

MIocene TO RECENT STRATIGRAPHY, STRUCTURAL
ARCHITECTURE AND TECTONIC EVOLUTION OF THE
ADANA BASIN, SOUTHERN TURKEY

CENTRE FOR NEWFOUNDLAND STUDIES

**TOTAL OF 10 PAGES ONLY
MAY BE XEROXED**

(Without Author's Permission)

RENEE BURTON

INFORMATION TO USERS

This manuscript has been reproduced from the microfilm master. UMI films the text directly from the original or copy submitted. Thus, some thesis and dissertation copies are in typewriter face, while others may be from any type of computer printer.

The quality of this reproduction is dependent upon the quality of the copy submitted. Broken or indistinct print, colored or poor quality illustrations and photographs, print bleedthrough, substandard margins, and improper alignment can adversely affect reproduction.

In the unlikely event that the author did not send UMI a complete manuscript and there are missing pages, these will be noted. Also, if unauthorized copyright material had to be removed, a note will indicate the deletion.

Oversize materials (e.g., maps, drawings, charts) are reproduced by sectioning the original, beginning at the upper left-hand corner and continuing from left to right in equal sections with small overlaps.

ProQuest Information and Learning
300 North Zeeb Road, Ann Arbor, MI 48106-1346 USA
800-521-0600

UMI[®]



National Library
of Canada

Acquisitions and
Bibliographic Services

395 Wellington Street
Ottawa ON K1A 0N4
Canada

Bibliothèque nationale
du Canada

Acquisitions et
services bibliographiques

395, rue Wellington
Ottawa ON K1A 0N4
Canada

Your file Votre référence

Our file Notre référence

The author has granted a non-exclusive licence allowing the National Library of Canada to reproduce, loan, distribute or sell copies of this thesis in microform, paper or electronic formats.

The author retains ownership of the copyright in this thesis. Neither the thesis nor substantial extracts from it may be printed or otherwise reproduced without the author's permission.

L'auteur a accordé une licence non exclusive permettant à la Bibliothèque nationale du Canada de reproduire, prêter, distribuer ou vendre des copies de cette thèse sous la forme de microfiche/film, de reproduction sur papier ou sur format électronique.

L'auteur conserve la propriété du droit d'auteur qui protège cette thèse. Ni la thèse ni des extraits substantiels de celle-ci ne doivent être imprimés ou autrement reproduits sans son autorisation.

0-612-83986-9



Memorial

University of Newfoundland

This is to authorize the Dean of Graduate Studies to deposit two copies of my thesis/report entitled

Miocene to Recent Stratigraphy, Structural Architecture
and Tectonic Evolution of the Adana Basin, Southern Turkey

in the University Library, on the following conditions. I understand that I may choose only ONE of the Options here listed, and may not afterwards apply for any additional restriction. I further understand that the University will not grant any restriction on the publication of thesis/report abstracts.

(After reading the explanatory notes at the foot of this form, delete TWO of (a), (b) and (c), whichever are inapplicable.)

The conditions of deposit are:

☒ (a) that two copies are to be made available to users at the discretion of their custodians,

OR

(b) that access to, and quotation from, this thesis/report is to be granted only with my written permission for a period of one year from the date on which the thesis/report, after the approval of the award of a degree, is entrusted to the care of the University, namely, _____ 19 ____, after which time the two copies are to be made available to users at the discretion of their custodians,

OR

(c) that access to, and quotation from, this thesis/report is to be granted only with my written permission for a period of _____ years from the date on which the thesis/report, after approval for the award of a degree, is entrusted to the care of the University; namely, _____, 19 ____; after which time two copies are to be made available to users at the discretion of their custodians.

Date

July 11, 2002

[Signature]
Dean of Graduate Studies

Signed

[Signature]

Witnessed by

[Signature]

NOTES

1. Restriction (b) will be granted on application, without reason given.

However, applications for restriction (c) must be accompanied with a detailed explanation, indicating why the restriction is thought to be necessary, and justifying the length of time requested. Restrictions required on the grounds that the thesis is being prepared for publication, or that patents are awaited, will not be permitted to exceed three years.

Restriction (c) can be permitted only by a Committee entrusted by the University with the task of examining such applications, and will be granted only in exceptional circumstances.

2. Thesis writers are reminded that, if they have been engaged in contractual research, they may have already agreed to restrict access to their thesis until the terms of the contract have been fulfilled.

**MIOCENE TO RECENT STRATIGRAPHY, STRUCTURAL ARCHITECTURE
AND TECTONIC EVOLUTION OF THE ADANA BASIN, SOUTHERN TURKEY**

by

Renee Burton

A thesis submitted to the
School of Graduate Studies
in partial fulfilment of the
requirements for the degree of
Master of Science

Department of Earth Sciences
Memorial University of Newfoundland

September-2002

Abstract

The Adana Basin of southeastern Turkey lies above the late Cretaceous-Eocene ophiolitic suture of the Afro-Arabian and Euro-Asian plates. The basin evolved in the Miocene and the sedimentary succession (0-6 km) records a complex tectono-stratigraphic history. Producing oilfields are present within the basin but the stratigraphic, sedimentological and structural controls on the fields have remained ambiguous. Advances in data accessibility and data quality have provided a new opportunity to re-examine the evolution of the basin in a modern context.

The Miocene to Recent succession is divided into three seismic megasequences by the three seismic unconformities. The unconformities include: B1, a progressively transgressed Type II sequence boundary that spans the Burdigalian-Serravalian interval, B2, a Type I sequence boundary that marks the onset of a basin wide forced regression in the Tortonian and B3 a laterally restricted transgressive sequence boundary that marks the maximum extent of Mediterranean desiccation and evaporite deposition in the basin.

Rapid lateral variations in sedimentary facies, complex growth stratal architectures and progressively-rotated local syntectonic unconformities are identified near buried thrust culminations within the Miocene succession. Three distinct structural provinces occur within the basin and include: 1) an E-W trending, buried southward-propagating growth fault-bend fold and thrust belt with associated carbonate reef buildups, 2) a prominent NNE-SSW trending basin-bounding culmination wall and local reverse faults that delimit the eastern flank of the basin, and 3) salt structures and an extensional listric fault fan that soles into salt in the southwest.

The Adana Basin documents a complex tectono-stratigraphic history during the Miocene. This is indicated by the highly variable nature of the Miocene sedimentology, stratigraphy and structural geology in space and time. Previous authors have proposed that the Miocene evolution of the Adana Basin resulted from periods of sea level variation, extensional and/or transtensional tectonism and intermittent periods of quiescence throughout the Miocene. In light of newly identified complex Miocene growth stratal architectures at buried thrust culminations, radical shifts in sedimentation style during the lower to late Miocene appears to have been largely controlled by compressional tectonics. The basin experienced an early to middle Miocene phase of south-directed thrusting, carbonate reef growth and subsequent drowning with continued basinward movement. The structural reorganization that led to the development of a proto-Kozan-Ecemis transtensional fault system during the late Serravalian marks the early docking of Arabia. Continued plate collision led to the development of a contractional culmination wall, associated with uplift of the Misis Mountains, that delimits the eastern basin edge. This uplift, in conjunction with a eustatic sea level fall led to a forced regression that climaxed in the Messinian with the desiccation of the Mediterranean Sea, and the precipitation of evaporates in basinal lows. Later, the sea returned to the southern parts of the basin, where delta progradation, delta toe collapse, and salt tectonics dominate the latest Miocene to Recent interval.

Table of Contents

Abstract i

List of Tables iv

List of Figures v

Acknowledgments vii

Chapter 1: Introduction 1

1.1 Study Area 1

1.1.1 Adana Basin 1

1.1.2 Misis Mountains 3

1.1.3 Cilicia and Iskenderun Basins 3

1.1.4 Taurus Mountains 4

1.2 Tectonic Framework 4

1.2.1 Tectonic Setting 5

1.2.2 Tectonic Evolution of Southeastern Turkey 8

1.3 Geological Setting 10

1.3.1 Neogene Basins of Southeastern Turkey 10

1.3.2 Adana Basin 12

1.3.3 Misis-Kyrenia Range 20

1.3.4 Eastern Taurus Mountains 25

1.4 Recent models of Neogene evolution of the Adana Basin 25

1.4.1 History of Shoreline Movements 27

1.5.2 Previous Tectono-Syntheses for the Adana Basin 31

1.5.3 Controls on Sedimentation 37

1.5 Scientific Objectives 38

Chapter 2: Stratigraphy 42

2.1	Lithostratigraphy	43
2.1.1	Basement to the Miocene Succession in the Adana Basin	44
2.1.2	Miocene Succession	51
2.1.3	Comments on lithostratigraphic contacts	67
2.2	Seismic Stratigraphy	69
2.2.1	Description of seismic features	73
2.2.2	Geographic distribution of seismic features	90
2.3	Correlation of surface and seismic data	98
2.3.1	Correlation and chronology of seismic markers and units	99
2.3.2	Comments on well data	102
2.4	Sequence stratigraphy	102
Chapter 3: Structural Geology 109		
3.1	Identification of structural features	109
3.2	Structural features in the Adana Basin	110
3.2.1	Northern Domain	113
3.2.2	Eastern Domain	127
3.3.3	Southwestern Domain	134
Chapter 4: Tectonic Synthesis 140		
4.1	Relative timing of deformation events	140
4.2	Tectonic-stratigraphic implications	144
4.2.1	Tectonic-stratigraphic analogs	144
4.2.2	Comparison with the Adana Basin	149
4.3	Miocene to Recent tectonic evolution of the Adana Basin	155
4.3.1	Phase 1	155
4.3.2	Phase 2	158
4.3.3	Phase 3	159

Chapter 5: Conclusions 161

5.1 Conclusions 161

Appendix A Methodology

Appendix B Lithologic/Biostratigraphic control data

Appendix C Surfer Map Data

List of Tables

Table 1.1: Williams et al., (1995) seismic units-lithologic units	16
Table 2.1: Characteristics of lithostratigraphic unconformities in the Adana Basin	68
Table 2.2: Summary of seismic stratigraphic frameworks for the Adana Basin	71
Table 2.3: Characteristics of prominent seismic unconformities in the Adana Basin	76
Table 2.4: Descriptive summary of seismic facies attributes	77
Table 2.5: Correlation of seismic and lithostratigraphic unconformities	100
Table 2.6: Correlation of seismic and lithologic units	103
Table 3.1: Structural-stratigraphic attributes of the Northern, Eastern and Southwestern Domains	112
Table 4.1: Constrained timing of deformation events for the Northern, Eastern and Southwestern Domains	141

List of Figures

- Figure 1.1: Location map of study area 2
- Figure 1.2: Plate tectonic configuration 6
- Figure 1.3: Regional geology and tectonic features 7
- Figure 1.4: Schematic tectonic evolution of the Maras region during the Neogene 11
- Figure 1.5: Stratigraphic framework for the Miocene - Recent basin fill of the Adana Basin 13
- Figure 1.6: Surficial geology map of the Adana-Misis region 15
- Figure 1.7: Previous seismic data sets in the Adana Region 18
- Figure 1.8: Simplified surface geology map of the Misis Mountains 21
- Figure 1.9: Schematic structural sections through the Misis Mountains and Iskenderun Bay 22
- Figure 1.10: Stratigraphic ranges identified using new micro-paleontological evidence in logged sections of the Misis Complex 23
- Figure 1.11: Thrust nappes of the Alada Mountains of the Eastern Taurus Range 26
- Figure 1.12: Comparison between eustatic and the relative sea level curves in the Adana Basin 28
- Figure 1.13: Summary of marginal vs deep basin deposition/non-deposition during the Messinian salinity crisis 30
- Figure 1.14: Schematic paleogeography maps of the Adana-Misis-Iskenderun region 32
- Figure 1.15: Schematic paleogeography maps of the Adana 33
- Figure 1.16: Tectonic evolution proposed by Williams et al., (1995)
- Figure 1.17: Tectonic evolution proposed by Pralle et al, (1994) 36
- Figure 1.18: Location of data set for the Adana study 39
-
- Figure 2.1: Composite surface geology map of the Adana- Misis region 45
- Figure 2.2: Stratigraphic template for the Adana Basin 46
- Figure 2.3: Stratigraphy at the Camardi-Nidge area 47
- Figure 2.4: Schematic distribution of Karaisal reef facies 59
- Figure 2.5: Seismic stratigraphic interpretation of Line 1 75

- Figure 2.6: Time structure map of the B1 unconformity (TWT) 78
- Figure 2.7: Time structure map of the B2 unconformity (TWT) 79
- Figure 2.8: Industry profiles Line 4 and Line 2 80
- Figure 2.9: Industry profiles Line 3 and Line 5 81
- Figure 2.10: Industry profiles Line 6 and Line 7 82
- Figure 2.11: Industry profiles Line 8 and Line 9 87
- Figure 2.12: Time isochore map of Megasequence 1 (TWT) 92
- Figure 2.13: Time isochore map of Unit 1 (TWT) 93
- Figure 2.14: Schematic sequence stratigraphic framework of the Adana basin 105
-
- Figure 3.1: Structural Domains of the Adana Basin 111
- Figure 3.2: Conjugate extensional fault sets in the Northern Domain 114
- Figure 3.3: Structural-stratigraphic interpretation of Line 4 115
- Figure 3.4: Schematic cross-section through Figure 3.1 117
- Figure 3.5: Northern Domain thrust traces superimposed on Unit 1 thickness distribution map 118
- Figure 3.6: High resolution detail of ramp anticlines in Line 3 and Line 4 120
- Figure 3.7: High resolution detail of Line 7 121
- Figure 3.8: Structural-stratigraphic interpretation of Line 12 122
- Figure 3.9: Structural-stratigraphic interpretation of Line 2 128
- Figure 3.10: Structural-stratigraphic interpretation of Line 13 129
- Figure 3.11: Schematic line drawings of reverse faults in the Eastern Domain 130
- Figure 3.12: High resolution detail of the eastern flank of the Adana Basin 131
- Figure 3.13: Structural-stratigraphic interpretation of Line 14 133
- Figure 3.14: Structural-stratigraphic interpretation of Line 1 135
- Figure 3.15: Structural-stratigraphic interpretation of Line 15 136
- Figure 3.16: High resolution detail of a salt roller in Line 1 139
-
- Figure 4.1: Depositional model of basin development within a foreland basin 145
- Figure 4.2: Variations in relationships between fold-thrust belt and foreland basin 146

- Figure 4.3: Morphology of satellite basins associated with fold-thrust belts 148**
- Figure 4.4: Miocene tectono-stratigraphic model for Phase I 152**
- Figure 4.5: Miocene tectono-stratigraphic model for Phase II 153**
- Figure 4.6: Miocene tectono-stratigraphic model for Phase III 154**

ACKNOWLEDGEMENTS

I would like to extend thanks to the Turkish Petroleum Corporation (TPAO) for providing the dataset for this study, to the Canada Newfoundland Offshore Development Fund for career development awards, the Department of Graduate Studies and the Earth Sciences Department of Memorial for internal funding support, and to the Buchans ASARCO and Canadian Society of Exploration Geophysicists for scholarship support.

A number of people have provided assistance and support over the course of this project. Many thanks to:

Drs. Jeremy Hall and Rick Hiscott for sharing their expertise and for always leaving their doors open.

Dr. Jim Wright and the faculty, staff and students of the Earth Science Department for making research at Memorial University such a positive experience.

Bob Leatherbarrow, Larry Sydora, Philip Benham, Veronique Dumas, Ewan Cumming and Laurie Davis for relaying a wealth of geological knowledge, techniques and perspectives during my intervening terms of employment.

My office mates Arden and Colleen for many great tips and for putting up with lots of plants, rocks, coffee cups and me!

Dianne and Alison for stimulating conversations, idea exchange and great coffee breaks.

Sincere thanks and gratitude to Drs. Ali Aksu and Tom Calon, my supervisors and mentors, whose guidance, moral support and instructive teachings were essential to the fruition of this project.

Deep thanks to my parents for introducing me to science and for providing a childhood filled with nature expeditions that put me on this path, and to Corinne and my grandparents for their confidence in me. Lastly, thanks to Jody and Dan for providing comic relief, adventurous diversions and encouragement along the way.

CHAPTER 1: INTRODUCTION

1.1 STUDY AREA

The geographic focus of this research project is the Adana Basin in southeastern Turkey. The study area is located between latitudes 36°30' N and 37°15' N and longitudes 34°45'E and 35°55'E (Figure 1.1). The onshore extent of the Adana basin is delimited by the Taurus Mountains in the north and west, by the Misis Mountains in the east, and by the Mediterranean Sea in the south. The marine extension of this large depocentre is the Inner Cilicia Basin, which lies directly south of the main Adana Basin. A second marine depocentre, the Iskenderun Basin, lies directly east of the Misis Mountains, and west of the Amanos Mountains.

1.1.1 Adana Basin

The Adana Basin covers a surface area of approximately 10 000 km². The elongate, northeast-southwest trending basin exhibits a range in topographic elevation from 1000 m ASL in northern areas to 0 m ASL along the southern shoreline. Three major rivers provide drainage from northern highlands of the Taurus Mountains through the Adana Basin to the Mediterranean coast. From west to east these are the Tarsus, Seyhan and Ceyhan rivers (Figure 1.1). Aksu et al. (1992b) cite estimates for the volume of sediment that is transported annually by these rivers. Minimum estimates of annual sediment yields range from 5462 x 10³ t for the Ceyhan River and 5185 x 10³ t for the Seyhan River to 129 x 10³ t for the Tarsus River. These rivers are recognized as the main present day suppliers of clastic sediment to the onshore Adana Basin and the marine basins of Cilicia and Iskenderun (Aksu et al., 1992b).

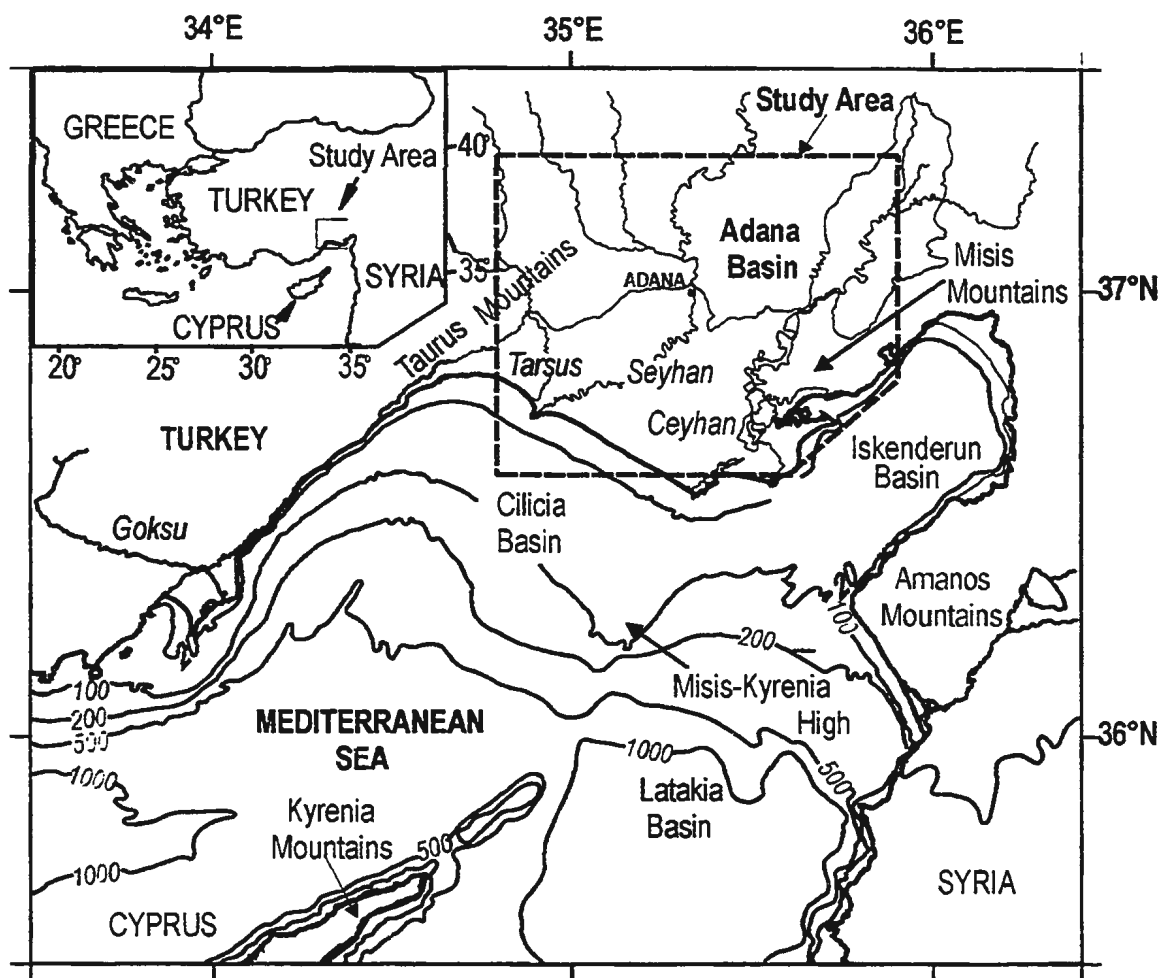


Figure 1.1: Location map of the Adana Basin. The location of the Tarsus Seyhan, Ceyhan and Goksu rivers is indicated. Bathymetric contours are expressed in metres.

1.1.2 Misis Mountains

The Misis Mountains form the eastern limit of the Adana Basin, and are oriented in a northeast-southwest direction (Figure 1.1). Bathymetric data indicate that this physiographical feature extends southward beyond the coastline into the Mediterranean Sea as the Misis-Kyrenia high, which separates the Cilicia and Iskenderun basins (Aksu et al., 1992a and b). Further south this northeast-southwest trending high outcrops again on the Island of Cyprus as the Kyrenia Range.

1.1.3 Inner Cilicia and Iskenderun Basins

The Inner Cilicia Basin represents the present day extension of the Adana Basin beyond the coastline to the southwest (Figure 1.1). The basin is delimited by the Taurus mountains in the west, the Adana Basin in the north and the submerged Misis-Kyrenia high to the east. Bathymetry data for the Cilicia Basin (Figure 1.1) reveal a shelf break in the 100 - 150 m water depth zone with a slope gradient of 1:140, and a steeper slope break in the 300-700 m water depth zone with a slope gradient of 1:50 (Aksu et al., 1992a). The basin contains a very thick (up to 3000 m) Plio-Quaternary sedimentary fill deposited by delta progradation feeding from the main rivers which drain the Adana Basin.

The Iskenderun Basin is a northeast-southwest trending, predominantly submarine basin located east of the Adana Basin (Figure 1.1). The basin is bound by the Misis Mountains to the west and the Amanos Mountains to the south and east. Bathymetric data indicates that the inner portion of the basin is quite shallow, with maximum water depths of

less than 100m. The outer portion of the basin, referred to as the Inner Latakia Basin (Aksu et al., 1992a), exhibits bathymetric features similar to those of the Cilicia Basin, where the sea floor drops rapidly from 100m to greater than 1km below the surface of the Mediterranean Sea.

1.1.4 Taurus Mountains

The Taurus Mountains form a northeast-southwest trending structural high that delimits the northern and western limits of the Adana Basin (Figure 1.1). A prominent lineament known as the Ecemiş Fault Zone divides the mountain belt into the Eastern and Western Taurides. This lineament is straddled by the narrow NNE - SSW-trending Çamardı Basin. The Çamardı Basin forms a shallow asymmetric depocentre, and is filled by an Eocene to Recent sedimentary succession that is thicker west of the Ecemiş Fault (~ 1000m), and thinner east of the Ecemiş Fault (~ 800m). Pre-Miocene rocks of Eastern Taurides extend northeastward beneath portions of the Miocene Adana Basin, and extend southward to the Mediterranean Sea.

1.2 TECTONIC FRAMEWORK

The African, Arabian and Eurasian tectonic plates lie in a collisional setting (Şengör and Yılmaz, 1981). The tectonic framework of the eastern Mediterranean is described in the following two sections. Section 1.2.1 provides an overview of the major tectonic elements in the region. Section 1.2.2 provides a summary of the tectonic evolutionary processes that

have contributed to the formation of the morpho-tectonic features of the region.

1.2.1 Tectonic setting

The south-easternmost portion of Turkey forms part of the Anatolian micro-plate, and occupies a unique tectonic position above the zone of suturing of the African, Arabian and Eurasian plates (Figure 1.2). A number of tectonic investigations have focused on the configuration and kinematics of this complex suture zone (e.g., Şengör and Yilmaz, 1981; Kelling et al., 1987; Karig and Kozlu, 1990). The Anatolian microplate is presently moving westward relative to the Eurasian, Arabian and African plates along a series of strike slip faults which include the North Anatolian and East Anatolian transform faults and their associated splays such as the Amanos and Eçemiş faults (Figure 1.2; Şengör and Yilmaz, 1981; Aksu et al., 1992).

The Bitlis-Zagros Suture zone (BZS) lies east of the tectonic triple junction of the African, Arabian and Anatolian plate boundaries (e.g., Karig and Kozlu, 1990). The African-Arabian plate boundary is represented by the Dead Sea Transform Fault (DST) which exhibits a sinistral sense of motion (Figs. 1.2 and 1.3). The Anatolian-Arabian boundary is represented by i) by the various strands of the sinistral East Anatolian (EAF) strike-slip fault, and ii) a belt of imbricated folds and thrusts, known as the Enginek Zone (Karig and Kozlu, 1990), which is the western extension of the Bitlis Zagros Suture Zone. The African-Anatolian plate boundary forms the third and southernmost tectonic element of the suture zone. This boundary changes progressively from convergence and subduction along the

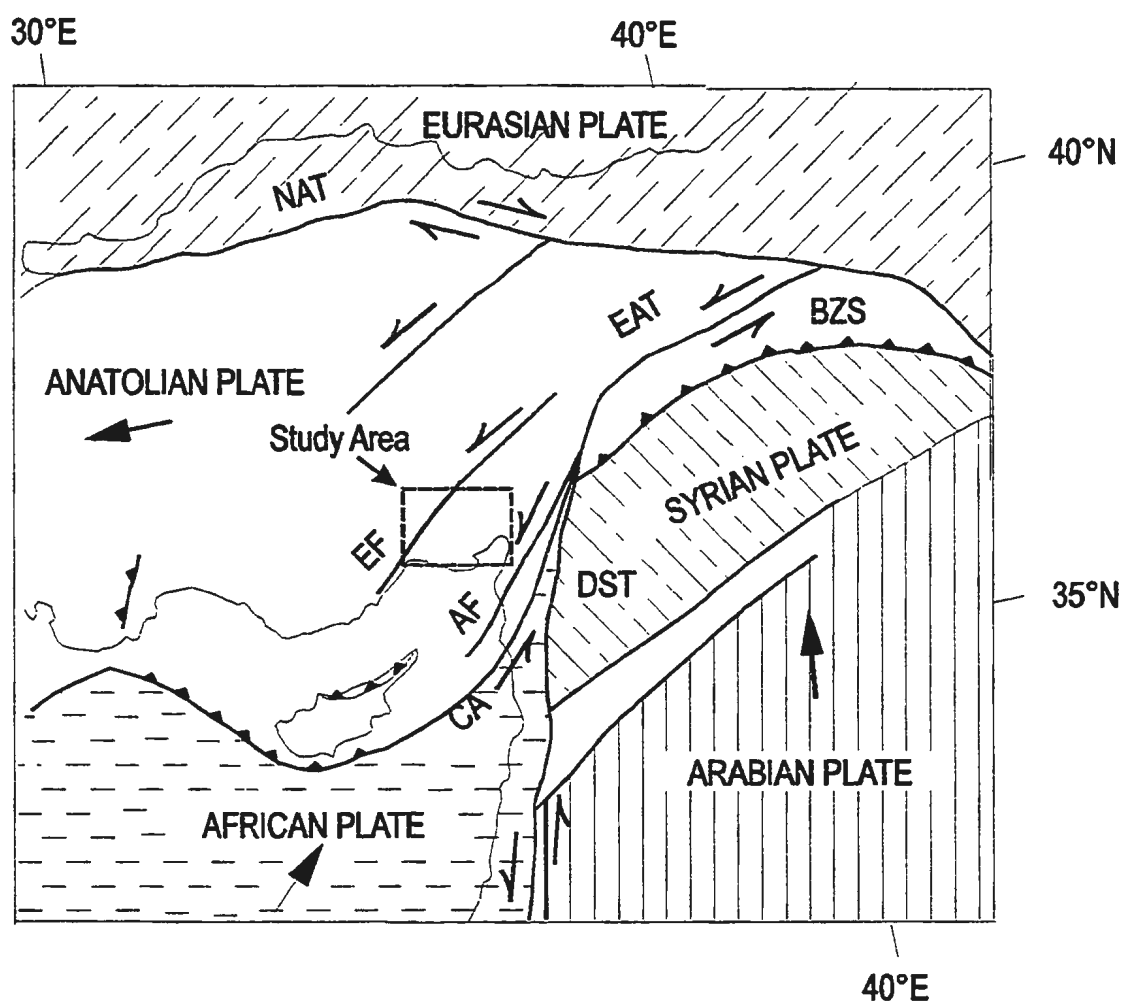


Figure 1.2: Tectonic setting of the Adana Basin. Note the location of the study area relative to the Bitlis-Zagros Suture zone (BZS), the Dead Sea Transform fault (DST), the east Anatolian Fault (EAT), the Amanos Fault (AF), the North Anatolian Fault (NAT) and the Ecemis Fault Zone (EF).

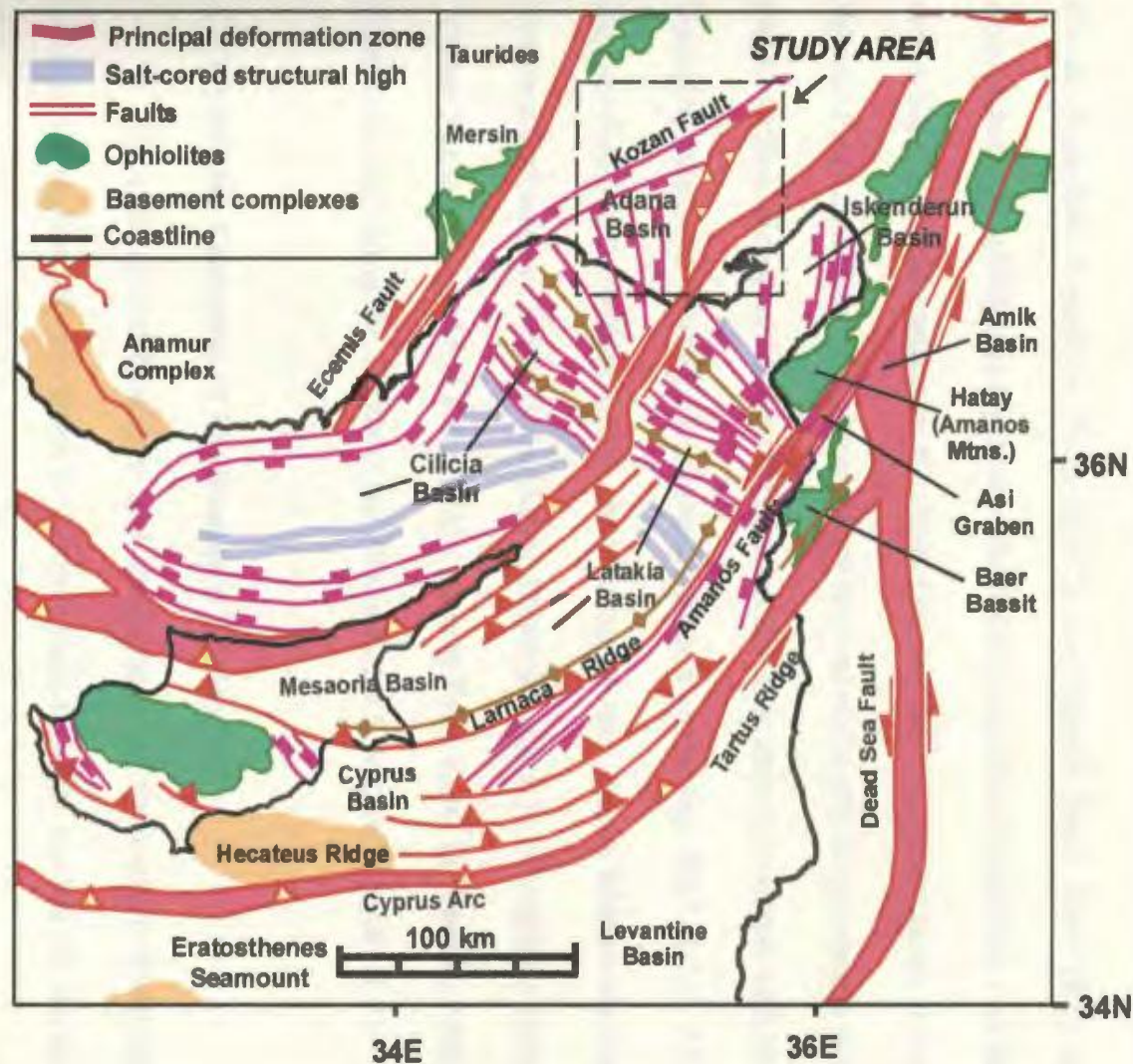


Figure 1.3: Regional Geology and tectonic features of the Adana Basin. The geological map is simplified to show the main structural elements of the area. The Neogene basin complexes are separated by major deformation zones combining various structural associations related to time and position in the evolution of the diffuse plate boundary. After Calon et al. (1998).

Cyprian Arc in the southwest, to sinistral strike-slip motion along the strands of the EAT in the northeast (Figs. 1.2 and 1.3).

Other important tectonic elements of the southeastern Mediterranean include the North Anatolian Transform Fault (NAT), the Eçemis Fault Zone (EF) and significant occurrences of ophiolite complexes. The North Anatolian Transform represents a dextral strike-slip fault which separates the Anatolian and Eurasian plates (Figs. 1.2 and 1.3). The Eçemis Fault Zone occurs as a corridor of sinistral strike-slip displacement which lies within the Anatolian microplate; this intra plate position is in marked contrast with the major plate-bounding positions of the fault zones mentioned above (eg. DST, EAF, AF, NAT). The Eçemis Fault Zone occurs within the portion of the Taurus Mountains that bounds the northern and western flanks of the Adana Basin (Figure 1.3). Ophiolites are exposed in the Taurus Mountains, on both sides of the Eçemiş Fault Zone in Amanos Mountains (Hatay Complex), and along the Syrian Coast (Baes Bassit Complex) (Figure 1.3).

1.2.2 Tectonic Evolution of Southeastern Turkey

The geologic architecture and stratigraphy of the eastern Mediterranean region records a complex tectonic history. Current plate tectonic models for the evolution of the Eastern Mediterranean conclude that the region has experienced a minimum of three tectonic phases. These phases include: 1) Permian to Triassic rifting and continental break-up, 2) passive margin subsidence and oceanic development and 3) ensuing collision of the African and Eurasian plates (e.g., Robertson, 1998). It is during this latest collisional phase that most

of the present day morpho-tectonic features of the eastern Mediterranean region developed. Aspects of the tectonic evolution of the eastern Mediterranean are presently reviewed in the context of pre-Neogene and post-Neogene events.

Pre-Neogene evolution of Southeastern Turkey

A number of tectonic models have attempted to delineate the pre-Neogene evolution of the Mediterranean region. One point of debate in existing literature focuses on the origin of various ophiolite bodies observed throughout the Mediterranean. The origin of these ophiolites is attributed to the creation and subsequent destruction of a Neotethys ocean. It is postulated that this large paleo-ocean consisted of a number of smaller ocean basins and intervening microplates. This ocean then experienced a significant collisional event that led to the tectonic emplacement of a variety of ophiolite bodies which are observed in the eastern Mediterranean today (Robertson and Woodcock, 1981). This 'Tethyan' perspective has been adopted by numerous authors in recent work (Vidal and Alvarez-Marrón, 2000; Karig and Kozlu, 1990; Kelling, 1987). Readers who wish to learn more on this subject are directed to the treatment of Pralle (1995), which provides an extensive summary of the pre-Neogene paleogeographic and tectonic evolution of Turkey.

Neogene tectonic evolution of southeastern Turkey

The tectonic evolution of southeastern Turkey has been largely controlled by strike-slip deformation during the Neogene (Kelling et al., 1987; Karig and Kozlu, 1990). These

strike-slip movements have been accompanied by components of extension and compression during the Neogene to recent interval. These contrasting components of extension versus compression-dominated strike-slip deformation exhibit a spatial and temporal variability which seems to indicate processes of strain partitioning within the orogen (Karig and Kozlu, 1990). Karig and Kozlu (1990) propose a tectonic model for the Neogene evolution of the Maras region (Figure 1.4) which involves a phase of Early Miocene transtension and a phase of late Miocene to Pliocene transpression.

1.3 GEOLOGICAL SETTING

Those portions of southeastern Turkey which are proximal to and encompass the suture zone of the Anatolian-African-Arabian plate collision have been the focus of a number of geological investigations in recent years. These investigations have resulted in a profusion of structural and stratigraphic observations pertaining to the sedimentary basins and structural highs of this region. Geological overviews of the Adana Basin, the Misis-Kyrenia Range and the Eastern Taurus Mountains are presented below.

1.3.1 Neogene Basins of southeastern Turkey

A series of genetically related Neogene Basins lie in close proximity to the Anatolian-African-Arabian triple junction of southeastern Turkey (Figure 1.3). Three basins within this complex which lie directly to the southwest of this tectonic feature are the Adana, Cilicia and Iskenderun Basins (Figs. 1.1 and 1.3). The basin complex is believed to have originated as

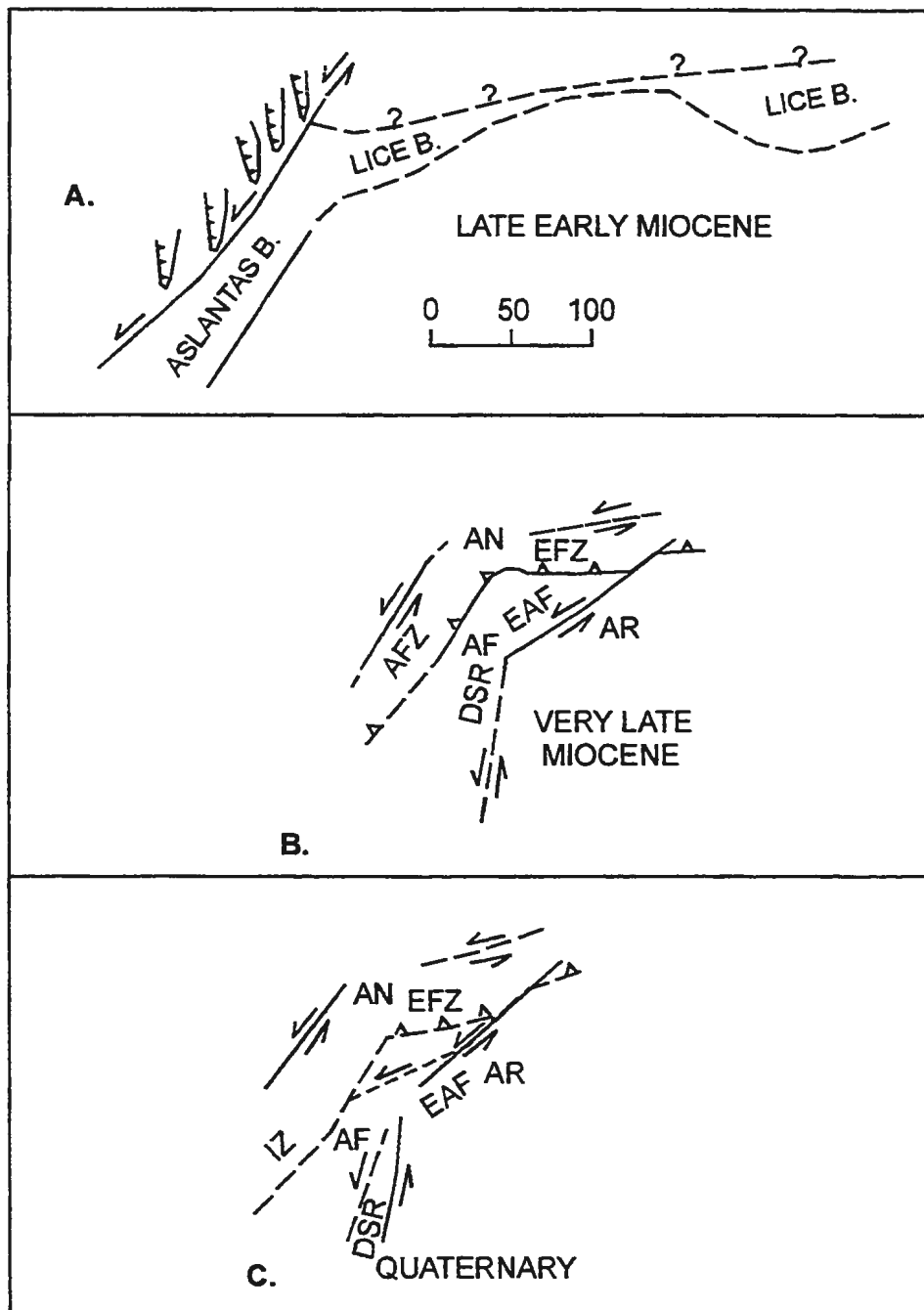


Figure 1.4: Schematic tectonic evolution of the Maras region during the Neogene: A. Late Early Miocene. Transtension along the Aslantas Fault Zone (AFZ) B. Latest Miocene - early Pliocene. Transpression along Aslantas and Enginek (EFZ) trends after initiation of the Eastern Anatolian Fault (EAF) and Dead Sea Rift (DSR). C. Quaternary. Conversion of Aslantas trend to the Iskenderun transtentional boundary (IZ). (Modified after Karig and Kozlu, 1990).

an effect of intra-plate extension which occurred in response to the inception and evolution of the triple junction (Aksu et al., 1992). Exploratory drilling in the Adana, Iskenderun and Cilicia basins has revealed a Miocene to Recent succession which exhibits maximum thicknesses of greater than 4-6 km. In each basin a Miocene to Recent succession lies unconformably above a deformed, partially eroded pre-Miocene basement. The Cilicia and Iskenderun basins are submerged below the Mediterranean Sea and as a result, researchers have had to rely heavily on subsurface sampling and mapping tools to study the sedimentary successions which they contain. In contrast, the terrestrial exposure of the Adana Basin has permitted surface sampling and mapping of the basement and cover successions.

1.3.2 Adana Basin

Numerous surface and subsurface studies within the Adana Basin indicate that the sedimentology, stratigraphy and structural geology of the basin is quite complex. A brief overview of the lithostratigraphic framework of the Adana Basin is provided below:

The sedimentary succession of the Adana Basin has been divided into a number of formations based on existing lithologic and biostratigraphic information. Yetis et al. (1995) provide a stratigraphic column for the Adana Basin (Figure 1.5) which indicates that the basin fill is divisible into nine lithostratigraphic formations representative of the Oligocene to Pliocene interval. This thick basin fill is topped by terrace alluvium of the Quaternary to Recent interval. Listed in order from oldest to youngest the Karsanti, Gildirli, Kaplankaya, Karaisalı, Cingöz, Güvenç, Kuzgun, and Handere formations form the Oligocene to Pliocene

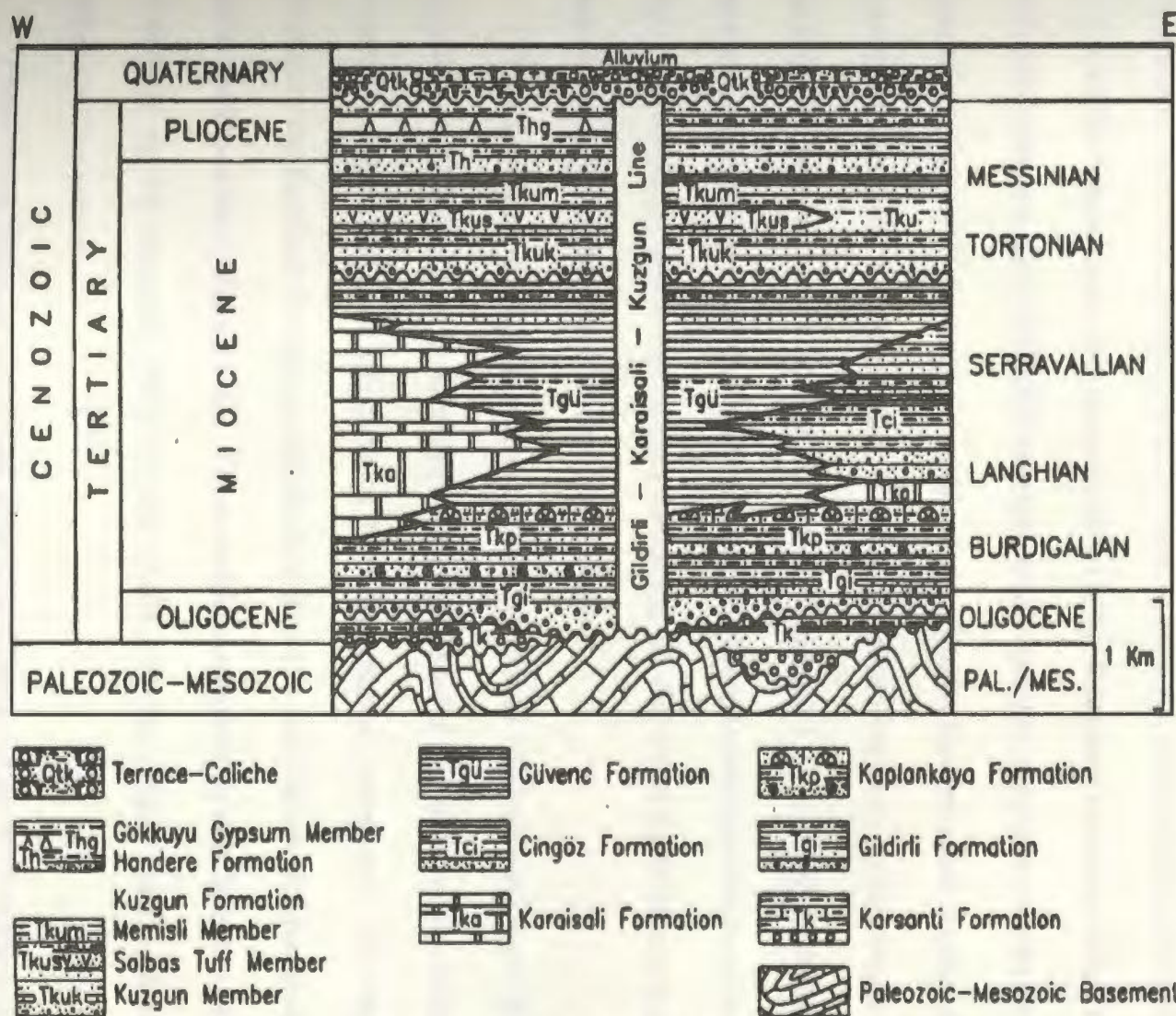


Figure 1.5: Stratigraphic framework for the Oligocene to Recent basin fill in the North-Central portion of the Adana Basin as proposed Yetis et al. (1995). This framework presents the results of a surficial geology mapping project limited to the north-central portion of the basin, and does not integrate the work of other authors in other portions of the Adana Basin.

succession of the Adana Basin (Figs. 1.5 and 1.6). The lateral extent of the various formations throughout the basin is summarized by Williams et al (1995) in Table 1.1a. This table indicates that most formations are present in both the northeastern and northwestern portions of the Adana basin, with the exceptions of the Karsanti Formation which is observed only in the northwest, and the Gildirli Formation which occurs only in the northeast. Notably, the question of possible diachroniety within the succession has remained largely unresolved. The individual formations of the Adana Basin succession have been defined based on a set of unique spatial, temporal and lithologic attributes. Figures 1.5 and 1.6 help to demonstrate the spatial and temporal aspects of each of the eight lithologic formations observed in the Adana Basin. The lithologic attributes of each formation are described by Williams et al. (1995). A summary of these observations is provided below.

The Karsanti Formation is composed of a mixture of Oligocene aged alluvial fan, fluvial, lagoonal and lacustrine deposits, while the Gildirli Formation, which occurs only in the north, consists of thick deposits of fluvial-lacustrine sediments. Carbonate reefs characterize the Karaisalı Formation which often occur in association with isolated basement highs in the Northwest (Figure 1.6). These reefal accumulations pass laterally into forereef and shallow marine deposits which in turn grade into the deeper marine clastics of the Kaplankaya Formation.

These lower units are succeeded upward and eastward by the Langhian-Serravalian aged Cingöz and Güvenç formations (Figs. 1.5 and 1.6). These formations consist primarily of turbidite deposits which suggest north and northwestern point source provenance and

Williams et al. (1995) distribution of lithological formations and correlation with seismic megasequences, Northern Adana Basin.				
Geological Time		NE Adana Basin	NW Adana Basin	Seismic Megasequence
Quaternary		Terrace Alluvium	Terrace Alluvium	Megasequence 3
Pliocene		-----	-----	
Miocene		Handere Formation	Handere Formation	Megasequence 3
	Messinian			
	Tortonian	Kuzgun Formation	Kuzgun Formation	Megasequence 3
		-----	-----	
	Serravalian	Guvenc Formation	Guvenc Formation	Megasequence 2
	Langhian	Cingoz Formation	Cingoz Formation	Megasequence 2
	Langhian	Karaisali Formation	Karaisali Formation	Megasequence 1
	Burdigalian	Kaplankaya Formation	Kaplankaya Formation	Megasequence 2
	Aquitania	Gildirli Formation	-----	
Oligocene		-----	Karsantii Formation	

Table 1.1: Williams et al. (1995) summary of stratigraphic data and seismic megasequence interpretations for the northern Adana Basin. Note i) apparent hiatus in the lithostratigraphy, and ii) the assignment of the Karaisali Formation to a separate megasequence.

south and southeastern paleocurrent directions. The Güvenç Formation is unconformably overlain by fluvial-deltaic deposits of the Kuzgun Formation. Shallow marine deposits of the Pliocene aged Handere Formation succeed the Kuzgun Formation. An abrupt erosional unconformity and evaporitic deposits of the Adana Group succeed the Handere Formation in the southwest; in the north and central and eastern portions of the basin the Handere Formation is conformably succeeded by Quaternary aged terrace alluvium of the Kuransa Formation.

ii. Subsurface geology

A. Stratigraphy

Aspects of the subsurface geology of the Adana Basin are also reported by Williams et al. (1995) and Pralle (1994). Figure 1.7 indicates the location and density of seismic data available for the Williams et al. (1995) and Pralle (1994) studies. The seismic data used in the Williams et al. (1995) study allowed the researchers to identify and interpret three seismic megasequences as well as a number of extensional and compressional structures. In ascending order the seismic megasequences of Williams et al. (1995) are described as follows:

Megasequence 1: bright reflectors which are interpreted as reefal deposits occur in association with the crests of interpreted extensional fault blocks.

Megasequence 2: parallel continuous reflectors which are interpreted as turbidite deposits demonstrate onlap at the base and truncation at the top; no growth strata

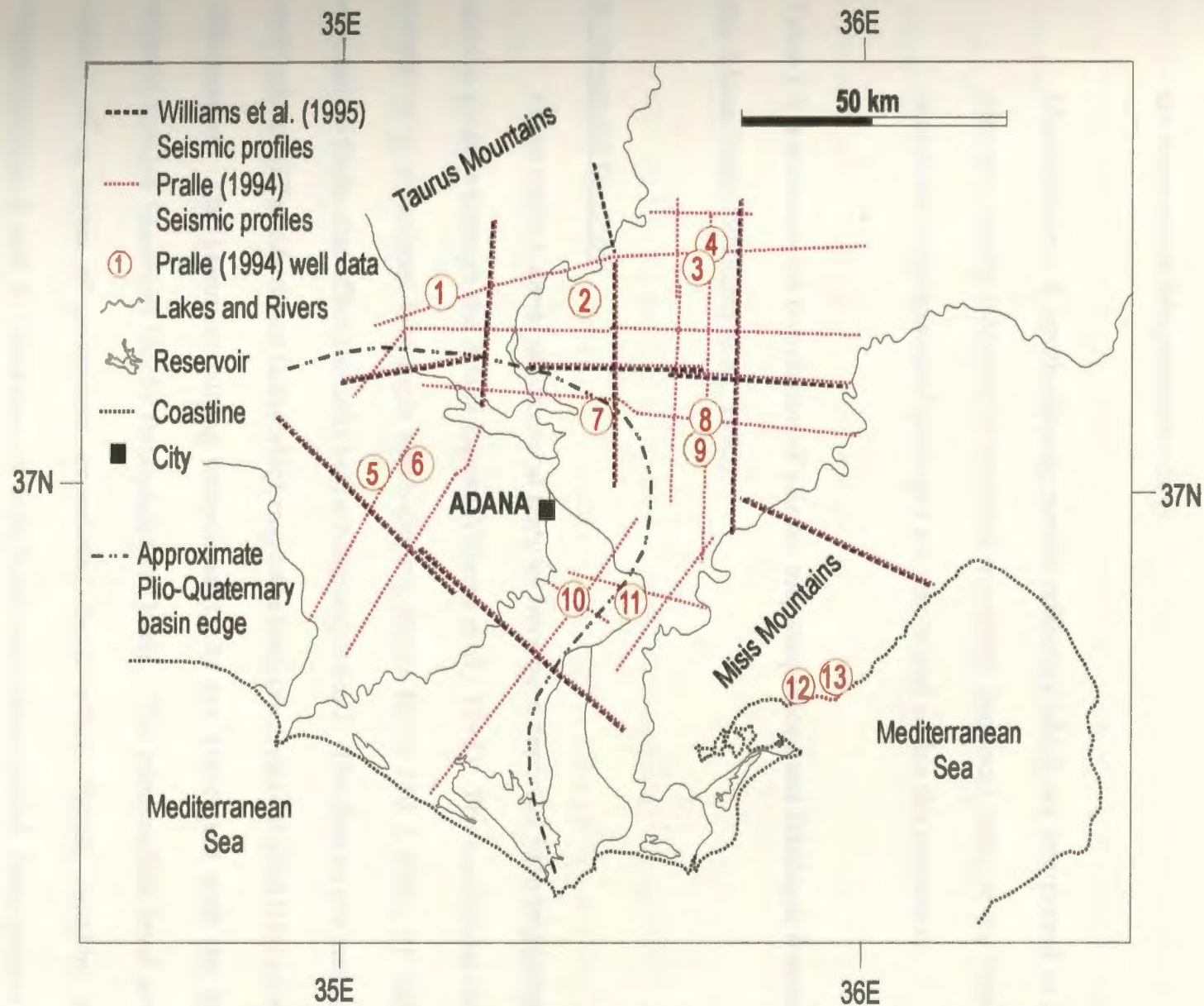


Figure 1.7: Location of previously available data in the Adana Basin from i) Williams et al. (1995) and ii) Pralle (1994). Note i) grid spacing and density of seismic data and ii) the distribution of available well data. Data provided courtesy of TPAO.

are observed in Megasequence 2.

Megasequence 3: south-dipping parallel reflectors which are interpreted as deltaic deposits contain evidence of erosional truncation and local onlap at the base; occasional progradational packages are also noted within the sequence.

Table 1.1 b indicates the correlation of seismic megasequences and lithologic formations of the Adana Basin (Williams et al., 1995).

B. Structural Geology

Three distinct levels of structural features have been reported from interpretation of seismic profiles through the Adana Basin (Williams et al., 1995). The lowermost structures consist of i) occasional low-angle north-dipping thrust faults and a series of high angle extensional faults that affect the units below Megasequence 2. The thrusts are interpreted as south-directed Tauride thrust faults which may have been reactivated during later extensional deformation. The basement cutting extensional faults are associated with the flanks of isolated horsted basement blocks throughout the basin. The intermediate level structures consist of a series of prominent extensional faults which display notable offset in Megasequences 2 and 3. Instances of both listric and tabular block fault geometries are observed within this structural level, and occasionally, opposing senses of dip are observed

within the main extensional faults. The uppermost level of structures noted with the Adana basin consist of two contrasting styles. In the southwest, a series of southwest directed listric extensional faults cut Megasequence 3; in the east, a series of high angle thrusts are interpreted as a positive flower structure which cut the units below Megasequence 3. Internal erosional unconformities are noted within Megasequence 3 to the west of this structure. These features suggest that deformation and development of the positive flower structure continued during deposition of Megasequence 3.

1.3.3 Misis-Kyrenia Range

The Misis-Kyrenia Range represents a structurally elevated segment of Cukurova basin fill (Gökçen et al., 1988). The northern terrestrial portion of this structural high is referred to as the Misis Mountains and/or Misis Complex which bounds the eastern limit of the Adana Basin (Figs. 1.1, 1.6 and 1.8). As described in Section 1.1.2, the Misis Mountains extend southward into the offshore as the Misis-Kyrenia high which lies south of the Adana Basin and underneath the Mediterranean Sea. Further south the Kyrenia Range of northern Cyprus represents the southern terrestrial extension of the submerged Misis-Kyrenia high. A number of recent stratigraphic and tectonic investigations have focused on the rocks of the Misis Mountains (Gökçen et al., 1988; Kelling et al., 1987; Karig and Kozlu, 1990). A brief summary of the Miocene geology of the Misis Mountains is provided below.

The rocks of the Misis Mountains are divisible into three lithologic formations based on biostratigraphic data (Figures 1.9 and 1.10; Gökçen et al. 1988). In ascending order the

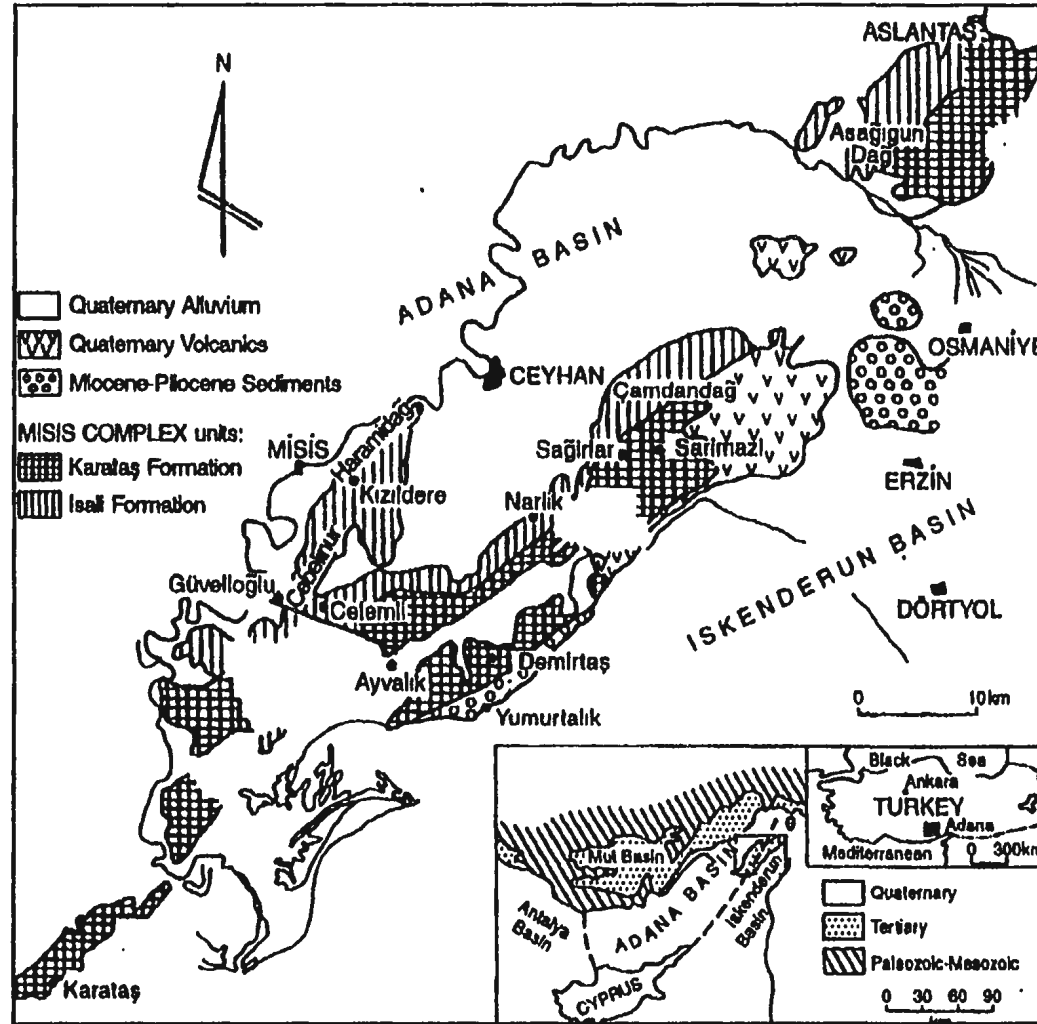


Figure 1.8: Simplified surface geology map of the Misis Mountains. Inset map indicates location of the map area relative to the Adana Basin. After Gokcen et al. (1985) and Yetis et al. (1995).

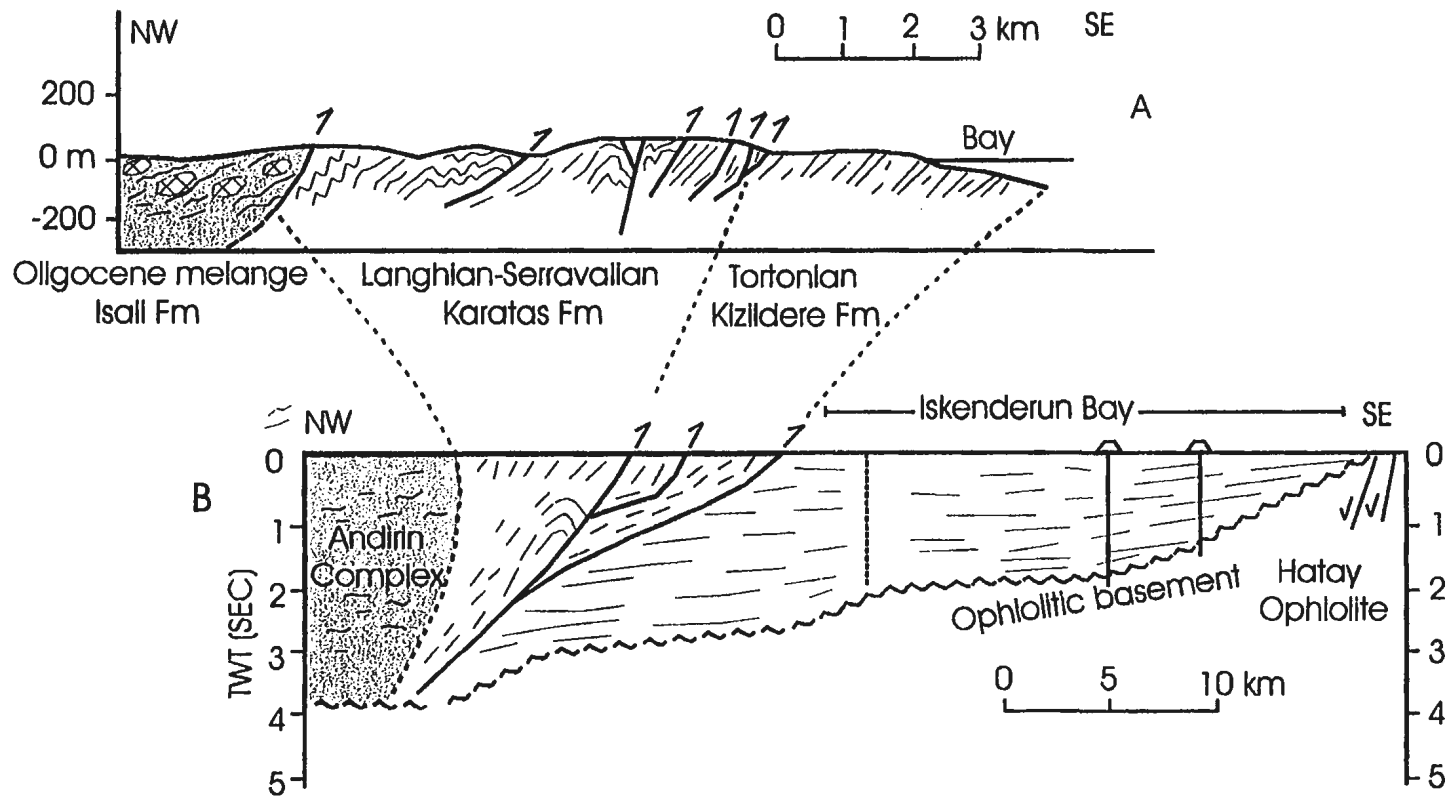


Figure 1.9: Schematic structural sections through the Misis Mountains and Iskenderun Bay. A) represents surface geological observations, after Kelling et al. (1987); B) illustrates observations from an interpreted seismic profile, after Karig and Kozlu (1990). Modified from Jackman (1995).

Isali, Karataş and Kızıldere formations are present in the Misis Mountains. The Isali Formation is dominated by olistostromic facies which formed during the Aquitanian interval. The Isali Formation is succeeded by time transgressive deposits of the Karataş Formation which span the Burdigalian to Tortonian interval. The formation is comprised of a potentially diachronous sequence of carbonate shelf, shallow marine, submarine fan and deep water basin plain facies. The Karataş Formation is in turn succeeded by Tortonian aged shallow marine and fluvial-deltaic deposits of the Kizildere Formation.

The structure of the sedimentary succession in the Misis Mountains has been a prominent focus of recent studies. These investigations indicate that the lithologic formations described above occur within an imbricate arrangement of predominantly northwesterly dipping thrusts. Schematic sections of the surface (Kelling et al., 1987) and subsurface (Karig and Kozlu, 1990) geology of the Misis Mountains are illustrated in Figure 1.9. These schematic cross sections indicates an increase in deformation toward the northwest from the gently deformed units of Iskenderun Bay to increasingly deformed units toward the Adana Basin. Three distinct observations can be made from Figure 1.10: 1) the Tortonian aged Kizildere occurs in the moderately deformed front of the imbricate thrust structure, 2) the Langhian to base Tortonian aged Karataş Formation occupies the central complexly folded and faulted zone of the imbricate, 3) the highly deformed Oligocene aged olistostromic melange of the Isali Formation is present in the northwestern-most portion of the sections. Exotic strips of pre-Miocene rocks that are observed within the Kalantas Formation appear to have been emplaced by regionally extensive strike slip movements (Kelling et al., 1987).

1.3.4 Taurus Mountains

The Eastern Taurus Mountains are composed of a series of imbricated thrust nappes (Tekeli et al., 1984; Yetiş et al., 1995). Structural and stratigraphic mapping of the Aladağ Mountain region reveals that a minimum of six different nappes are present within the imbricate pile (Figure 1.11). These nappes are divisible into allochthonous and para-autochthonous categories based on nappe lithology and relative transport distance. The para-autochthonous nappes consist of five predominantly carbonate-bearing nappes which in ascending order are the Yahyalı, Siyak Aladağ, Minaretepeler, Çataloturan and Beyaz Aladağ nappes (Figure 1.11). Each of the para-autochthonous nappes is overlain by the allochthonous Aladağ Ophiolite nappe (Tekeli et al., 1984), which exhibits the diagnostic petrological characteristics of an ophiolite sheet. Each nappe is host to a unique set of stratigraphic features, however, the primary goal of this section is to report the simplified geology of the Eastern Taurides. The Miocene to Recent stratigraphy of the Eastern Taurides are summarized and presented in Chapter 2, in reference to the location of the Eçemiş Fault Zone (Figure 1.3), a major left lateral strike slip zone which was most active in the post-Paleocene to pre-Lutetian interval (Yetiş, 1984b).

1.4 RECENT MODELS OF NEOGENE EVOLUTION OF THE ADANA BASIN

The terrestrial exposure, accessible nature and hydrocarbon potential of the Adana Basin has resulted in the accumulation of a wealth of geologic observations for the Neogene succession. Syntheses of these data have provided valuable paleogeographic and tectonic

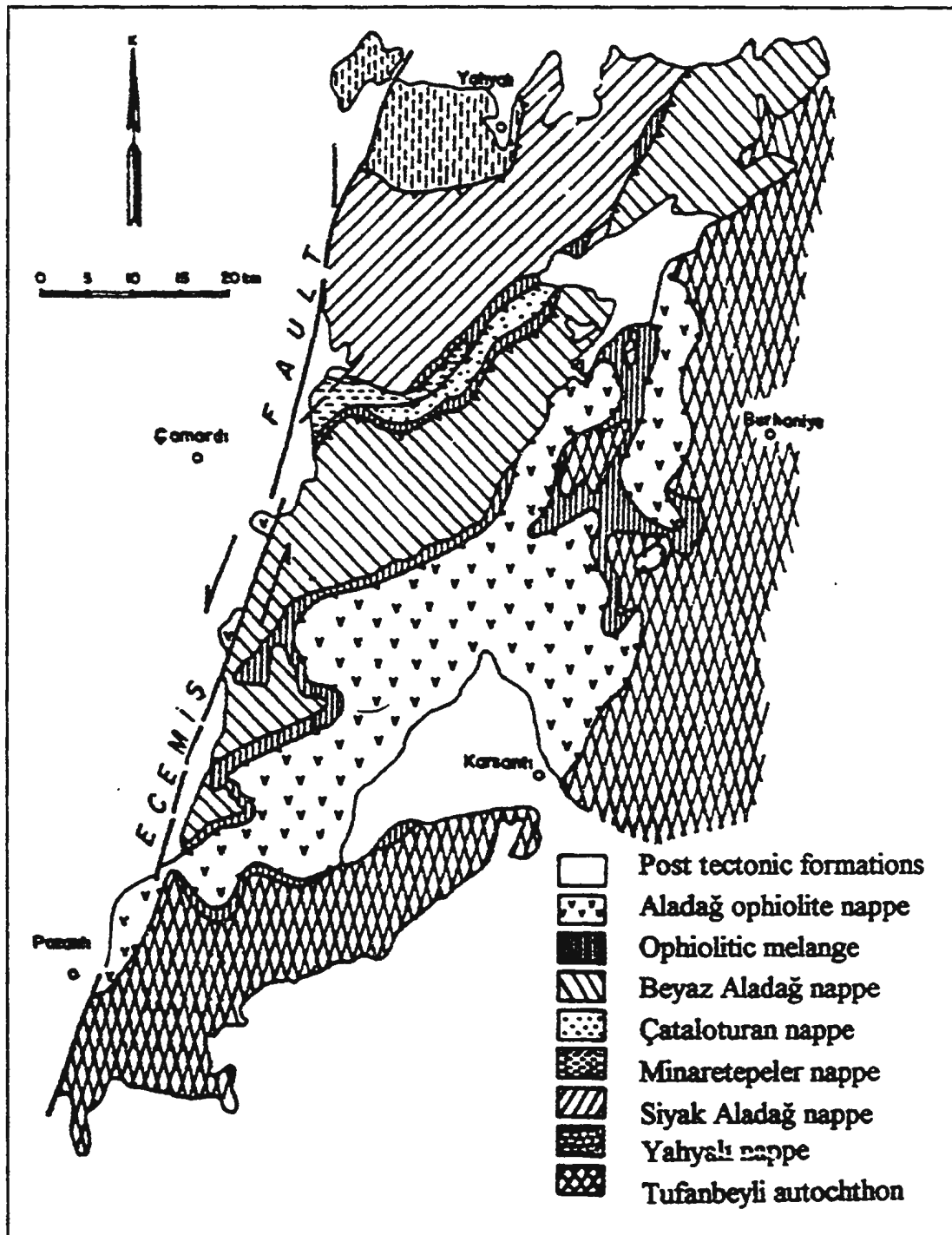


Figure 1.11: Thrust nappes of the Aladağ Mountains, Eastern Taurus Range. After Tekeli et al. (1984).

models for the Adana Basin (e.g. Yalçın and Görür, 1984; Williams et al., 1995). An overview of previous conclusions and syntheses pertaining to the Neogene evolution of the Adana Basin is provided in Sections 1.4.1-1.4.3.

1.4.1 History of shoreline movements

Previous sedimentological and stratigraphic studies in the Adana region indicate that the area has experienced a number of relative sea level fluctuations during the Neogene. An extensive early Miocene transgressive event is evident in the geological record of the southeastern Mediterranean. New sedimentological evidence (Gökçen et al., 1988) suggest this relative sea level rise occurred as a time-transgressive process which spanned the early Burdigalian to Serravalian interval. Comparison of relative sea level curves for the Adana Basin (Figure 1.12) with the global eustatic curves of Haq et al. (1987) reveal that this transgression occurred at a time when global sea level was dropping (Görür, 1994). As a result of these observations, the early to middle Miocene sequences deposited during this interval have often been interpreted as the products of new basin opening, however, Yılmaz et al. (1988) propose that the mid-Miocene sequences may be the products of marine readvancement into the area as a response to the formation of a lateral fault system. Görür (1994) comments that this rapid early Miocene transgression may have resulted from the combined effect of tectonically induced subsidence and a short term sea level rise.

The early to middle Miocene rise in sea level was succeeded by a sizable regression in southeastern Mediterranean during the Tortonian-Messinian interval. This relative sealevel

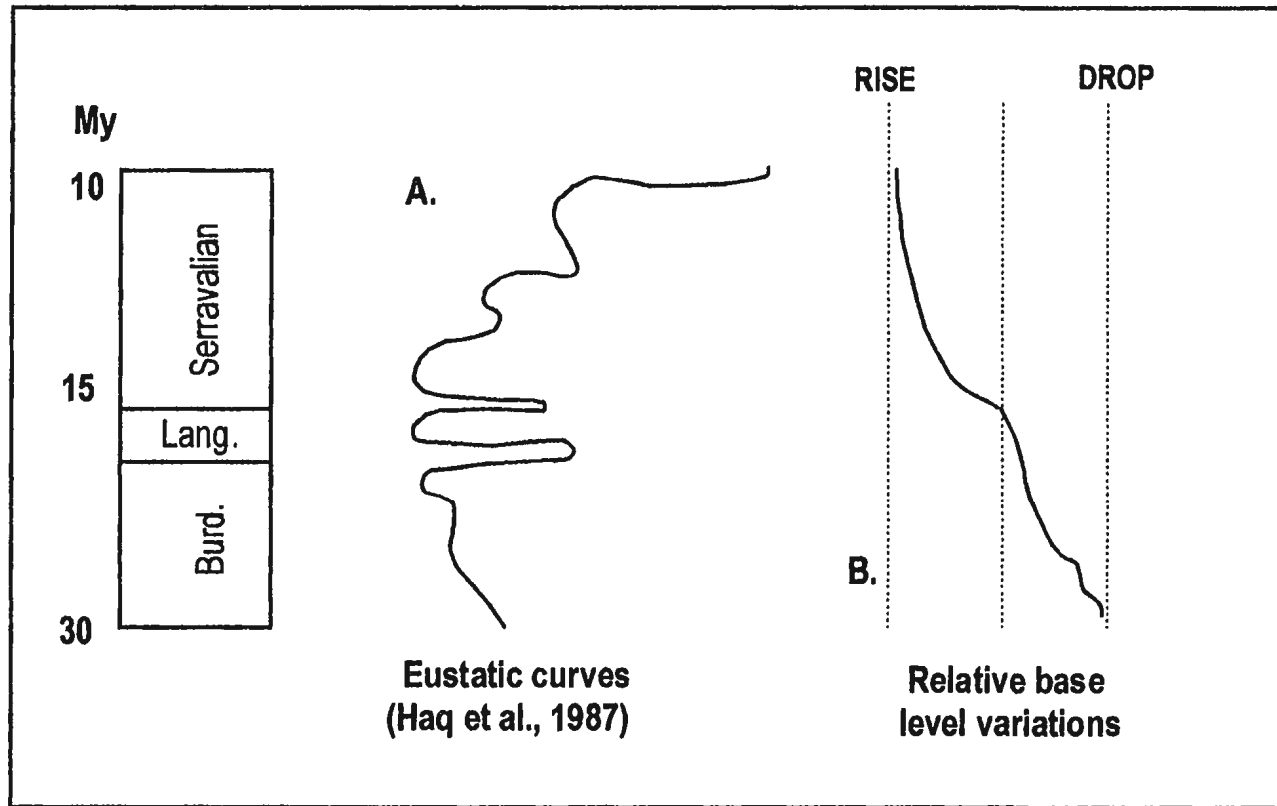


Figure 1.12: Comparison between A) regional eustatic sealevel curves generated for the Burdigalian to Serravalian interval by Haq et al.(1987) and B) local relative base-level variations indicated by sedimentological investigations (Gorur,1994)of the Karaisali Formation, along the northwestern flank of the Adana Basin. After Gorur (1994).

drop was very significant in many parts of the eastern Mediterranean, where extensive dessication of the Mediterranean Sea produced significant evaporite deposits at this time (Mulder et al., 1975). This event appears to correspond to a period of sea level fall which is reflected in global eustatic sealevel curves for the Messinian interval (Clauzon et al., 1996). However, the effects of this event within the Mediterranean region are quite pronounced with respect to other regions. For this reason, the Messinian interval has been the subject of numerous eastern Mediterranean studies. Mulder (1973) concludes that a significant regression in the late Miocene led to the “isolation, reduction in size and increased compartmentalization of the Mediterranean depositional area”. This substantial drop in relative sea level, coincident with creation of local accommodation space, resulted in the precipitation of thick evaporite deposits on the order of 1km + thick in the more restricted portions of the Mediterranean (Mulder, 1973). Intervening highs and basinal margins experienced exposure and erosion at this time (Figure 1.13; Clauzon et al., 1996). The presence of such notable events within the sedimentary basin fill of the eastern Mediterranean Neogene basins may suggest that localized tectonic activity was a primary control on shoreline movement and sedimentation at this time.

Recent sedimentological and paleogeographic research in the Adana basin has addressed the issue of shoreline movements during the Miocene (Yalçın and Görür, 1984; Gökçen et al., 1998). At various times during the Miocene to recent interval, the Cukurova and Adana basins experienced shifts in the relative position of the paleo-shoreline (Figs. 1.4.3-1.4.4). A landward advance of the paleo-shoreline is evident during the Burdigalian to

Stages	Ma	THE SALINITY CRISIS IN THE DEEP BASIN AND ON A MARGIN (SICILY)	
		DEEP BASIN	MARGIN (SICILY)
ZANCLEAN	5.2	CLAYS	TRUBI
	5.3		
MESSINIAN	5.4	EVAPORITES	EROSION
	5.5		
	5.6		
	5.7	CLAYS	UPPER EVAPORITES
	5.8		LOWER EVAPORITES
			CALCARE DI BASE
	5.9		TRIPOLI

Figure 1.13: Summary of marginal versus deep basin deposition and non-deposition in the Mediterranean during the Messinian salinity crisis. Note a) the sharp mid-Messinian shift from evaporite deposition to erosion along the margin, and b) clay deposition to evaporite deposition in the deep basins. After Clauzon et al. (1996).

Serravalian interval (Figure 1.14 a-b; Figure 1.15 a-b); this event appears to correspond with the early to middle Miocene transgression discussed above. A seaward advance or south-directed retreat of the paleo-shoreline is indicated in the Serravalian to Messinian Interval (Figs. 1.14 b-c; Figure 1.15 b-d); this event is correlatable with the extensive Messinian regression described in the preceding paragraphs. Further shifts in the location of the paleo-shore of the Adana Basin include a landward directed re-advancement in the Pliocene (Figure 1.15 e) and a seaward directed retreat in the Quaternary which approximates the position of the coast today (Figure 1.15 f).

1.4.2 Previous tectonic syntheses for the Adana Basin

The tectonic and stratigraphic evolution of the Adana Basin is a complex issue which has remained largely unresolved. Two recent studies have addressed this concern and at present two tectonic models for the Neogene evolution of the Adana Basin are available for review. The first model (Williams et al., 1995) suggests that the Adana basin formed within a complex system dominated by a convergent plate tectonic setting. A second evolutionary model (MA thesis by Pralle, 1994) suggests the basin evolved in a tectonic setting which was controlled by oblique convergence. Brief summaries of each model are outlined below:

The Williams et al model:

Williams et al., (1995) present the evolution of the Adana Basin in three key stages which are outlined in Figure 1.16. Stage 1 (Eocene to Oligocene) involves thrust emplacement of the Taurus Mountain belt and creation of the Adana Basin (Figure 1.16 a-c).

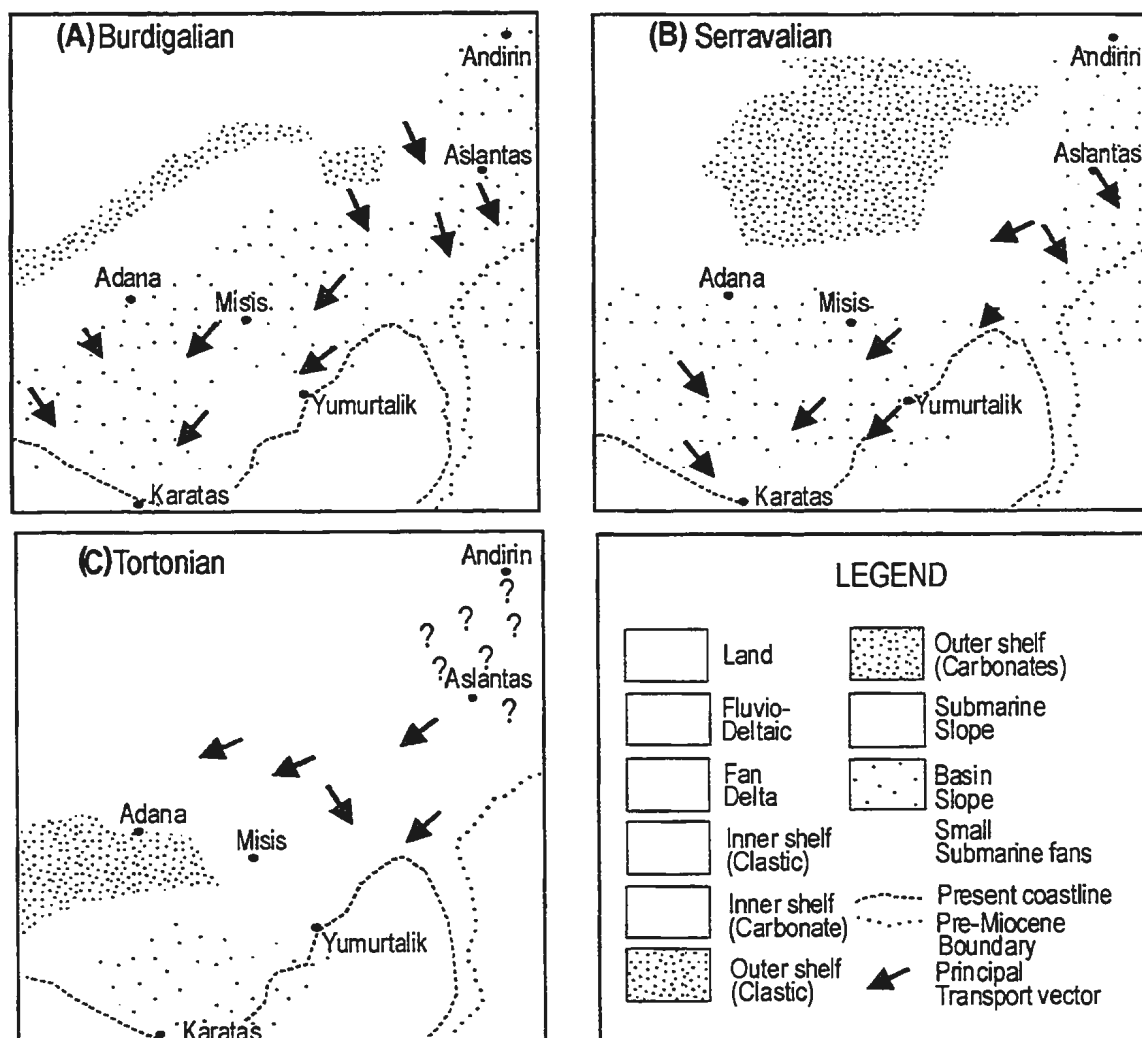


Figure 1.14: Schematic paleogeography maps of the Adana-Misis-Iskenderun region. Note movement of the shoreline and carbonate deposits through Burdigalian to Tortonian time (A - C). After Gocken et al. (1988).

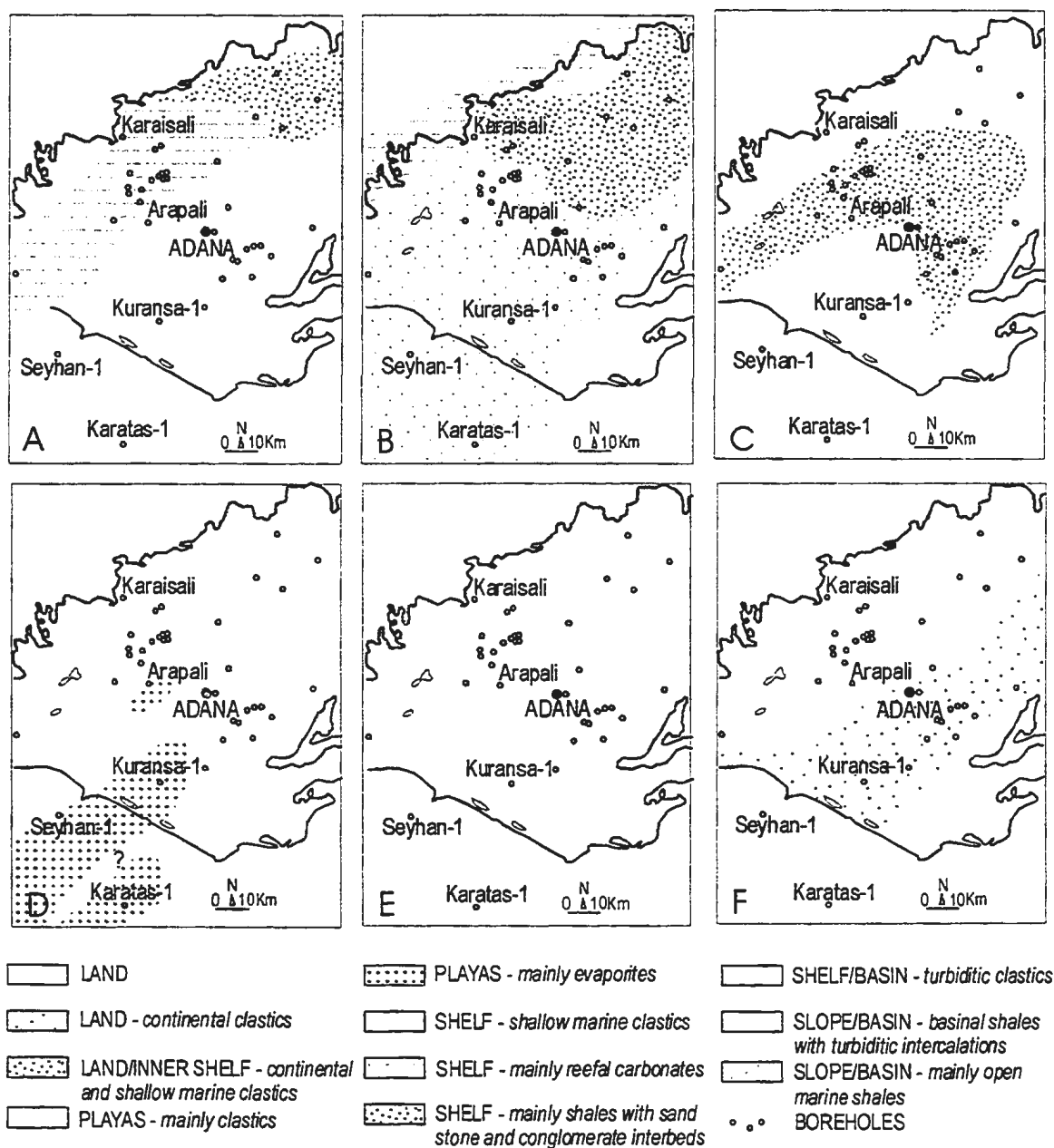


Figure 1.15: Schematic Miocene paleogeographic maps of the Adana Basin. Note shifts in the location of the Land/Shelf transition from A (oldest) to F (youngest). After Yalcin and Gorur, (1984).

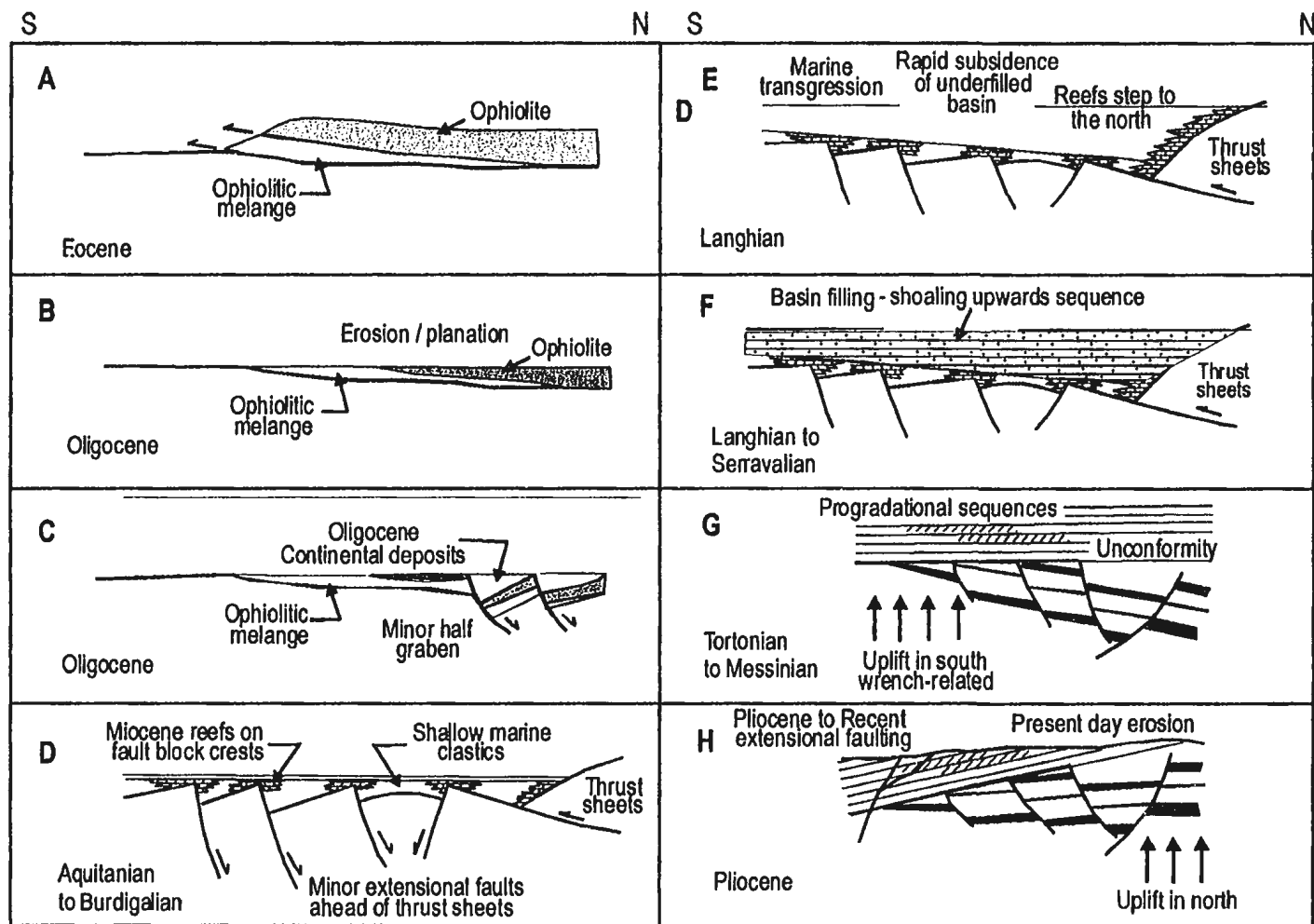


Figure 1.16: Eocene to Pliocene tectonic evolutionary model for the Adana region. Stage I (a-c): Eocene to Oligocene evolution of southern Anatolia; Stage II (d-f): early to middle Miocene evolution of Megasequence 2 of the Adana Basin; Stage III (g-h): Late Miocene to Pliocene evolution of the northeastern Adana Basin. After Williams et al. (1995).

Stage 2 (early to middle Miocene) begins with early Miocene rifting, horst block formation and reef accumulation on the basement highs (Figure 1.16 d-e). In the latter part of Stage 2 the basin deepens and infills in as a result of rapid flexurally induced subsidence and passive turbidite deposition (Figure 1.16 f). Stage 3 (middle to late Miocene) involves further extensional faulting, coupled sinistral wrench faulting and erosional truncation (Figure 1.16 g-h). These events are accompanied with and followed by variable periods of continental and shallow marine sedimentation, localized progradation and later minor extensional faulting.

The Pralle model:

Pralle (1994) presents an alternative model for the tectonic evolution of the Neogene Adana and Iskenderun basins. This model involves two key tectonic phases, and is divisible into six schematic stages as indicated in Figure 1.17. Pralle states that the first tectonic phase is dominated by transtensional deformation in the Early to mid Miocene, although this is not clear in Figure 1.17, while the second phase is dominated by transpressional deformation in the Messinian to Pliocene interval (Figure 1.17). In light of these findings Pralle suggests that the basins represent a zone of strain transfer between two significant sinistral transform faults. Stages I-III (Mesozoic - Paleogene) of Pralles' model involve ophiolite emplacement, thrust emplacement of the Taurides and olistostrome development along the Arabian Platform. In Stage IV (Middle Miocene) Pralle states that the Adana and Iskenderun basins formed as a result of extensional deformation, while initial infill of the basins is the result of continued thrusting and growth of the Taurides. Stage V (Messinian) highlights evaporite deposition

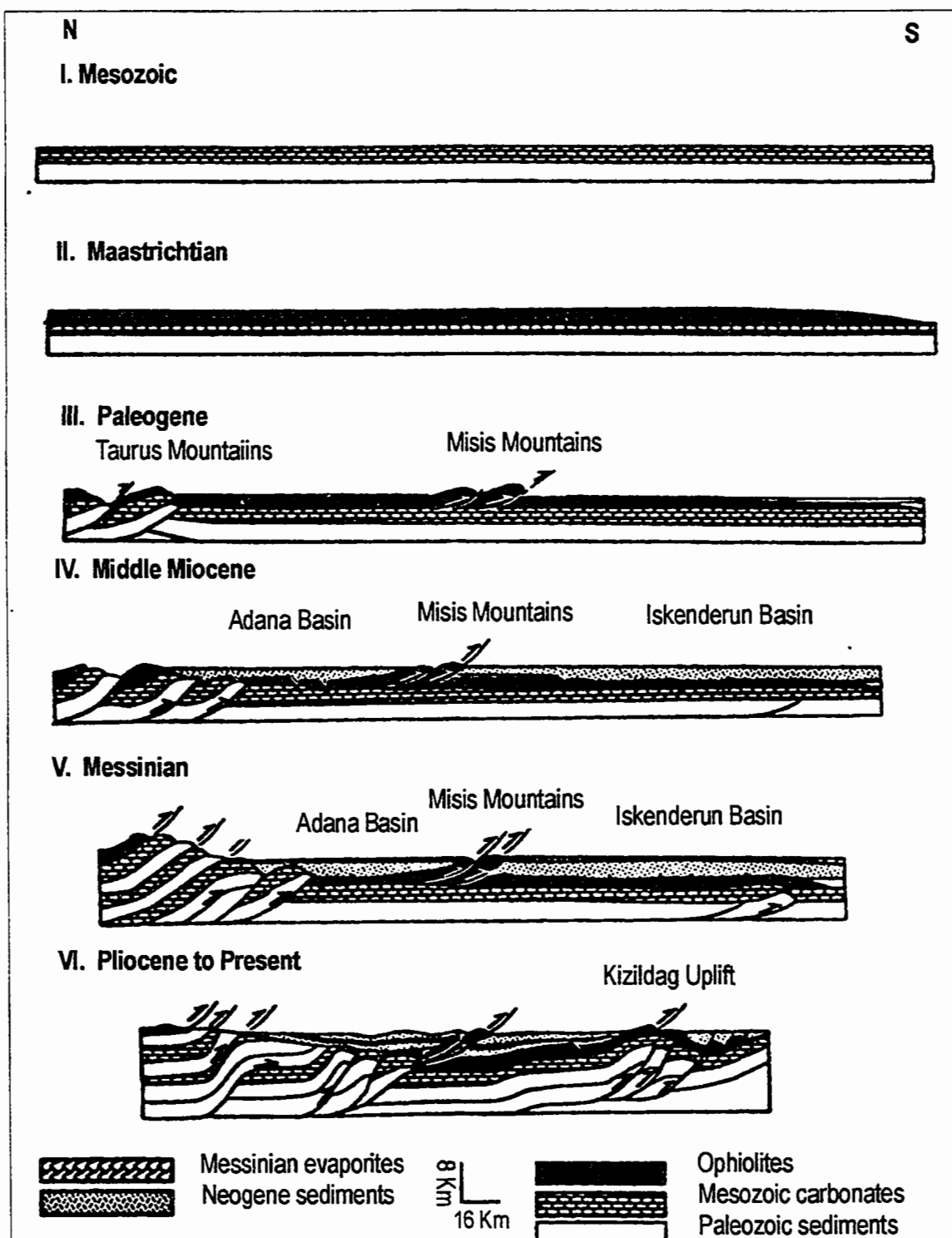


Figure 1.17: Mesozoic to Pliocene tectonic evolutionary model for southeastern Turkey (Adana -Misis-Iskenderun region). Discussed in text. After Pralle, (1995).

through much of the Mediterranean while Stage VI is dominated by compression. This compression resulted in further uplift of the Misis Mountains, creation of the Kizildag uplift in the East, and deformation of the basement and Miocene cover successions of both basins.

The preceding models present contrasting evolutionary histories for the Miocene Adana Basin. Williams et al., (1995) propose a history characterized by lower to mid-Miocene extension and subsidence, Tortonian uplift, and Messinian to Recent extension, while Pralle details a tectonic history of early to mid-Miocene transtension followed by Messinian to Recent transpression. The contrasting models likely reflect differences in i) the size and location of the data sets used in the analyses, and ii) the approach and application of tectonic theory. The results of both studies provide a valuable starting point, from which, further examination of the Adana Basins' evolutionary history (this study) can proceed.

1.4.3 Controls on sedimentation

The Neogene basins of southeastern Turkey contain sedimentary sequences which developed during a period of complex tectonic activity. Extensive investigations of these sedimentary successions has led Kelling et al., (1987) to conclude that the collision of the Anatolian-African-Arabian plates is recorded in the sedimentary basins of the eastern Mediterranean. Yılmaz et al. (1988) conclude that large scale crustal convergence in this region controlled the lithologic and spatial character of the sedimentary deposits in the Iskenderun, Maras and Andirin region. The highly variable, coeval sedimentary sequences of this region have been interpreted as syn-tectonic deposits which were controlled by

“differing deformational effects along the orogenic system” (Yılmaz et al., 1988).

The terrestrial exposure of the Adana Basin has provided a unique setting where surface characteristics of this syn-tectonic basin-fill can be examined and tied to the subsurface architecture of the basin. An iterative tectono-stratigraphic investigation of the structure and stratigraphy of the Miocene basin fill of the Adana Basin may reveal much about the tectonic conditions which controlled sedimentation in the Eastern Mediterranean during this time.

1.5 SCIENTIFIC OBJECTIVES

New data provided by Turkish Petroleum Corporation (TPAO) for this study consist of a dense grid of seismic reflection profiles complemented by well data (Figure 1.18). The principal data used in this investigation include more than 1000 km of multi-channel onshore seismic reflection profiles, representing a significant increase in the amount of available data compared to the datasets covered in previous investigations (e.g., Pralle, 1994 and Williams et al., 1995; see Figure 1.7). This expanded seismic data set varies in vintage from 1977 to 1994, with subsurface penetrations that vary from 3.00 to 5.00 seconds two-way travel time (TWT). Previous work has revealed that the basin-fill imaged in the seismic profiles represents primarily rocks related to the Miocene evolution of the Adana Basin, with the exception of Plio-Quaternary rocks which are restricted to the southwestern corner of the study area (Figure 1.7). The volume and location of the newly acquired data will provide greater resolution of subsurface geological aspects relating to the Miocene evolution of the

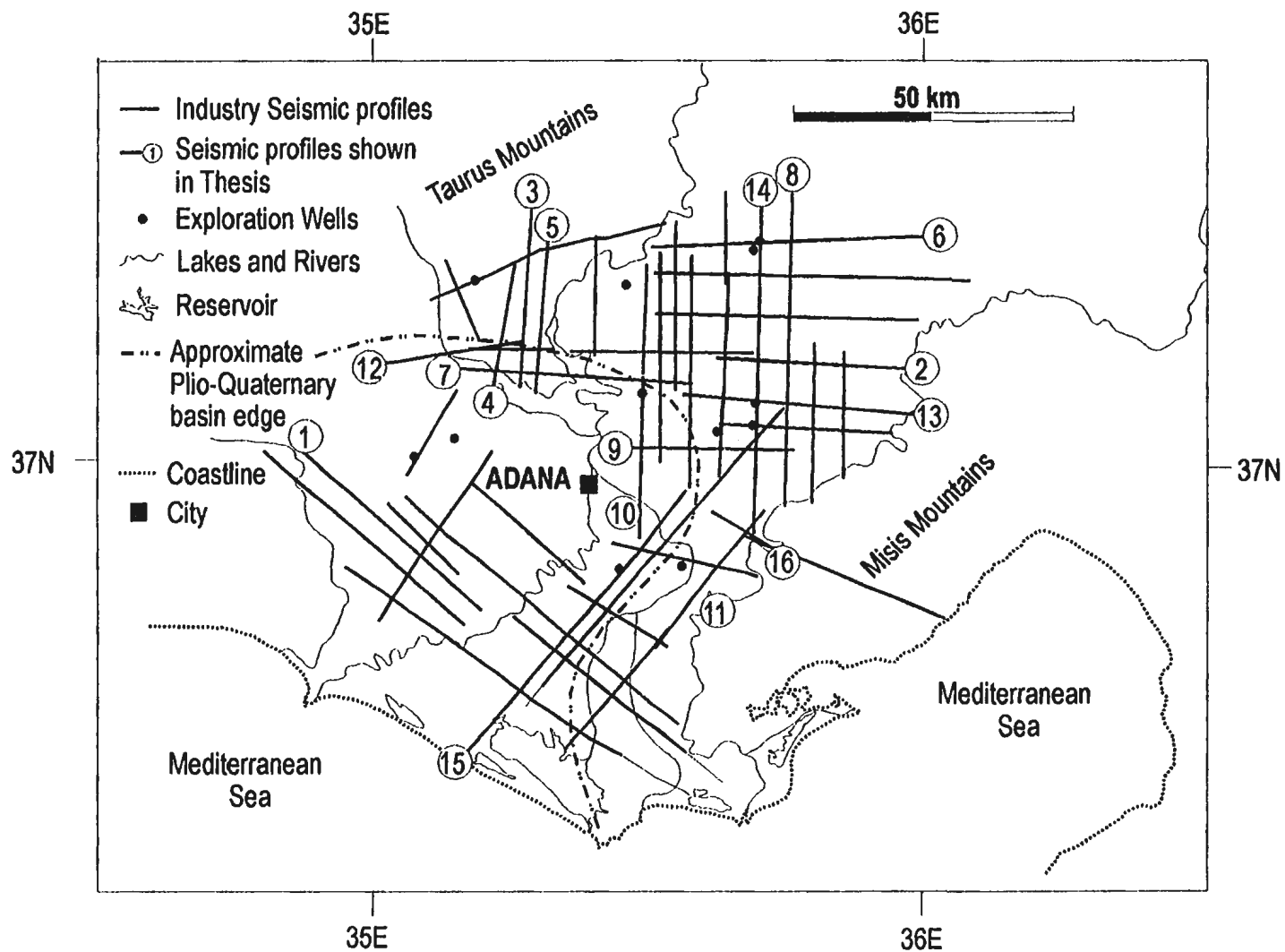


Figure 1.18: Location of seismic data and well control used in this study. Note i) grid spacing and density of seismic data and ii) the distribution of available well data. Data provided courtesy of TPAO.

Adana Basin, and will provide a tie for the geology of the land - sea transition between the Adana and Cilicia basins. The reader is referred to Appendix A for a review of the methodology used in this investigation.

The primary focus of the present investigation is the Miocene tectonic evolution of the Adana Basin. Three main objectives are pursued:

1) To establish a seismic-stratigraphic framework for the Miocene succession of the Adana Basin, and to identify any spatial and temporal relationships which exist within this seismic framework. Noteworthy aspects of the Plio-Quaternary basin fill are reported but the primary emphasis remains on the Miocene succession. Correlations are made with previously published lithostratigraphic surface and well data. In this way a holistic temporal and spatial framework for the Miocene stratigraphy of the Adana Basin is presented.

2) To establish the structural architecture of the basin. Emphasis remains on the Miocene succession, but noteworthy aspects of the Plio-Quaternary succession are reported. Structural features are highlighted and examined using applied techniques of structural (sub-surface) analysis. Timing of deformation is ascertained through examination of the relationships between the established stratigraphic framework and the structures, notably using growth stratal architectures.

3) To develop a model for the tectonic controls on the basin fill by integrating the

stratigraphic/structural results. Thus, a tectonic model for the evolution of the Miocene succession of the Adana Basin is presented as an overall synthesis of this investigation.

CHAPTER 2: STRATIGRAPHY

The stratigraphy of the Adana Basin has received particular attention in recent studies and an abundance of published work is available for review (Yalçın and Görür, 1984; Gökçen et al., 1988; Yetiş, 1988a; Karig and Kozlu, 1990; Pralle, 1995; Williams et al., 1995; Yetiş et al., 1995; Kelling et al., 1997 etc). However, the naming of many stratigraphic units, their definitions, and their ages are notably inconsistent. Consequently a detailed stratigraphic review is necessary for the purpose of this study. Extensive sedimentological work in the region has provided a number of detailed surface geology maps (Schmidt, 1961; Ozer et al., 1974; Yalçın and Görür, 1984; Görür, 1985, 1994; Gökçen et al., 1988; Yetiş, 1988a; Karig and Kozlu, 1990; Pralle, 1995), exploratory drilling within the basin has supplied numerous well data (TPAO internal reports; Pralle, 1995, see Appendix B), and paleontological studies have constrained ages for many of the mapped lithologic units (Schmidt, 1961; Benda et al., 1977; Görür, 1977, 1985, 1994; Gürbüz and Gökçen, 1985, Tanar, 1985; Yetiş 1988a; Nazik and Gürbüz, 1992; Özelik, 1993; Ünlügenç et al, 1993; Kelling et al., 1997). Recent seismic stratigraphic treatments of the area have further provided a seismic stratigraphic framework for the basin (Williams et al., 1995, Pralle, 1995), but no significant sequence stratigraphic work has been published for the Adana Basin to date.

This study attempts to establish both a lithostratigraphic framework (based on a comprehensive review of recent outcrop studies), and a seismic stratigraphic framework (based on interpretation of the current seismic data set) for the Adana Basin. These

frameworks will then be tied together using existing well data to create a chronostratigraphic template for the Adana Basin. This is followed by the author's attempt to summarize these data in a sequence stratigraphic model. This synthesis will establish the temporal and spatial relationships between various units within the basin and will aid in establishing the stratigraphic and tectonic evolution of the basin since the early Miocene.

2.1 Lithostratigraphy

The Adana Basin is one of the major Neogene basins of the Taurus Orogenic Belt (Yalçın and Görür, 1984). The basin hosts an approximately 6000 m- thick sedimentary succession which spans the Miocene to Recent interval. The basin is bounded by the Taurus Mountains in the north and northwest and the Misis Mountains in the east (Figure 1.1). To the south the Cilicia is the marine extension on the on land Adana Basin. The genetically related Iskenderun Basin (Aksu et al., 1992) lies east of the Misis Mountains.

The Adana Basin lies in close proximity to the Maras triple junction, and has been the focus of a multitude of sedimentologic, lithologic, and biostratigraphic studies. These studies indicate that the region records a complex stratigraphic history involving dramatic facies and paleo-environmental variation, as well as radical shifts in drainage patterns and sandstone provenance (Yalçın and Görür, 1984; Gökçen et al., 1988; Yetiş, 1988a; Karig and Kozlu, 1990; Yetiş et al., 1995; Kelling et al., 1997 etc). Within existing previous work, the reported interpretations for many lithologic units (e.g. names, descriptions, ages, stratigraphic position) are inconsistent and confusing. The following lithostratigraphic review is based primarily on

the revised stratigraphic framework for the northeastern Mediterranean, as proposed by Yetis et al. (1995) (refer to Figs. 1.5 and 1.6). Additional sedimentological, biostratigraphic, and paleogeographic evidence are presented, where relevant, to support the incorporation of lithostratigraphic divisions, correlations and map results from other previous works. The surficial geology map (Figure 2.1) and stratigraphic template (Figure 2.2 and Table 2.1) utilized in this chapter were constructed by the author and reflect the results of relevant previous sedimentological, lithostratigraphic and surface mapping projects in the Adana region (eg. Görür, 1992; Kelling et al., 1987; Yetis et al., 1988; Turkish Government maps).

Yetis et al. (1995) divide the Miocene sedimentary succession in the Adana basin into three groups of sedimentary deposits: i) pre-transgressive deposits, ii) transgressive deposits and iii) regressive deposits. Within this framework, the succession is further divisible into eight formations and four members.

2.1.1 Basement to the Miocene succession in the Adana Basin

The basement to the Miocene succession in the Adana Basin consists of a number of Paleozoic to Oligocene units (Figure 2.1). A thick cover of Miocene rocks prevents the outcrop of basement rocks within the basin, however, pre-Miocene rocks outcrop in a number of areas to the north and northwest (eg., Camardi-Nidge area; Figs. 2.1 and 2.3) and in areas to the east and southeast (Misis and Amanos Mountains, Figure 2.1). Recent studies (Görür, 1985; Pralle, 1995; Karig and Kozlu, 1990) have provided some insight into the lithology of the basement rocks, and these data have been useful in identifying (or excluding) potential

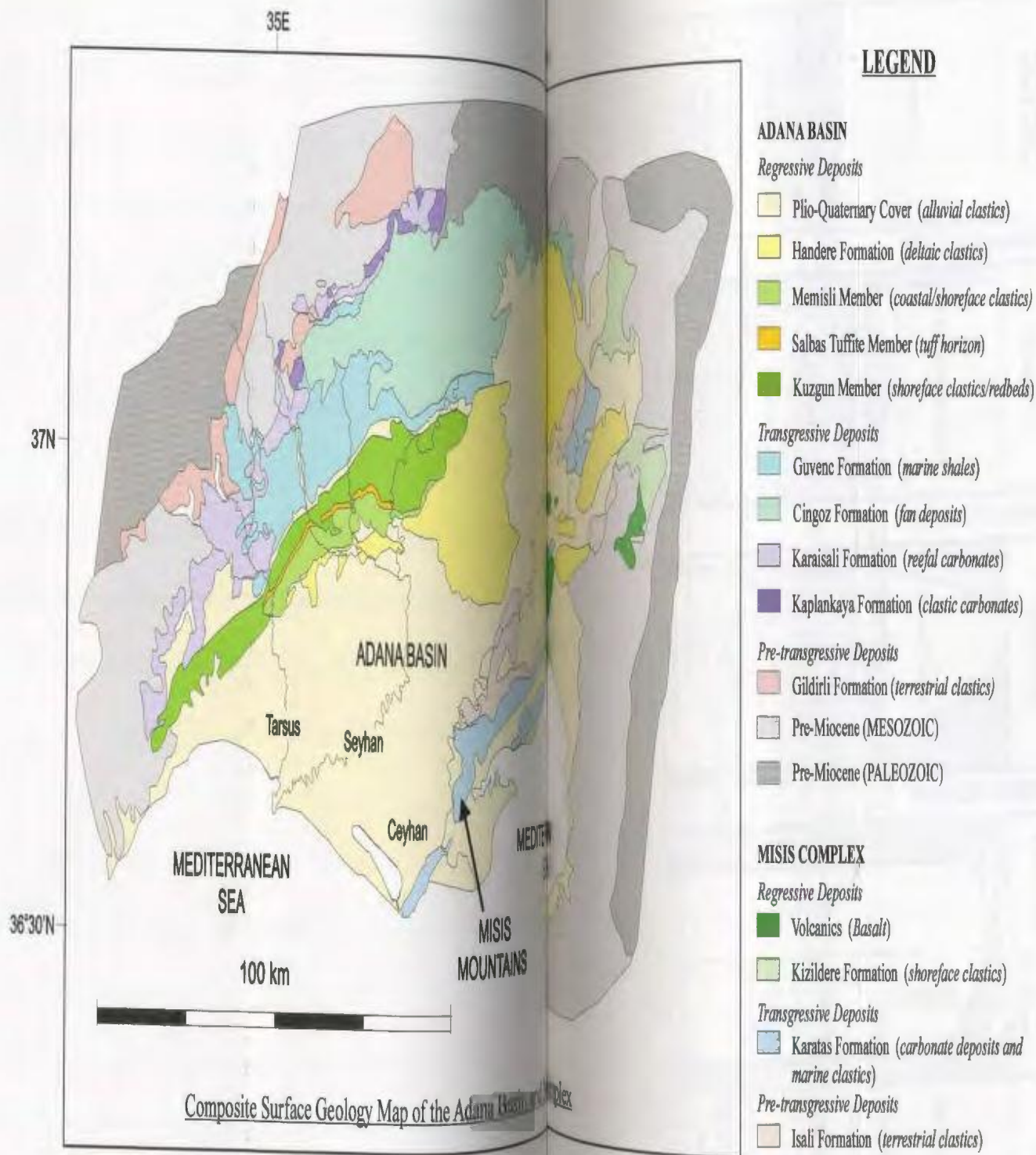


Figure 2.1: Composite Surface geology map of the Adana-Misis Region. This map is based on data previously reported by i) Gorur (1992) ii) Kelling et al. (1987) iii) Yetis et al. (1988) into existing Turkish surface geology maps of the region. The map illustrates the outcrop distribution of lithologic units discussed in Section 2.

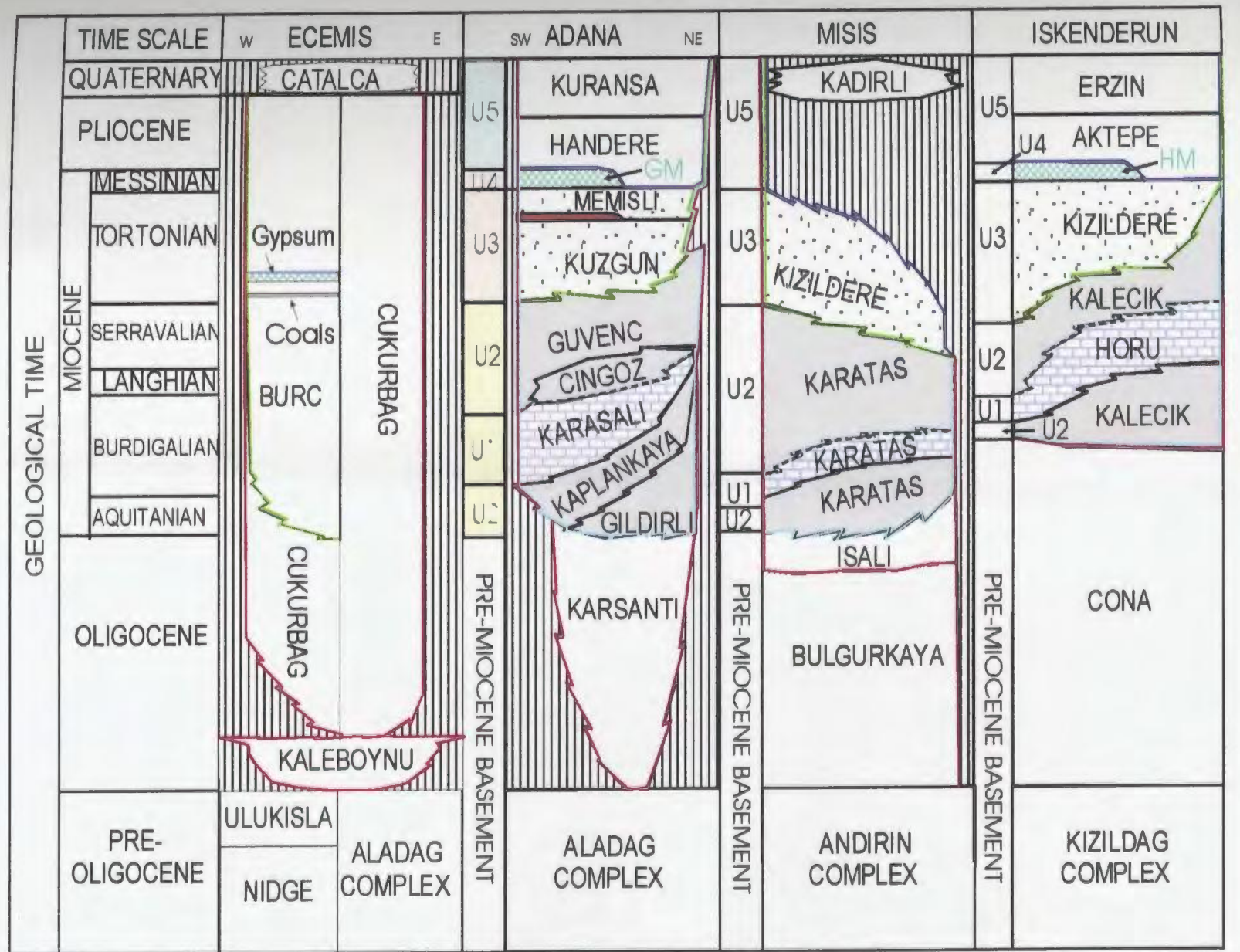


Figure 2.2: Stratigraphic template for the Miocene succession in the Adana Basin.

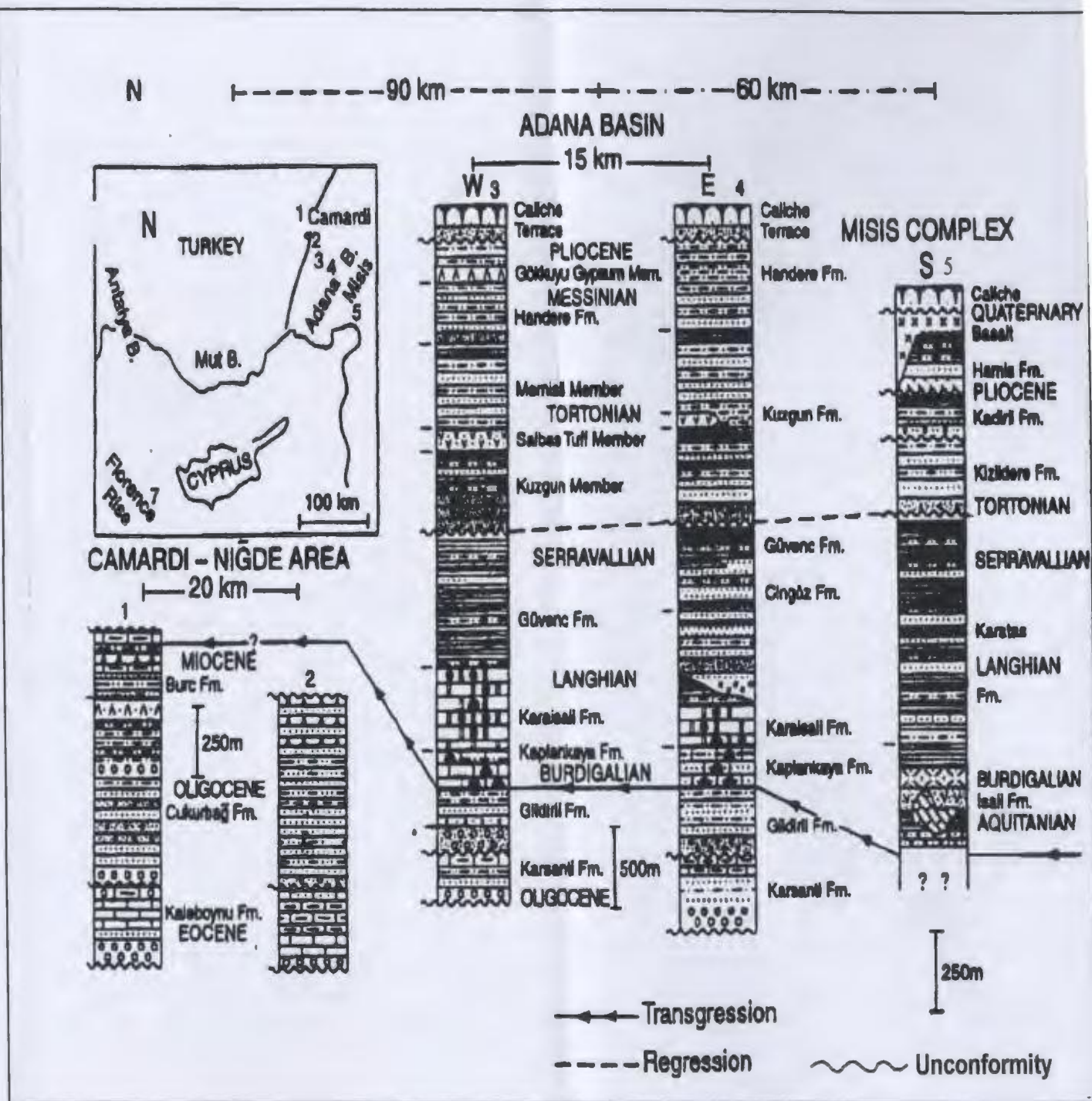


Figure 2.3: Oligocene to Pliocene successions in the northeastern Mediterranean region (Sections 1 & 2: Camardi Nigde area; Sections 3 & 4: Adana Basin; Section 5: Misis Complex). Correlations between successions, as proposed by Yetis et al. (1995) illustrate i) the progressive on of a time transgressive marine ravinement surface related to the mid-Cenozoic marine transgression and ii) the near synchronous nature of the Late Miocene regression. After Yetis et al. (1995).

provenance regions for a number of Miocene formations. Lithostratigraphic summaries of the Eastern Taurus and Misis Mountains are provided in the following sections.

Eastern Taurus

The Taurus Mountains bound the western and northern flanks of the Adana Basin (Figure 1.1) and represent the southernmost tectonic zone of the Menderes-Taurus Platform. The easternmost portion of these mountains, known as the Eastern Taurus, is composed of a number of pre-Neogene lithostratigraphic units which outcrop to the west and north of the Neogene Adana Basin (Figure 2.1). Published geologic investigations of the Eastern Taurus region are sparse, however recent works within the Aladağ Mountains in the western portion of the Eastern Taurus (Tekeli et al., 1984; Yetiş, 1984b; Yetiş et al., 1995) are available for review. These works focus on the portion of the Aladağ Mountains which encompasses the Eçemiş Fault Zone; for the purpose of this study the stratigraphy of this region will be briefly reviewed.

The pre-Neogene basement of the Çamardı area of the Aladağ Mountains is stratigraphically and structurally complex (Figure 1.11) (Tekeli et al., 1984). Yetiş et al. (1995) describe four key lithologic units within the pre-Neogene basement rocks of the Çamardı area. From oldest to youngest these units are the Niğde Metamorphics, the Maden Formation, the Demirkazık Formation and the Mazmılı ophiolitic melange (Yetiş et al., 1995). The Niğde Metamorphics outcrop west of the Eçemiş Fault zone (Figure 1.11) and represent the oldest rocks within the Çamardı area. The Maden Formation is composed of massive

limestones which represent the Permian to Triassic interval, while the Demirkazık Formation is dominated by platform carbonates from the Upper Triassic to Jurassic interval. The Mazmili Ophiolitic Melange is interpreted to have formed in a continental shelf environment prior to tectonic emplacement above the relatively autochthonous carbonate during the late Campanian to Maastrichtian interval (Yetis et al., 1995).

The pre-Neogene basement rocks of the Eastern Çamardı Block are overlain with discordance by the Lutetian aged Kaleboynu Formation, the Oligocene aged Çukurbağ Formation, the Miocene aged Burç Formation and Quaternary alluvium (Figure 2.3, Sections 1 and 2). The Kaleboynu Formation is limited in outcrop, but investigations reveal the unit displays a wide variation in lithology from conglomerate and shallow marine clastics to thick limestone deposits. The formation exhibits transgressive onlap relations with underlying units and consequently bears evidence of a rapid marine transgression into the Çamardı area during the Eocene (Yetis, 1984b; Yetis et al., 1995). The Çukurbağ Formation consists predominantly of fluvial-deltaic red beds and conglomerates which Yetis et al. (1995) conclude are notably similar to Oligocene deposits in the Karsanti Basin to the east. The Miocene aged Burç Formation is observed west of the Eastern Çamardı Block (Figure 2.3, Section 1) and represents an upwards shift from swamp and lacustrine environments to a drier fluvial terrestrial setting.

Misis Mountains

Recent work by Gokçen et al. (1988) has revealed that the Misis Mountains are comprised of a fault bounded slice of complex and intensely deformed rocks, which sits

juxtaposed between the relatively undeformed and gently folded strata of the Adana and Iskenderun basins (Figure 1.9). Miocene rocks of the Iskenderun Basin are underlain by an ophiolitic basement that is correlated with the Hatay ophiolite of the Amanos Mountains. This ophiolitic sheet is thought to extend westward and may constitute the basement of much of the Cukurova Basin Miocene succession.

The rocks of the Misis Mountains are divisible into three lithologic formations based on biostratigraphic data as indicated in Figure 1.10 (Gökçen et al. 1988). In ascending order the Isali, Karataş and Kızıldere formations are present in the Misis Mountains (Figure 2.3, Section 5). The Isali Formation is Aquitanian in age, and contains lithologic features which are diagnostic of an olistostromic facies (Gökçen et al., 1988). Biostratigraphic studies indicate that the overlying Karataş Formation represents the Burdigalian to Tortonian interval, which represents a time-transgressive sequence (Figure 1.10). This formation is characterized by deep marine facies and potentially diachronous carbonate shelf progradation in the Burdigalian - Tortonian interval. The Karataş Formation is also comprised of basin plain and submarine fan deposits of the Langhian interval, shallow marine and deep marine deposits of the Serravalian interval, and basin plain/turbidite deposits of the Early Tortonian interval.

The Karataş Formation is overlain by the Kızıldere Formation (Figs. 1.10 and 2.3, Section 5; Table 1.1). The Tortonian aged Kızıldere Formation records important lithologic and sedimentologic variability from base to top. Lithologic variation within the Kızıldere is evident in the change from fluvial-deltaic facies near the base of the formation to increasingly shallow marine clastic facies in the middle and upper portions. While the lower facies indicate

relatively consistent southwest paleo-transport directions, the upper shallow marine facies record variable flow vectors with bar migration directed to the northeast, south and southwest (Gökçen, 1988). Contact relations between the Kızıldere Formation and adjacent overlying units are in all places discordant or structural in nature.

2.1.2 Miocene Succession in the Adana Basin

The Miocene succession of the Adana Basin is represented by eight formations and six members (Figs. 2.1 and 2.2). From oldest to youngest, the Gildirli, Kaplankaya, Karaisalı, Cingöz, Güvenç and Kuzgun formations form the Miocene Aquitanian to Messinian portion of this succession. These successions contain lithologies which are often correlative to units in surrounding areas, particularly in the Misis Complex and the Cilicia and Iskenderun basins (Pralle, 1995, Yetiş et al, 1995). A summary of previous biostratigraphic data for various lithologic units within the Adana Basin is included in Appendix B.

Pre-transgressive deposits

Yetiş et al. (1995) define the lowermost sedimentary package of Miocene age within the Adana Basin as consisting of pre-transgressive deposits of the Gildirli Formation (Figs. 2.1 and 2.2).

Gildirli Formation

The Gildirli Formation has formerly been defined as consisting of both the Çakmak

and Kabalak Tepe members (Görür, 1979; Yalçın and Görür, 1984; Görür, 1992); however the fossiliferous Kabalak Tepe Member has recently been distinguished from the Gildirli Formation by Yetiş and Demirkol (1986). The Kabalak Tepe Member is now referred to as the Kaplankaya Formation (Yetiş et al, 1995).

The Gildirli Formation is composed of a series of 2-20 m thick fining upward cycles which contain erosive bases (Yetiş et al., 1995). The base of each cycle is overlain by poorly sorted conglomerate that passes upward into pebbly sandstone, sandstone and alternating sandstone and siltstone layers. Each cycle is topped by 20-30 cm of reddish brown, poorly consolidated and parallel laminated mudstone. Clast composition within the Gildirli Formation consists of Paleozoic carbonate lithoclasts as well as quartz, chert and occasional igneous rock fragments (Görür, 1985). Nodular calcrete units are also observed within the Gildirli Formation, and consist of either small spherical concretions or short narrow columns arranged perpendicular to bedding (Yetiş et al, 1995). No fossil evidence has been identified within the Gildirli Formation.

The thickness of the Gildirli Formation appears to have been controlled by pre-Miocene topography, where maximum thicknesses of 300 m are observed in pre-Miocene troughs, while thickness over paleotopographic highs decreases substantially (Yalçın and Görür, 1984). In some localities the Gildirli Formation is observed to unconformably overlie Paleozoic and Mesozoic successions of the Taurides, as well as tilted beds of the Karsanti Formation (Figure 2.3, Sections 3 and 4). In paleotopographic depressions, Gildirli sediments pass upward and laterally into the Kaplankaya Formation, while on topographic highs Gildirli

sediments are overlain directly by Karaisalı reefal facies. A lack of fossils prevented any conclusive dating of the Gildirli Formation, but stratigraphic relationships between the Gildirli Formation and other units assigns a relative age bracket of late Oligocene to basal Miocene (Aquitanian ? - early Burdigalian) to this unit (Yetiş et al., 1995). The formation has been interpreted to exhibit an alluvial fan character.

Recent work by Pralle (1995) correlates the Gildirli Formation in the Adana Basin with the Langhian-Serravalian aged Kaleçik Formation in the Iskenderun Basin. The Gildirli-Kaplankaya-Karaisalı-Cingöz-Güvenç successions of the Adana Group is also broadly correlative to the Karataş Formation in the Misis Complex (Gökçen et al., 1988) (Figure 2.2).

Transgressive Deposits

Transgressive deposits comprise the intermediate sedimentary package within the Miocene succession of the Adana Basin. The transgressive sequence represents a thick siliciclastic succession (Kaplankaya, Cingöz and Güvenç formations), which internally contains local reefal and platform carbonate patches of various ages (i.e. the Karaisalı Formation; Figs. 2.1 and 2.2).

Kaplankaya Formation

Lithology within the Kaplankaya Formation varies from alternating sandstone (occasionally pebbly) and siltstone layers in the lower half of the formation, to fossiliferous marls and sandy limestones in the upper half as carbonate content increases upward (Yetiş et

al, 1995). Clasts of the Kaplankaya Formation are represented mainly by Cretaceous carbonate mudstones, and fossil fragments, although iddingsites have also been noted within the formation (Görür, 1985). Fossil remains described within this formation include echinoids, bivalves, gastropods, algae, corals and small benthic foraminifera.

The Kaplankaya Formation exhibits vertical and lateral transitions into both the underlying Gildirli Formation and the overlying reefal Karaisali and basinal units of the Güvenç Formation (Figs. 2.1 and 2.3, Sections 3 and 4); (Yetiş et al, 1995). However, where the Gildirli Formation is absent on topographic highs, the Kaplankaya Formation overlies Paleozoic and Mesozoic units with discordance. Thickness of the Kaplankaya Formation is variable (5-100 m) and appears to be controlled by the pre-existing topography (Yetiş et al, 1995). The Kaplankaya Formation is interpreted to exhibit characteristics of a shallow marine depositional environment. Foraminiferal assemblages of the Kaplankaya Formation observed in different localities indicate Burdigalian (Benda et al. 1977), and Burdigalian to early Langhian (Yetiş, 1988a) ages (Appendix B). Yetiş et al (1995) conclude that the diachronous deposition of the coastal to shallow marine Kaplankaya Formation may be the result of an early Miocene marine transgression into the Adana Basin.

Cingöz Formation

The Cingöz Formation is divisible into 2 interfingering units: the Ayva and Topalli members (Görür, 1985). A third unit, the Köpekli shale, was previously included in the Cingöz Formation (Schmidt, 1961), but has since been re-assigned to the Güvenç Formation

(Yetiş, 1988a, Yetiş et al, 1995). The redefined Cingöz Formation is described by Yetiş et al. (1995) as a single lithostratigraphic unit in which characteristics of the Ayva and Topalli members have been combined.

The basal portion of the Cingöz Formation is composed primarily of medium grained, moderately sorted, channelized conglomeratic sandstones which overlie shales of the Kaplankaya and Güvenç formations. Conglomerate clast composition is variable, and includes carbonate mudstone, recrystallized limestone and igneous lithologies. These clasts are commonly rounded and pebble- sized, but increase to boulder size in some localities. Yalçın and Görür (1984) also noted moderately developed planar bedding, medium to large scale planar cross-stratification, and occasional localized slump features. Large scale slump-scar features and erosive conglomeratic feeder-channel complexes are present in the northern portion of the Adana Basin (Figure 2.3, Section 4) (Yetiş et al., 1995).

Basal deposits of the Cingöz Formation are transitionally succeeded by interbedded sandstones and shales of roughly equal proportions. The sandstone beds exhibit very fine to coarse grain size, are moderately to well sorted, and show variable thickness on the scale of centimeters (Yalçın and Görür, 1984). Internal grading, erosive bases and bottom structures such as groove casts, tool marks, scour and fill, flute casts are also noted within the sandstone units. The intervening shale units are fissile, silty, and calcareous; the shale is locally carbonaceous and contains abundant quartz, calcite and feldspar.

Recent work by Gürbüz and Kelling (1992 and 1993) has revealed that the Cingöz Formation represents the deposits of two small coeval submarine fan systems in the northern

portion of the Adana basin during the middle Miocene. Each fan deposit is characterized by a period of channelized inner fan deposition, followed by thickening upward cycles interpreted to represent a shift to middle fan lobe sedimentation. Lower fan-basin plain siltstones and shales succeed these middle fan sediments. The basal deposits of the Cingöz Formation have been interpreted as proximal turbidites, while the upper deposits are interpreted by Gorur (1985) to represent laterally equivalent distal turbidites. Yetiş et al. (1995) conclude that the Cingöz Formation is partly coeval with and partly superimposed upon the Kaplankaya, Karaisalı and Güvenç formations, and that fans observed within the Cingöz Formation are retrogradational in style. The Cingöz Formation ranges in thickness from 1000 m in the west to 3200 m in the east (Gülbüz, 1993). The basinal shales of this formation have been dated by recent foraminiferal studies (Gülbüz and Kelling, 1992; 1993) as late Burdigalian to Serravalian in age (Appendix B).

Similar Burdigalian-aged basin plain, sandy lobe and fan deposits are observed in the upper portion of the Karataş Formation of the Misis Complex (Figure 2.3, Section 5); these deposits are largely restricted to the southwestern sector of the complex (e.g. Karataş and Haylazlı sections, Gökçen et al., 1988).

Güvenç Formation

Previous works on Miocene units of the Adana Basin (e.g. Turkish Petroleum Corporation, internal reports) describe the Seyhan Group, which is defined as including both the Cingöz and Güvenç formations; however, most recent stratigraphic treatments make no

reference to the Seyhan Group (e.g. Yalçın and Görür, 1984; Yetiş et al., 1995). Further reorganization of the stratigraphy of the Adana Basin (Yetiş, 1988; Yetiş et al., 1995) has redefined the Güvenç Formation to include both the Güvenç and Köpekli shales. These silty, calcareous microfaunal- rich shales are partly coeval with and partly overlie the Kaplankaya, Karaisalı and Cingöz formations (Figure 2.2). The lower portion of the Güvenç Formation begins with slope and forereef deposits which pass upward into basinal shales (Yetiş et al., 1995). The basal to middle portion of the Güvenç Formation records increasing water depth as indicated by decreasing thickness and number of sandstone layers as well as shifts from benthic to dominantly planktonic foraminiferal assemblages. The middle to upper portion of the formation is characterized by abundant pyritization which suggests poorly oxygenated environmental conditions. The basinal shales are transitionally succeeded by storm-dominated shelf deposits (Gürbüz, 1993), which indicate a general shallowing of the basin. Increased sandy detritus, benthic foraminifera and nannofossils observed within the uppermost part of the Güvenç Formation indicate the prevalence of more shallow-marine conditions at this time (Yetiş et al., 1995). Contact relations between the Güvenç Formation and the overlying Kuzgun Formation are often disconformable.

The maximum observed thickness of the Güvenç Formation is estimated at 2340 m (Schmidt, 1961; Görür, 1977), but thickness varies significantly across the basin (Figure 2.3, Sections 3 and 4). Foraminiferal assemblages obtained from the formation indicate deposition during the Burdigalian to lower Tortonian interval (Appendix B).

Karaisalı Formation

As described above, siliciclastic deposits of the Kaplankaya, Cingöz, and Güvenç formations are observed to overlie, grade laterally into, or be succeeded by discontinuous, irregularly distributed carbonate deposits of the Karaisalı Formation. The Karaisalı Formation consists of six sub-facies: corallgal packstone and boundstone, corallgal wackestone and packstone, globigerinid packstone (Alibeyli Fm) and wackestone, globigerinid algal packstone, globigerinid argillaceous wackestone (Figure 2.4; Görür, 1979, 1980). Each sub-facies contains varying combinations of allochems such as coralline algae, corals, foraminifera, echinoderms, molluscs, and minor amounts of *Halimeda*, Bryozoa and worm tubes (Appendix B). The formation is interpreted to represent a carbonate shelf reef complex. Complex interfingering relationships between these six sub-facies are commonly observed within the Karaisalı Formation as a result of the formation of reefal deposits on paleotopographic highs, talus deposits on the steep submarine forereef slopes and finer carbonate muds in more distal portions of the basin (Yalçın and Görür, 1984). The reef complex eventually onlapped to the north across denuded Tauride units (Figure 1.15 a-b; Yalçın and Görür, 1984; Yetiş et al., 1995). Thickness of the Karaisalı Formation ranges from 10 - 350 m and vertical and lateral transitions have been observed between Karaisalı facies and Kaplankaya, Güvenç and Cingöz units (Figure 2.1). Foraminifera and algae present within the Karaisalı Formation indicate an age range of Burdigalian to Serravalian (Appendix B), which is consistent with the lateral and vertical relationships outlined above (Yetiş, 1988a).

The limestones of the Karaisalı Formation in the Adana Basin appear to be

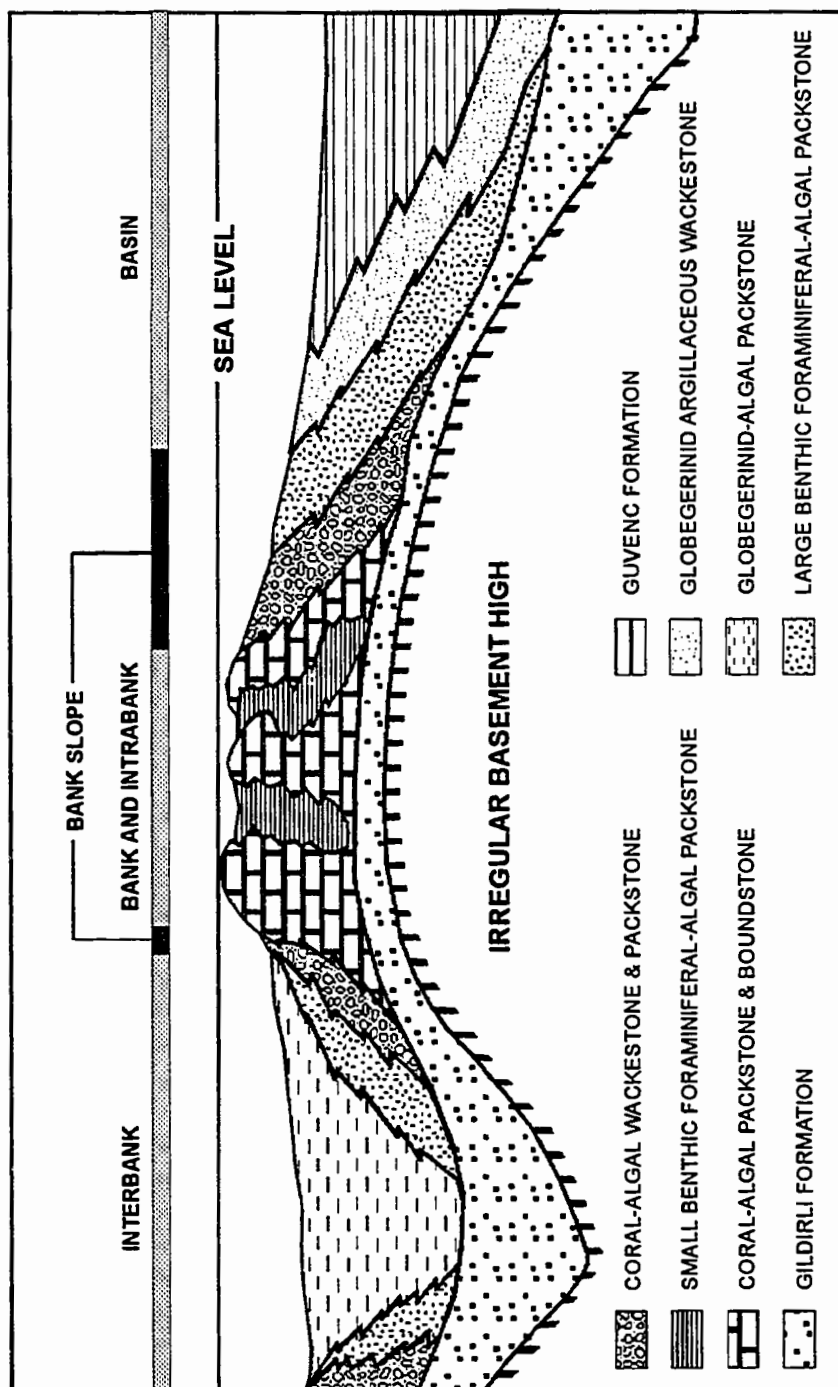


Figure 2.4: Schematic distribution of Karaisali Limestone subfacies as observed in outcrop above irregular basement highs along the Karaisali Embayment, northwestern Adana Basin (modified from Gorur, 1985).

correlative with the carbonates of the Horu Formation in the Iskenderun Basin (Pralle, 1995). Although the Karaisalı Formation is not described in the Misis Complex, diachronous carbonate shelf progradation has been noted within the Karataş Formation (eg Haylazlı Section, Gökçen et al., 1988).

Regressive Deposits

The youngest sedimentary package in the Adana Basin is comprised by the Kuzgun, Handere and Kuranşa formations (Yetis et al., 1995) (Figs. 2.1 and 2.2). A regionally extensive middle Miocene unconformity forms the base of the regressive deposits throughout much of the Adana Basin. This unconformity outcrops in the northern portion of the basin, landward of which, late Miocene regressive deposits occur as outlier deposits. These isolated, northernmost occurrences of regressive deposits are separated from underlying transgressive and pre-transgressive deposits by localized, late Messinian to Pliocene erosional unconformities.

Kuzgun Formation

The Kuzgun Formation forms the base of the regressive deposits within the Adana Basin (Yetis et al., 1995). The Kuzgun Formation has traditionally been subdivided into six interfingering members: Kocaveliler, Caparlı, Kepaz, Kurbanlı, Cubiklar, and Sarnelli members (Schmidt, 1961; Yalçın and Görür, 1984). The formation as described above is transitionally succeeded by the Adana Group which consists of coastal, lagoonal and

evaporitic units (e.g. Sucular Formation, Kosan Shale, Memisli Sandstones; Yalçın and Görür, 1984). Yetiş and Demirkol (1986) have attempted to redefine the traditional stratigraphic treatment of this Tortonian-Pliocene succession by assigning coastal and lagoonal clastic facies of the Adana Group to the underlying Kuzgun Formation, and assigning evaporites of the Adana Group to the overlying Handere Formation. This revision serves to simplify this complex sedimentary succession and allows for better correlation of these units with similar units elsewhere in the Mediterranean (Yetiş et al., 1995). For the purpose of this study the stratigraphic description of Yetiş and Demirkol (1986) will be adopted, as summarized below. The Kuzgun Formation of Yetiş and Demirkol (1986) consists of three units which in ascending order are the Kuzgun, Salbaş Tuffite and Memişli members (Figure 2.3, Section 3).

Kuzgun Member

The Kuzgun Member consists of red and yellow medium- to coarse-grained sandstones and sandy to pebbly conglomerates, with lesser amounts of yellow-green and red siltstones and shales. These deposits are fining-upward successions that consist of crossbedded conglomerates and pebbly sandstones with erosive bases and silty tops. Sedimentary structures noted within the succession include both high- and low-angle crossbedded sandstones, intercalated reddish brown muds, nodular calcrete horizons, and greenish grey *Ostrea*-rich sandstones, siltstones and shales. The rapid lateral facies variations described for the Kuzgun Member of Yetiş and Demirkol (1986) appears to correspond to

those described for the Kuzgun Formation of Yalçın and Görür (1984). The paleogeographic interpretation of this unit suggests that these sediments represent prograding alluvial, deltaic, beach, bar, lagoonal and shallow-water deposits (Yalçın and Görür, 1984).

Contact relations between the Kuzgun Member and underlying units are highly variable throughout the Adana Basin. Deposits of the Kuzgun Formation appear to be relatively conformable with underlying levels of the Güvenç Formation in outcrop, yet seismic profiles indicate the contact is often unconformable (Yetiş et al., 1995). Furthermore, toward the basin edges, and particularly in the west, the Kuzgun Member onlaps earlier Miocene and pre-Miocene units. The member has a maximum thickness of 443 m, and contact relations between the Kuzgun Member and overlying units are variable (discussed below). Benthic foraminifera, gastropods, bivalves, and teeth (*Hipparion* spp) within the Kuzgun Member indicate a Late Serravalian to Tortonian age of deposition (Appendix B; Yetiş, 1988a).

Salbaş Tuffite member

Yetiş and Demirkol (1986) define the Salbaş Tuffite member as equivalent to Schmidt's (1961) upper Tuff Member (Yetiş et al., 1995). The lower portion of the Salbaş Tuffite member consists of transitional volcanoclastic sandstones, siltstones and shales which form a transition between rocks of the underlying Kuzgun member with the tuffite horizon above. The tuff horizon itself contains variable percentages of silt and clay, exhibits a lenticular geometry on a regional scale, and has a maximum thickness of 15 m (Yetiş et al., 1995) (Figs. 2.1 and 2.3, Sections 3 and 4). Gastropods and vertebrate teeth isolated within

the Salbaş Tuffite Member indicate a Tortonian age (Appendix B; Yetiş, 1988a). Yalçın and Görür (1984) conclude that widespread tuff horizons within the Tortonian succession are indicative of increased volcanic activity within, or proximal to, the Adana Basin at this time.

Memişli Member

The Sucular Formation and Memişli Sandstone of the Adana Group (Schmidt, 1961; Yalçın and Görür, 1984) have been re-defined as the Memişli Member of the Kuzgun Formation (Yetiş and Demirkol, 1986; Yetiş et al., 1995). The lower portion of the Memişli Member consists of basal conglomerates and coarse sandstones which commonly exhibit cross-stratification and ripple marks. Thick organic-rich, bioturbated siltstones form the tops of many of these fining-upward sequences of the lower Memişli Member. These deposits are equivalent to the fluvial channel and bar deposits of the Sucular Formation as outlined in Yalçın and Görür's (1984) description of the Adana Group. Yellowish-green oyster-rich pebbly sandstones and intercalated siltstones and mudstones prevail higher in the Memişli Member. This portion of the member is essentially equivalent to the shallow-marine and lagoonal deposits of the Memişli Sandstone of the Adana Group (Yalçın and Görür, 1984). Coral growths, gastropods and rare planktonic foraminifera present within these sandstones indicate a Tortonian - Messinian age range for the upper part of the Memişli Member (Appendix B; Yetiş et al., 1995).

The Memişli Member has an observed maximum thickness of 434 meters (Yetiş et al., 1995), and contact relations range from transitional with the underlying Salbaş Tuffite

Member and the overlying Handere Formation (Figure 2.3, Section 3), to discordant where it rests directly on the Kuzgun Member sandstones (Figure 2.3, Section 4). Yetiş et al., (1995) propose penecontemporaneous erosion of the intervening tuffite unit as an explanation for this observed discordance. The range of units described within the Kuzgun Formation are interpreted by Yalçın and Görür (1984) to represent deposits of alluvial fan, deltaic and shallow marine character. The formation is broadly correlative with the Kızıldere Formation of both the Misis Complex and the Iskenderun Basin based on the presence of tuff horizons in each location (Gökçen et al., 1988; Pralle, 1995; Yetiş et al., 1995).

Handere Formation

The Handere Formation consists primarily of a thick sequence of grey to yellow thinly bedded lagoonal siltstones and shales, with channelized to lenticular sandstone and conglomerate interbeds. Yetiş and Demirkol (1986) have recently redefined this formation by including the Gökkuyu Gypsum Member, an evaporitic unit previously assigned to the Adana Group. Lagoonal sediments are up to 25 m thick, display flaser-like interbeds, and contain abundant oysters, gastropods and ostracods (Yalçın and Görür, 1984). Maximum thicknesses noted for the Handere Formation are in excess of 450 m. Faunal evidence indicates a Messinian to Early Pliocene age for this unit (Appendix B; Gürbüz and Gökçen, 1985; Yetiş, 1988a; Yetiş et al., 1995). The paleogeographic interpretation of Yalçın and Görür (1984) concludes that the widespread shallowing observed during the late Tortonian climaxed during the Messinian. This resulted in widespread dessication of the Adana Basin

and development of the saline lakes, playas and sabkhas in which the Handere Formation evaporites precipitated.

The Gökkuyu Gypsum Member

Evaporitic units of the Gökkuyu Gypsum Member outcrop in the southwestern part of the Adana Basin (Figure 2.3, Section 3), but are absent in the north (Figure 2.3, Section 4) (Yetiş et al., 1995). In outcrop these units are observed as 0.25–5 m thick stringers of gypsum within a succession of soft grey sandstones and siltstones. Pebbly horizons which contain gypsum clasts have also been noted within the succession (Yetiş, 1988a). These reworked horizons provide supporting evidence to Yalçın and Görür's (1984) paleogeographic interpretation that these rocks formed in a terrestrial environment which experienced erosion during the Messinian.

Notable evaporitic horizons have also been intersected in exploration wells in the southern part of the Adana Basin. The thicknesses of intersected evaporites range from 100 m in Arapali-1 (Pralle, 1995), to 400 m in Kuranşa-1 and 900 m in Seyhan-1, both located in the Inner Cilicia Basin (Turkish Petroleum well data, Appendix B). This suggests that the evaporites thicken toward the south and thin toward the north. Yalçın and Görür (1984) note that gypsum and anhydrite dominate the lower portion of the intersected evaporites, while a thick succession of halite dominates the upper portion; numerous deep channel incisions are also observed within the evaporite succession and attest to erosion during the Messinian to Pliocene. Figure 1.15 d indicates the non-palinspastic depositional environments for the

origin of these evaporites as proposed by Yalçın and Görür (1984).

The Messinian to Pliocene Handere Formation of the Adana Basin can be correlated with the Aktepe Formation of the Iskenderun Basin (Figure 2.2) (Pralle, 1995). Pralle (1995) also correlates the Gökkuyu Gypsum Member (GM) of the Adana Basin with the Haymanseki Member evaporites (HM) of the upper Kızıldere Formation in the Iskenderun Basin. No Messinian-aged deposits have been recognized in the Misis Complex (Figure 2.3, Section 5) (Gökçen et al., 1988; Yetiş et al., 1995). This is in contrast with the thick Messinian deposits observed in the Adana, Iskenderun and inner Cilicia basins which flank the Misis high. Yetiş et al., (1995) conclude that the absence of Messinian deposits in the Misis Complex might be explained if the area was emergent at this time. The presence of late Miocene-Pliocene channel incisions within Misis Complex rocks (Schmidt, 1961; Yetiş et al., 1995) supports the conclusion that the Misis Complex experienced terrestrial conditions and erosion at this time.

Kuraşa Formation

The Late Pliocene-Quaternary deposits of Kuraşa Formation and overlying Recent alluvium and caliches form the uppermost regressive deposits within the Adana Basin (Yalçın and Görür, 1984). The Kuraşa Formation consists primarily of unconsolidated to loosely cemented sands, gravels and silts. The depositional style of this unit indicates alluvial and estuarine origins (Yalçın and Görür, 1984). The Kuraşa deposits are, therefore, viewed as representative of the deltaic sedimentation which exists in the Adana Basin today. Maximum

thicknesses for the Kuraşa Formation appear to be highly variable in outcrop, ranging from to 0 to 1300 m (Yalçın and Görür, 1984; Yetiş et al, 1995).

The Kadirli Formation of the Misis Complex and the Erzin Formation of the Iskenderun Basin represent alluvium deposits which are correlative to the Kuraşa Formation of the Adana Basin (Kozlu, 1987; Pralle, 1995).

2.1.3 Comments on Lithostratigraphic Unconformities

The preceding lithostratigraphic review identifies four prominent lithostratigraphic unconformities, which divide the Miocene Adana Basin succession (Figure 2.2). The characteristics of each lithostratigraphic unconformity are summarized in Table 2.1 and briefly outlined below.

The lowermost Miocene lithostratigraphic unconformity in the Adana Basin is represented by a regionally extensive base Miocene angular unconformity, which marks the top of pre-Miocene basement in the Adana Basin. The lower to middle Miocene transgressive deposits are separated from underlying pre-transgressive deposits and pre-Miocene basement rocks by a prominent Burdigalian to Serravalian time-transgressive unconformity. Where pre-transgressive deposits are absent, the time-transgressive lower Miocene unconformity and the base Miocene angular unconformity are coincident (Figure 2.2). The Tortonian unconformity occurs as a variable surface of apparent onlap, downlap and localized erosional truncation that marks the base of the regressive deposits. The uppermost unconformity is a prominent Messinian erosional unconformity which is restricted to the southern portion of the Adana

Table 2.1: Characteristics of Miocene to Recent lithostratigraphic contacts observed in the Adana Basin.

Litho-stratigraphic contact	Formations Directly Below Contact	Formations Directly Above Contact	Erosional Truncation	Onlap	Distribution
Messinian Dessication Unconformity	- Handere Fm (Gökkuyu Gypsum Member only) - Kuzgun Fm - pre-Miocene basement	- Handere Fm (excluding Gökkuyu Gypsum Member)	yes	yes	- largely restricted to the south, - erosional outliers noted in the north
Tortonian Regressive Unconformity	- Güvenç Fm - Cingöz Fm - pre-Miocene basement	- Kuzgun Fm	yes	yes	- regional, unconformable in the north-central region, but becomes conformable toward the south
Burdigalian to Serravalian Time-transgressive Unconformity	- Gildirli Fm	- Güvenç Fm - Cingöz Fm - Karaisalı Fm - Kaplankaya Fm	no	yes	- regional, but most developed in outcrops in the northwest
Base Miocene Unconformity	- pre-Miocene basement	-Gildirli Fm	yes	yes	- regional

Basin. Toward the north, the Messinian unconformity merges with the underlying Tortonian unconformity. All unconformities appear to merge above structural highs which delimit the basin edges to the North, West and East of the Adana Basin.

2.2 Seismic Stratigraphy

Over the last decade Turkish Petroleum (TPAO) has supported a number of recent studies in the Adana region, resulting in an increase in access to industry seismic profiles of the region. Access to previously inaccessible seismic data sets is allowing researchers to apply the principles of seismic stratigraphic analysis to the Adana Basin and to consider the stratigraphic architecture of the basin in a modern context. Two differing seismic stratigraphic frameworks previously proposed for the Miocene succession are based on the seismic data sets illustrated in Figure 1.7 (Williams et al., 1995; Pralle, 1995). Offshore seismic stratigraphic treatments of the inner Cilicia-Adana Basin (Aksu et al., 1992a; Aksu 1992b) explore the architecture and sedimentary history of only the Quaternary portion of the Adana, Cilicia and Iskenderun Basins.

New data made available to the principal researchers of the East Mediterranean Research Group (Memorial University of Newfoundland) by TPAO has more than doubled the number of industry seismic profiles used in previous studies (Figure 1.18). Consequently this study aims to reconcile both previous seismic stratigraphic treatments (below) in a new expanded seismic stratigraphic framework (Section 2.2.1).

I. Seismic Study: Williams et al (1995)

Williams et al. (1995) applied the principles of seismic stratigraphic analysis to a data set of 11 industry seismic profiles (300 km) provided by Turkish Petroleum Corporation (Figure 1.7). The data set provides good coverage of the northern portion of the Adana Basin, but coverage of the southern part of the basin is sparse. The seismic stratigraphic framework proposed by Williams et al. (1995) consists of two megasequence boundaries and three megasequences as summarized below:

Megasequence 1 (M1) occurs above seismic basement, is dominated by a bright internal reflection configuration and is interpreted as Lower Miocene reef accumulations which occur preferentially on extensional horst block crests. The seismic megasequence is correlated with a Langhian aged Karaisali Formation (Table 2.2).

Megasequence 2 (M2) is described as a package of parallel continuous reflectors which are interpreted to represent the deposits of turbidite activity. The megasequence is inferred to be the result of passive infill into a relatively deep basin due to a lack of identifiable growth features within the seismic profiles, however local onlap is noted at the base of the succession. This megasequence is correlated with the early to middle Miocene deposits of the Kaplankaya, Cingöz and Güvenç formations (Table 2.2).

Megasequence 3 is characterized by largely south dipping parallel reflectors, which locally onlap a truncated Megasequence 2. Progradational features are noted in the northeastern extent of the megasequence and it is postulated that these features may represent deltaic deposits. Megasequence 3 is correlated with the mid- to- late Miocene-Pliocene

Table 2.2: Past and present: seismic stratigraphic frameworks and lithologic correlations for the Adana Basin.

Series	Stages	A. Williams et al., 1995		B. Pralle, 1994		C. This Study		
Quaternary		Terrace alluvium				Kuraşa Fm	Unit 5	MGS3
Pliocene				Kuraşa/Erzin Fm Aktepe Fm Kadirli Fm	P3 P2 P3	Handere Fm		
M i o c e n e	Messinian	Handere Fm	M3	Handere Fm Haymanseki Fm	M3b M3a	Gökkuyu Gypsum Mbr (Handere Fm)	Unit 4	MGS2
	Tortonian	Kuzgun Fm		Kuzgun Fm, Kızıldere Fm, Cingöz Fm, Horu Fm, Kalecik Fm, Köpekli Fm	M2	Kuzgun Fm	Unit 3	
	Serravalian	Güvenç Fm	M2			Güvenç Fm Cingöz Fm	Unit 2	
	Langhian	Cingöz Fm			M1	Kaplankaya Fm	Unit 1	MGS1
		Karaisalı Fm	M1			Gildirli Fm		
	Burdigalian	Kaplankaya Fm	M2	Karaisalı Fm Gildirli Fm	M1	Karaisalı Fm		
Pre-Miocene						Karsanti Fm Paleozoic and Mesozoic rocks	Basement	Basement

deposits of the Kuzgun and Handere formations (Table 2.2).

II. Seismic Study: Pralle (1994)

Pralle (1994) proposed a seismic stratigraphic framework for the Adana Basin using a seismic data set of 27 industry seismic profiles provided by Turkish Petroleum Corporation (Figure 1.7). This data set is complemented with core and/or geophysical well data for 11 wells in the Adana Basin in addition to seismic and well data for the adjacent Iskenderun Basin. The seismic/stratigraphic approach implemented by Pralle identified 2 prominent bounding surfaces, one lessor erosional surface and four key units within the Miocene to Recent succession (Table 2.2). Pralle establishes ties between well data and the seismic profiles by developing synthetic seismograms. These results were used to reconcile seismic reflection and lithostratigraphic data at the onset. As a result, written descriptions of individual seismic facies attributes are omitted in favor of a report on the stratigraphic evolution of the reconciled seismic-lithostratigraphic units. Pralle's seismic stratigraphic framework is presented in Table 2.2 and summarized below:

M1 is the lowermost Miocene aged seismic stratigraphic unit in Pralle's framework of the Adana and Iskenderun basins (Table 2.2). The unit is interpreted as Burdigalian in age and is correlated with deposits of the Karaisalı and Gildirli formations in the Adana Basin and the Horu and Kalecik formations in the Iskenderun basin. These units lie with unconformity upon pre-Neogene basement, and both the carbonate and clastic deposits exhibit thickness and distribution variations which appear to be controlled by paleotopography.

M2 represents an early Langhian-late Tortonian aged succession which Pralle has correlated with the Cingöz, and Kuzgun formations of the Adana Basin and the Kızıldere Formation of the Iskenderun Basin (Table 2.2). The transgressive Cingöz Formation is interpreted as distal and proximal turbidite fan deposits which are succeeded by variable inner shelf, lagoonal and deltaic deposits of the regressive Kuzgun Formation.

The M3 seismic stratigraphic unit represents the upper Miocene interval, and includes Messinian aged clastics of the Handere Formation (M3a) and evaporites of the Haymasseki Formation (M3b) in the Adana and Iskenderun basins. Continued regression resulted in significant dessication at this time, which was accompanied by subaerial erosion and evaporite deposition.

The P1-P3 unit represents the youngest, Pliocene aged unit of Pralle's seismic stratigraphic framework. The unit is divisible into the lower Pliocene aged Kadirli Formation (P1), the Pliocene aged Aktepe Formation (P2) and the Plio-Quaternary deposits of the Kuranşa and Erzin formations (P3) of the Adana and Iskenderun basins.

2.2.1 Description of Seismic Features

A new expanded seismic stratigraphic framework is proposed for the Adana Basin based on a dataset of 53 industry seismic profiles and varied well data (Figure 1.2). The density of onshore seismic data varies throughout the Adana Basin, such that spacing between seismic reflection profiles ranges between 3 and 10 km. The water reservoir for the city of Adana creates a data gap through the centre of the seismic data grid. To the north, the

seismic grid is dense, with frequent line intersections which permit detailed correlation of prominent seismic reflectors across the area. Toward the south, seismic interpretation and correlation of seismic reflectors is more challenging, due in part to complex structuring, and less frequent line intersections. A new seismic stratigraphic framework of the Adana Basin is outlined below.

The seismic succession is divisible into three distinct seismic megasequences (MGS 1-3) by two prominent regional unconformities (B1-2) and one laterally restricted local unconformity (B3) (Figure 2.5, Table 2.3). The seismic megasequences (MGS1-3) are further divided into 5 seismic units (Tables 2.2 and 2.4). Each acoustic unit exhibits a unique set of internal and external attributes and a distinctive set of contact relations with observed B1, B2 and B3 seismic unconformities. Time-structure maps of the B1 and B2 seismic unconformities are presented in Figures 2.6 and 2.7. The B1 surface forms a deep NE-SW trending trough. The B1 basin edge extends northward of the B2 basin edge, and falls outside the study area. The B2 surface forms a shallow NE-SW trending trough, with a basin edge that is located within the northern portion of the study area.

Seismic basement

The basement to the Miocene seismic succession occurs as an acoustically opaque package which is bounded at the top by the B1 unconformity (Figs. 2.5, 2.8 to 2.10). The vertical thickness of seismic basement imaged on seismic profiles in the Adana Basin ranges from 2.0 to 4.0 seconds TWT, but penetration is limited to the uppermost interval.

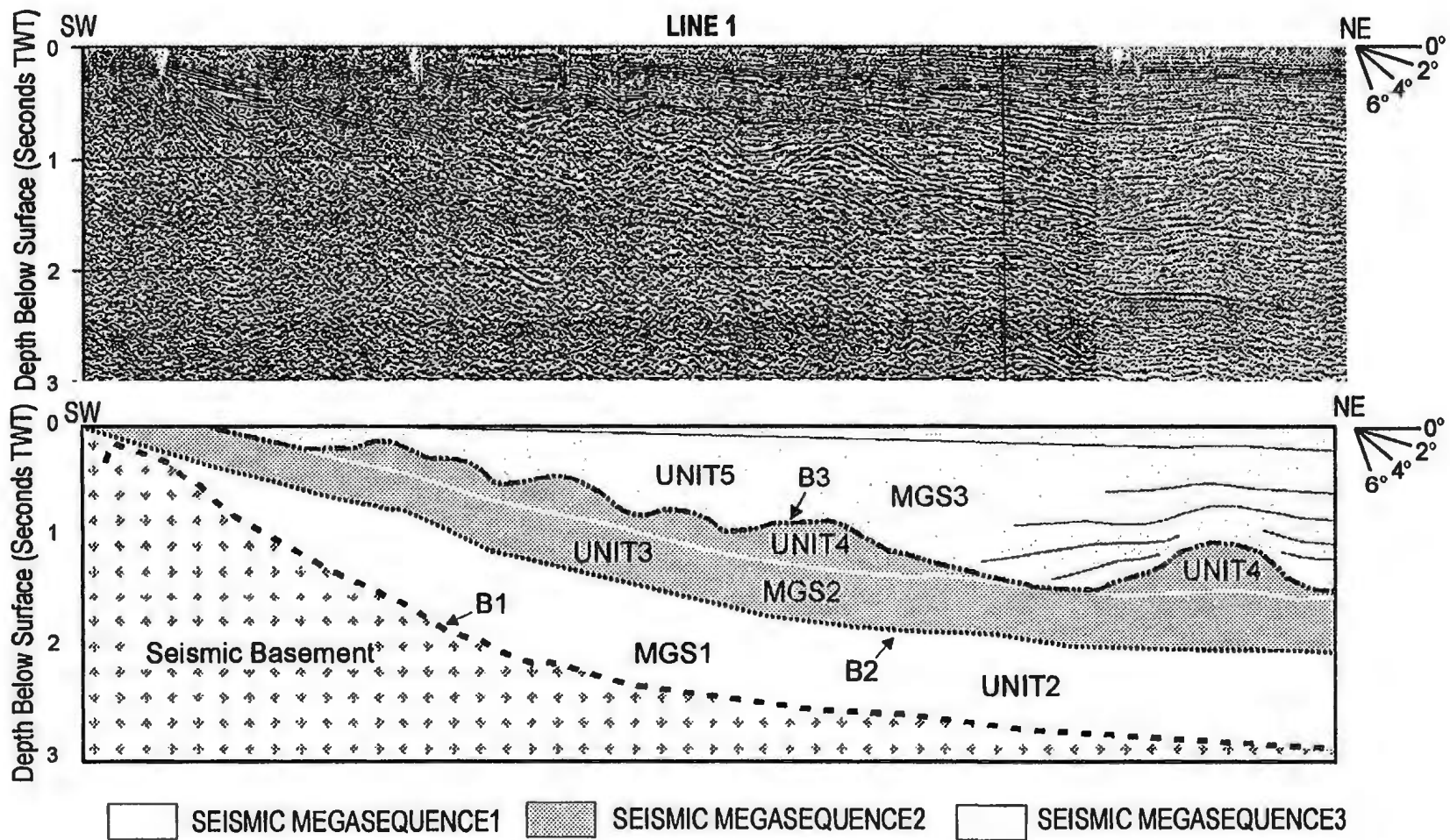


Figure 2.5: Line 1. The B1, B2 and B3 seismic markers divide the seismic succession into three seismic megasequences (MGS1, MGS2, MGS3), which are further divisible into seismic Units 1 to 6. Note: the absence of Unit 1 in this profile is due to the variable distribution of Unit 1 within the study area.

Table 2.3: Characteristics of prominent seismic markers in the Adana Basin.

Seismic Marker	Amplitude and Continuity of marker	Units directly below	Units directly above	Erosional Truncation	Onlap/ Apparent Downlap Surface	Depth to Marker (TWT)	Distribution
B3	- moderate to high amplitude - rolling, semi-continuous	Unit 4 Unit 3 Unit 2 Basement	Unit 5	varies: - present in shallow areas - not apparent in deeper areas	onlap	0-2*s	Observed only in the southwest; extends to the surface along the western flank of the basin; increases in depth from surface toward the south
B2	varies: (i) single, high amplitude, continuous (ii) stacked twin moderate amplitude, semi-continuous	varies: Unit 2 Unit 1 Basement	Unit 3	yes	yes	0-3 s	Basin wide, unconformable, present as a hard reflector in the north and central part of the basin; Toward the south the unconformity begins to lose its character, and becomes conformable.
B1	- high amplitude - fragmented, continuous	Basement	varies: Unit 2 Unit 1	varies: - not apparent in basement lows - often present on basement highs	varies locally: - apparent onlap - apparent downlap	0-4 s	Basin wide, but extends below the limit of resolution in deeper areas (> 4.0 seconds TWT) in the south

Table 2.4: Descriptive summary of seismic facies attributes in the Adana Basin.

Unit	Depositional Interpretation	Seismic Facies	External Form	Internal Reflection Configuration	Amplitude	Continuity	Onlap/Offlap Relations
U5	terrestrial/ coastal	sheet	uniform	-parallel (horizontal to inclined) -uppermost part is often transparent and chaotic	moderate to high	- relatively continuous -discontinuous in uppermost part	-onlap -apparent downlap
U4	evaporites	mounds	convex upward	-moderate transparency -parallel (undulating?) to sub-parallel (irregular)	low	semi-continuous	variable
U3	coastal	wedges to lenses	stacked successive lenticular wedges	-parallel (slightly undulating) to hummocky discordance -subparallel oblique clinoforms noted in NE	variable high or low	semi-continuous to discontinuous	-offlap -downlap -apparent truncation or toplap
U2	basin slope and floor	onlap fill	uniform to convex downward	-parallel (low angle inclination to large wavelength undulating folds) -occasionally transparent	high	relatively continuous	-onlap -apparent downlap
	basin slope and floor	onlap fill to mound	uniform to convex upward	-parallel (inclined) to divergent -lenticular to hummocky -alternating railroad tracks and transparent layers	variable high or low	variable high or low	-onlap onto highs -apparent downlap basin floor
U1	coastal-shelf?	mound	convex upward	-irregular to discordant -hummocky to chaotic	low to moderate	semi-continuous	-onlap -downlap?
Basement	acoustic basement	-----	-----	-chaotic to parabolic	high	relatively continuous	-----

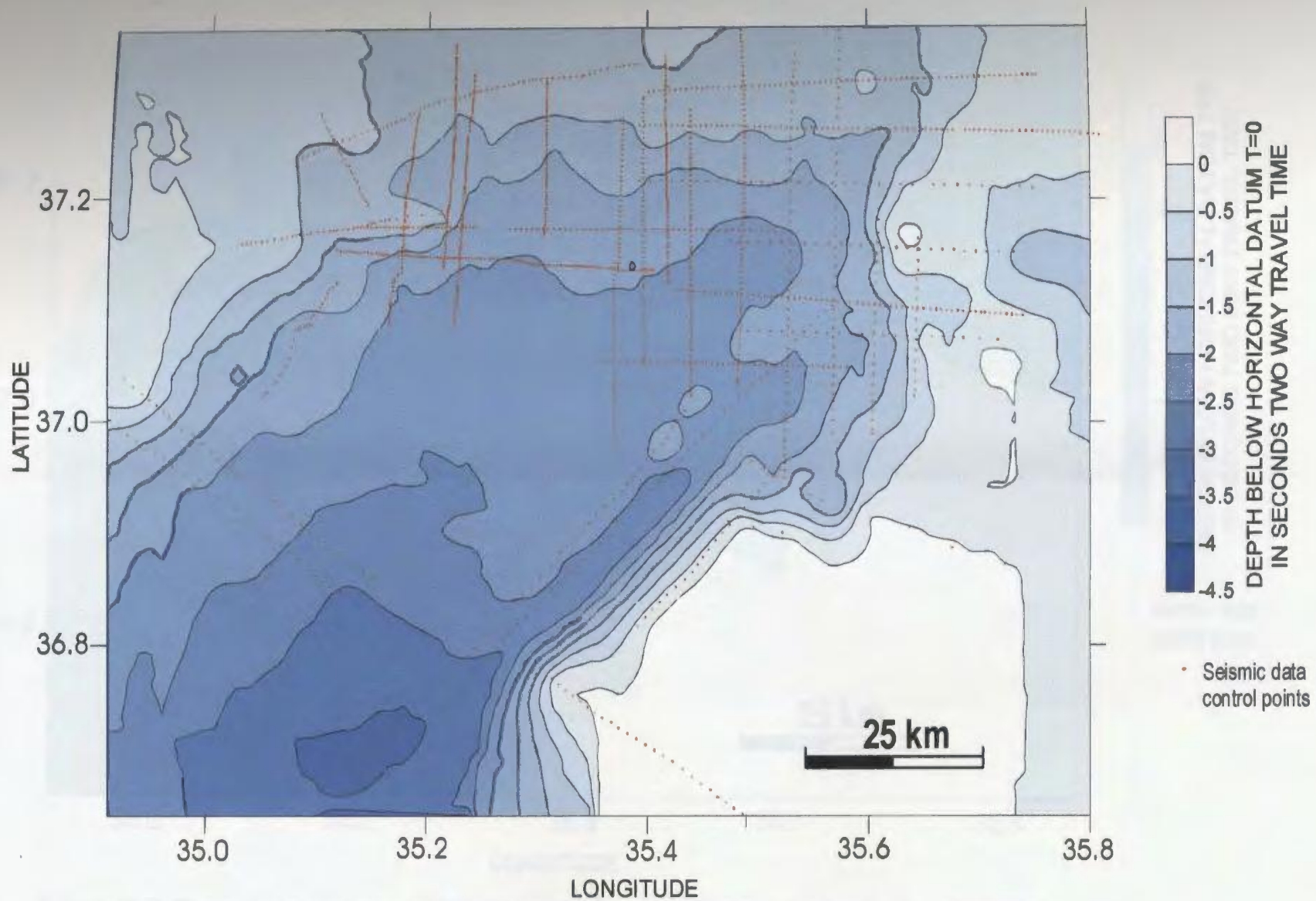


Figure 2.6: Time-structure map of the B2 seismic unconformity. Depth below horizontal datum ($t = 0$) in seconds, TWT. Note the position of a deep trough adjacent to a prominent, northeast-southwest trending structural high along the eastern limit of the basin.

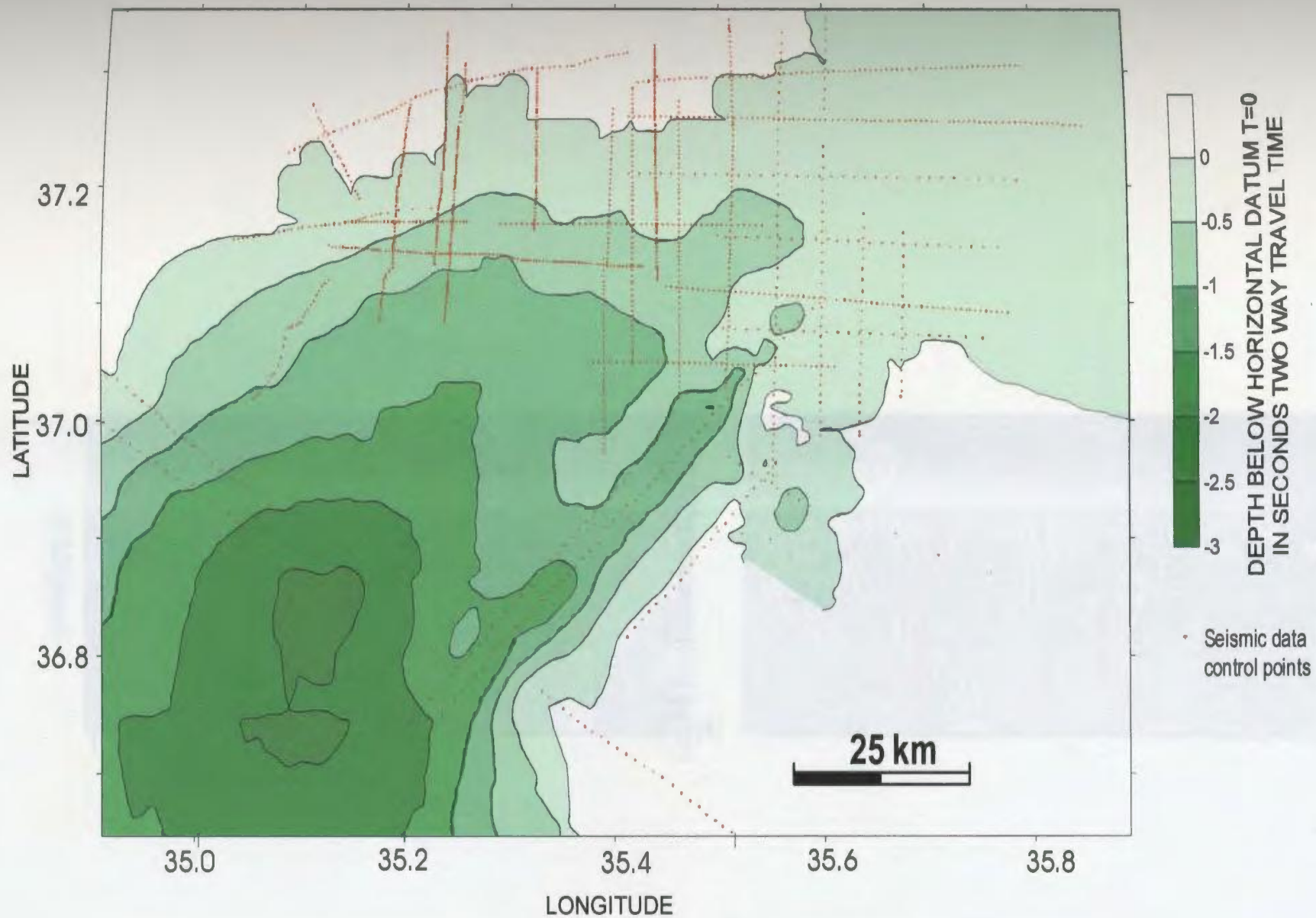


Figure 2.7: Time-structure map of the B1 seismic unconformity. Depth below horizontal datum ($t = 0$) in seconds, TWT. Note: i) B1 is delimited by a $T=0$ basin edge in the north and east; ii) a narrow trough lies adjacent to the northeast-southwest trending structural high along the eastern limit of the basin.

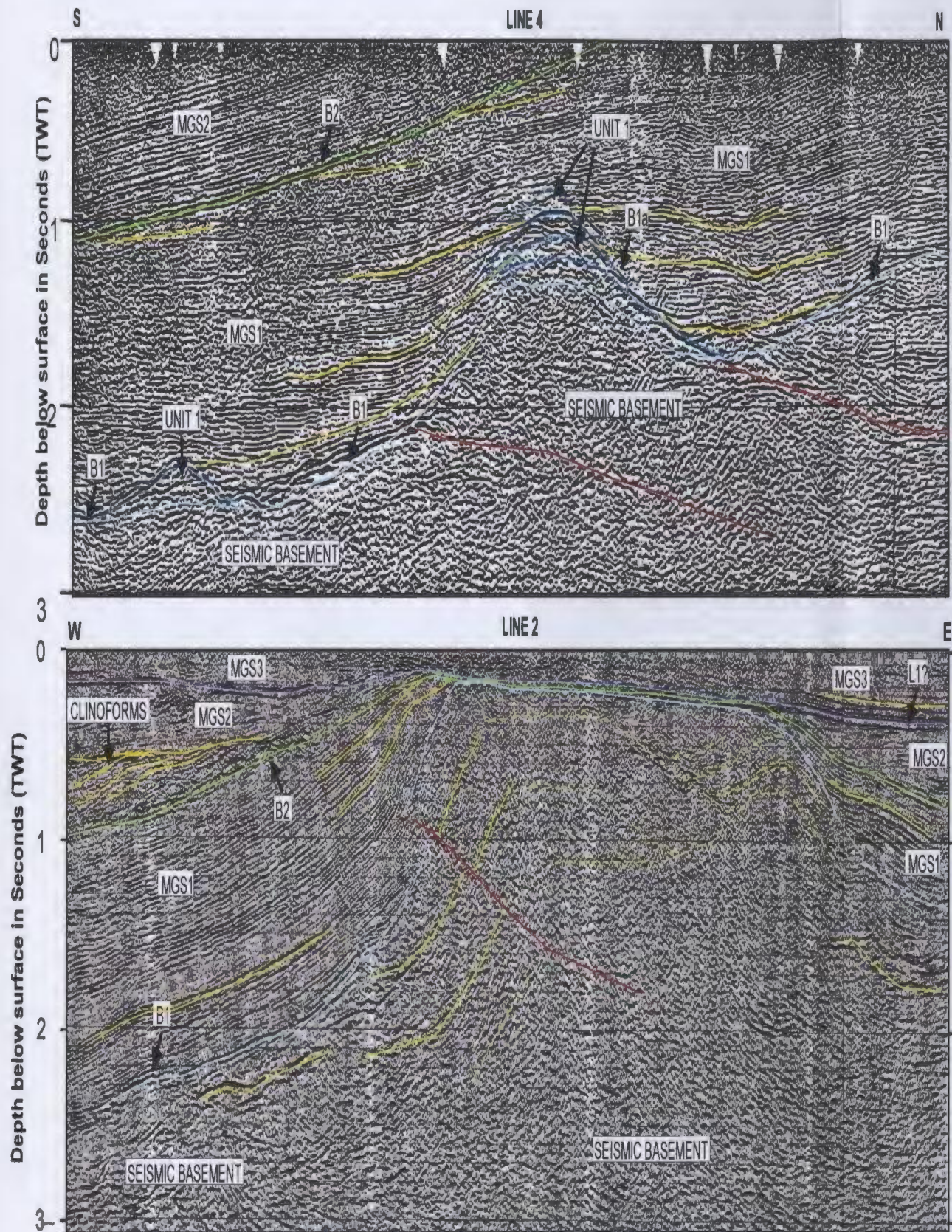


Figure 2.8: Seismic stratigraphic interpretation for the north-central portions of a) Line 4 and b) Line 2. Note the position of the B1(blue) and B2(green) unconformities, and the variable stratal geometries indicated in yellow. Refer to Figure 1.18 for line locations.

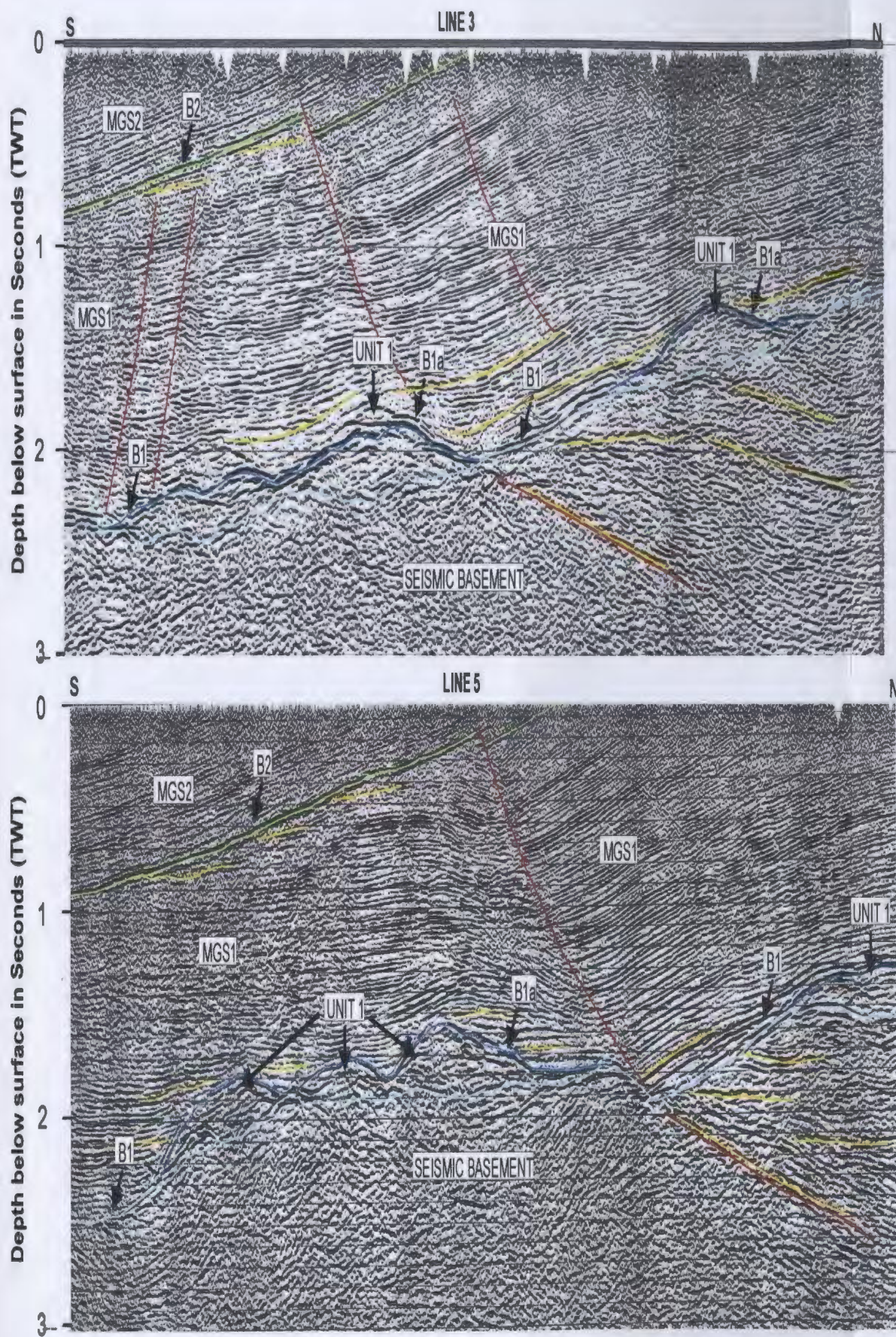


Figure 2.9: Seismic stratigraphic interpretation for the north-central portions of a) Line 3 and b) Line 5. Note the position of the B1(blue) and B2(green) unconformities, and the variable stratal geometries indicated in yellow. Refer to Figure 1.18 for line locations.

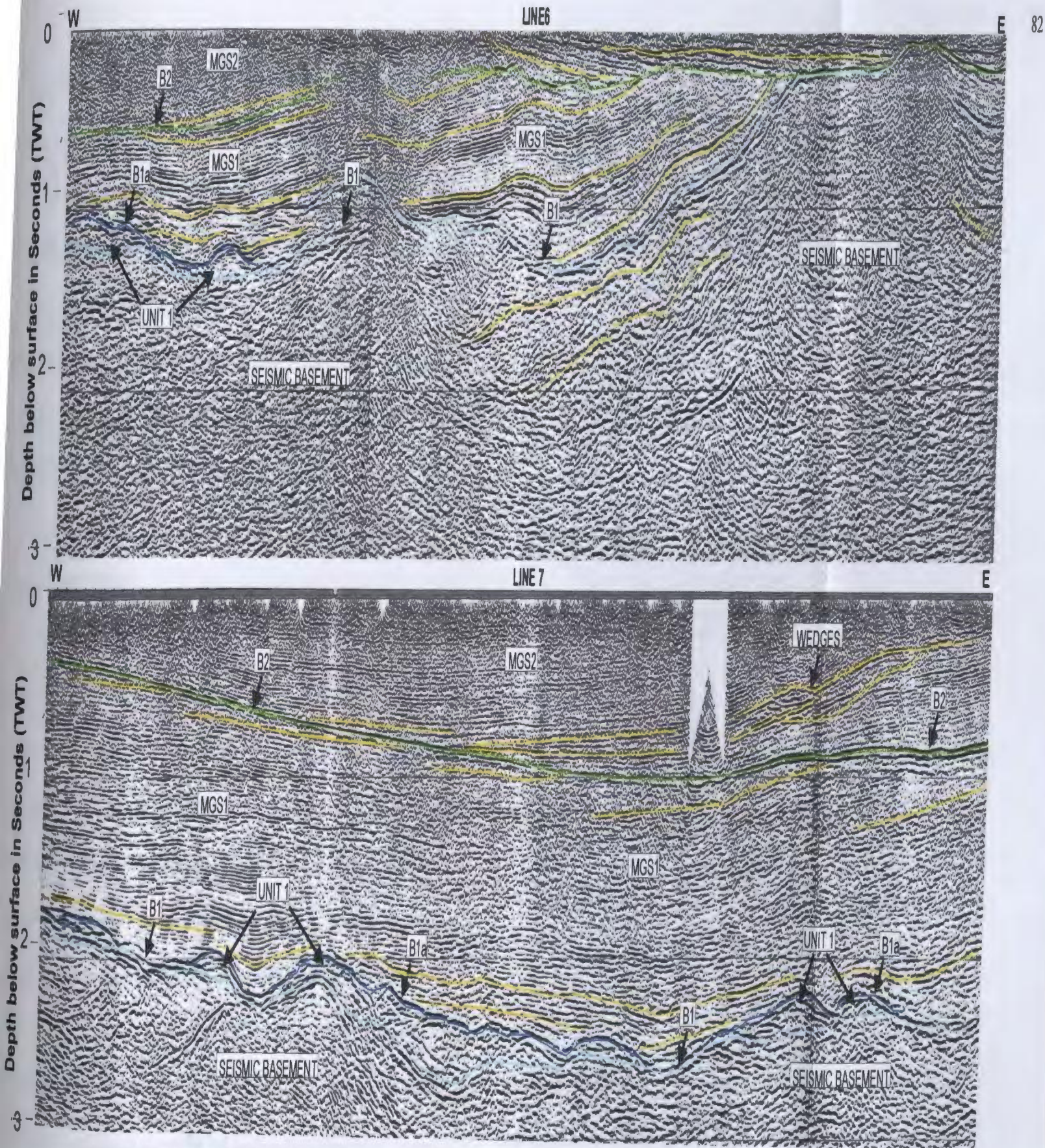


Figure 2.10: Seismic stratigraphic interpretation for the north-central portions of a) Line 6 and b) Line 7. Note the position of the B1(blue) and B2(green) unconformities, and the variable stratal geometries indicated in yellow. Refer to Figure 1.18 for line locations.

The seismic basement is characterized by a relatively continuous, high amplitude, chaotic to parabolic internal reflection configuration which becomes opaque at depth. The upper limit of the seismic basement is irregular, and occasionally contains moderate amplitude truncated dipping reflectors (eg. Figs. 2.8 a and 2.9 b). Large discontinuous high amplitude dipping events are present throughout the northern portion of the Adana Basin, and appear to occur in association with basement thrust culminations. Seismic profiles of the basin flanks image the greatest vertical thickness of seismic basement, which exceeds 4.0 seconds TWT (Figure 2.8 b).

Megasequence 1 (MGS1)

Seismic megasequence 1 overlies seismic basement with an irregular topography defined by the B1 unconformity (Figs. 2.5, 2.8 b and 2.9 a). It exhibits variable apparent downlap and onlap onto the B1 unconformity, and is bounded at the top by erosional truncation defined by B2. MGS1 is dominated by parallel-dipping to large wavelength undulating reflectors that are high in amplitude at the base, but which become increasingly transparent toward the top. The megasequence comprises a 0 to 2.3 second TWT thick sedimentary package which is divisible into Units 1 and 2, where Unit 1 forms an thin, discontinuous irregularly distributed seismic unit, and Unit 2 forms a thick, continuous seismic stratigraphic unit that forms most of MGS1. Where Unit 1 is present, the contact between the units 1 and 2 is observed as a hummocky, high amplitude unconformity (B1 a). Where Unit 1 is absent, Unit 2 lies above seismic basement, and the B1 unconformity represents the

combined B1 - B1a seismic unconformity..

Unit 1

Unit 1 is represented by bright convex upward mounds which consist of moderate amplitude, irregular to discordant, hummocky internal reflectors set in a semi-transparent background (Figs 2.8 a , 2.9 and 2.10 b). The unit is traceable in several of the profiles as a semi-continuous string of 0.2 to 0.4 seconds TWT thick mounds which are often located on or near topographic highs of the underlying seismic basement. Unit 1 mounds are unconformably onlapped by overlying seismic units, but local onlap relationships are varied and complex and (Figs 2.8 a and 2.9). In the east, Unit 1 is often overlain by Unit 2 with variable apparent downlap and onlap contacts.

Unit 2

Unit 2 consists of parallel (westward inclined) to divergent reflectors that exhibit a lenticular to hummocky internal geometry and a slight large wavelength folded external geometry. The reflectors vary in amplitude from groups of strong railroad track reflections to layers which are almost transparent; continuity of the reflectors ranges from high in undeformed areas to moderate in areas above basement highs. The unit has a uniform to convex upward external geometry and shares characteristics of both onlap fill and mound facies. The unit rests on Unit 1 and/or the B1 surface with contact relations that range from onlap at basin margins and basement highs to apparent downlap along portions of the basin

floor. Unit 2 is disconformably succeeded by the B2 unconformity and seismic megasequence 2 in the south-central portion of the study area. In contrast, seismic megasequence 1 is steeply inclined, erosively truncated and succeeded by the B2 unconformity and seismic megasequence 2 along the easternmost basin edge (Figs 2.8 a and 2.9 a). Successive folded, local unconformities (onlap, offlap) are visible within the lower, middle and upper portions of Unit 2 (Figure 2.8 a and b).

Megasequence 2 (MGS2)

Seismic megasequence 2 is imaged as a relatively undeformed succession which gently onlaps truncated seismic basement and MGS1 deposits along the B2 surface (Figs. 2.5, 2.8 to 2.10). It is represented by seismic Units 3 and 4, which exhibits significant lateral and vertical variation. Seismic megasequence 2 thickens from a basin edge in the north, to 2.5 seconds TWT in the south. The upper limit of MGS2 is delimited in the south-central portion of the basin by the laterally restricted south-dipping B3 unconformity, which is restricted to the southwestern and south-central portions of the basin and relates to the localized presence of seismic Unit 4 (Figure 2.5). North of the outcrop edge of the B3 unconformity, the upper limit of Megasequence 2 is approximated as surface of the earth ($t = 0$ Seconds TWT). However, north of the B3 unconformity, the uppermost portion of seismic megasequence 2 is highly attenuated and contains local unconformities. The seismic strata contained in this uppermost interval may represent the disconformable deposits the younger seismic megasequence 3.

Unit 3

Unit 3 consists of semi-continuous to discontinuous high and low amplitude reflectors with an internal reflection configuration that varies between parallel and hummocky discordance. The external geometry of the unit exhibits significant lateral variation; uniform sheets, stacked wedges, and oblique clinoforms are observed at different locations within the basin (Figs. 2.9 to 2.11). High amplitude discontinuous convex down reflector sets within a low amplitude to semitransparent background are noted higher in the unit; erosional down-cutting of the Unit 3 is also observed.

Evidence of local onlap, offlap and downlap, are noted at different locations along the B2 unconformity, which forms the lower boundary of the unit. Apparent truncation and/or toplap is also noted along the tops of clinoform structures near the top of the unit. The upper boundary of Unit 3 is visible as the B3 unconformity in the southwest (Figure 2.5), as a local unconformity in some areas to the east (Figs 2.8 b and 2.11), and as a disconformity in the north (Figs. 2.8 a and 2.9). The thickness of the Unit 3 ranges from 0 to 0.7 seconds TWT on interpreted profiles, but thickness estimations in the south-central area have been impeded by poor imaging, complex structuring and correlation problems.

Unit 4

Unit 4 is a highly variable, acoustically transparent seismic unit that is restricted to the south and southwest portions of the study area. The unit occurs as a series of discontinuous, fault modified lenticular packages which range in thickness from 0 to 0.8 seconds TWT

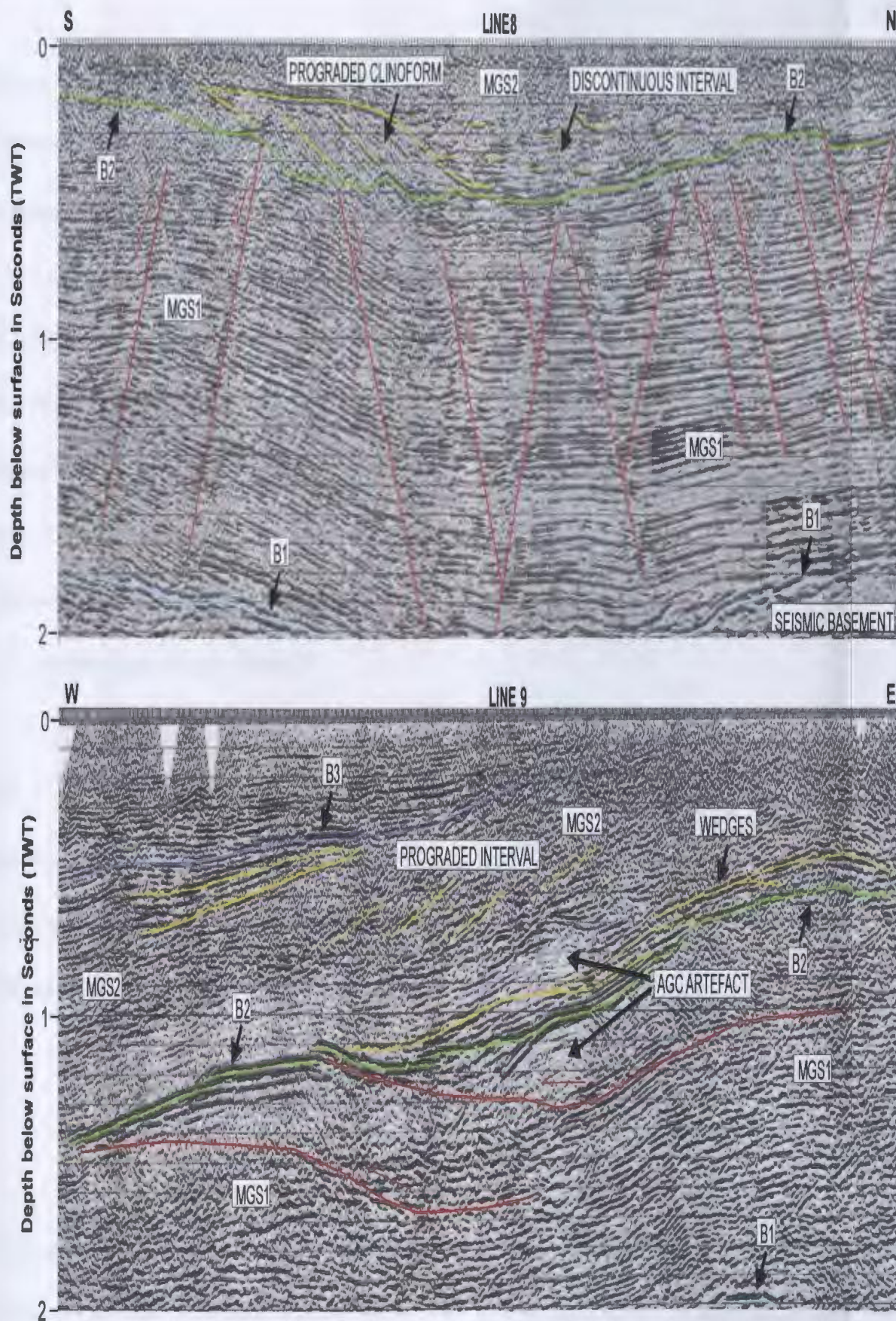


Figure 2.11: Seismic stratigraphic interpretation for a) the north-central portions of Line 8 and b) the central portion of Line 9. Note the position of the B2 (green) unconformity, and the variable stratal geometries associated with it (indicated in yellow). Refer to Figure 1.18 for line locations.

(Figure 2.5). The external forms of the unit are comparable to those of salt rollers, pillows, and welds observed in halokinetic regimes. The unit consists of a few semi-continuous to discontinuous, moderate amplitude, dipping reflectors which are set in an acoustically transparent background. Unit 4 is bounded at the base by a gently dipping moderate to high amplitude semi-continuous reflector, and the top by the high amplitude undulating B# unconformity. Both the base and top of the unit are structurally modified, and in places the surfaces merge to form topographic lows. Seismic imaging through the unit is quite poor, although resolution increases in areas where packages of Unit 4 thin near areas of structural/stratigraphic pinch-out (Figure 2.5). The unit is only observed in the southwest and south-central portions of the Adana Basin at depths of 0.4 to 1.9 seconds TWT.

Megasequence 3 (MGS3)

Megasequence 3 forms the uppermost seismic megasequence in the Adana Basin. The megasequence is bounded at the base by the B3 unconformity. The MGS3 succession ranges from 0 to 2.5 seconds TWT in vertical thickness. The characteristics of seismic Unit 5 are outlined below.

Unit 5

Unit 5 is represented by parallel, horizontal to inclined, moderate to high amplitude continuous reflectors (Figure 2.5). The unit exhibits a uniform sheet-like external geometry and evidence of local onlap, apparent downlap and erosional down-cutting is seen in different

locations. The unit is bounded at the base by B3 along the basin edges in the southwest and local unconformities in the east. Toward the south, contact relations between Unit 5 (MGS3) and Unit 3 (MGS2) become conformable in the south-central portion of the basin. The uppermost portion of Unit 5 becomes chaotic, discontinuous and parabolic near its upper bounding surface, which is seen to be the upper limit of the seismic profiles (0 seconds TWT). Thickness of Unit 5 ranges from 0 to 0.8 seconds TWT in most areas but increases to 2.5 seconds TWT in the south.

Regional Seismic Unconformities

B1

The B1 unconformity is a high amplitude, fragmented but laterally continuous hard reflector (Figs. 2.8 to 2.10). It exhibits an irregular to rolling topography throughout the basin, and ranges in depth below surface from 0 to 0.5 seconds TWT at the north-eastern and north-western basin edges to 4.0+ seconds TWT in the central and southern portions of the basin. Units below the B1 unconformity are often show evidence of erosional truncation, and units above B1 lie in angular unconformity with those below (Figs. 2.8 and 2.10). Along the eastern basin edge B1 becomes disconformable as units above and below the marker become parallel (eg. Figure 2.10 a).

B2

The B2 unconformity is a smooth dipping, occasionally fragmented, laterally

continuous reflector which exhibits local variation in amplitude and morphology (Figs. 2.8 to 2.11). The marker varies from a very hard continuous dipping single reflection (Figure 2.8 a and 2.9 b) to moderate amplitude semi-continuous stacked twin reflectors that form wedge morphologies (Figure 2.11 a, b). The B2 marker ranges in depth below surface from 0 to 0.7 seconds TWT in the northeast to 1.0 to 2.5⁺ seconds TWT in the central and southern portions of the basin. Units below the B2 surface are often truncated and lie in angular unconformity with overlying units (Figure 2.8 a), however to the south the seismic marker decreases in amplitude and becomes conformable at depth.

B3

The B3 unconformity is a rolling semi-continuous moderate to high amplitude reflector that forms the base of seismic megasequence 3 (Figure 2.5). The marker varies in depth below surface from 0 to 2.0 seconds TWT and is present only along the southwestern and south-central portions of the basin. Contact relations of units above and below B3 are unconformable near the basin edge but become conformable in the south. B3 is cut by a number of faults and Unit 5 exhibits onlap and growth features above elevated portions of the B3 seismic unconformity.

2.2.2 Geographic Distribution of Seismic Features

The preceding descriptions of seismic features in the Adana Basin reflect observations that are based on the interpretation of two dimensional seismic profiles. A three dimensional,

regional distribution of the seismic succession can also be revealed in many parts of the basin through gridding, cross-line correlation, and subsurface mapping of selected seismic features. The lateral and vertical extent of many of these features is revealed in time-structure maps of the B1 and B2 seismic unconformities (Figs. 2.6 and 2.7), and vertical thickness maps of megasequence 1 and Unit 1 (Figs. 2.12 and 2.13).

Regional Seismic Unconformities

The seismic succession of the Adana Basin is divided locally or regionally by the B1, B2 and B3 seismic unconformities as described in Section 2.2.1. The three dimensional character of these markers can provide valuable tectono-stratigraphic clues as to how topography may have influenced the depositional style of overlying units. Figures 2.6 and 2.7 represent depth from a horizontal surface datum ($t = 0$ seconds TWT) to the B1 and B2 regional unconformities consecutively. Limited data coverage over the restricted B3 unconformity has prevented the development of a comprehensive map of the B3.

B1

The B1 seismic marker is a surface which occurs as a deep NE-SW trending trough with maximum depths below the horizontal datum ($t = 0$) approaching 4 seconds TWT (Figure 2.6). The marker extends outside the study area to the north, south and west, but terminates along an elevated mappable edge to the east. The trough-shaped marker shows

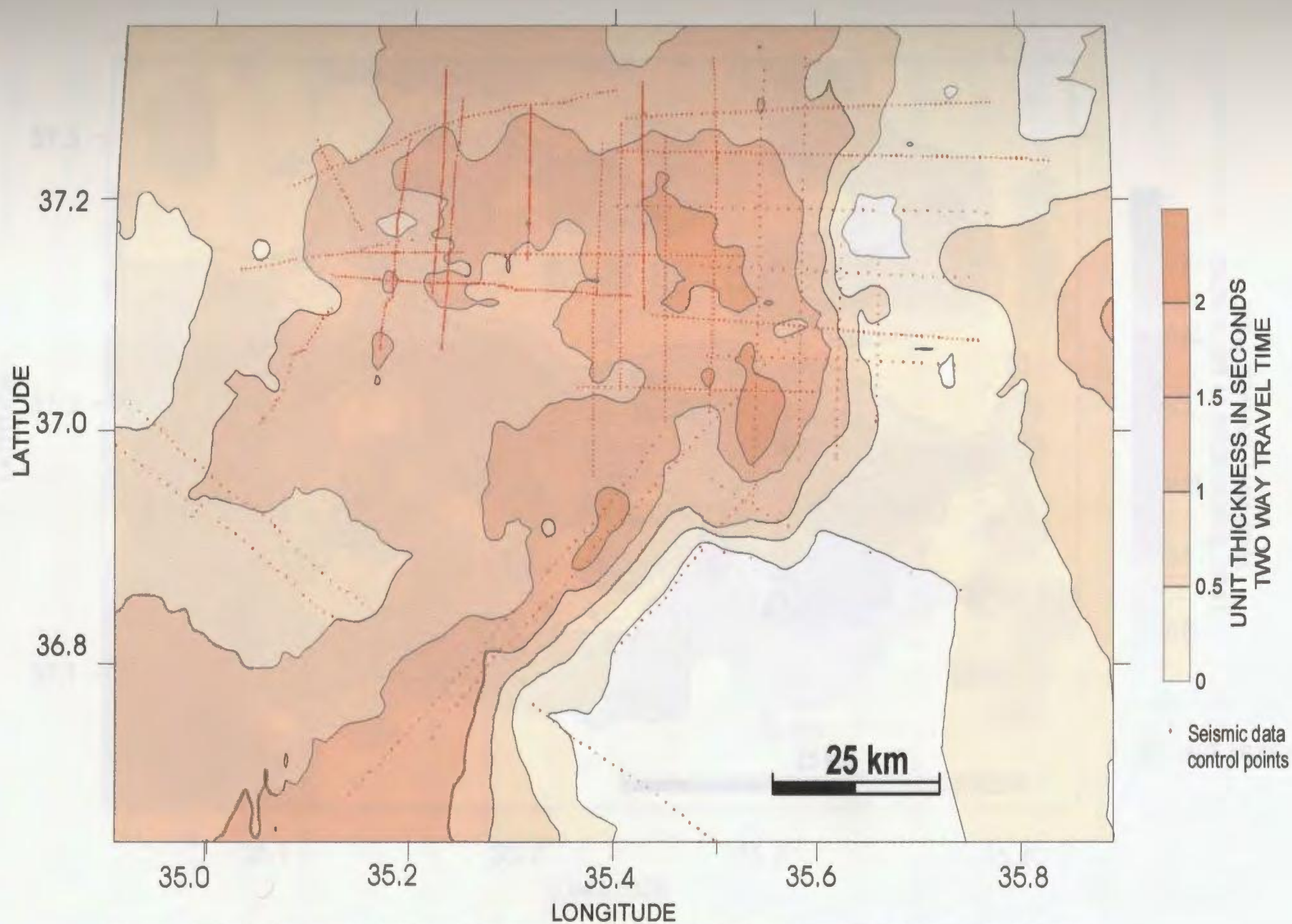


Figure 2.12: Thickness distribution map of seismic Megasequence 1 (interval between B1 and B2 seismic unconformities). Vertical thickness in seconds, TWT. Note the wedge - shaped morphology of Megasequence 1, which thickens eastward before thinning abruptly and/or terminating against the eastern basin edge.

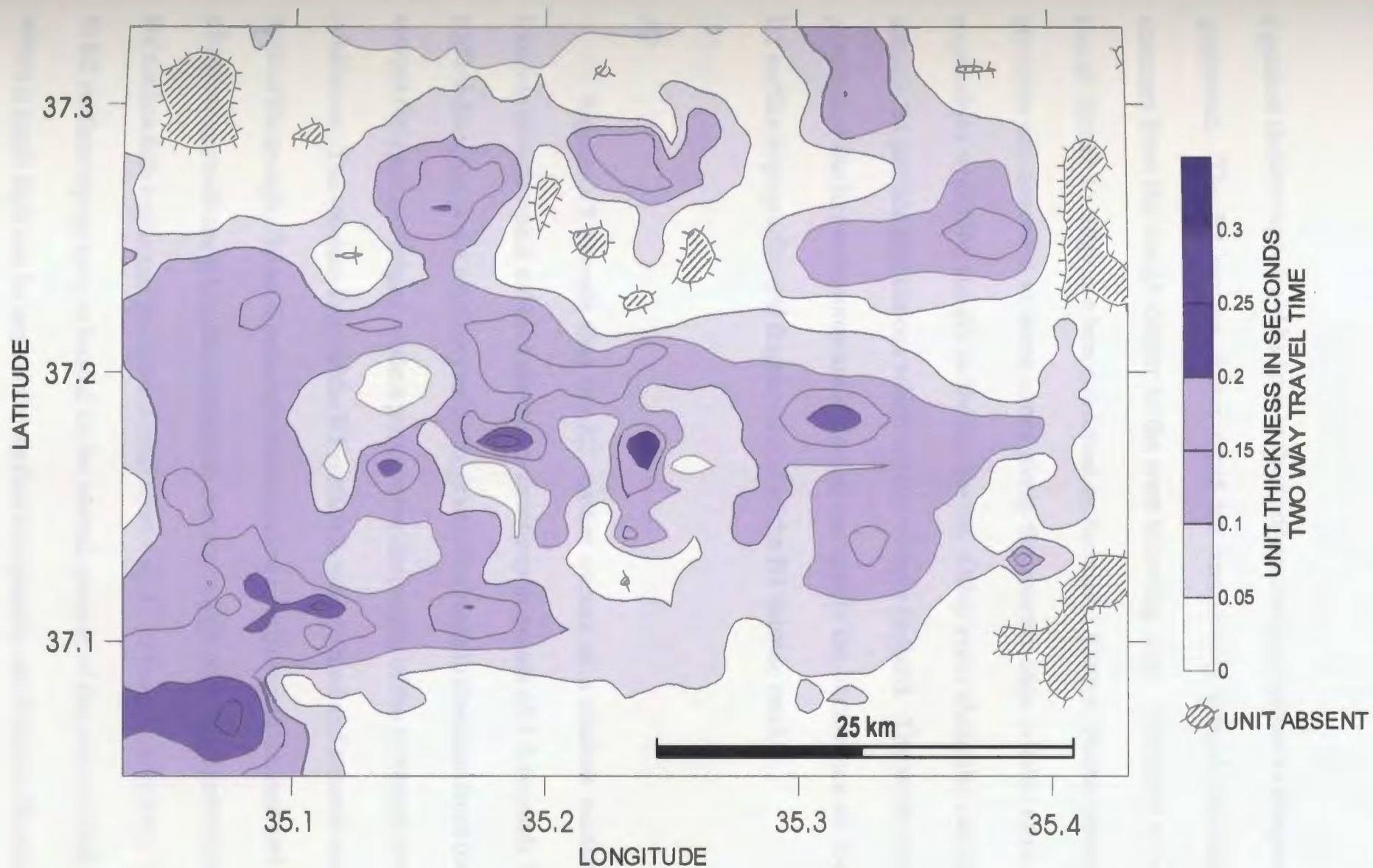


Figure 2.13: Thickness distribution map of the seismic Unit 1 in the northwestern portion of the study area. Vertical thickness in seconds, TWT. Note the east-west trending thickness distribution of Unit 1 within the map area. Refer to Figures 1.18 and 2.6 for seismic control in the northwestern portion of the study area.

a gradual shallowing toward its apex in the northeast and a progressive deepening toward the southwest. The B1 surface shows rapid but consistently spaced increases in elevation contours from the trough center to the west bounding edge. Elevation increases from the trough center to edge are less consistent in the east. Abrupt, closely spaced increases in elevation are observed in some areas along the eastern edge which result in B1 surface expressions which dip steeply to the northwest. Other areas along the eastern edge exhibit arcuate B1 surface expressions which are less steeply inclined. The north and northwestern portions of the basin demonstrate a marked increase in the occurrence of local variation in B1 surface topography and fragmentation of the B1 seismic marker.

B2

Figure 2.7 reveals that the B2 marker occurs as a shallow northeast-southwest trending trough which exhibits elevation variations in excess of 2.5 seconds TWT. The B2 surface demonstrates a relatively uniform, gradual increase in elevation from the trough center toward the apex and edges, while a progressive deepening of the surface is noted toward the southwest. The western limit of the B2 surface is well defined and extends northward to the apex of the trough. B2 surface terminations are less continuous in the east and the B2 surface often merges with the B1 surface along the eastern trough edge. The terminating edge of the B2 surface falls inside and southward of all observed B1 surface terminations. Local variation in B2 surface topography is limited to the central portion of the eastern flank of the trough, where a small high can be seen in the surface topography and frequent fragmentation of the

B2 marker is observed.

B3

The B3 seismic marker is observed only along the southwest and south-central portions of the basin. Seismic imaging indicates that the marker forms an irregular undulating surface which exhibits rapidly increasing depth toward the south-central portion of the basin. The traceable western limit or surface terminations of the B3 marker falls inside and southward of all observed B2 surface terminations.

Seismic Succession

The regional distribution of the seismic succession of the Adana Basin will be described in relation to the distribution of the seismic markers which divide it. Figure 2.6 represents depth to the B1 surface from a horizontal datum ($t = 0$ TWT), but it also provides information about the overlying succession which is bounded at the base by the B1 surface and the top by the present day surface of the earth ($t = 0$ TWT). The figure indicates that the seismic succession above the B1 surface fills topographic lows, and forms a northeast-southwest trending deposit with vertical thicknesses that range from 0 to 4.0 seconds TWT. The total seismic succession is divisible into three megasequences as outlined in Section 2.2.1.

Seismic Megasequences and Units

Seismic Basement

Seismic basement is observed in all locations throughout the basin. The unit underlies B1 and B2 directly along the western, northern and eastern boundaries of the study area and represents the outermost identifiable seismic interval along the basin edge.

Megasequence 1

Megasequence 1 lies directly above the B1 surface throughout the basin, and forms an irregularly shaped NNE-SSW trending deposit (Figure 2.12). The megasequence displays a wedge-shaped external geometry and maximum vertical thicknesses of the deposit exceed 2.2 seconds TWT. The deposit extends out of the study area to the northeast and southwest and is thickest in the northeast. The megasequence thins and terminates gradually from the center to western edge across widely spaced thickness contours but from the center to the eastern edge it thickens to 2.2 + seconds TWT and then terminates abruptly in a wedge-like geometry against seismic basement highs. The thickest parts of megasequence 1 occur in two northeast-southwest trending depressions, which extend along the eastern and northern basin edges. These depressions are separated by a small ridge with a similar orientation. The larger depression reveals an irregular internal geometry, where contour lines extend outward toward the northeastern and eastern deposit edges with trough-like geometries. Crossing line ties indicate that Unit 2 shows a gradual thickening toward the south and central portions of the basin and abrupt thinning toward the basin edges.

The regional distribution of Unit 1 is best observed in the northern portion of the basin. Unit 1 is also apparent in the central and eastern portions of the basin, however the unit is not imaged in the southern portion of the basin, where it descends to depths of greater than 4.0 seconds TWT. Figure 2.13 presents a high resolution time-isochore map of Unit 1 in the northwest corner of the Adana Basin. The map indicates an east - west trend in the distribution of Unit 1 mounds in the study area; on a regional scale Unit 1 deposits are often observed in association with local topographic highs of the underlying seismic basement (Figure 2.8 a).

Megasequence 2

Megasequence 2 (Units 3 and 4) is bound at the base by the B2 surface and at the top by the B3 unconformity (in the south) and the present day surface of the earth (in the north) as discussed in Section 2.2.1. The deposit exhibits a broad clastic wedge-shaped geometry which partially fills the trough formed by the B2 unconformity. The megasequence is thinnest along the basin edges, but thickens 1.0 seconds TWT in the south-central portion of the trough. Megasequence 2 exhibits different external geometries in different parts of the basin. The unit occurs as a series of thin, stacked lenticular wedges along the northern basin edge,, as inclined sheets in the south-central portion of the basin, and as oblique clinoforms adjacent to steeply inclined portions of the eastern basin edge. Unit 4 is limited to the southwestern portion of the basin and occurs in a series of NNE-SSW trending roller and pillow features below the B3 unconformity. The terminating edge of megasequence 2 is prominent in the

west and is traceable up to the northernmost tip of the deposit, where it extends outside the study area. The depositional edge of Megasequence 2 is located south of the Megasequence 1 deposit edge, which extends northward beyond the limit of the study area. The terminating edge of Megasequence 1 deposit reappears close by on the eastern side, but is located east relative to the Megasequence 2 deposit edge.

Megasequence 3

Megasequence 3 (Unit 5) is bound at the base by the B3 unconformity and at the top by the present day surface of the earth as discussed in Section 2.2.1. The deposit is largely confined to the southern portion of the Adana Basin, where it forms the uppermost seismic fill to the trough formed by the B2 unconformity. Megasequence 3 appears to reflect halokinetic movements of Unit 4 (MGS2), that may have contributed to local folded geometries observed in the otherwise uniformly-dipping Unit 5 seismic interval. Unit 5 forms a broad sheet-like deposit that thickens southward, and thins toward the basin edges.

Section 2.3 : Correlation of Surface And Seismic Data

The stratigraphy of the Adana Basin has been described separately in terms of surface data (Section 2.1) and seismic data (Section 2.2). These surface and seismic data will be reconciled to address the temporal and spatial relationships that exist within the Miocene succession in the Adana Basin. Correlation of existing lithostratigraphic surface data and seismic subsurface data is proposed through linkage of unconformable surfaces described in

outcrop (previous work), with those observed in seismic profiles (this study). Once these surfaces are correlated, many individual seismic and lithostratigraphic units are also correlated based on similarity of features, such as external geometry, stratigraphic position and regional distribution.

2.3.1 Correlation and Chronology of Seismic Markers and Units

A number of lithostratigraphic contacts and seismic markers have been described in the Miocene succession of the Adana Basin (Sections 2.1 - 2.2). Four prominent unconformities identified within the Neogene sedimentary succession of the Adana Basin, are correlated with three prominent seismic unconformities (B1, B2 and B3) identified in the seismic succession (Table 2.5). Correlations are based on similarity of stratigraphic position and regional distribution, as follows:

B1

The B1 seismic unconformity is regarded as a composite unconformity that is correlated with the base Miocene erosional unconformity and the often-synonymous lower Miocene time-transgressive unconformity (Section 2.1; Table 2.5). This correlation is based on a number of shared criteria, which include: (i) stratigraphic position - at the base of a thick sedimentary succession and associated with lenticular Unit 1 deposits, which occur in association with basement highs, (ii) contact relations - no observed erosional down-cutting of underlying units; variable apparent downlap and onlap relations with overlying strata (iii)

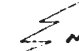
SEISMIC UNIT	SEISMIC SEQUENCE	TIME			LITHOLOGIC UNIT
UNIT5	MGS3	Q	QUATERNARY	Q	KURANSA FM
		P	PLIOCENE	P	HANDERE FM
B3					MESSINIAN U/C
UNIT4	MGS2	M	MESSINIAN	M	GOKKUYU GYPSUM MB
UNIT3		I	TORTONIAN	I	KUZGUN FM
B2		O		O	TORTONIAN REGRESSIVE U/C
UNIT2	MGS1	C	SERRAVALIAN	C	GUVENC FM
		E	LANGHIAN	E	CINGOZ FM
N E		BURDIGALIAN	N E	Progressive Unconformities  KARAISALI FM	
UNIT2					KAPLANKAYA FM
			AQUITANIAN		GILDIRLI FM
B1					BASE MIOCENE U/C
SEISMIC BASEMENT	-----		PRE-MIOCENE		KARSANTI FM + Mezosoic and Paleozoic Basement complexes

Table 2.5: Correlation of seismic markers and lithostratigraphic markers

regional distribution - the B1 surface is present basin wide, but is most apparent in the east and less pronounced in the west. Figure 2.2 indicates the position of the merged base Miocene - time-transgressive B1 unconformity in space and time, and demonstrates that this composite surface represents the late Burdigalian to Serravalian time interval. This surface is equivalent to the D Ia denudational surface of Erol, (1990).

B2

The B2 seismic unconformity is correlated with the Middle Miocene regressive unconformity described in Section 2.1 (Table 2.5). Shared characteristics include: (i) stratigraphic position - located in the middle of the thick sedimentary succession, (ii) contact relations - down-cutting erosional truncation of underlying units; onlap of overlying units, (iii) regional distribution - surface is prominent throughout the north-central portion of the basin, but loses its characteristic seismic signature within a conformable succession toward the south. Figure 2.2 indicates that the B2 regressive unconformity formed during the late Serravalian to mid-Tortonian interval. The Middle Miocene B2 unconformity is equivalent to the D Ib denudational surface of Erol, (1990).

B3

The B3 seismic unconformity is equivalent to the prominent, laterally restricted Messinian unconformity in the Adana Basin (Section 2.1; Table 2.5) on the basis of the following shared criteria: (i) stratigraphic position - located above both the transgressive B1

and regressive B2 unconformities in the upper part of the thick sedimentary succession, (ii) contact relations - erosional truncation at the basin edge; onlap of overlying units throughout (iii) regional distribution - surface is observed only along the south-western flank of the basin. The Messinian B3 unconformity corresponds to the DII denudational surface of Erol, (1990).

The seismic megasequences described in Section 2.2 have also been tied to the lithostratigraphy. These correlations are in accordance with the correlation and chronology of the seismic markers which bound them, as outlined in Section 2.3.1 (Figure 2.2; Table 2.6).

2.3.2 Comments on Well Data

Well data (e.g. cross sections, well logs, synthetic seismograms) obtained from Turkish Petroleum Corporation (internal reports) and Pralle (1995) reveal lithostratigraphic and depth information that is useful in tying the surface and seismic data together (Appendix B). Pralle examined well data provided by Turkish Petroleum Corporation in a modern context and used these data to generate synthetic seismograms/time-depth curves for the basin. These new time-depth conversions have allowed for increased accuracy in correlation of wells to seismic data and have provided a useful reference that lends further support to the correlations proposed in Section 2.3.1. A tabulated summary of well data, lithological contacts and correlations with seismic unconformities is presented in Appendix B.

2.4 Sequence Stratigraphy

The Miocene succession of the Adana Basin is divisible into three distinct

Table 2.6: Correlation of seismic megasequences, lithologic formations and seismic units

Seismic Megasequence	Lithostratigraphic Formations	Seismic Units
Megasequence 3	Kuraşa Formation Handere Formation (excluding the Gökkuyu Gypsum member)	Unit 5 Unit 5
Megasequence 2	Handere Formation (Gökkuyu Gypsum member only) Kuzgun Formation	Unit 4 Unit 3
Megasequence 1	Cingöz Formation Güvenç Formation Karaisalı Formation Kaplankaya Formation	Unit 2 Unit 2 Unit 1 Unit 2
Acoustic Basement	Gildirli Formation Pre-Miocene Basement	Basement

megasequences (MSQ1 - MSQ3), which overlie a pre-Miocene basement succession (Figure 2.14). MSQ1 forms the lowermost megasequence, and is separated from underlying basement rocks by a Type II sequence boundary (Van Wagoner et al., 1988), which represents a rate of eustatic fall less than or equal to the rate of basin subsidence. This boundary extends northward beyond the limits of the study area and is correlated with seismic megasequence 1 (MGS1). In contrast, MSQ2 is bounded at the base by a Type I sequence boundary (Van Wagoner et al., 1988), where the rate of eustatic fall exceeds the rate of subsidence. This boundary truncates underlying strata in the north-central portion of the basin, but becomes a correlative conformity in the southernmost portion of the basin. MSQ2 is correlated with seismic megasequence 2 (MGS2). MSQ2 thins to the north and terminates basin-ward of the underlying MSQ1 succession. MSQ3 forms the youngest megasequence in the Adana Basin, and is separated from MSQ2 by a marine flooding surface that followed the climax of widespread dessication of the Mediterranean Sea. MSQ3 thins toward the north, and is correlated with seismic megasequence 3 (MGS3). The sequence stratigraphic character of each megasequence is examined in further detail below.

MSQ1

The lower sequence boundary of the MSQ1 corresponds with the time transgressive B1 seismic marker and represents a period in which successive early - middle Miocene transgressive deposits of seismic megasequence 1, progressively onlapped basement rocks in a northwesterly (landward) direction (Figure 2.14). The lowermost portion of the MSQ1 is comprised of aggradational early Miocene deposits (Kaplankaya and Karaisali formations),

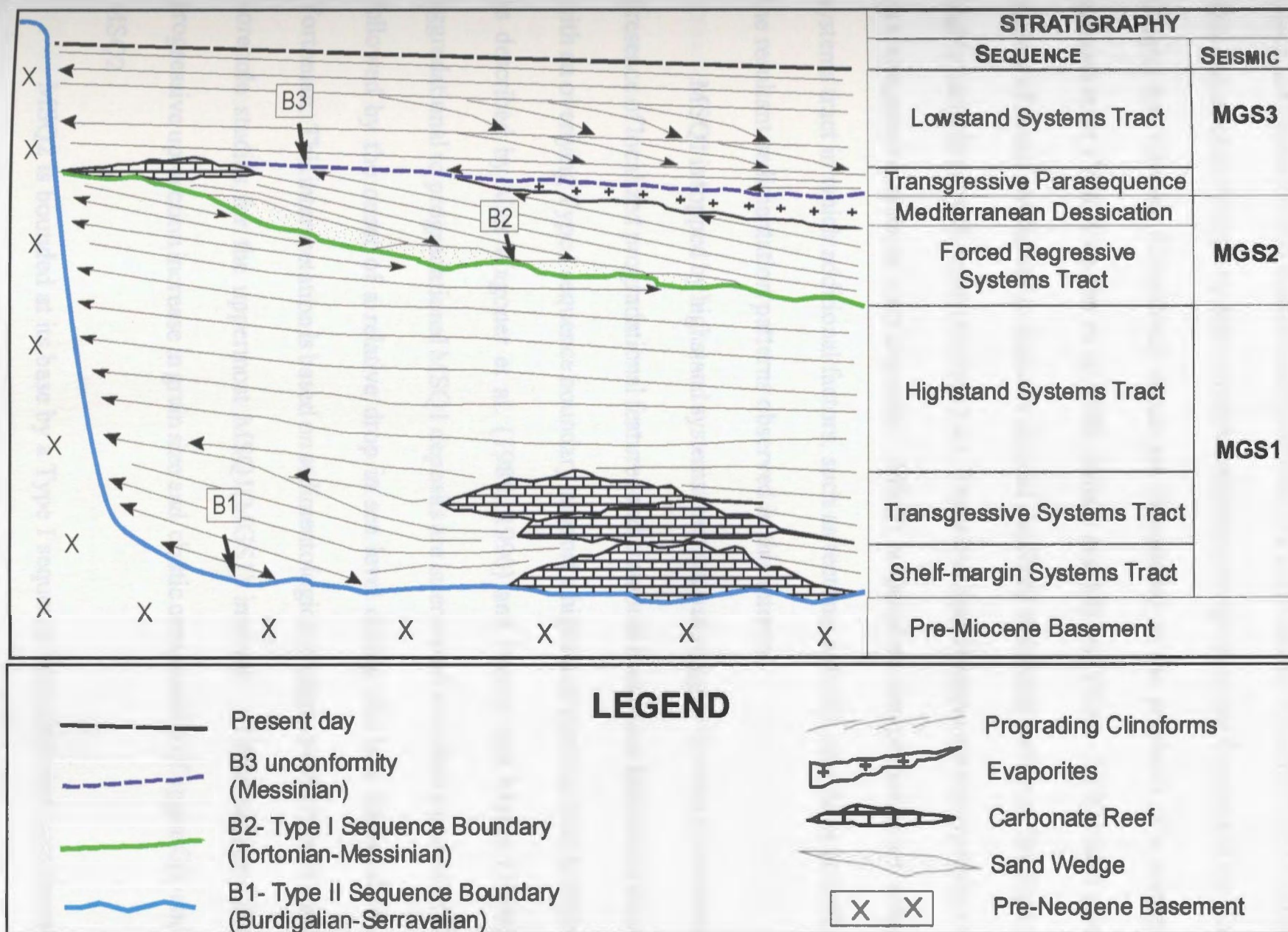


Figure 2.14: Schematic sequence stratigraphic framework for the Adana Basin. Note the location, timing and nature of sequence bounding surfaces (eg. B1, B2; B3) within the Miocene succession.

which are interpreted as depositional products of a shelf-margin systems tract (Figure 2.14). This sequence is overlain by early - middle Miocene retrogradational deposits of the Karaisalı, Cingöz and Güvenç formations, which are interpreted as the products of a transgressive systems tract (Van Wagoner et al., 1988, Emery and Myers, 1996). MSQ1 also contains a variety of lesser stratigraphic features such as localized erosional surfaces, fan deposits and highly variable growth strata (Section 2.2). These localized features are not typically reported in transgressive systems tract deposits. MSQ1 is therefore interpreted as a transgressive systems tract in which additional factors, such as tectonic activity, may have contributed to the resultant sedimentation patterns observed in this interval.

MSQ1 is topped by highstand systems tract deposits (upper Güvenç Formation). The presence of localized progradational features and erosional truncation features in association with an overlying Type I sequence boundary support a highstand systems tract interpretation as described by Van Wagoner et al. (1988, 1990) and Emery and Myers (1996). The aggradational to progradational MSQ1 deposits are interpreted to reflect a period of flooding followed by the onset of a relative drop in sea level during the late Serravalian-earliest Tortonian. This interpretation is based on sedimentological changes noted in both surface and borehole studies for the uppermost MSQ1(MGS1) interval. These changes include a progressive up-section increase in grain size and clastic composition of upper Güvenç shales.

MSQ2

MSQ2 is bounded at its base by a Type I sequence boundary that corresponds with the regressive, Middle Miocene B2 unconformity (Figure 2.14). This megasequence

represents a period characterized by relative sea level drop (from moderate to extreme), which resulted in subaerial exposure, erosional truncation and a basin-ward shift in facies during the Tortonian to Messinian interval. The B2 unconformity forms an abrupt contact between terrestrial / shallow marine clastics and underlying deeper marine shales of the MSQ1 Güvenç Formation. The basal sequence of MSQ2 (MGS2) is comprised primarily of terrestrial redbeds and shoreface deposits of the Tortonian to base Messinian-aged Kuzgun Formation. The regressive nature of MSQ2, in conjunction with the presence of stranded sand wedges above the B2 unconformity, is consistent with architectures that are deposited during a Forced Regressive systems tract on a ramp margin (Emery and Myers, 1996). Posamentier et al., (1992, 1993) indicate that forced regressive sand wedges of the Forced Regressive systems tract form during sealevel fall along a ramp margin, where there is no bypass of sediment to the basin floor.

The regression recorded by MSQ2 climaxed in the Late Messinian interval with the dessication of the Mediterranean Sea, precipitation and deposition of the Gökkuyu Gypsum Member evaporites, and subaerial to terrestrial erosion of newly exposed MSQ1 and MSQ2 strata. MSQ2 is bounded at the top by the B3 unconformity, which represents the upper limit of Mediterranean dessication and evaporite deposition in the Messinian (Table 2.2, Figs. 2.5; 2.14).

MSQ3

MSQ3 is bounded at its' base by a combination erosional unconformity reworked at

a marine flooding surface, which corresponds with the laterally restricted, Late Messinian B3 unconformity (Figure 2.14). Basal MSQ3 strata that onlap eroded MSQ2 strata and MSQ2 evaporites represent a transgressive parasequence, which reflects the return of the Mediterranean Sea to the southern portions of the Adana Basin during the Late Messinian (Figure 2.5). The upper limit of this parasequence is represented by a subtle maximum flooding surface, above which, progradational fluvial-deltaic deposits of the Handere (Pliocene) and Kuranşa (Recent) formations occur. The stratigraphic architecture of the prograding deposits is consistent with a lowstand systems tract interpretation as described by Van Wagoner et al. (1988, 1990) and Emery and Myers (1996). The remainder of MSQ3 is characterized by terrestrial-fluvial-deltaic deposits, and the present-day position of the shoreline reflects the continued regressive character of MSQ3.

CHAPTER 3: STRUCTURAL GEOLOGY

A variety of geological structures are present within the Miocene succession of the Adana Basin (Williams, 1995; Pralle, 1995). This statement has an important implication for the stratigraphic observations reported in Chapter 2, which have not yet been examined for evidence of structural deformation. The data presented in Chapter 2 therefore reflect the present day, deformed state character of the Miocene succession. At this time it is appropriate to shift our focus to the distribution and structural style of prominent geologic structures which affect the Miocene succession. A number of structures have already been reported (Chapter 1, Section 1.3), however advances in data accessibility, data quality and seismic interpretation techniques have warranted a reinvestigation of the structural geology of the Adana region. Chapter 3 presents the findings of this investigation and includes a summary of structural features that are identified within the basin. The structural-stratigraphic architecture of these features is examined and when possible, the timing of deformation is constrained.

3.1 Identification of structural features

The stratigraphic analysis presented in Chapter 2 has contributed to our understanding of the position, continuity and chronology of a number of critical stratigraphic horizons throughout the basin. In the structural analysis presented in this chapter these critical markers are examined for evidence of structural truncation, offset, duplication, or absence on both

local and regional scales. The reader is referred to Appendix C for a review of the sub-surface mapping techniques used in this study.

3.2 Structural features in the Adana Basin

A minimum of three different structural features affect at least three different stratigraphic levels within the Miocene succession of the Adana Basin. These features have been identified in seismic reflection profiles and mapped to reveal geographic distribution trends. Figure 3.1 represents the horizontal map projection of prominent structural features observed within the Adana Basin. The figure illustrates that the study area is comprised of three distinct structural domains. Listed clockwise from the northwest, these domains are: the Northern Domain, the Eastern Domain and the Southern Domain (Figure 3.1). Major defining attributes for each structural domain include i) which critical stratigraphic markers are deformed and ii) which type and class of faults appears to dominate that deformation. Other diagnostic attributes include: i) the frequency, trend and distribution of structural features, ii) the presence and nature of syntectonic unconformities, iii) the presence and nature of onlap, offlap, and growth stratal patterns, and iv) observed associations with specific seismic units or features. The structural-stratigraphic attributes observed in the Northern, Eastern and Southern domains are summarized in Table 3.1 and addressed in Sections 3.2.1-3.

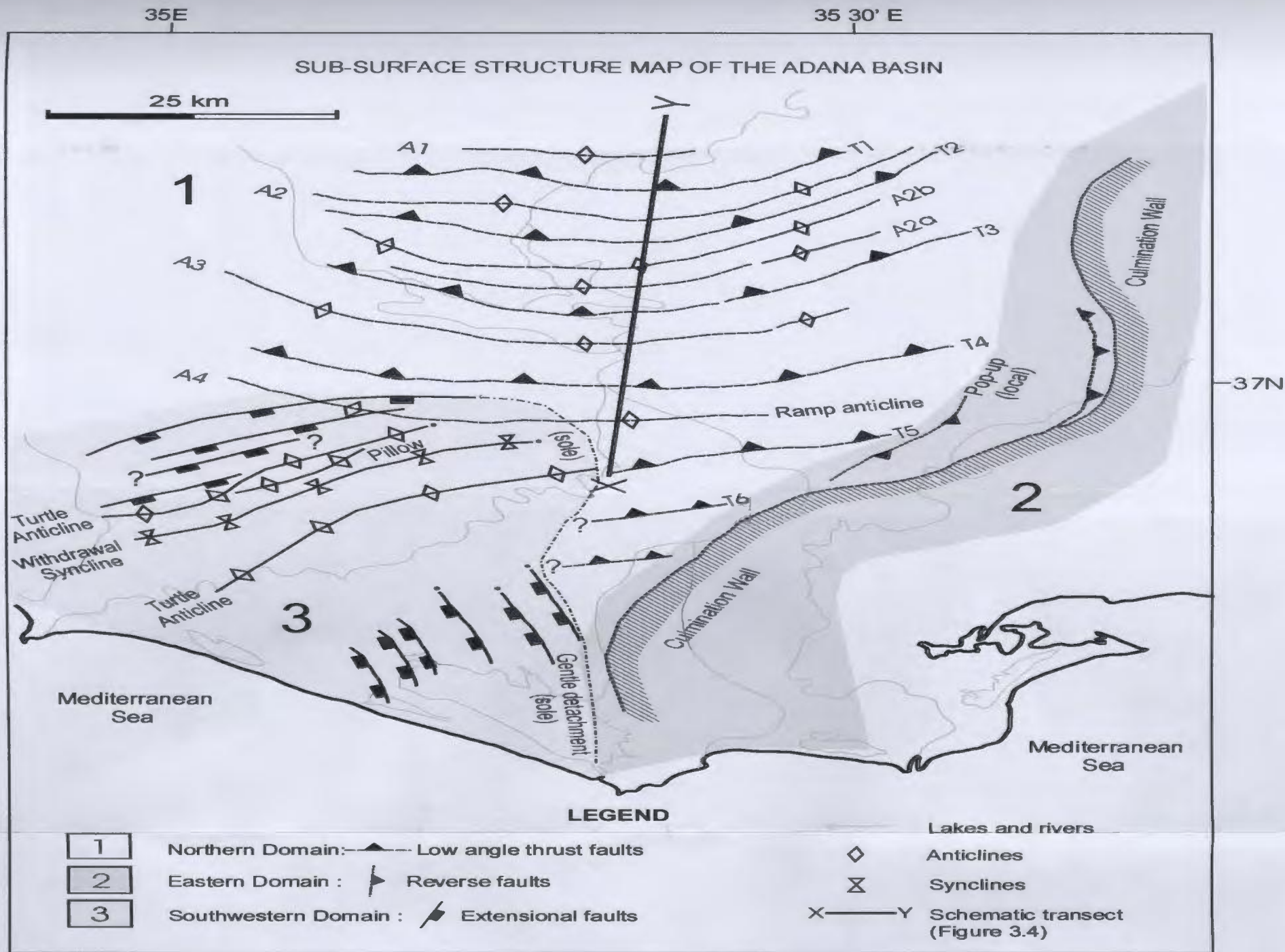


Figure 3.1: Structural Domains of the Adana Basin. Note location of schematic X-Y transect (Figure 3.4).

Table 3.1: Structural stratigraphic attributes of the Northern, Eastern and Southwestern Domains. Y = imaged in seismic profiles; N = not imaged in seismic profiles.

Attributes	Structural provinces of the Adana Basin		
	Northern Domain	Eastern Domain	Southwestern Domain
Location in study area	North & Central Adana Basin	Eastern flank of Adana Basin	South & Southwest Adana Basin
Dominant structural features	ramp anticline-syncline pairs	reverse-faulted structural high	extensional fault fan; rollover anticline
Fault class	low angle thrusts	i) reverse faults ii) minor extensional faults	extensional - listric
Transport direction	S	WNW	SSE
Salt bodies	N	N	salt rollers, diapirs, welds
Deformed unconformity(s)	B1	B1 and B2	B3
Local unconformities	Y	Y	Y
apparent onlap/ folded onlap/ downlap	Y	Y	Y
wedging of strata	medium small	large scale	small scale
bed thickening	Y	Y	Y
carbonate mounds	Y (common)	Y (uncommon)	N
clinoforms	N	Y	N
sub-basins	numerous; small to medium in scale	sub-basins are large in scale	frequent; small scale

3.2.1 Northern Domain

Structure

The most extensive structural domain in the study area is imaged in association with the B1 unconformity, in the northern portion of the Adana Basin (Figs. 3.1 and 3.2). Toward the south, the B1 unconformity descends to depths below surface of greater than 3 seconds TWT, where many of the stratigraphic and structural features of the lower basin fill fall below the limit of fine-scale resolution. Figure 3.2 illustrates the conjugate nature of extensional faults mapped in the Northern Domain. Figure 3.3 is a representative seismic reflection profile which illustrates the dominant structural-stratigraphic architecture observed in the northern domain. This line reveals the deformed nature of the B1 unconformity which occurs in association with a prominent anticline-syncline pair. These topographic basement highs and lows are observed throughout the northern domain and occur in association with underlying low-angle north-dipping fault plane features (Figure 3.3). The fault surfaces exhibit a dip sense that is parallel to the dip of strata on the backlimbs of the anticlines; in the up-dip direction the fault surfaces terminate against the B1 unconformity. Typically, this intersection occurs near the inflection point between the anticline-syncline pair. Upwards-narrowing kink band geometries (Suppe et al., 1991) are also imaged within the seismic strata that surround prominent anticline-syncline pairs (Figure 3.3). On occasion, these bands exhibit an apparent normal fault plane geometry, however closer examination reveals that MGS1 strata are kinked rather than offset along these planes.

A series of arcuate east-west trending thrust sheets and *ramp anticline* ridges have

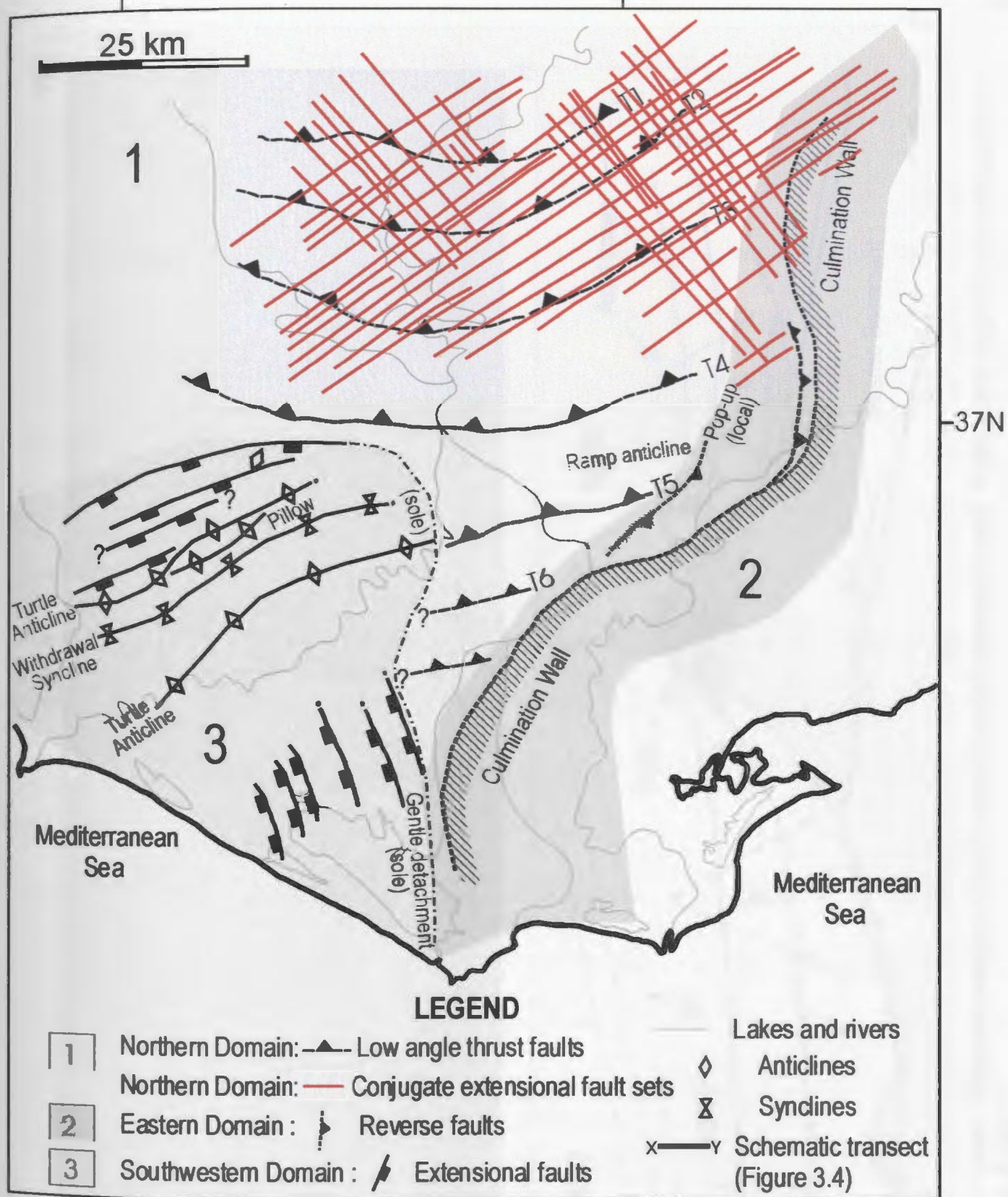


Figure 3.2: Superposition of conjugate extensional fault set trends (in red; mapped by the Eastern Mediterranean Research Group) with fault structures mapped in this study. Refer to Figure 2.11a (Line 8) for representative sub-surface character of the conjugate fault sets.

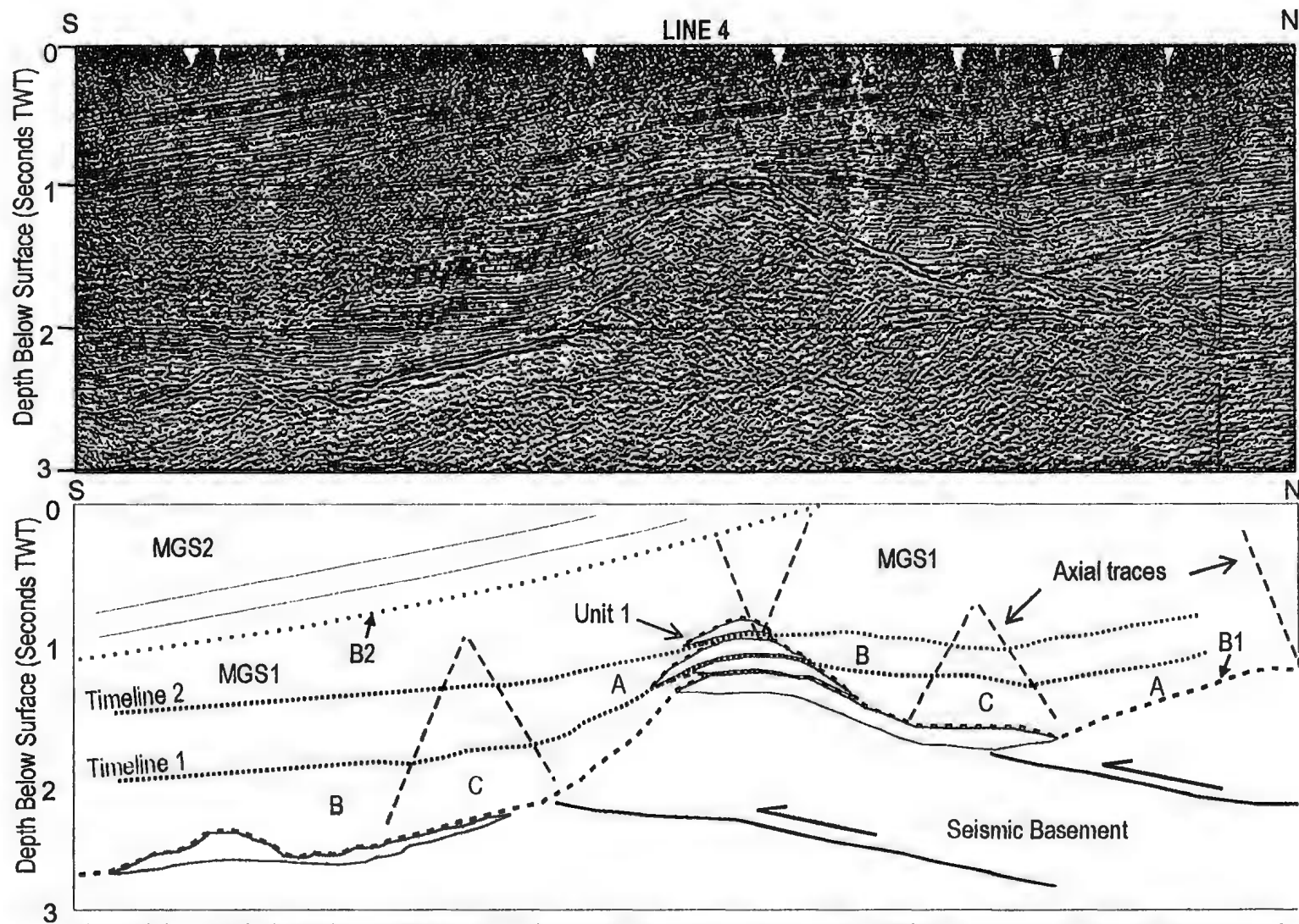


Figure 3.3: Line 4. Note the presence of Unit 1 above thrust basement highs. Refer to text (page 125) for discussion of locations A, B and C.

been mapped across the Northern Domain (Figure 3.1). The structures are mapped relative to the hanging wall cut-offs of the B1 unconformity. Figure 3.4 provides a schematic illustration of the X-Y transect located in the Northern Domain (Figure 2.5). Figure 3.4 indicates that anticlinal ridges A1 to A5 form a stacked succession, within which, the southernmost anticlinal ridge, A5, occupies the lowest stratigraphic position and the northernmost ridge, A1, occupies the highest stratigraphic position (Figure 3.4). Southward of the X-Y transect, the T6 and T7 thrust sheets are noted to exhibit greater structural relief and incorporate younger strata than observed in anticlines A1-A5. The successive, stacked geometry of these basement highs, in conjunction with the position of anticlines above planar ramps and synclines in front of fault plane tips is suggestive of a thrust-dominated structural style in the Northern Domain. These low angle, south-directed thrust sheets display maximum relief in seismic profiles that are oriented in a north-south orientation (Figure 3.3), and display intermediate relief on oblique lines. Little structural relief is observed in seismic profiles that are oriented in an east-west strike direction; in contrast, these lines are dominated by lateral ramp and stacked horizontal thrust sheet geometries that are consistent with south-directed bulk transport. Figure 3.5 reveals the coincident nature of the thick occurrences of Unit 1 mounds and the mapped position of basement-derived ramp anticlines. Unit 1 attains maximum thickness on thrust sheet crests, thins rapidly away from these crests, and is absent in the adjacent leading-edge synclines.

The anticlines depicted Figure 3.4 reflect the position and relief of the basement-derived portion of each structure, which occurs in association with the B1 unconformity. As

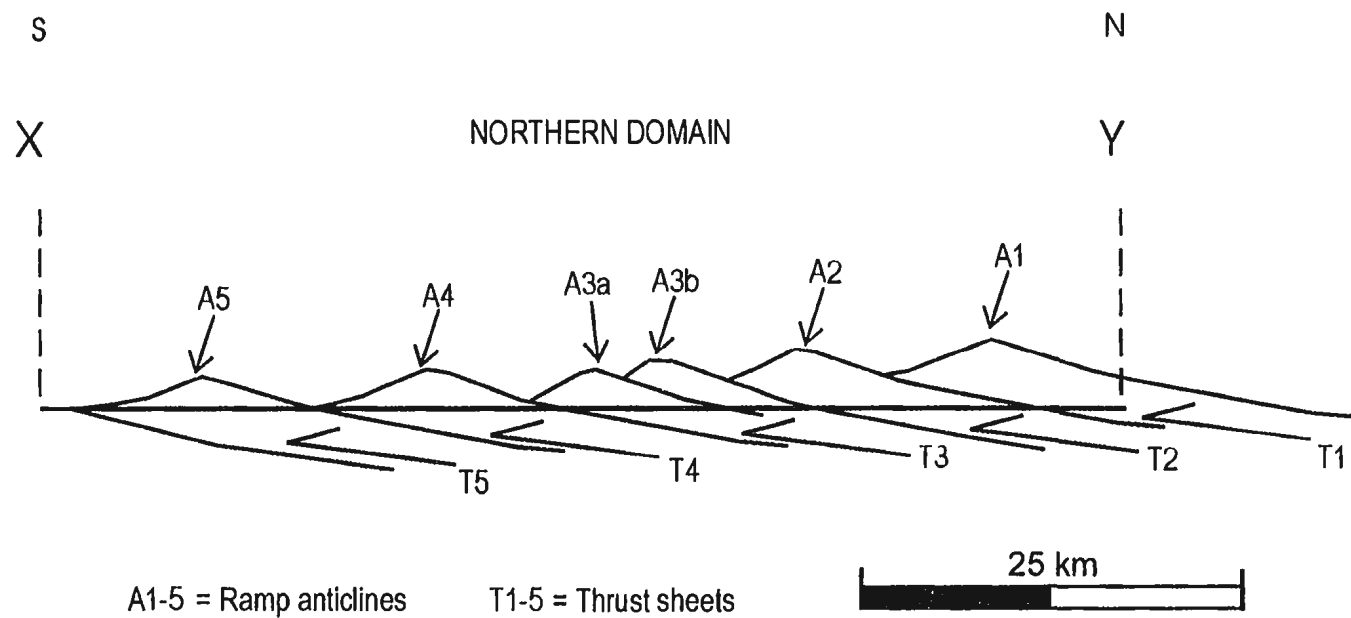


Figure 3.4: Schematic transect X-Y through the Northern Domain of the Adana Basin. Location of transect is indicated in Figure 3.1. Note i) stacked geometry of basement blocks ii) hinterland dipping fault planes, iii) south directed transport direction.

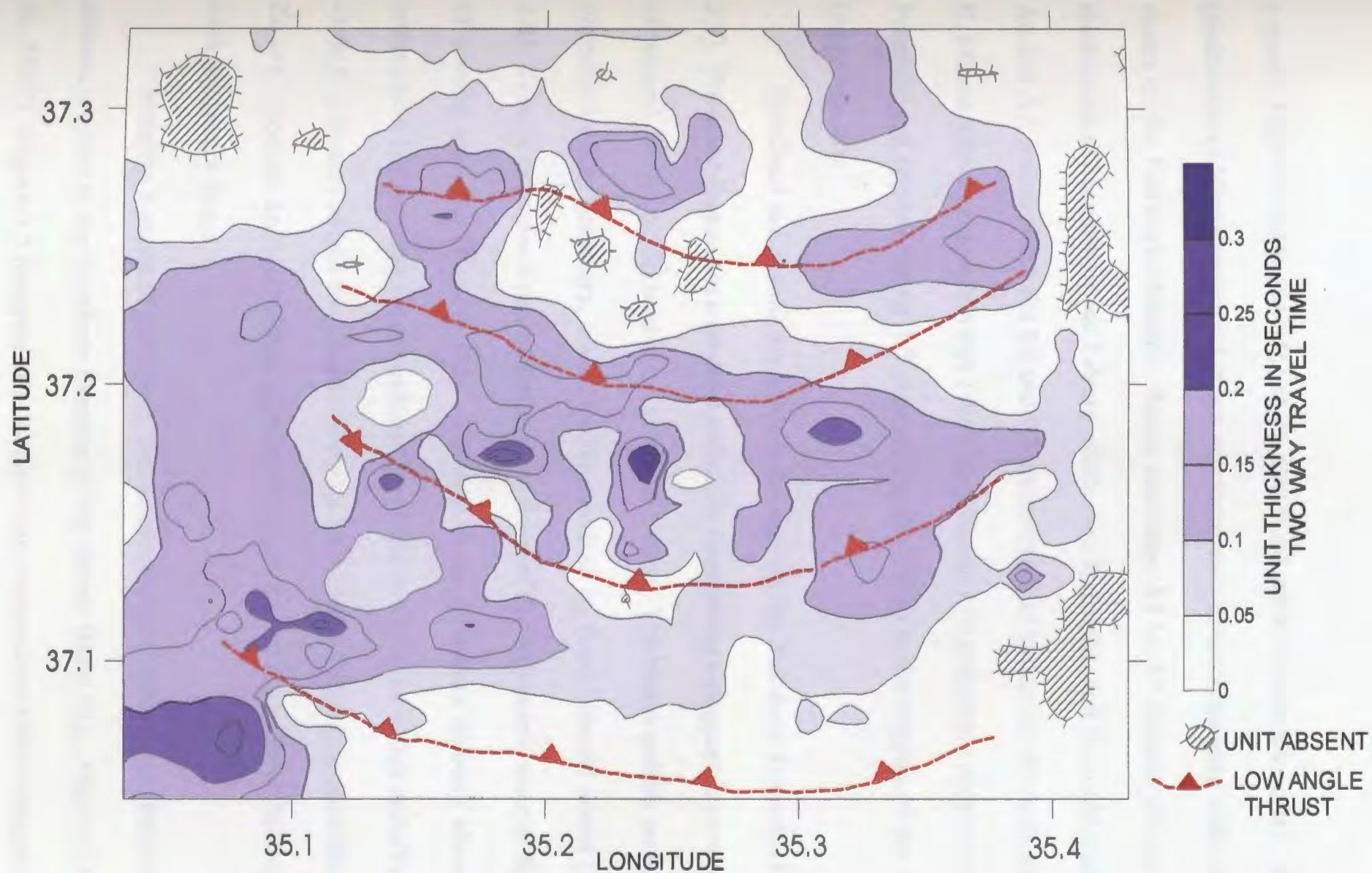


Figure 3.5: Superposition of mapped low angle thrust fault traces and the Unit 1 thickness distribution map (from Figure 2.13) in the north-central portion of the Adana Basin. Note the east-west trend of the thrust fault traces and Unit 1 deposits. In general, Unit 1 deposits thicker than 0.2 seconds TWT occur between successive thrust traces.

a result, Figure 3.4 does not depict the structural relief of units above B1, although varied thicknesses of Megasequence 1 strata are observed within the hanging walls of certain thrust sheets in the Northern Domain. Ramp anticlines A3 to A5 contain progressively greater thicknesses of Megasequence 1 strata within their forelimbs, and the southernmost anticlines, A6 and A7, include both the B1 and B2 unconformities within the forelimb succession. The K. Mihmandar-1 exploration well (Well 10 in Figure 1.7) indicates a repetition of the Kuzgun Formation at approximately 1.5 seconds depth (TWT) in the vicinity of the T6 thrust sheet (Appendix B).

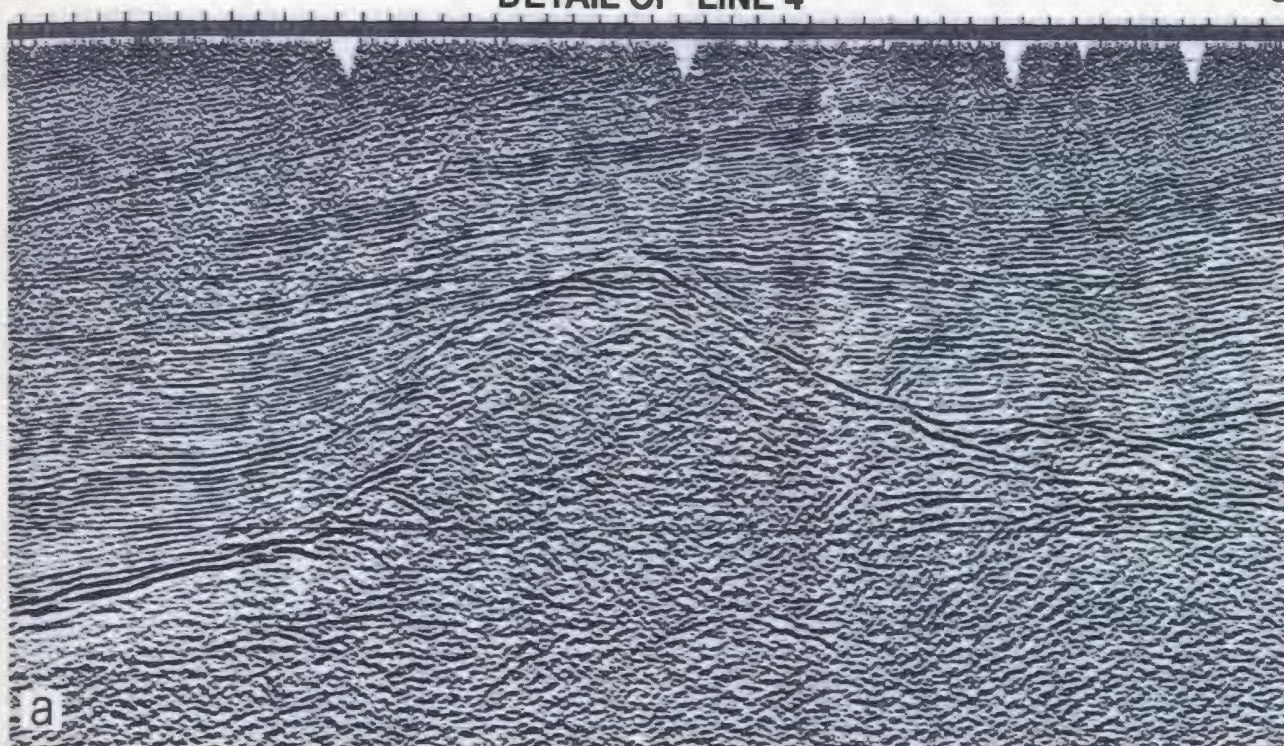
Synclinal sub-basins are evident throughout the Northern Domain (Figures 3.6 and 3.7). These sub-basins are contained within the intervening topographic lows above the series of stacked, basement derived ramp anticlinal ridges. The basins exhibit an internal *piggyback basin* geometry, which is characterized by three internal zones (A - C) (Figure 3.8). Zone A occupies a position directly in front of the prominent, steeply-dipping forelimb of a ramp anticline (Figures 3.3). Notably, Zone A occurs directly above the point of intersection between the B2 unconformity and the thrust faults which underlie the anticlines. Zone B is occurs above the shallow-dipping back limb of the ramp anticline (Figures 3.3). Zone C occupies an intermediate position between Zones A and B in the central portion of each piggyback basin.

Notably, a series of previously described conjugate extensional faults are apparent in seismic profiles in the Northern Domain of the Adana Basin (e.g., Figure 2.11; Williams et al., 1995). Figure 3.2 illustrates the location and orientation of the conjugate faults sets, as

N

DETAIL OF LINE 4

S



N

DETAIL OF LINE 3

S



Figure 3.6: Closeups of a) LINE 4 and b) LINE 3 (see Figures 1.18, 2.8 and 3.3 for location and scale. Note variable stratal architectures in the vicinity of ramp anticline crests.

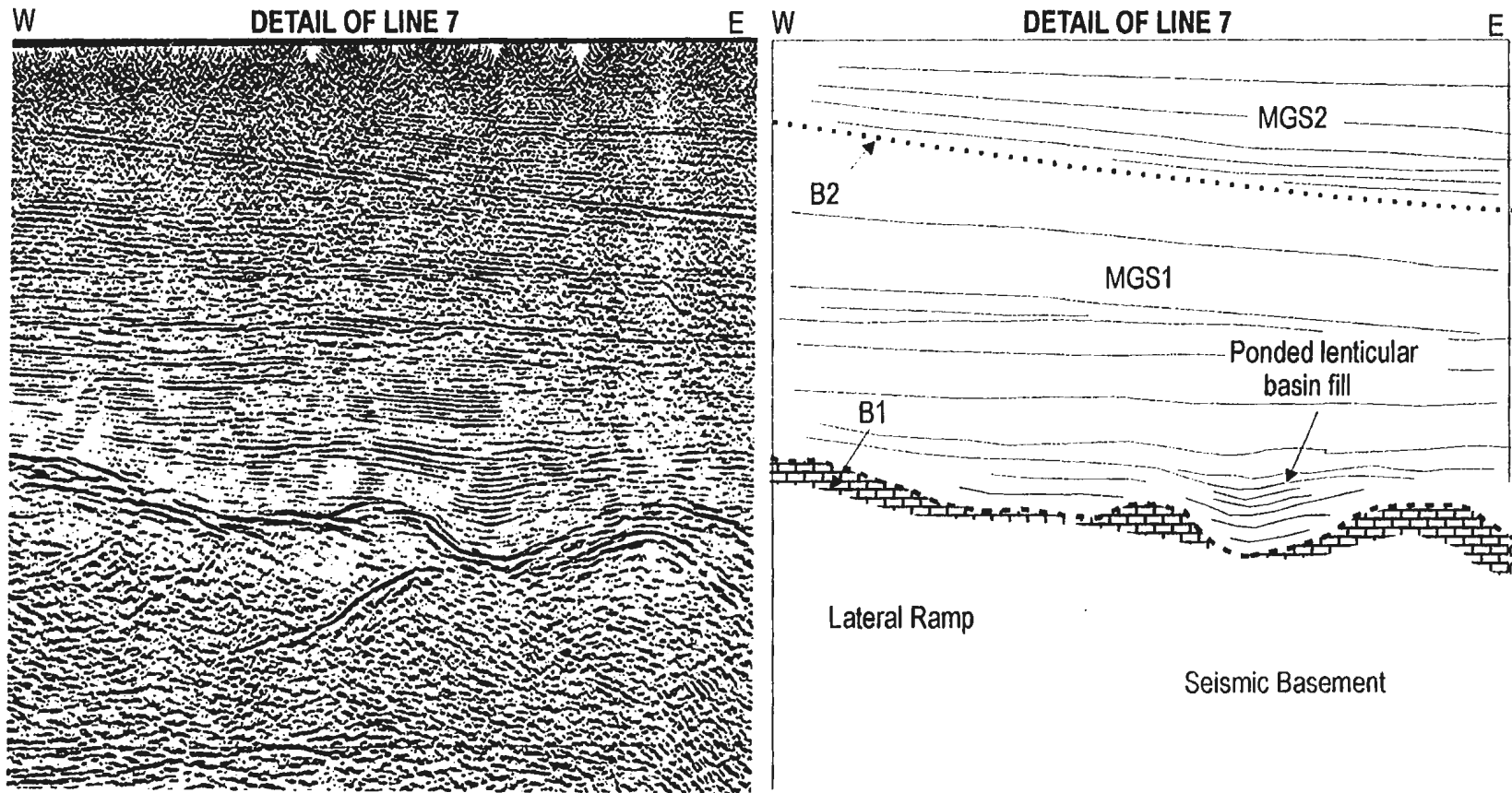


Figure 3.7. High resolution detail of LINE 7. Note i) the presence of Unit 1 above seismic basement, ii) the ponded lenticular geometry of basinfill in B1 topographic lows and iii) the lateral ramp geometry of a basement thrust sheet. Refer to Figure 1.18 for line location.

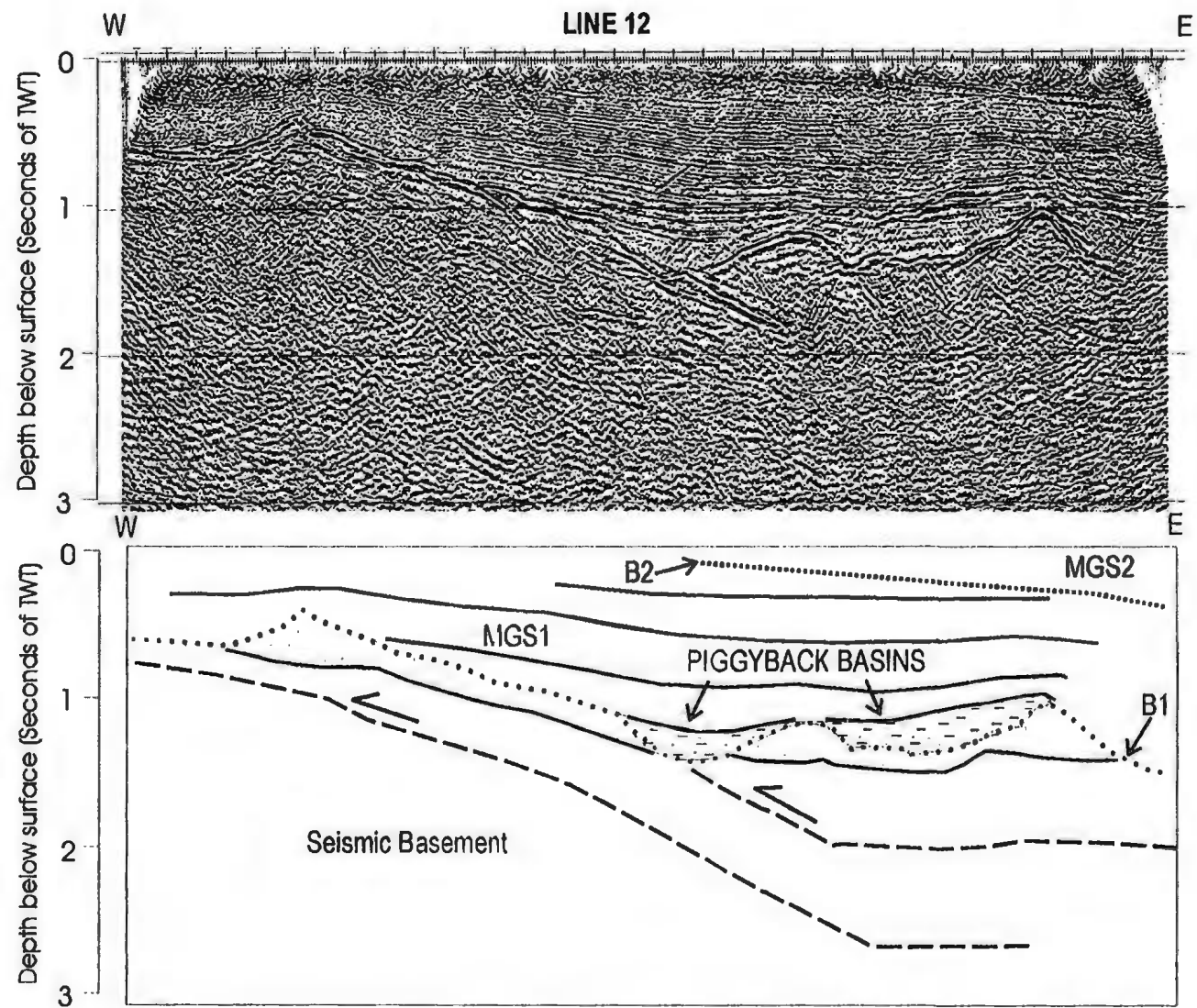


Figure 3.8: LINE 12. Note the presence of Piggyback basins above thrust sheets.

mapped by principle researchers of the Eastern Mediterranean research group (unpublished data, 1998). These structures are contained within the Megasequence 1 interval, and typically extend downward from the B2 toward the B1 unconformity. Occasionally, an extensional fault is observed to cut either the B1 or B2 unconformity; however this is an uncommon event, marked by small to negligible offsets. Localized, apparent extensional fault geometries are also observed within the MGS1 succession, but clear offsets must be identified in each case to determine if these features do in fact represent extensional faults. No MGS1 growth strata, progressive local unconformities or unique seismic units are observed in association with the conjugate extensional faults in the Northern Domain. As a result, while the presence of these structures is noted, the primary focus of the stratigraphic-structural investigation in the Northern Domain remains of the thrust fault structures.

The geometry of thrust anticline-syncline pairs in the Northern Domain exhibits a marked similarity with geometries reported for various thrust related folds in published literature (Medwedeff, 1989; Hardy and Poblet, 1994). Apparent normal fault style geometries on the flanks of thrust anticlines that do not show evidence of clear offset are consistent with stratal geometries reported in growth fault bend folds (Medwedeff, 1989).

Stratigraphic-structural architectures

Figure 3.3 indicates that the basement-involved anticline-syncline pairs of the northern domain are succeeded by a highly variable MGS1 Miocene succession, which is comprised of i) Unit 1 carbonate deposits, and/or ii) Unit 2 siliciclastic deposits. These adjacent and

often contemporaneous deposits exhibit contrasting geographic distributions and stratal architectures such that laterally restricted Unit 1 deposits occur above anticlinal highs while Unit 2 deposits fill the adjacent synclinal lows. The stratal geometries of ramp anticlines and synclinal sub-basins of the northern domain are described below.

Localized syntectonic unconformities and platform carbonate facies are commonly observed in association with ramp anticlines in the northern domain. Figure 3.6 presents a high resolution detail of the ramp anticline crest imaged in Figure 3.3. A series of complex syntectonic unconformities and laterally restricted Unit 1 mounds occur above the crest of the anticlinal ridge. The stacked syntectonic unconformities onlap ridge flanks with varying degrees of angularity (Figures 3.3 and 3.6). The B1 surface forms the steepest unconformity of the group, while each successively younger local unconformity shows a progressive up-section decrease in dip angle toward the crest flanks. Where the local unconformities extend onto or across anticlinal crests, the unconformities are observed to be erosional and often merge together within mounded Unit 1 seismic reflection events.

The Unit 1 mounds lie on or near the crests of ramp anticlines (Figure 3.3). These mounds represent the seismic facies equivalent to the platform carbonate reef facies of the Karaisalı Formation. The time isochore map for the Unit 1 seismic facies shows that the subsurface distribution of this facies has rapid lateral thickness changes (Figure 3.5). The thickest Unit 1 reef deposits occur in three to four approximately east-west trending arcuate ridges which are separated by intervening areas with little to no Unit 1 development. It is also of note that Unit 1 reef occurrences are often coincident with local syntectonic unconformities

along the flanks and tops of the anticlines. The seismic reef facies extends outward along the lower local erosive unconformity for a short lateral distance before it is onlapped and overlapped by younger MGS1 strata (Figure 3.3). A similar event is noted at along a stratigraphically higher local unconformity.

The piggyback basins described in the preceding structure sub-section exhibit a variety of complex MGS1 basinfill architectures. Local instances of onlap, offlap, downlap, overlap contacts, progressive unconformities, and pond, fan and wedge stratal geometries are imaged within piggyback basinfill deposits of the northern domain. Strata located in Zone A exhibit a progressive forelimb-directed onlap onto steeply dipping anticline forelimbs along a series of syntectonic erosional unconformities (Figure 3.3). These onlapping reflectors often exhibit a folded geometry within the lower portion of the sub-basin such that a relatively flat lying onlap reflector steepens and curves upward toward the forelimb of the anticline (Figure 3.3). Folded onlap reflectors show maximum curvature near the base of anticlinal flanks; up-section this curvature diminishes to negligible at anticline crests. The down-dip contact relations of Zone A strata include minor instances of ponded onlap and downlap upon isolated highs within the B1 topography; however, in most profiles the contact appears conformable. Strata in Zone B tend to show a greater variety of contact relationships with the pre-Miocene basement. Figure 3.3 reveals that the lowermost strata in Zone B lie above the B1 unconformity and the backlimbs of ramp anticlines in an apparent downlap configuration. Along the flanks of the piggyback basins (Zones A and B) strata can be traced briefly up dip before terminating in an apparent onlap configuration against the forelimb of the next ramp

anticline. Figure 3.3 also reveals that successive piggyback basin strata exhibit an apparent downlap configuration in the lowermost section. Up-section, this stratal architecture changes progressively to a ponded onlap configuration against the flanks and crests of adjacent anticline ridges.

The localized syntectonic unconformities which occur along the flanks and crests of ramp anticlines extend into the piggyback basin-fill. These local unconformities occur as local erosional surfaces which change progressively basinward to minor surfaces of toplap, offlap or downlap. Further basinward, these surfaces lose their seismic character and become apparent conformities within the MGS1 strata.

Stratal geometries are varied within the piggyback basins of the northern domain. Evidence of localized stratigraphic wedging, sediment ponding, and fanned bed thickening are observed. Significant wedging of basin-fill strata can be observed along the flanks of many anticlinal ridges. Two successive, stacked stratigraphic wedges are imaged in Zone A strata (Figure 3.3). Each wedge thins rapidly from 0.5 seconds TWT thickness to 0 seconds TWT thickness at the crest of the anticline. Wedges are also present in Zone B strata (Figure 3.3), but stratal thickness on the backlimb is more uniform, and wedges are only apparent in areas that are most proximal to the crest of the anticline. Evidence of minor ponding is also observed in the basal portion of sub-basin strata. Ponded strata are often imaged as semi-transparent lenticular packages which contain a few disorganized to chaotic internal reflectors. The laterally restricted packages fill the narrow trough-like sub-basins which occur between successive anticlines. Divergent seismic reflectors observed in Zone B strata are

suggestive of slump and debris flow deposits proximal to steeply-dipping anticline limbs (e.g. Gilbas 2 well, Appendix B).

3.2.2 Eastern Domain

The second structural domain in the Adana Basin is located along the eastern edge of the study area (Figure 3.1). Figures 3.9 and 3.10 are representative seismic profiles through the Eastern Domain, which display a dramatic change in structural-stratigraphic style from that observed in the Northern Domain (Table 3.1). These seismic profiles image a prominent structural high that delimits the eastern boundary of the basin. In most locations this structural high is present as a progressively-eroded culmination wall (eg. Line 6). In the vicinity of Line 13 and Line 16, the culmination wall is accompanied by synthetic reverse faults that cut both the B1 and B2 unconformities and disrupt much of the Miocene succession (MGS1-3) (Figs. 3.1, 3.11 and 3.12). The local reverse fault imaged in Figure 3.9 displaces the MGS1 succession and seismic basement such that hanging wall cutoffs for the B1 seismic unconformity are displaced (Figures 3.9, 3.10). Intersections of the younger and older fault planes create unique “piercing points” of reference, which are used herein to assess relative movement along the fault. Close examination of displaced piercing points indicate a larger component of vertical separation combined with a lesser component of horizontal separation across the reverse fault. The geometry of the culmination wall / reverse fault system imaged in Figure 3.9 is interpreted by Williams et al., (1995) as a positive flower structure.

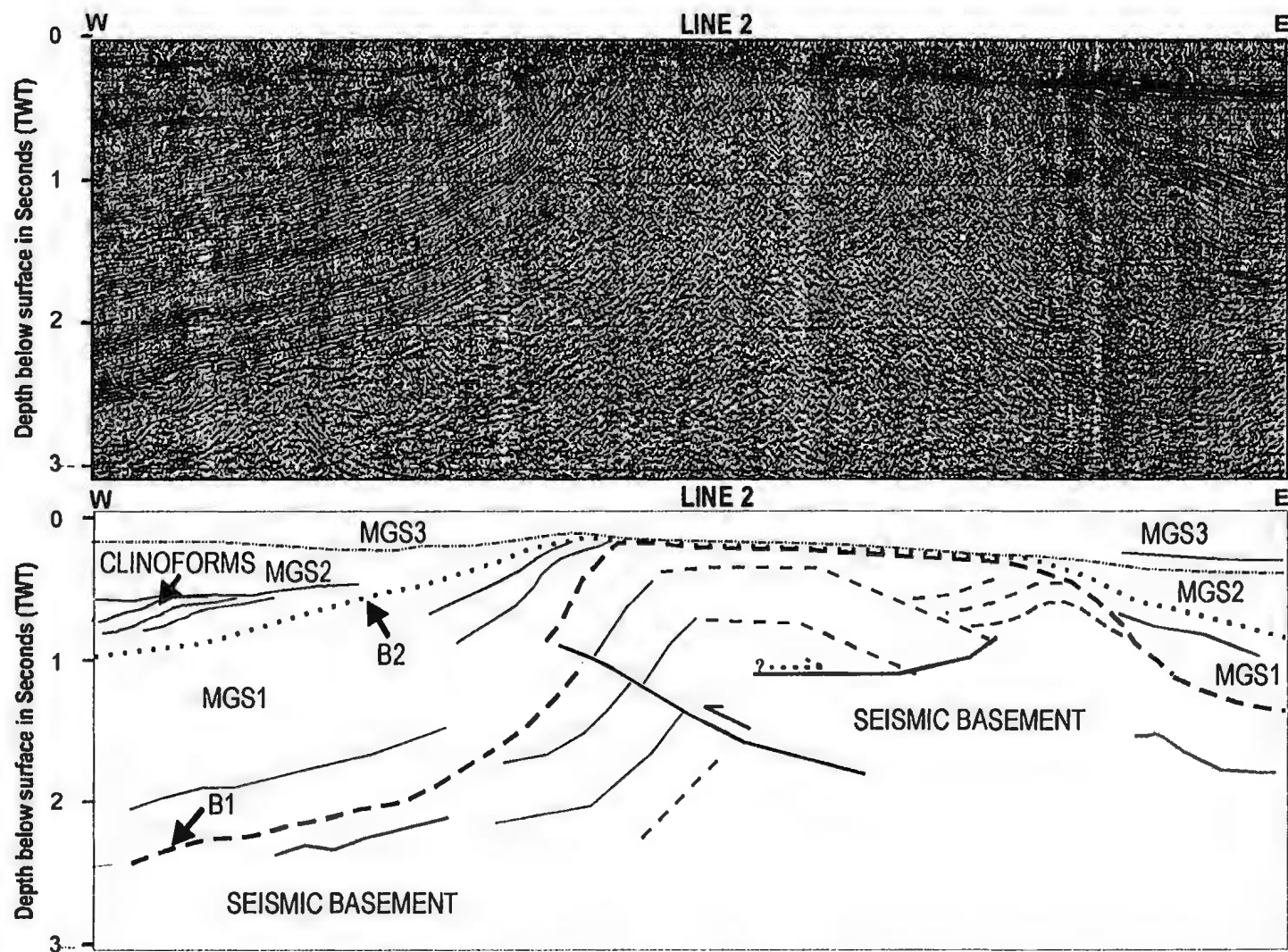


Figure 3.9: Structural-stratigraphic interpretation of Line 2. Note the position of the B1 and B2 unconformities, and the variation in stratal geometries. Refer to Figure 1.18 for line location and Figure 2.8 for enlarged seismic profile.

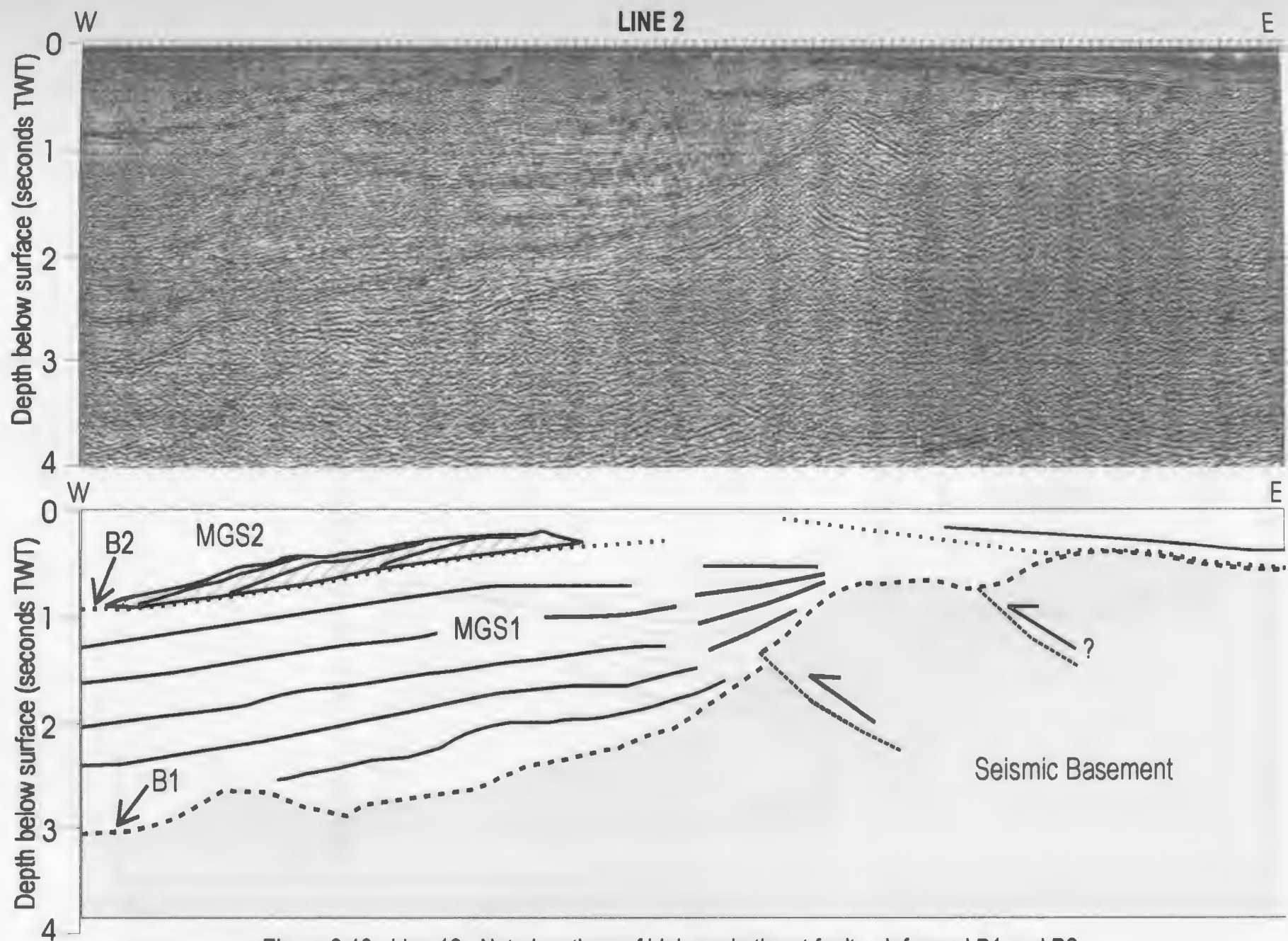


Figure 3.10: Line 13. Note locations of high angle thrust faults, deformed B1 and B2 unconformities, and progradational clinoforms.

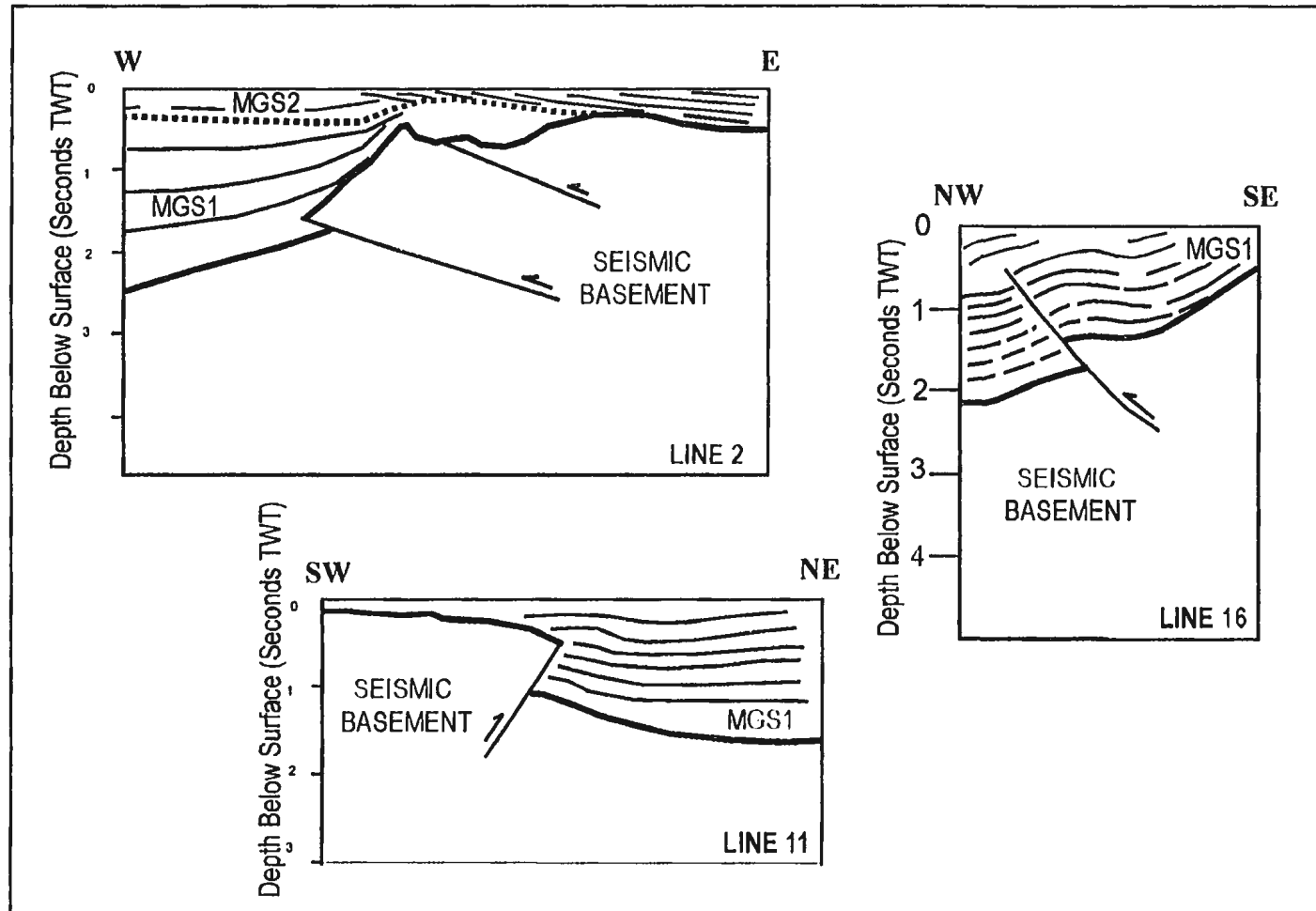


Figure 3.11: Schematic line interpretations of Lines 2, 11 and 16 (See Figure 1.18 for line locations). Note that thrust fault planes exhibit much higher dips than those imaged in the Northern Domain. Lines 2, 11 and 16 are oriented approximately perpendicular to Eastern Domain structures to illustrate structural relief.

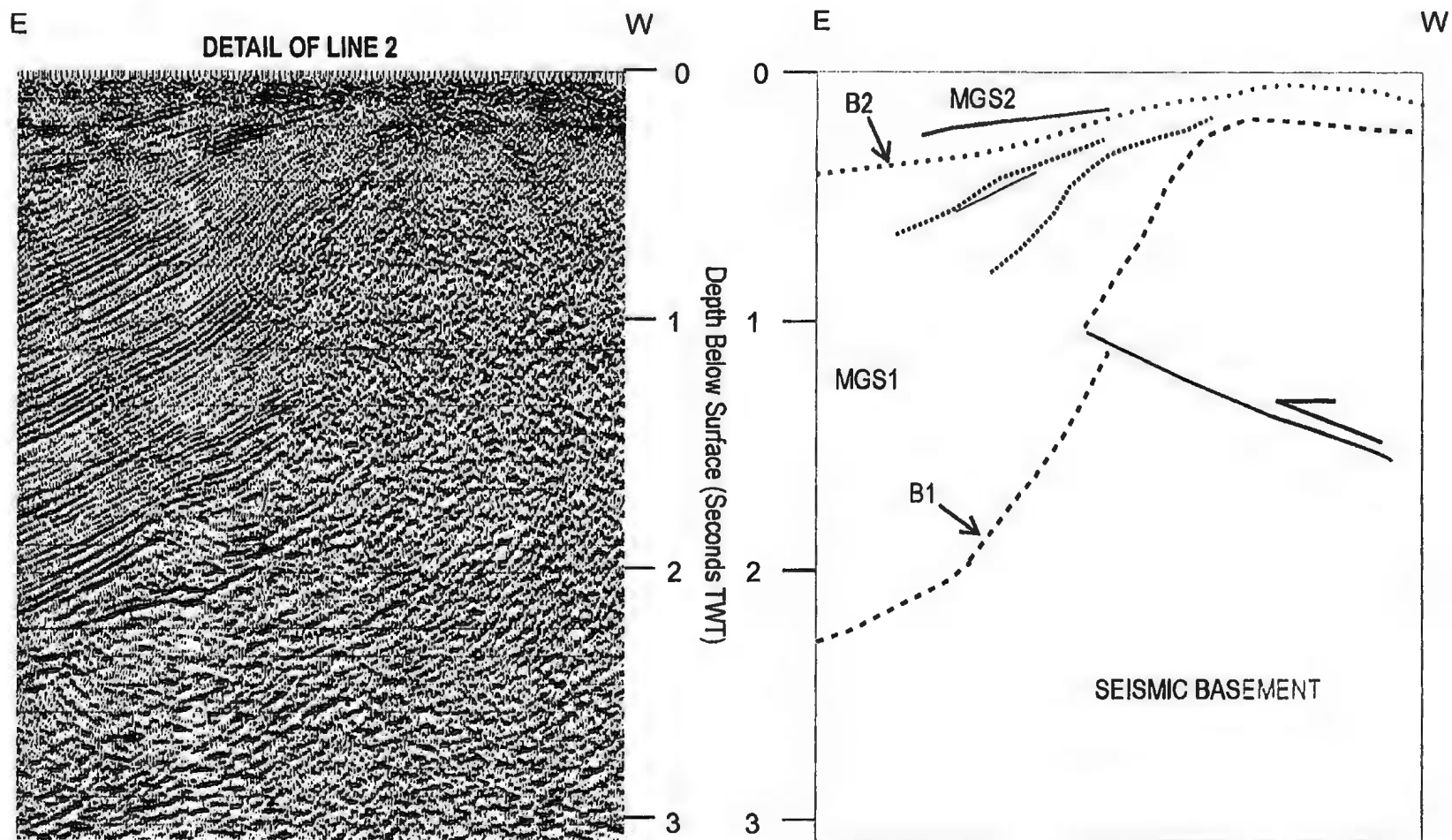


Figure 3.12: High resolution detail of Line 2. See Figure 3.9 for location.. Note abrupt truncations in the lower portion of MGS1 and the series of local unconformities located in upper MGS1 strata along the flank of the thrust basement high.

Stratigraphic-structural architecture

The western flank of the culmination wall is imaged as an abrupt, steeply-dipping contact that forms the eastern boundary of a 2.0 second (TWT) thick stratified seismic succession (MGS1-2). This thick seismic succession is structurally juxtaposed against a seismic basement that outcrops at surface in the Misis Mountains (Figure 3.9). Two distinct contact relations are observed between the strata of MGS1 and the structural high. Figure 3.13 presents a detail of the western flank, where the lower half of Megasequence 1 terminates abruptly against a steeply-dipping folded unconformity. This portion of Megasequence 1 is represented by a tilted stratigraphic succession of uniform thickness which maintains the dip of the unconformity at the top of the underlying basement blocks. Stratal architectures of the Northern Domain (apparent downlap, bed thickening and wedging) are occasionally discernable directly above the B1 unconformity.

The upper MGS1 succession exhibits a high degree of lateral and vertical variability. An abrupt contact between the uppermost portion of MGS1 and juxtaposed basement rocks is imaged in Figure 3.9. A progressive increase in the dip angle of MGS1 strata is noted with increasing proximity to the west flank of the culmination wall (Figure 3.13). These steeply dipping strata exhibit a prominent wedge shaped stratal architecture in which a 1.0 second TWT thick upper MGS1 package rapidly pinches out at the crest of the anticline structure. The wedged strata are punctuated by a number of local progressively shallowing syntectonic unconformities which demonstrate onlap and folded onlap relations with the forelimb and crest of the anticlinal feature.

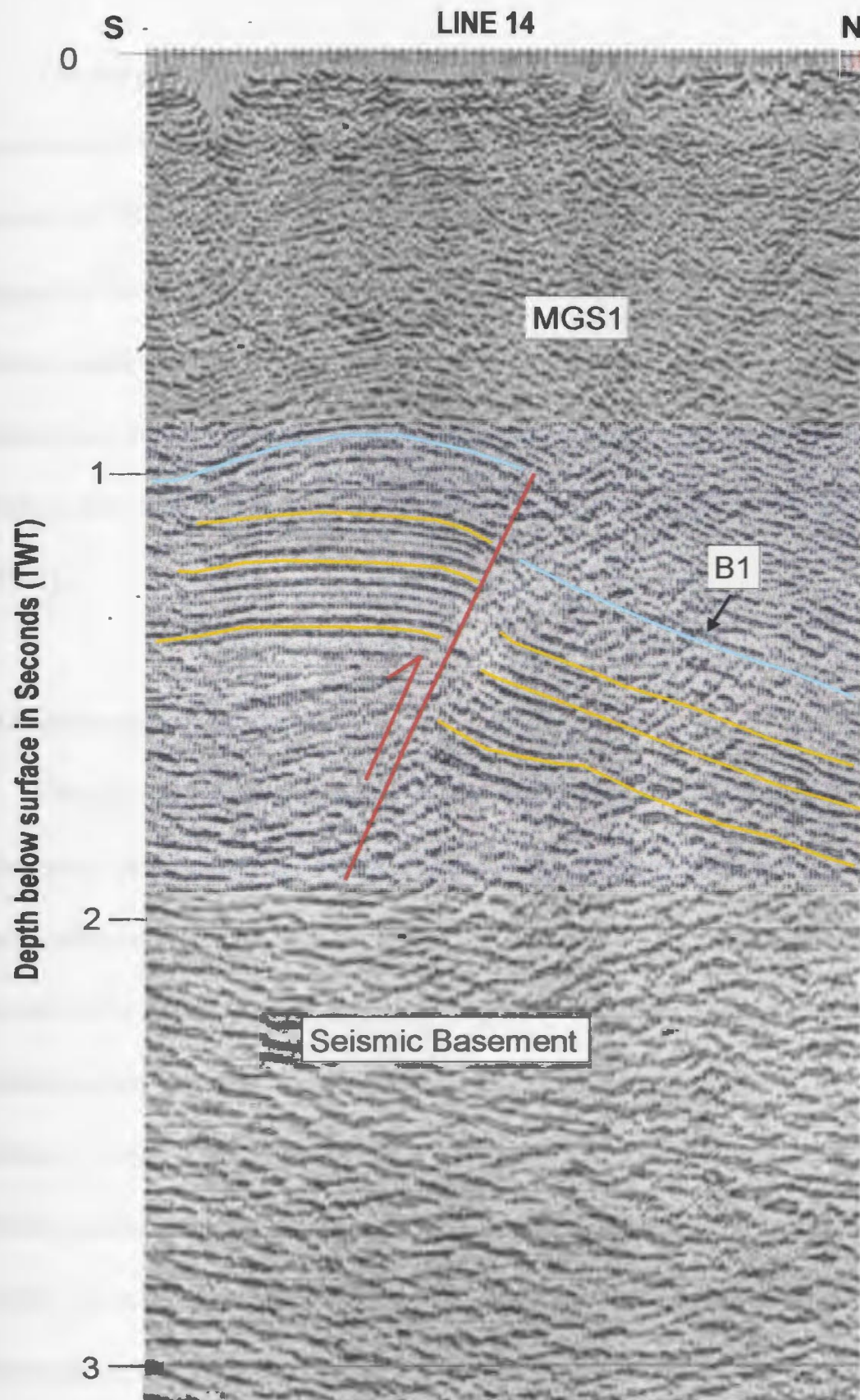


Figure 3.13: Local reverse fault imaged at the southern end of Line 14.

The progressive syntectonic unconformities described in the upper portion of MGS1 extend upward into the MGS2 and MGS3 successions. Progradational clinoforms appear within the MGS2 interval of the stratigraphic wedge (Figure 3.9). These features occupy a stratigraphic position which is proximal to, but down dip from, the culmination wall. The Tortonian aged B2 unconformity forms a more abrupt regional erosive unconformity (and offlap surface) between MGS1 and MGS2 strata. It often occurs in association with a series of stacked less than 0.1 second TWT thick lenticular progradational packages (Figures 3.9 and 3.10).

3.2.3 Southwestern Domain

The third structural domain in the Adana Basin is restricted to the southwest and south-central portions of the basin (Figure 3.1). Figures 3.14 and 3.15 are representative seismic reflection profiles that illustrate the dominant structural-stratigraphic architectures observed in the Southwestern Domain. Figure 3.1 indicates that the Southwestern Domain is characterized by extensional faults, turtle anticlines, withdrawal synclines and salt structures. Extensional faults in the northwest portion of the domain dip toward the south-southeast, while similar structures in the southeast dip toward the west-southwest. In both locations the extensional fault fans sole into a gentle detachment surface (Figure 3.1). The detachment surface demarcates the southern and southwestern limits of a broad, structurally elevated platform that occupies the northern and eastern portions of the Adana Basin. Southward of the platform, the MGS3 succession thickens rapidly from zero to greater than

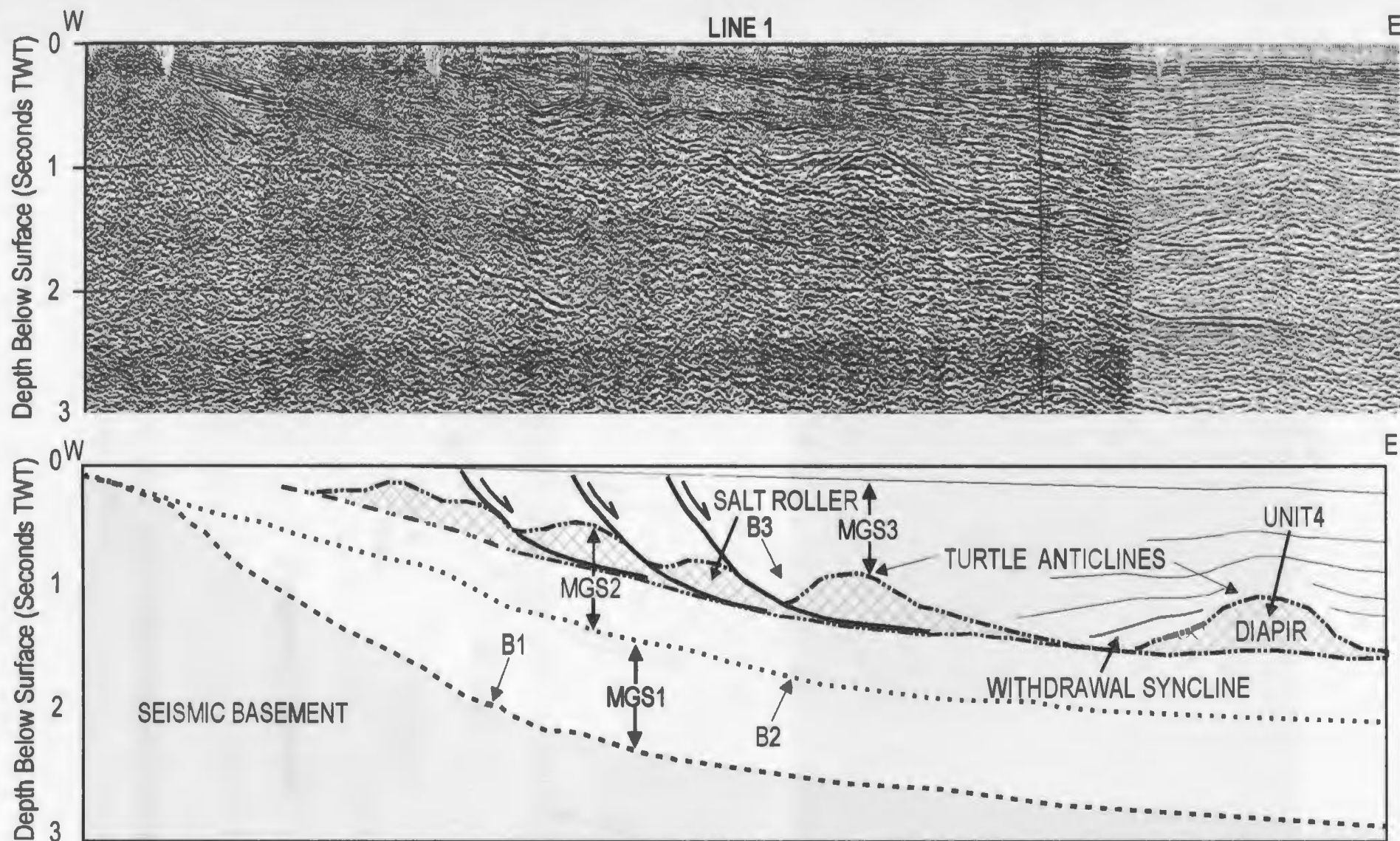


FIGURE 3.14: Line 1. Note the association between salt structures in MGS2 and the location of listric normal faults in MGS2 and MGS3.

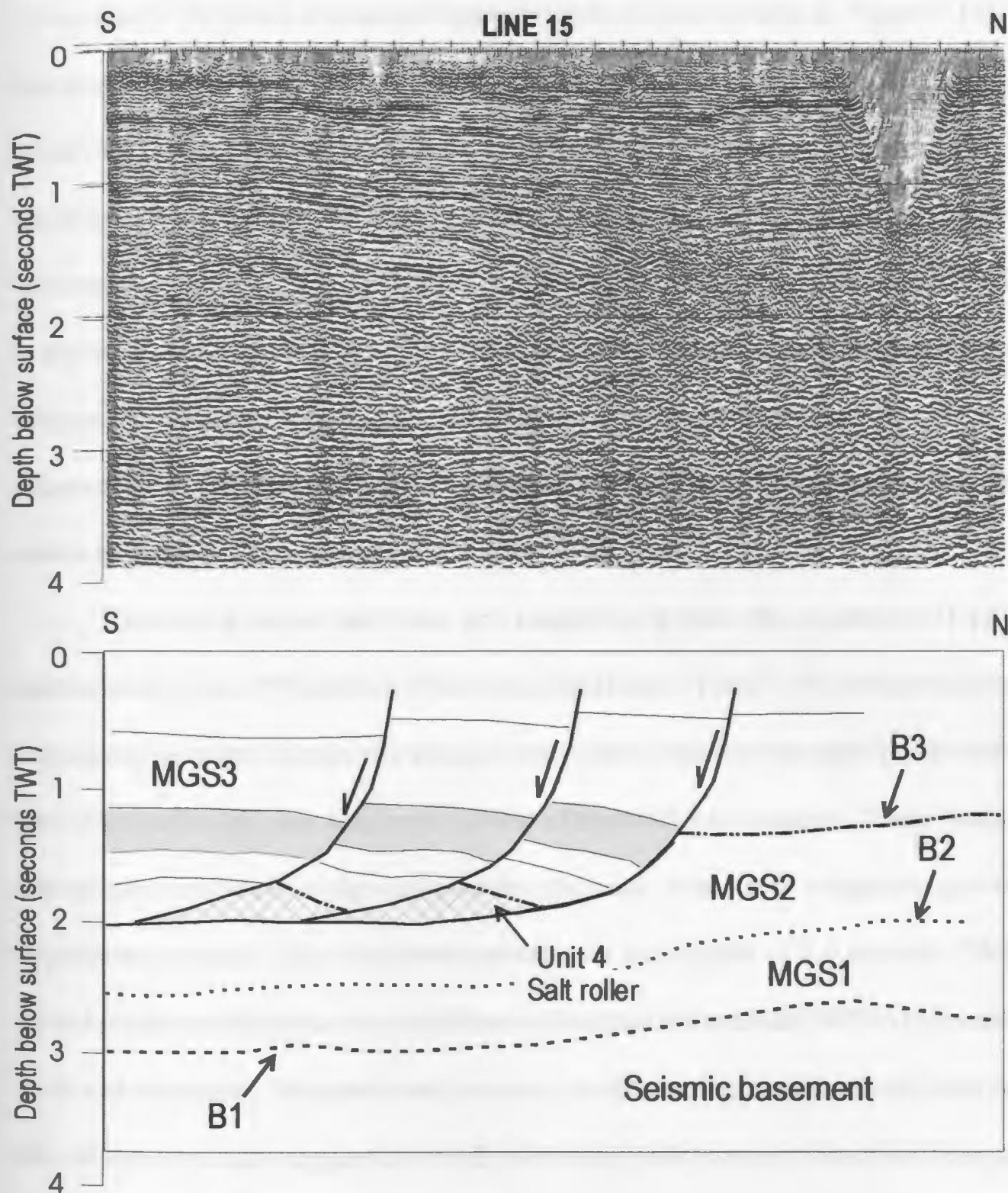


Figure 3.15: South end of Line 15. Note extensional listric rollover structure and associated salt bodies.

2.0 seconds TWT over a distances of approximately 25 kilometres (e.g., Figure 3.14). Within this deep Messinian to Recent depocentre, the upper portion of MGS2 and the lower portion of MGS3 is controlled by extensional faults and salt structures. A pair of ENE-WSW trending salt-cored turtle anticlines apparent in Figure 3.14 are separated by an intervening withdrawal syncline. Unit 4 (MGS2) evaporites within the turtle anticlines attain thicknesses in excess of 0.4 seconds TWT. The flanks and crests of both turtle anticlines are variably onlapped by overlying MGS3 strata, which exhibit flat-lying to folded onlap geometries. The adjacent withdrawal syncline is filled by an apparently downlapping MGS3 succession, which attains thicknesses in excess of 1.4 seconds TWT.

Extensional listric fault fans are imaged in in both the southwest (Line 1) and southernmost (Line 15) portions of the study area (Figs. 3.1 and 3.15). In both locations, the extensional fault fans consist of a series of listric faults that cut the upper portion of MGS2, the B3 unconformity, and the lower portion of the MGS3 succession. These faults display a progressive decrease in dip angle toward the base, where they merge along a common detachment surface. This detachment surface sits at a depths of 2.0 seconds TWT in the central portions of the basin, but it shallows to less than 0.3 seconds TWT in the west (Figure 3.14) and the north. The nature and geometry of offset reflectors in both the fault fans, and the roll-over structure suggest an overall south-west bulk transport direction for extensional features of the Southwestern Domain. These structures occur in association with Unit 4 Messinian evaporites and a variable middle to upper MGS3 (Messinian to Recent) succession.

Unit 4 evaporites exhibit considerable thickness variations in association with listric

normal faults of the Southwestern Domain. Close examination of Line 1 reveals that salt welds, salt rollers and salt-cored anticlines delimit the lower boundary of the fault fan (Figure 3.14). The complex Messinian aged B3 unconformity is interpreted as a variable contact surface which separates MGS3 hanging wall strata from MGS2 salt rollers, salt-cored anticlines and salt welds that form the base of the extensional fault fan, which acts as detachment horizon. Two successive salt rollers are imaged below the B3 unconformity in Line 1; these features occur as 0.1-0.3 second TWT thick convex, flat-bottomed mounds which form the lowermost portion of the footwall for listric normal faults. Figure 3.16a presents a high resolution detail of a salt roller from Line 1. This detail reveals that MGS3 strata that overly the salt rollers occur as localized curved wedges, which display variable apparent downlap, onlap and folded onlap contact relations with footwall blocks.

Salt welds and salt-cored anticlines are also imaged below the B3 unconformity in Line 1 (Figure 3.14). Salt welds are identifiable as locations at the base of the listric fault fan where Unit 4 deposits are absent, and deformed MGS3 strata in the hanging wall of a listric fault lie with angularity on undeformed MGS3 strata in the footwall. These salt-free fault bound contacts often appear unconformable, but are clearly structural features only traceable over short distances. The salt-cored turtle anticlines occur as larger 0.1-0.6 second TWT thick Unit 4 mounds, which appear to “bulge” upward into overlying MGS3 strata (Figure 3.16b). MGS3 strata thin toward, onlap onto and succeed the salt-cored anticlines. Higher in the section, upper MGS3 (Middle-Upper Pliocene) reflectors show positive relief above the easternmost turtle anticline imaged in Line 1, but remain undeformed in adjacent areas.

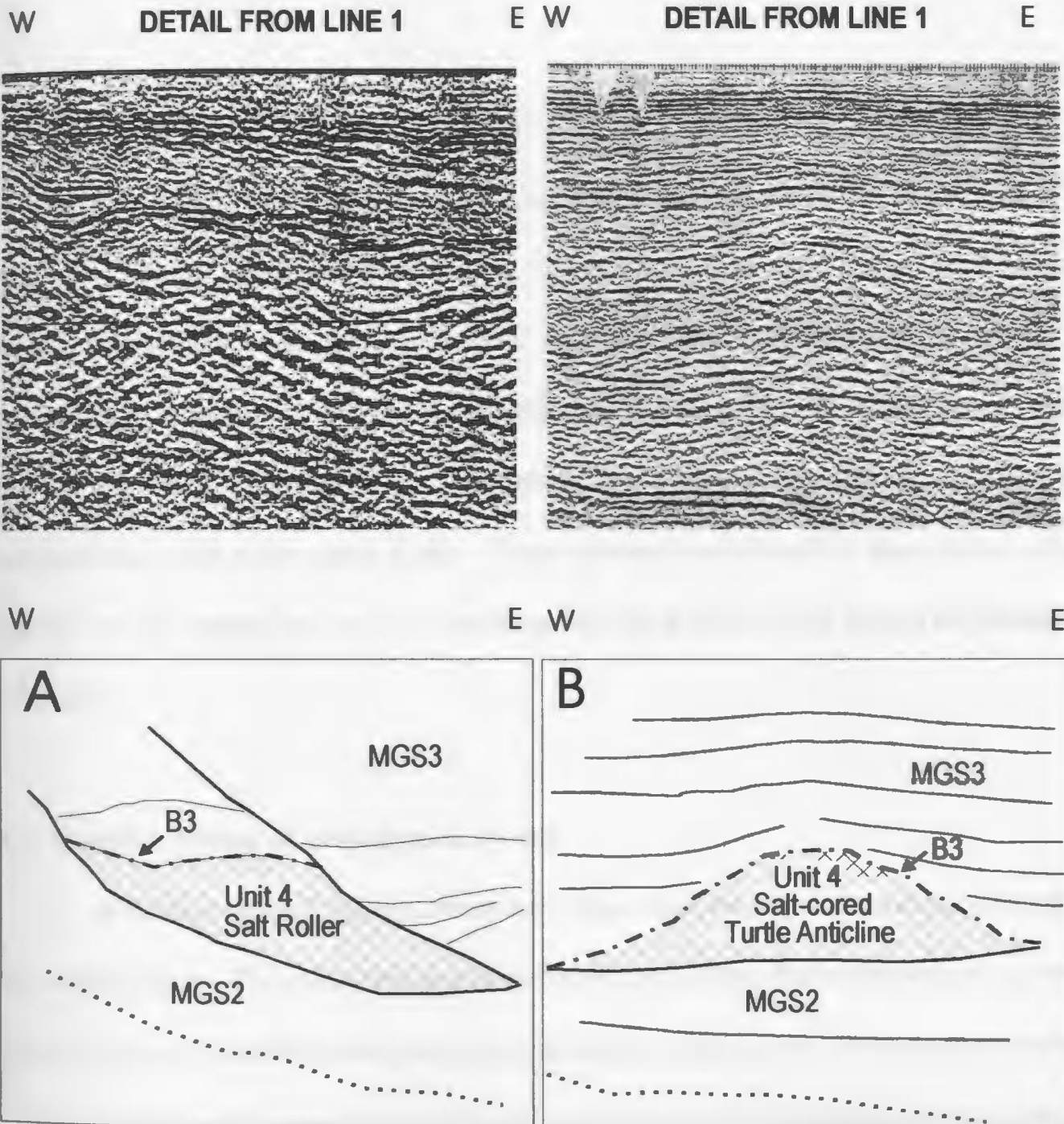


Figure 3.16: High resolution details of Line 1. A) Salt Roller B) Salt-cored Turtle Anticline. Refer to Figure 3.14 for scale and location details.

CHAPTER 4: TECTONIC SYNTHESIS

The Adana Basin documents a complex tectono-stratigraphic history during the Miocene. This is indicated by the highly variable nature of the Miocene sedimentology, stratigraphy and structural geology in space and time. New evidence presented in this study reveal 1) local variation in onlap and offlap relationships at the B1, B2 and B3 unconformities, and 2) localized progressive unconformities and complex growth strata near thrust culminations within the Adana Basin. These structural-stratigraphic features provide new insight into the timing and nature of deformation which affected the Adana Basin during the Miocene.

4.1 Relative timing of deformation events

A number of geologic structures have been described in the Miocene succession of the Adana Basin. The study area has been divided into three distinct structural domains on the basis of structural style and structural-stratigraphic architecture. Various age-constrained critical stratigraphic markers and units show evidence of deformation in these structural domains. The chronology of each structural domain is summarized in Table 4.1 and outlined below.

Chronology of the Northern Domain

Based on the relative timing of deposition to structural growth of the anticlines, the

Table 4.1: Constrained timing of deformation events for the Northern, Eastern and Southwestern Domains. Refer to Figures 2.2 and 2.14 for details relating to sedimentological and stratigraphical conditions, and timing of Hiatus events.

----- PRE-DEFORMATION XXXXX SYN-DEFORMATION ////////// POST-DEFORMATION

Phase	Structural Province	Pre-Miocene	Miocene						Pliocene	Quaternary
			Aquitanian	Burdigalian	Langhian	Serravalian	Tortonian	Messinian		
1	Northern Domain (Low angle thrusts)	-----	XXXXXXXXXXXXXXXXXX			////////////////////////////////////				
	Northern Domain (Conjugate extensional fault sets)	-----				XX	////////////////////////////////////			
2	Eastern Domain (Culmination wall and local reverse faults)	-----				XXXXXXXXXXXXXXXXXX			//////////	
3	Southwestern Domain (Extensional listric faults fans and salt tectonics)	-----						XXXXXXX		///

stratigraphic succession of the Northern Domain is divisible into pre-growth, syn-growth and post-growth strata. Stratified units of the basement involved in the thrust sheets are interpreted as pre-growth strata and were deposited prior to crustal shortening. Syn-growth strata are represented by Burdigalian-Serravalian aged deposits of Unit 1 (where present), and by much of the MGS1 succession (late Burdigalian-early Tortonian). In the northern portion of the Northern Domain the Tortonian aged B2 unconformity appears unfolded, unbroken and unaffected by growth of underlying thrust features. The uniformly dipping Tortonian-Recent-aged MGS2 succession, which lies above the B2 unconformity is interpreted to represent post-growth strata with respect to the structural features observed in the Northern Domain. The conjugate extensional fault sets observed within the Northern Domain structures offset MGS1 strata without evidence of growth. This observation indicates that the extensional faults were not active during the deposition of most of the MGS1 succession, and represent younger, possibly upper Serravalian to Tortonian events.

Chronology of the Eastern Domain

The stratigraphic succession of the Eastern Domain is similarly divisible into pre-growth, syn-growth and post-growth strata. Pre-Miocene basement and strata from the lower half of MGS1 (lower to middle Miocene) are interpreted as pre-growth strata which were deposited prior to the initiation and development of the eastern basin-bounding culmination wall and localized high-angle reverse faults. Syn-growth strata of the Eastern Domain are represented by the upper portion of MGS1 (late Serravalian-Tortonian) and the lower to middle portion

of the MGS2 succession (Tortonian-Messinian). The unfolded flat-lying strata of the uppermost portion of MGS2, as well as local outliers of MGS3, are interpreted as post-growth strata with respect to formation of structural features observed in the Eastern Domain.

Chronology of the Southwestern Domain

The stratigraphic succession of the Southwestern Domain is divisible into pre-growth, syn-growth and post-growth strata. Pre-Miocene basement, MGS1 transgressive deposits and lower MGS2 (pre-Messinian) regressive deposits are interpreted as pre-growth strata which were deposited prior to the initiation and evolution of the listric fault fan, roll-over structures and salt-cored turtle anticlines. Syn-growth strata of the Southwestern Domain are represented by upper MGS2 strata, which represent the Messinian-Lower Pliocene geologic time interval. Post-growth strata are represented by the undeformed, flat-lying strata from MGS3 (Pliocene to Recent).

Table 4.1 summarizes the chronology of Northern, Eastern and Southwestern Domains and reflects the relative timing of deformation events which have affected the Miocene to Recent succession in the Adana Basin. The table reveals that low angle thrusts events in the Northern Domain developed in the early Miocene and dominated the stratigraphy until the end of the Serravalian interval. The base of the Tortonian interval marks a shift to the development of high angle thrust events in Eastern Domain. Table 4.1 further reveals that these high angle thrusts persisted into the Pliocene along the eastern edge of the study area. Meanwhile, stratal architectures reflect a shift to extension in the Southwestern

Domain where post-Messinian faulting and halokinetic activity dominate the stratigraphy until the Late Pliocene.

4.2 Tectonic-stratigraphic Implications:

Many complex tectono-stratigraphic relationships are present within the Miocene to Recent sedimentary succession in the Adana Basin. Following the development of the plate tectonic theory, an extensive array of tectono-stratigraphic field and laboratory investigations throughout the world have led to the development of geological models for a variety of plate tectonic configurations. Many of these models attempt to summarize and predict various aspects that are likely to occur in a given tectonic plate configurations, such as structural style, depositional environments and sedimentation patterns. Aspects of the foreland basin model will be outlined and compared with those of the Adana Basin to assess the suitability of the model as an analog for the Miocene structural evolution of the Adana Basin.

4.2.1 Tectono-stratigraphic analog

The Foreland Basin Model:

The tectono-stratigraphic architecture of the Adana Basin exhibits a marked similarity with architectures observed in modern and ancient foreland basins. Foreland basins develop as foredeeps in front of active thrust belts and provide accommodation spaces for sediments which are eroded and shed basinward off thrust high (Figure 4.1). Over time, a foreland basin sedimentary succession may become dissected or incorporated into an active thrust belt

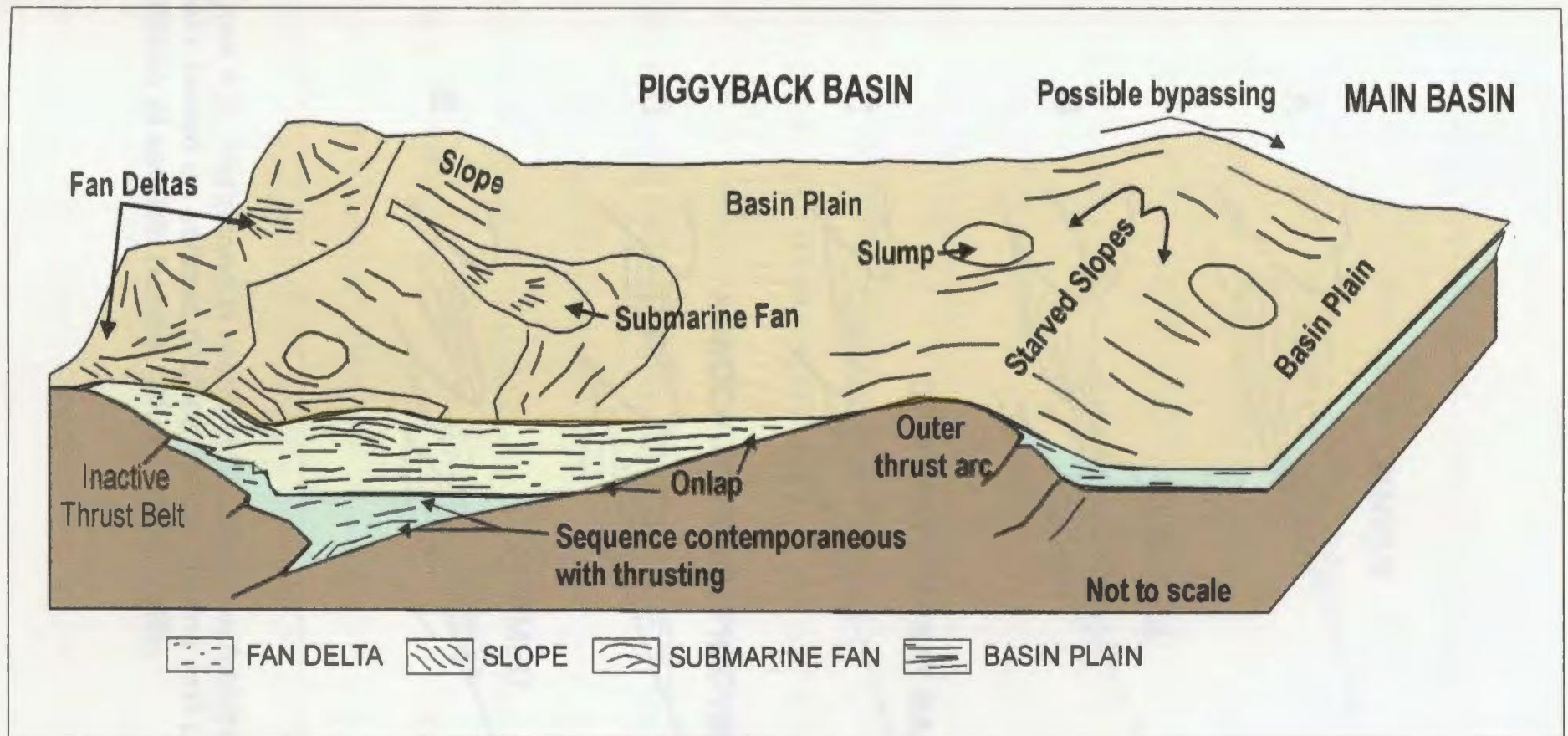


Figure 4.1: Depositional model of basin development within a foreland basin setting. Note I) the distribution of depositional environments relative to the location of the thrust front and II) the architecture of the sequences that fill the piggy back basin. After Ori et al. (1986).

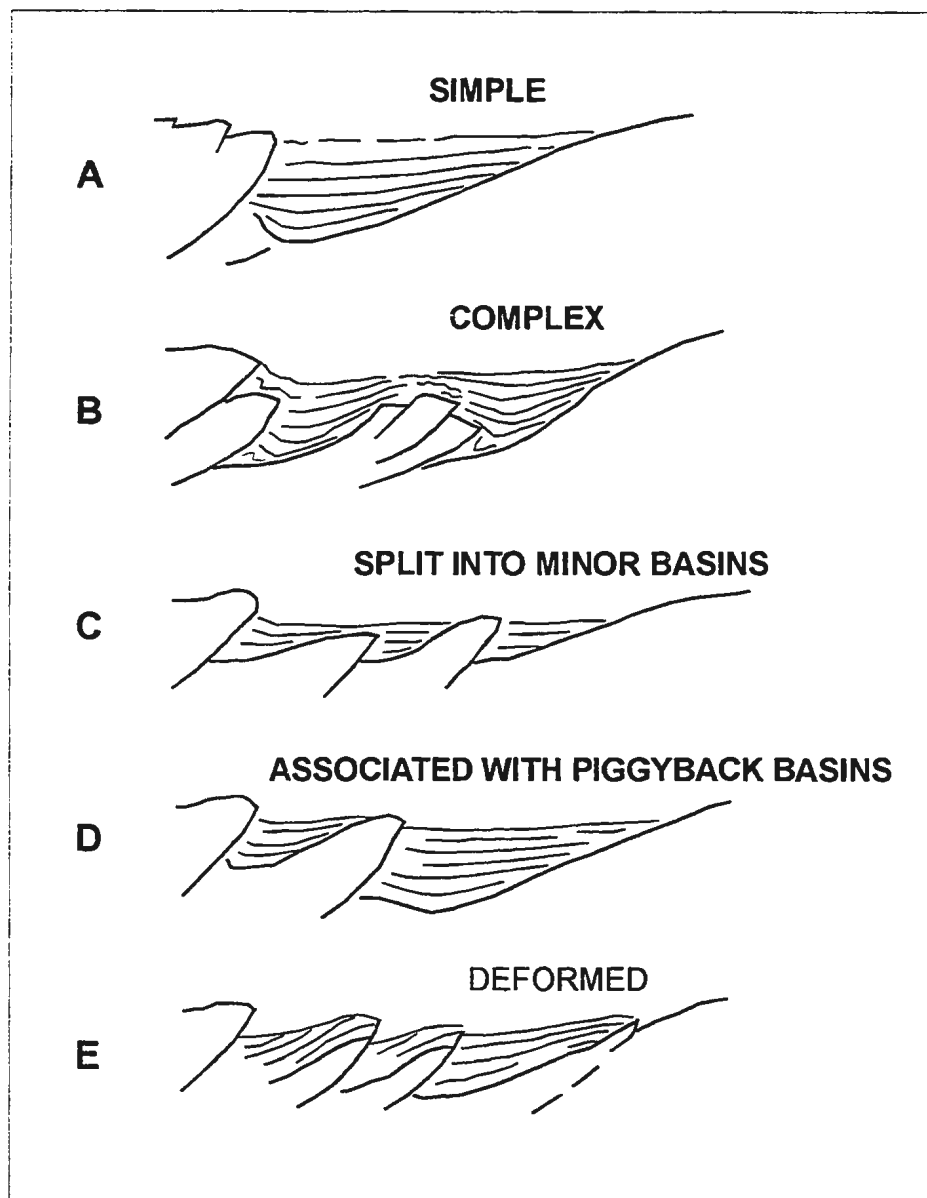


Figure 4.2: Variations in relationship between fold-thrust belt and foreland basin, based on seismic profiles. Minor basins and piggyback basins are varieties of satellite basins. After Lucchi (1986).

as thrusts propagate progressively basinward (Figure 4.2). In this circumstance, contemporaneous deformation, erosion and sedimentation can occur, the combined effect of which, is documented in the complex sedimentary growth successions which form within and proximal to the fold and thrust belt. Two depocentres that commonly host such strata are presented in Figure 4.3. *Toe troughs* (C) are localized depocentres which form directly in front of thrust sheet tips. During piggyback thrust propagation these and other pre-existing basins may be uplifted and transported above newly activated thrust sheets as *Piggyback basins* (D). Despite the low preservation potential of growth strata in foreland fold and thrust belt settings, such features may be preserved in locations where sufficient accommodation space is coupled with a plentiful sediment supply and rapid sediment accumulation rates. Ori and Friend, (1984) have used a variety of seismic, borehole and outcrop data to identify the Po Basin in Italy and the Ebro Basin in Spain as two examples of piggyback basin complexes. Continued research in this field has contributed greatly to our understanding of both the stratal architecture and the tectonic significance of growth deposits which form in foreland fold and thrust belt settings.

A variety of tectono-stratigraphic features have been described in the sedimentary deposits of foreland fold and thrust belts (Allen et al., 1986; Ori et al., 1986; Ricchi, 1986; Medwedeff, 1989; Suppe, 1992; Zoetemeijer et al., 1992; Hardy and Poblet, 1994; Poblet et al., 1999 etc). Features such as coupled wedge-shaped toe troughs and piggyback basins are commonly positioned on opposing flanks of thrust ramp anticlines. Syntectonic unconformities and carbonate platform deposits are often observed along ramp anticline

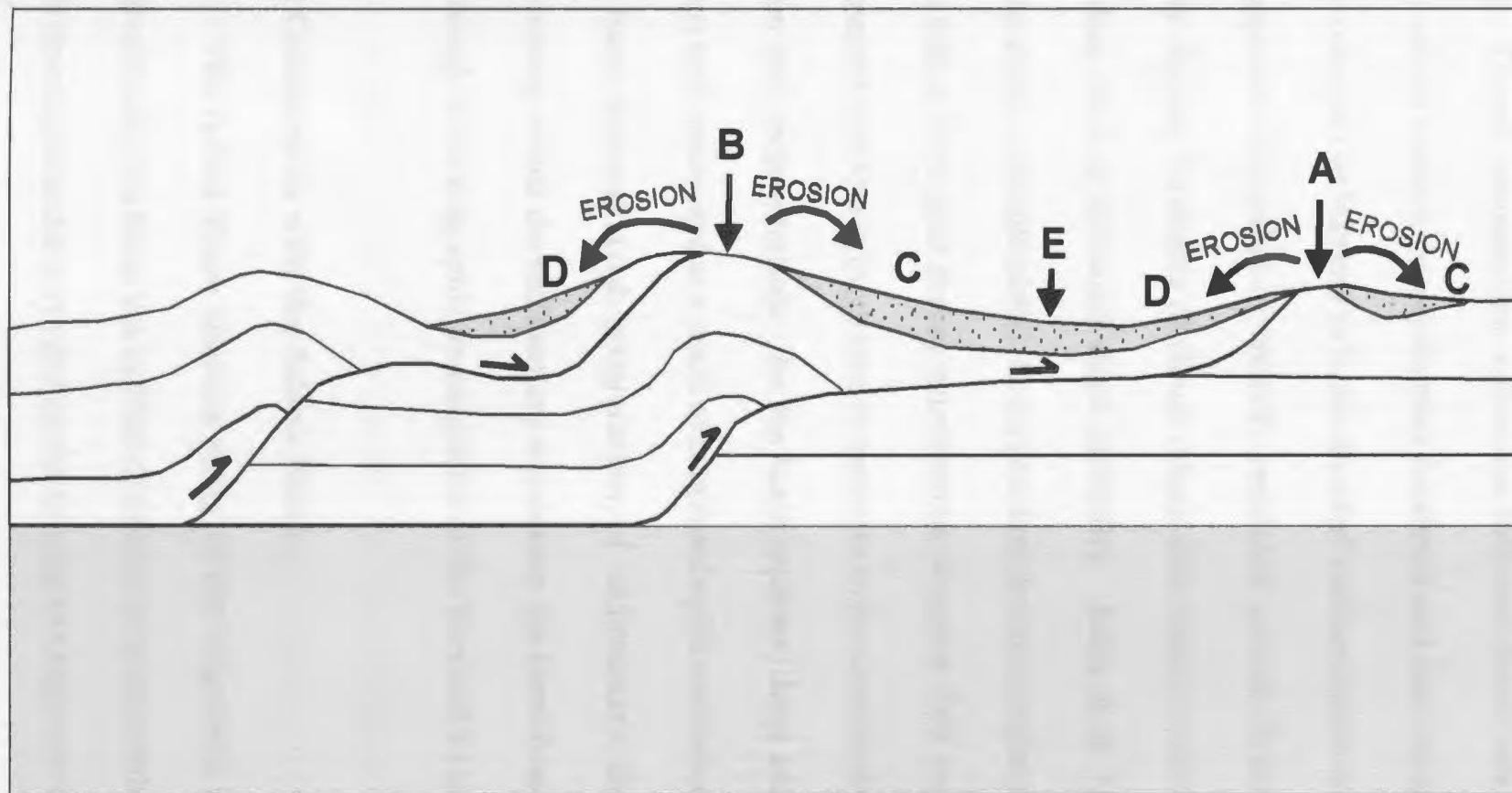


Figure 4.3: Morphology of satellite basins associated with fold-thrust belts. Note the position of piggyback basins (D) above thrust backlimbs and toe troughs (C) in front of thrust forelimbs. Piggyback basins and toe troughs reflect architectures observed on the flanks of asymmetric satellite basins. The central zone (E) of a satellite basin may appear conformable with underlying basement strata. Modified from Ori et al. (1986).

crests. Thrust culminations within the fold and thrust belt generally occur as a series of ridges which contain steeply dipping forelimbs and less steeply dipping back limbs. These ridges often act as barriers to basin-directed sedimentation and therefore contribute to the development of ponded or laterally restricted growth stratal deposits (Figure 4.2). The steeply dipping forelimbs of thrust ridges also impose controls on sedimentation style by providing sites of increased slope instability. Allen et al. (1986) indicate that submarine slumps, slides, turbiditic debris flows and denudation complexes are often observed in growth strata which form near thrust culminations in active fold and thrust belts. Foreland basin successions develop through time in response to the combined processes of shortening, uplift, erosion and sedimentation. As the basin evolves, deep and shallow marine depositional settings shift basinward as a result of continued uplift and/or incorporation into the thrust belt. This basin-directed axial progradation of sedimentary facies can result in a notable diachroneity within the sedimentary succession, the identification of which can be assisted by a thorough biostratigraphic investigation of the foreland basin succession.

4.2.2 Comparison with the Adana Basin

The Adana Basin contains many of the diagnostic elements of a foreland basin. Geographically, the basin lies in front of a series of large south-directed Tauride thrust sheets which developed in the north during the Eocene to Oligocene interval. Further south, in front of the Cilicia-Adana Basin complex, a zone of active convergence and subduction has been documented near Cyprus (Aksu et al., 2003; Hall et al., 2003). Structurally, the lower to

middle Miocene succession of the Adana Basin is dissected by a series of progressive south-directed low angle thrust faults. In the northern portion of the basin, these thrusts occur in association with Early Miocene (Burdigalian to Langhian) stratigraphy; further south, these thrusts dissect progressively thicker stratigraphic sections and incorporate Middle Miocene (Serravalian to Tortonian) strata. Carbonate reef deposits occur along the crests of most ramp anticlines, and biostratigraphic analyses indicate that reefs in the north of the Adana Basin formed in the Burdigalian, while reefs located to the south near the Misis Complex, formed during the Tortonian. Thrusts imaged in the southernmost portion of the Adana Basin incorporate successively thicker Miocene successions, which include the Tortonian aged B2 seismic unconformity and overlying Kuzgun deposits.

The sedimentary succession that is dissected by the early to middle Miocene south-directed thrust structures contains a variety of stratal architectures and features which are often observed in foreland basins. Progressive syntectonic unconformities occur in both the Northern and Eastern domains of the Adana Basin. While the structural style of each domain differs, evidence of uplift is observed in both settings, and the resultant progressive unconformities exhibit geometric similarities. Progressive unconformities in the Northern Domain occur in piggyback basin depocentres, which developed between successive thrust sheets. Sedimentation within these sub-basins was therefore, contemporaneous with uplift and progressive steepening of individual thrust sheet forelimbs. The rotational geometry is discernable within seismic profiles of folded growth strata which flank ramp anticline crests; this rotation is imaged as an up-section decrease in stratal and local unconformity dip angles.

Hardy and Poblet (1994) have generated similar geometries in numerical models of growth sedimentation and progressive limb rotation which are comparable to those observed in the Mediano anticline, Pyrenees, Spain.

The progressive unconformities observed in the Eastern Domain appear as isolated composite progressive unconformities, which display a similar up-section decrease in dip angle. However, these features occur at the flank of a prominent culmination wall that presently forms the eastern margin of the Adana Basin. Lower portions of the MGS2 seismic succession are imaged as pre-growth strata which terminate abruptly against local reverse faults. Up-section, a shift to progressive unconformities, rotational growth strata and denudational complexes are observed along the flanks of the uplifted basement high. The appearance of southwest-directed progradational features in MGS2 growth strata provide further evidence of an abrupt increase in erosion and sedimentation in the northeast portion of the Adana Basin in the Tortonian to Pliocene interval. Sedimentological provenance studies of the Adana Basin indicate that these progradational deposits were sourced from newly uplifted rocks of the Misis Mountains in the east. This marks a radical shift in sediment provenance and drainage patterns within the Adana Basin, which was previously dominated by sediment sourcing from the north and west. These shifts in sediment provenance, in conjunction with the identification of denudational complexes set within deepwater deposits of the Güvenç Formation, indicate that a major change in tectonic activity occurred in the Adana Basin in the middle Miocene.

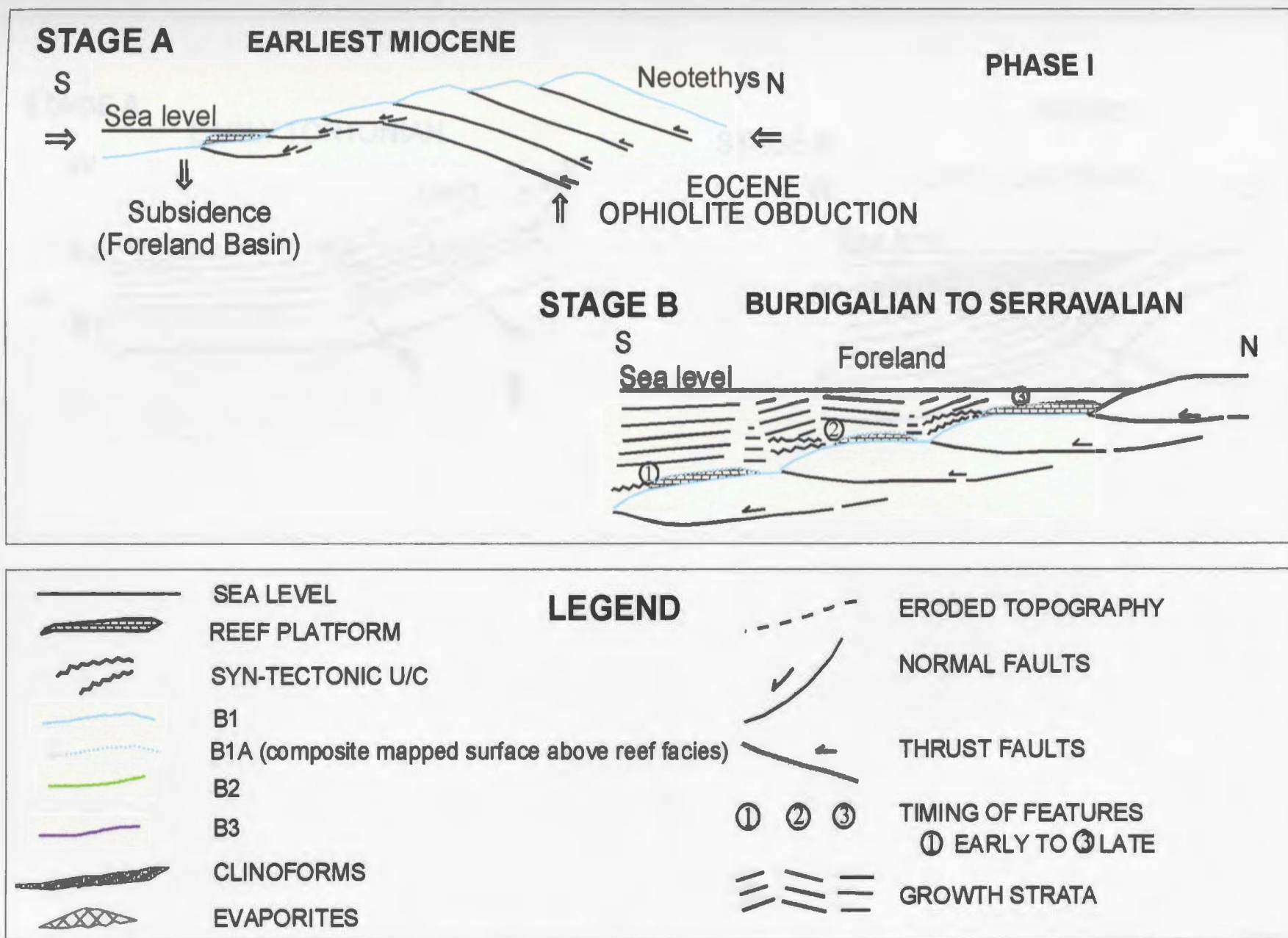


Figure 4.4: Miocene tectono-stratigraphic model for Phase I in the Adana Basin. Phase I is linked to structural-stratigraphic observations reported in the Northern Domain. Explanations of Stages A and B are provided in text section 4.3.

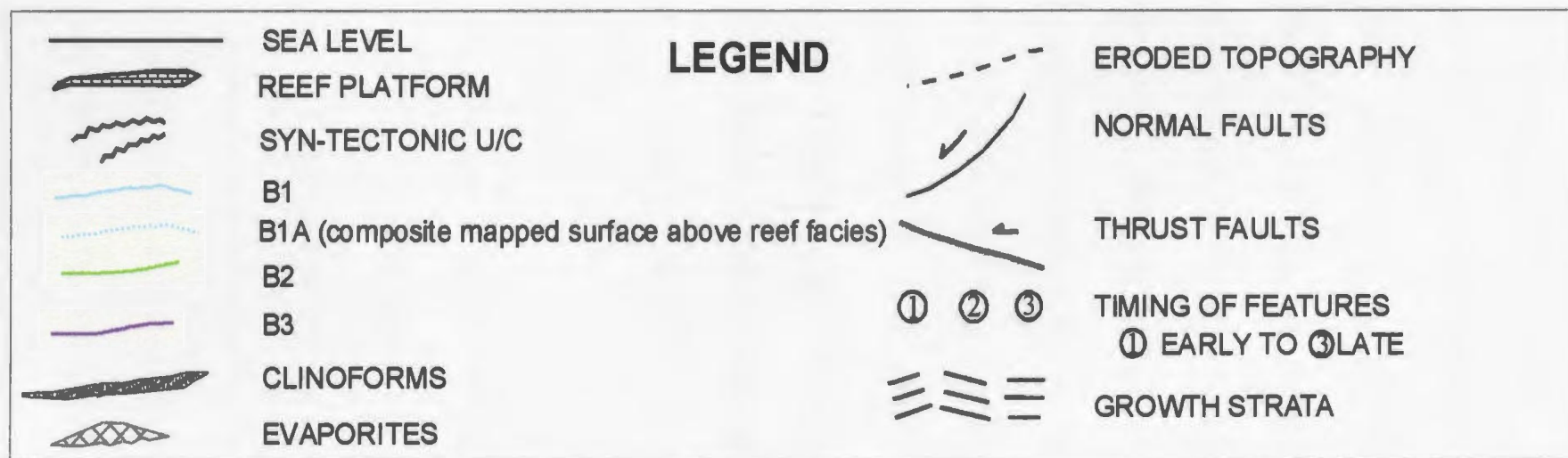
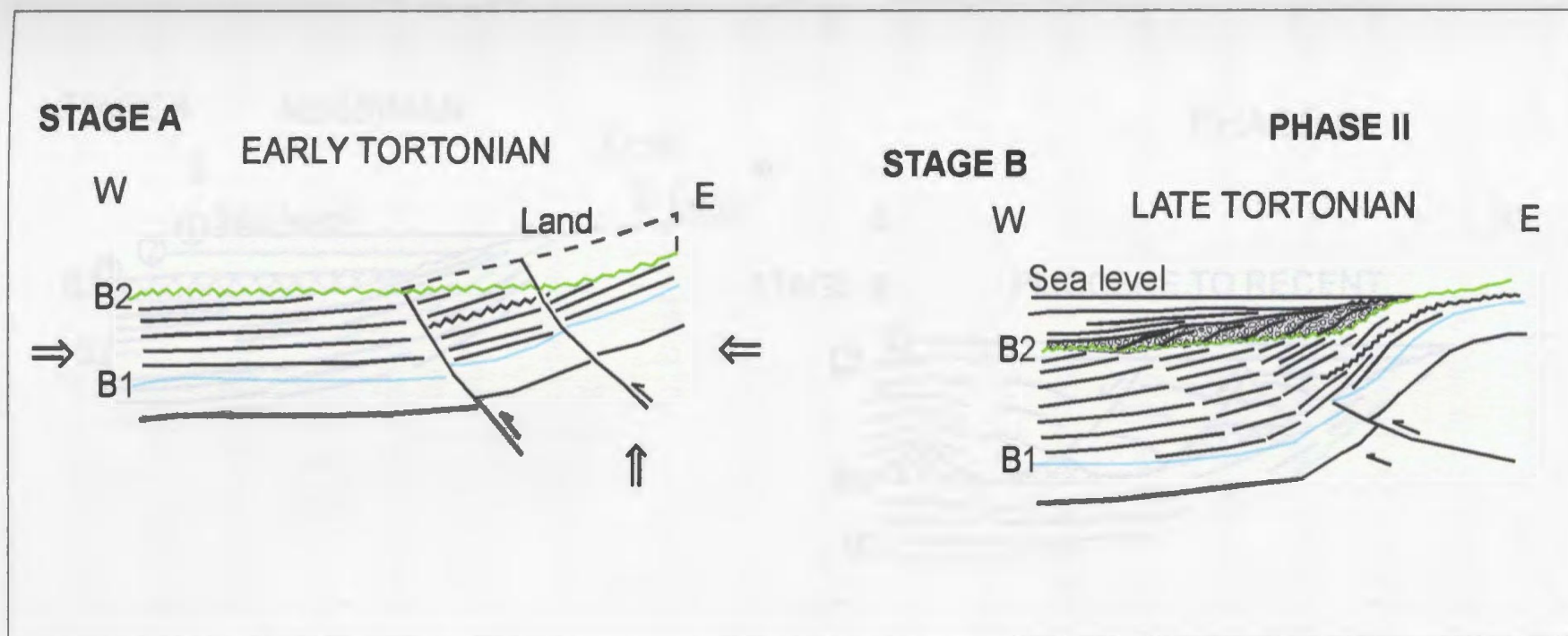


Figure 4.5: Miocene tectono-stratigraphic model for Phase II in the Adana Basin. Phase II is linked to structural-stratigraphic observations reported in the Eastern Domain. Explanations of Stages A and B are provided in text section 4.3.

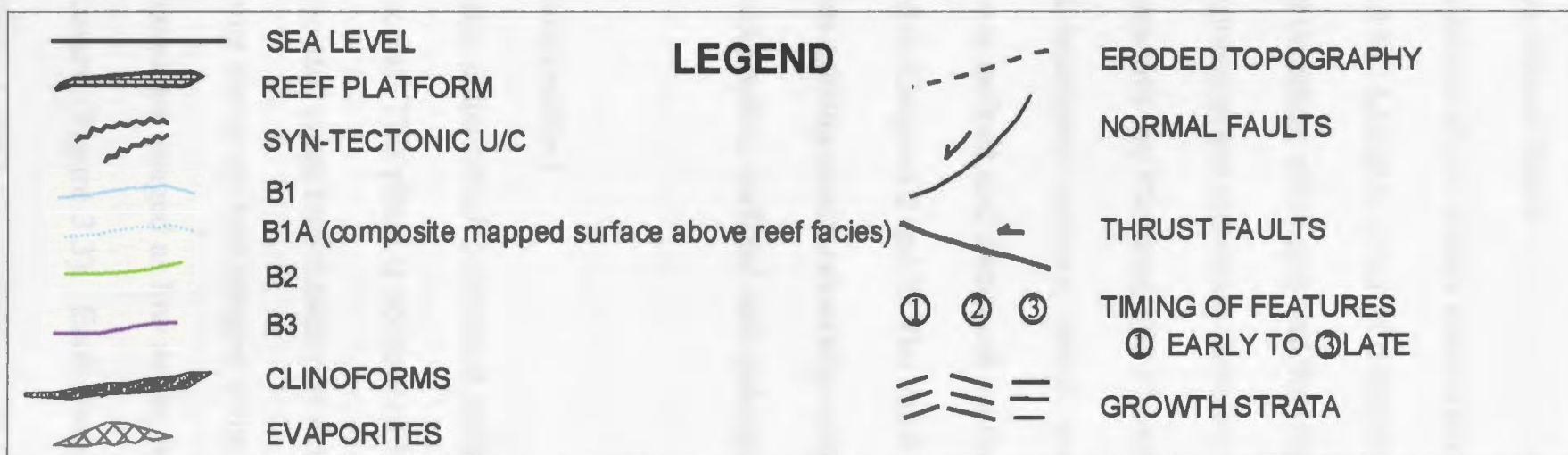
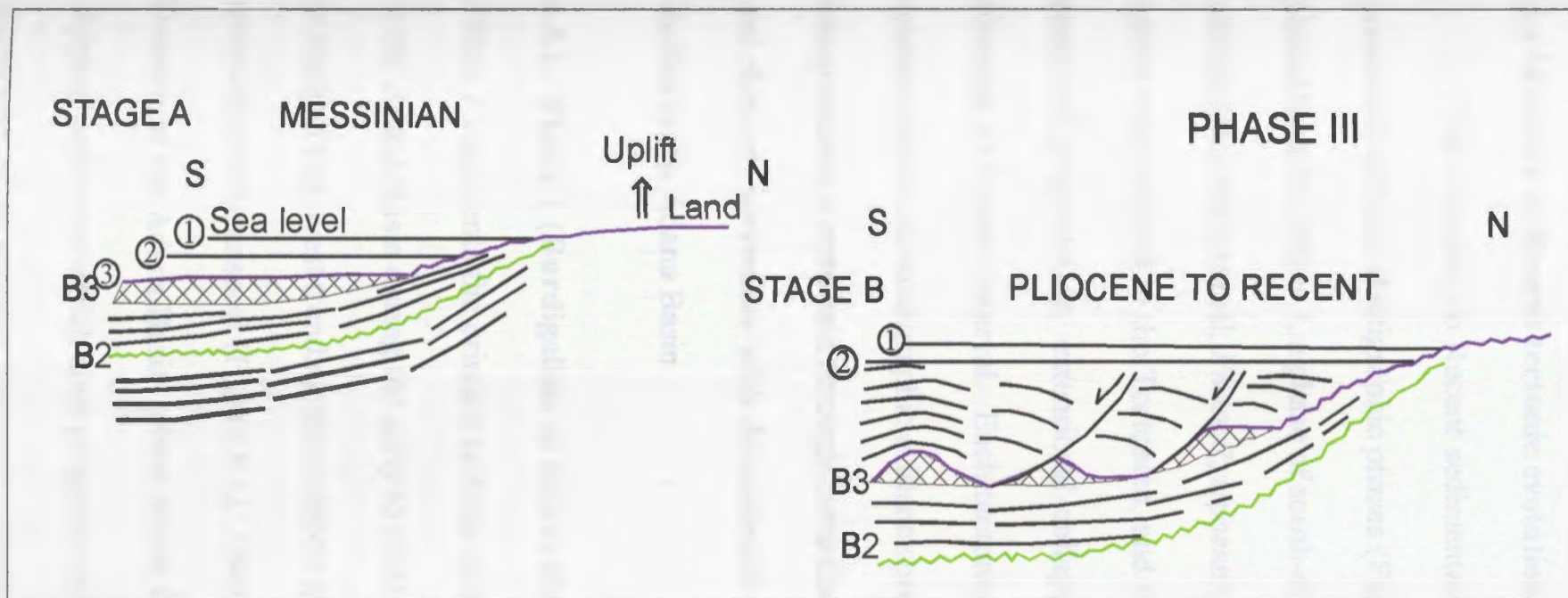


Figure 4.6: Miocene tectono-stratigraphic model for Phase III in the Adana Basin. Phase III is linked to structural-stratigraphic observations reported in the Southwestern Domain. Explanations of Stages A and B are provided in text section 4.3.

4.3 Miocene to Recent tectonic evolution of the Adana Basin

The Miocene to Recent sedimentary succession of the Adana Basin records three prominent tectono-stratigraphic phases (Figs 4.4-4.6). Listed in order of occurrence, these phases include: *Phase 1*, a phase of south-directed thrusting which spanned the Oligocene to middle Miocene interval, *Phase 2*, a phase of compression and southeast-directed thrusting, which was initiated in the Tortonian, and continues into the Pliocene, and *Phase 3*, a late phase of progradation, extensional collapse and halokinetic activity, which spanned the Pliocene to Recent interval. Each tectonic phase is defined and discussed on the basis of seismic-structural/stratigraphic evidence presented in Chapters 2 and 3. The validity of each interpretation is examined through comparison with existing structural-stratigraphic analogs and through agreement with documented biostratigraphic, surficial and paleogeographic studies in the Adana Basin.

4.3.1: Phase 1 (Burdigalian to Serravalian Compression)

Phase 1 represents the primary tectono-stratigraphic phase which controlled sedimentation in the Adana Basin during the early to middle Miocene. This phase is dominated by a series of stacked east-west trending thrust sheets and associated piggy back basins that demonstrate south-directed transport (Figure 3.1). *Phase 1* thrust sheets are best imaged in the Northern Domain of the Adana Basin, where thrust fault planes are imaged as low angle, hinterland-dipping reflectors which step progressively northward (Figure 3.3). Each thrust sheet is comprised of an acoustic basement succession which ranges in thickness from 0.8 to 1.0

second TWT. The structural-stratigraphic architecture of these features suggests that thrust sheets formed in the uppermost levels of thick piles of obducted pre-Miocene ophiolitic thrust sheets which lie to the north and west of the study area (Figs 1.11 and 2.1). The formation and progressive basinward movement of thrusts in the Northern Domain was most likely achieved through gravity-driven processes similar to those outlined by Allen et al. (1986).

Seismic-stratal architectures observed at the flanks and tops of individual thrusts reveal that many of these thrusts were simultaneously eroded along their crests and buried along their flanks. As progressive thrust sheets descended into the shallow marine setting of the south, carbonate platforms developed preferentially on thrust submarine highs and were later drowned during continued basinward movement. This interpretation accommodates the presence of localized carbonate platform reef facies, complex growth strata and local unconformities, as observed within seismic profiles in the study area.

The internal architecture of the thrust belt may best fit a model in which successive internal thrusts developed within the Adana Basin and effectively dissected the sedimentary succession. The thrusts moved progressively basinward. The leading edge of the thrust front then jumped to the south, in a position in front of the internal stack. This deep-seated thrust carried the stacked succession of internal thrusts and their associated sub-basins, piggy back-style, deeper into the basin. Such a model could accommodate for the observed landward directed onlap and apparent downlap relations observed above the B1 unconformity, as well as the localized transgressive character of the Karaisalı Formation.

Continued basin-directed movement of thrusts in the Northern Domain led to the

progressive development of ramp anticlines in a shallow marine setting. Uplifted basement highs extended into the photic zone, where simultaneous carbonate platform deposition and erosion reshaped the thrust culminations. As thrust sheets continued to propagate in a basinward direction, existing thrust sheets crests and platform reef features were successively drowned as they descended below the photic zone. Each successively higher thrust sheet most likely experienced an initial rise into the reef-nurturing photic zone, followed by the same basinward descent and drowning as its predecessors. In this fashion a series of platform reef deposits of the Karaisalı Formation stepped stratigraphically up-section, and transgressed a series of basinward-shifting thrust sheets, during a period in which eustatic sea level may have been rising, stationary or falling. Görür (1994) used sedimentological and biostratigraphic data in the Karaisalı Formation to produce a nonpalimpsestic relative sea level curve of the Burdigalian to Serravalian interval for the Adana Basin (Figure 1.12). The study reveals that reef features of the Karaisalı Formation document a consistent, relative sea level rise in the Adana Basin which spans the Burdigalian to Serravalian interval. This consistent, localized transgression spans a time in which eustatic sea levels of Haq et al (1987) rose slightly during the Burdigalian, fluctuated during the Langhian, and dropped significantly through the Serravalian time interval (Figure 1.12). Therefore, a poor correlation between local basin trends and postulated worldwide eustatic events is seen.

The documentation of a long duration relative sea level rise in the Adana region has led researchers to conclude that tectonic controls may have contributed to the event. Pralle (1994) proposes that the Adana Basin formed in response to extensional deformation, and

was then dominated by transtensional tectonics in the early to middle Miocene interval. Williams et al. (1995) propose that the observed transgression may be attributed to the rapid subsidence caused by early to middle Miocene extension. Yetis et al. (1995) make reference to an alternate model, which proposes that early Miocene subsidence and transgression in the Adana region can be attributed to crustal-scale extension generated by a back-arc “roll-back” mechanism along the Hellenic-Cyprus subduction zone (e.g. Postma et al., 1993). The data acquired through the course of this study reveal that compression-dominated tectonics were a primary control on the architecture and evolution of the Adana Basin from the early to middle Miocene. Extensional fault arrays observed within the north-central portion of the basin appear to have formed later, during the Serravalian to base Tortonian interval. The development of middle Miocene extensional fault sets in the Northern Domain may relate to the westward propagation of a transtensional (proto-Ecemis - Kozan Fault) system associated with the early docking of Arabia. These observations lend further support to the interpretation that south-directed thrust tectonics controlled the relative sea level changes, depositional styles and sedimentation patterns observed in the early to middle Miocene succession of the Adana Basin.

4.3.2: Phase 2 (Tortonian to Pliocene compression)

A second phase of compression spanned the Tortonian to Pliocene interval in the Adana Basin (Figure 4.4). This phase of compression resulted in the development of a prominent culmination wall, with local isolated reverse faults, in an area recognized regionally

as the western flank of the Misis structural high. Growth strata and progressive unconformities are not imaged in association with these structures in the lower half of the tilted MGS2 succession. This suggests that the lower portion of MGS2 contains pre-growth strata, while the upper MGS2 and MGS3 successions contain syn-sedimentary deposits that formed during the development of the Misis high. Phase 2 uplift was coincident with a documented eustatic sea level drop in during the Tortonian to Messinian interval (Haq et al., 1987). The combined effect of uplift on an existing foreland basin ramp setting, during a time eustatic sea level fall led to the development of a forced regression. This forced regression resulted in the development of a series of stacked, stranded sand wedges that occur in association with the Tortonian B2 unconformity (Figure 2.14). The climax of the forced regression was punctuated by extensive dessication of the Mediterranean Sea, which resulted in widespread evaporite deposition and erosion during the Messinian interval.

4.3.3: Phase 3 (Pliocene to Recent extensional collapse and halokinetics)

A late phase of extensional collapse and halokinetic activity spanned the Pliocene to Recent interval in the Adana Basin (Figure 4.4). Following the widespread dessication of the Mediterranean Sea, and the precipitation of thick evaporites sequences within the Adana Basin, the sea returned to the southernmost portions of the study area. As a result, the Adana Basin was influenced mainly by terrestrial and shallow marine erosion and deltaic progradation during the latest Messinian to recent interval. Sediments were eroded from the structurally elevated northern, western and eastern flanks of the basin, and were transported

southward, where they were deposited as deltaic deposits above the the evaporitic sequences. As the deltas thickened and prograded basinward, a gentle detachment horizon formed within the Messinian evaporites. The development of a detachment horizon led to basin-directed extensional collapse of the Messinian to Recent sedimentary pile along a series of listric fault in the southernmost portions of the Adana Basin. Localized salt tectonics accompanied the this extensionsional collapse, and resulted in the development salt rollers, welds, turtle anticlines and diapirs in the Southwestern Domain of the Adana Basin. Stratal architectures observed on the flanks of salt cored - turtle anticlines and diapirs indicated that salt structures remained active into the late Pliocene.

CHAPTER 5: CONCLUSIONS

The Adana Basin of southeastern Turkey lies above the late Cretaceous-Eocene ophiolitic suture of the Afro-Arabian and Euro-Asian plates. The Miocene to recent stratigraphy, structural geology and tectonic evolution of the oil-producing basin can be summarized as follows:

1. The early to middle Miocene succession records the development of a foreland piggyback basin, in which sedimentation was largely controlled by southward-propagating thrust sheets. Seismic reflection profiles reveal that irregularly-distributed basement highs are, in fact, progressively-transgressed anticline crests of successive thrust sheets. Transgressive system tract reef deposits are imaged on ramp anticline crests, slumps deposits and denudational complexes are imaged in intervening frontal synclines, and progressively rotated syntectonic unconformities are imaged at ramp anticline flanks. Continued basin-directed movement of thrust sheets likely controlled the drowning of successive reef deposits, which are succeeded by deeper marine Highstand systems tract deposits. Notably, the thickness of Miocene strata contained within thrust sheet hanging walls increases substantially in the southernmost thrust sheets, and likely reflects a jump of the thrust front toward the south.
2. During the late Serravalian, a series of conjugate extensional fault sets developed, prior to, or coincident with, the development of a regionally extensive Type I sequence boundary (B2). These events were followed by uplift in the east, represented by the development of a prominent N-S trending culmination wall and local reverse faults associated with the Misis Mountains. The B2 unconformity is succeeded by Forced

Regressive systems tract deposits in the northern uplifted portions of the basin, which consist of Tortonian-aged stranded sand wedges and are incised by fluvial channels. A series of southwestward-prograding clinoforms, complex growth stratal architectures and progressively rotated syntectonic unconformities are observed in association with the flanks of the culmination wall. These features suggest that the basin bounding structure had already gained significant relief prior to the Messinian.

3. The late Miocene stratigraphic succession records a regionally extensive dessication event, characterized by evaporation of the Mediterranean Sea, precipitation of evaporates in basinal areas, and erosion of exposed areas, that marks the culmination of the Forced Regressive systems tract. The significant uplift observed along the eastern Flank of the basin at this time may have contributed to the rapid and extensive retreat of the Mediterranean Sea recorded in the Adana Basin during the Messinian.

4. Late Messinian strata record a transgressive parasequence, which marks the return of the Mediterranean Sea to the southern portions of the basin. The Pliocene to Recent interval is characterized by the development of thick deltaic Lowstand systems tract deposits. In the southernmost portion of the basin these deposits contain extensional collapse structures that sole into salt, as well as various salt structures. The processes of erosion, lowstand fluvio-deltaic progradation and tectonism are still active in the Adana Basin today.

References

- Allen, P.A., Homewood, P. and Williams, G.D. 1986. Foreland basins: an introduction: International Association of Sedimentologists Special Publication 8, 3-12.
- Aksu, A.E., Calon, T.J., Piper, D.J.W, Turgut, S, and E.K. Izdar, 1992 a. Architecture of late orogenic basins in the eastern Mediterranean Sea. *Tectonophysics*, 210: 191-213.
- Aksu, A.E., Uluğ, A., Piper, D.J.W., Konuk, T. and Turgut, S., 1992 b. Quaternary sedimentary history of Adana, Cilicia and Iskenderun Basins, Northeast Mediterranean Sea. *Marine Geology*, 104: 55-71.
- Bridge, C., Calon, T.J., Hall, J. and Aksu, A.E., 2003. Salt tectonics in two convergent margin basins of the Cyprus Arc, Eastern Mediterranean. *Marine Geology*, in press.
- Calon, T.J., Hall, J. and Aksu, A.E., 2003 a. Origin and evolution of the Mesaoria Basin, Cyprus: linkage with the Eastern Mediterranean. *Marine Geology*, in press.
- Calon, T.J., Aksu, A.E., and Hall, J., 2003 b. The evolution of the outer Latakia and eastern Mesaoria Basins, Eastern Mediterranean. *Marine Geology*, in press.
- Clauzon, Georges, Suc, Jean-Pierre, Gautier, Francois, Berger, Andre and Loutre, Marie-France, 1996. Alternate interpretation of the Messinian salinity crisis: controversy resolved? In *Geology*: April 1996: v. 24; no.4; p 363-366; 3 figures.
- Emery, D. and Myers, K.J., 1996. *Sequence Stratigraphy*. Blackwell Science Ltd. London 297p.

- Gökçen, S.L., Kelling, G., Gökçen, N. and Floyd, P.A., 1988. Sedimentology of a late Cenozoic collisional sequence: the Misis Complex, Adana, southern Turkey. *Sedimentary Geology*, Vol. 59: 205-235.
- Görür, N., 1985. Depositional history of Miocene sediments on the NW flank of the Adana Basin. *Proc. Sixth Colloquium on Geology of the Aegean region*, Izmir, 185-208.
- Görür, N., 1992. A tectonically controlled alluvial fan which developed into a marine fan-delta at a complex triple junction: Miocene Girdirli Formation of the Adana Basin, Turkey. In *Sedimentary Geology*, Vol. 81, p. 243-252.
- Görür, N. (1994). Tectonic control in the development of a lower miocene reef at a complex triple junction: depositional history of the Karaisali Formation of the Adana Basin. In *Geologie Mediterranee Tome XXI* (1-2), 1994 p 49-67.
- Gürbüz, K. and Kelling, G., 1992. Internal/external controls on submarine fan development: two examples from the Neogene of southern Türkiye. 29th Int Geol Congress, Kyoto (abstracts) 2:p. 292.
- Gürbüz, K., and Kelling, G., 1993. Provenance of Miocene submarine fans in the northern Adana Basin, southern Turkey: a test of discriminant function analysis. *Geol J* 28:277-293.
- Hall, J., Aksu, A.E., Calon, T.J. and Yaşar, D., 2003 a. Varying tectonic control on basin development at an active microplate margin: the Iskenderun - Latakia Basin complex, Eastern Mediterranean. *Marine Geology*, in press.

- Hardy, S., and Poblet, J., 1994. Geometric and numerical model of progressive limb rotation in detachment folds. *Geology*, Vol 22: 371-374.
- Haq, B.U., Hardenbol, J., and Vail P.R., 1987. The chronology of fluctuating sea level since the Triassic. In *Science* 2335 p. 1156-1167.
- Karig, D.E. and Kozlu, H., 1990. Late Paleogene - Neogene evolution of the triple junction region near Maraş, south-central Turkey. *Journal of the Geological Society, London*, 147: 1023-1034.
- Kelling, G., Gökçen, S.L., Floyd, P.A., Gökçen, N., 1987. Neogene tectonics and plate convergence in the eastern Mediterranean: new data from southern Turkey. *Geology*, 15: 425-429.
- Kozlu, H. 1987. Structural development and stratigraphy of Misis-Andirin region. 7th Biannual Petroleum Congress of Turkey. p.104-116.
- Medwedeff, D.A., 1989. Growth fault-bend folding at southeast Lost Hills, San Joaquin Valley, California. *American Association of Petroleum Geologists Bulletin*, Vol 4: 133-146.
- Mulder, C.J. (1973)
Tectonic framework and distribution of Miocene evaporites in the Mediterranean
In *Messinian events in the Mediterranean* Koniniljke Nederlandse Akademie van Webnschappen.

- Mulder, C.J; Lehner, P. And Allen, D.C.K., 1975. Structural evolution of the Neogene salt basins in the eastern Mediterranean and the Red Sea. In *Geologie en Mijnbouw*, Volume 54 (3-4) p. 208-221.
- Ori, G.G. and Friend, P.F., 1984. Sedimentary basins formed and carried piggyback on active thrust sheets. *Geology*, 12: 475-478.
- Ori, G.G., Roveri, M. and Vannoni, F., 1986. Plio-Pleistocene sediments in the Apenninic-Adriatic foredeep (central Adriatic Sea, Italy): International Association of Sedimentologists Special publication 8, 183-198.
- Özer, B., Bijou-Duval, B., Courrier, P. and Letouzey, J., 1974. Geology of Neogene Basins of Antalya, Mut and Adana. In: Proceedings of the 3rd Petroleum Congress of Turkey, Turkish Association of Petroleum Geologists, p. 57-84.
- Perinçek, D. et al., 1987. New observations on strike-slip faults in east and southeast Anatolia. 7th Biannual Petroleum Congress of Turkey. p. 89-103.
- Poblet, J., Munoz, J.A. Trave, A. and J. Serra-Kiel, 1999. Quantifying the kinematics of detachment folds using the 3D geometry: application to the Mediano anticline (Pyrenees Spain). *GSA Bulletin*, in press.
- Pralle, N., 1994. Geometric and numerical model of progressive limb rotation in detachment folds. *Geology*, Vol 22: 371-374.
- Ricci-Lucchi, F., 1986. The Oligocene to recent foreland basins of the northern Apennines: International Association of Sedimentologists Special publication 8, 105-139.

- Şengör, A.M.C. and Yılmaz, Y., 1981. Tethyan evolution of Turkey: a plate tectonic approach. *Tectonophysics* 75: 181-241.
- Suppe, J., Chou, G.T. and Hook, S.C., 1991. Rates of folding and faulting determined from growth strata. *In* McClay, K.R., ed., *Thrust Tectonics*: London, Chapman & Hall. 105-121.
- Uffenorde, H., Lund, J.J. and Georgi, K.H., 1990. Biostratigraphy of the Neogene in the Iskenderun Basin. Turkish Association of Petroleum Geologists, Proceedings of the 8th Petroleum Congress of Turkey, 363-370.
- Van Wagoner, J.C., H.W. Posamentier, R.M. Mitchum, P.R. Vail, J.F. Sarg, T.S. Loutit, and J. Hardenbol, 1988. An overview of the fundamentals of sequence stratigraphy and key definitions, *In*: Sea level changes: an integrated approach: Soc. Econ. Paleontologists and mineralogists Special Publ. 42: 39-45.
- Van Wagoner, J.C., R.M. Mitchum, K.M. Campion and V.D. Rahmanian, 1990. Siliciclastic sequence stratigraphy in well logs, cores and outcrops: AAPG Methods in Exploration Series No. 7, Tulsa, Okla., 55p.
- Williams, G.D., Ünlügenç, U.C., Kelling, G. and Demirkol, C., 1995. Tectonic controls on stratigraphic evolution of the Adana Basin, Turkey. *Journal of Geological Society of London*, 152: 873-882.
- Yalçın, N.M. and Görür, N., 1984. Sedimentological evolution of the Adana Basin. *In*: Tekeli, O. and Göncüoğlu, M.C. (Eds.), *Proceedings of the International Symposium on the Geology of the Taurus Belt*, Ankara, 165-172 pp.

- Yetis, C., 1988a. Reorganization of the Tertiary stratigraphy in the Adana Basin, southern Turkey. *Newsl Stratigr* 20 (1): 43-58.
- Yetiş, C., Kelling, G., Gökçen, S.I. and Baroz, F., 1995. A revised stratigraphic framework for Late Cenozoic sequences in the northeastern Mediterranean region. *Geol. Rundsch.*, 84: 794-812.
- Yılmaz, Y. et al., 1988. Tectonic Evolution of the Miocene Basins at the Amana Mountains and the Maras Region. *TAPG Bulletin*, Vol. 1/1, p. 52-72.
- Yılmaz, Y., 1993. New evidence and model on the evolution of the southeast Anatolian orogen. *Geological Society of America Bulletin*, Vol. 105, p. 251-271.
- Zoetemeijer, R., Sassi, W., Roure, F., and Cloetingh, S., 1992. Stratigraphic and kinematic modeling of thrust evolution, northern Appenines, Italy. *Geology*, 20: 1035-1038.

APPENDIX A – METHODOLOGY

APPENDIX A - METHODOLOGY

A1. Data Collection

Compilation of the Lithostratigraphic Review:

A comprehensive lithostratigraphic review of previous surface and subsurface studies in the Adana Basin was undertaken to clarify inconsistencies in the multitude of diverse published stratigraphic schemes available within the region. The resulting lithostratigraphic review is based primarily upon the revised stratigraphic framework for the northeastern Mediterranean, as proposed by Yetis et al (1995). Additional sedimentological, biostratigraphic and paleogeographic evidence are presented, where relevant, to support the incorporation of lithostratigraphic divisions, correlations and map results from other previous works. The surficial geology map and stratigraphic template presented in Chapter 2 were constructed by the author to reflect the results of the present lithostratigraphic review.

Delineation of Seismic Unconformities:

Standard seismic interpretation techniques were applied to the dataset used in this study. Full-size and 50% reduced paper copies of all industry seismic profiles were generated for use during the seismic interpretation procedure. Key horizons representing reflection discontinuities were identified in key profiles located in the north-central portion of the dataset (e.g., Line 7). The more continuous horizons (B1, B2) were delineated and correlated across the seismic data grid (using coloured pencils), on the basis of cross-line ties, reflection character, and stratigraphic position (Table 2.2). Additional local discontinuities were also highlighted on profiles where apparent. Once critical unconformities were mapped across the north-central portion of the seismic grid, well data, limited grid ties, and jump correlations were utilized to increase confidence in tracking the B1 and B2 unconformities into the southern portion of the dataset. An additional seismic unconformity, B3, was identified and delineated locally in the southernmost portion of the data.

Delineation of Seismic Units:

Seismic units were identified in seismic profiles and delineated with coloured pencils on the basis of internal reflection configuration, amplitude, continuity and external form (Table 2.4). The geographic locations of prominent

seismic units were noted, and where possible were correlated through the seismic grid for inclusion on subsurface maps (e.g., Unit 2).

Correlation and Chronology of Surface and Sub-surface Data:

Correlations between seismic horizons and reported, age-constrained, lithostratigraphic unconformities were achieved on the basis of similarity in stratigraphic position and regional distribution. Similarly, seismic megasequences were correlated with lithostratigraphic sequences according to the spatial correlation and chronology of the unconformities that bound them. Additional correlations of seismic facies and lithostratigraphic units were achieved using borehole data from the area (see correlations in Table B.1, Appendix B).

Sequence Stratigraphy:

A sequence stratigraphic framework was constructed for the Miocene succession in the Adana Basin. This framework was established through analysis of the results of the stratigraphic assessment presented in text Sections 2.1-2.3 in relation to sequence stratigraphic principles as outlined, for example, in Sequence Stratigraphy (Emery and Myers, 1996).

Identification of Structural Features:

Structural features were identified in seismic profiles by examining the B1, B2 and B3 seismic unconformities for evidence of structural truncation, offset, duplication or absence on both local and regional scales. Individual structural features were tracked and correlated using standard procedures of mapping through a seismic grid. Line orientations and density of line crossovers played important roles in aiding in the visualization of structures, following the established standard that dip profiles reflect maximum structural relief, strike lines reflect virtually no structural relief and oblique lines reflect intermediate relief. Various cross-sectional and longitudinal lines provided additional confirmation for the interpreted orientations and geometries of various fault features within the basin. Once structures were identified, hanging wall cut-offs, and any apparent stratal architectures, growth packages or associated seismic facies were examined in an attempt to ascertain the style and timing of deformation. Fault locations, geometries and heave and throw directions were recorded for inclusion on map patterns.

Notes on Seismic Imaging:

The quality of seismic imaging is greatly reduced in certain portions of the Adana Basin. Areas of significantly reduced seismic imaging were examined in an effort to determine whether these data reflect surface culture or possible subsurface conditions. In certain locations surficial features such as reservoirs, rivers, coastlines and residential areas within the study area have disrupted seismic acquisition and have created breaks in the seismic signal on some lines (see Figure A1). Along the eastern portion of the study area, significant diminishment and/or total loss of seismic signal is observed consistently across a number of profiles (see Figure A2). No surface culture-related data breaks are apparent in the vicinity of this north-northeast – south-southwest trending area of lost seismic image. However, borehole data obtained proximal to zones of reduced seismic imaging indicate the presence of complex structures and steeply dipping strata (e.g., Wells #10 and #11 in Appendix B). Seismic imaging is also noted to diminish significantly beneath thickened deposits of Unit 4 evaporites in the southwest portion of the basin.

A2. Sub-surface Mapping Techniques

Two different sub-surface mapping procedures were implemented during this study to reflect the geographic distribution of the collected stratigraphic and structural data. The significance of the resultant maps and the techniques used in each mapping procedure are outlined below:

Surfer Mapping Procedure

A series of time-structure and time-isochore maps were generated using the SURFER 7.0 statistical contouring package. Appendix C contains the data spreadsheet and provides the equations used in the SURFER mapping exercise. SURFER data filter and gridding reports are also included in Appendix C. Time-depth conversions were not attempted due to the high degree of lateral variability and deformation of seismic facies across the study area. Furthermore, the suite of time-structure and isochore maps generated in this study have provided sufficient results upon which observations relating to the timing and evolution of Miocene succession can be drawn. Time-structure maps reflect Two Way Travel (TWT) time, in seconds, from a horizontal surface datum, $t = 0$, to the B1 and B2 seismic unconformities. A time structure-map of the local B3 seismic unconformity was also attempted; however, the limited lateral extent of the horizon, sparse grid ties and numerous data gaps precluded mapping of this horizon on a scale that could contribute to our understanding of the Miocene

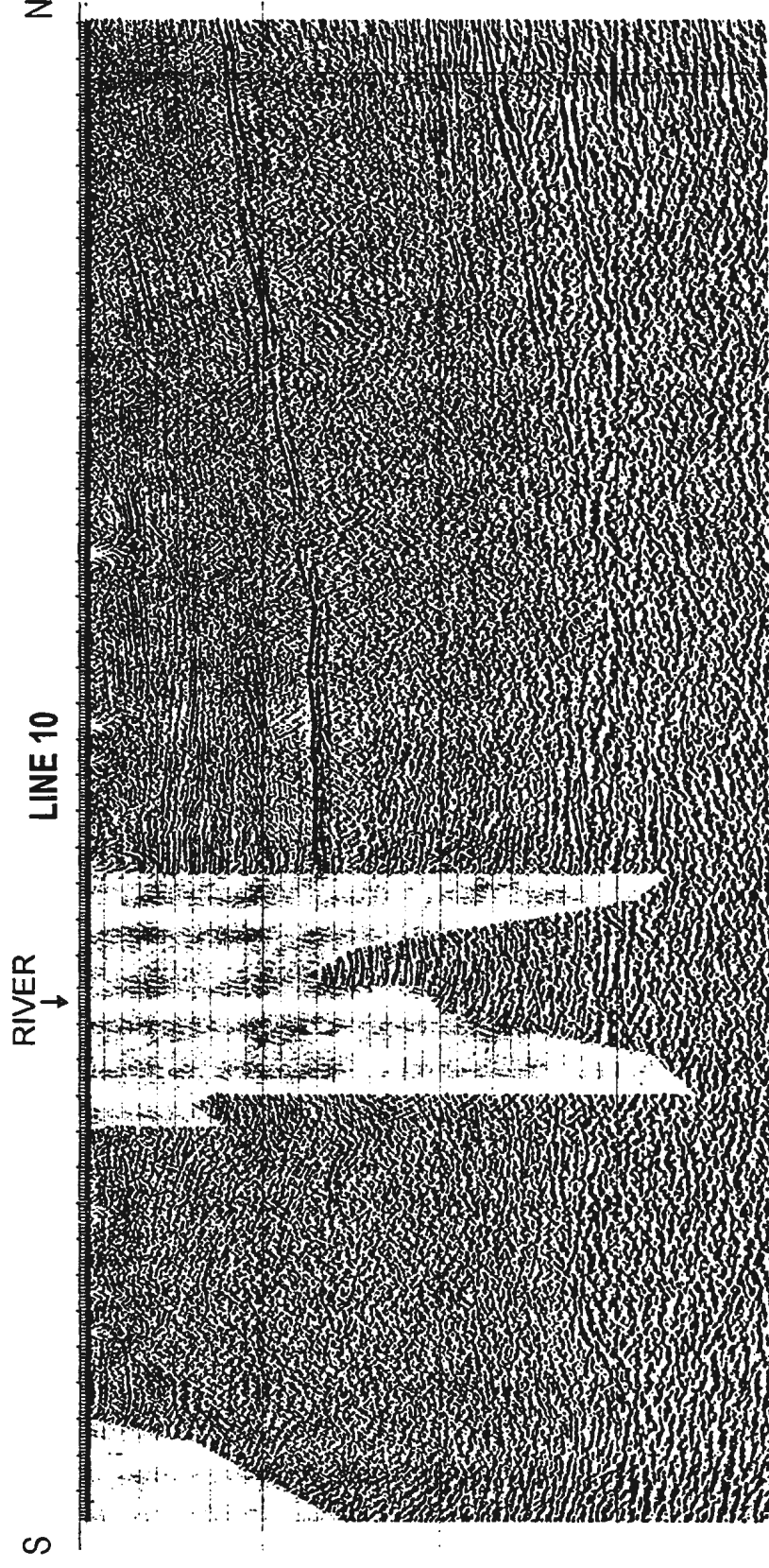


Figure A1: Line 10. Note the temporary break in seismic imaging at the location of a river.

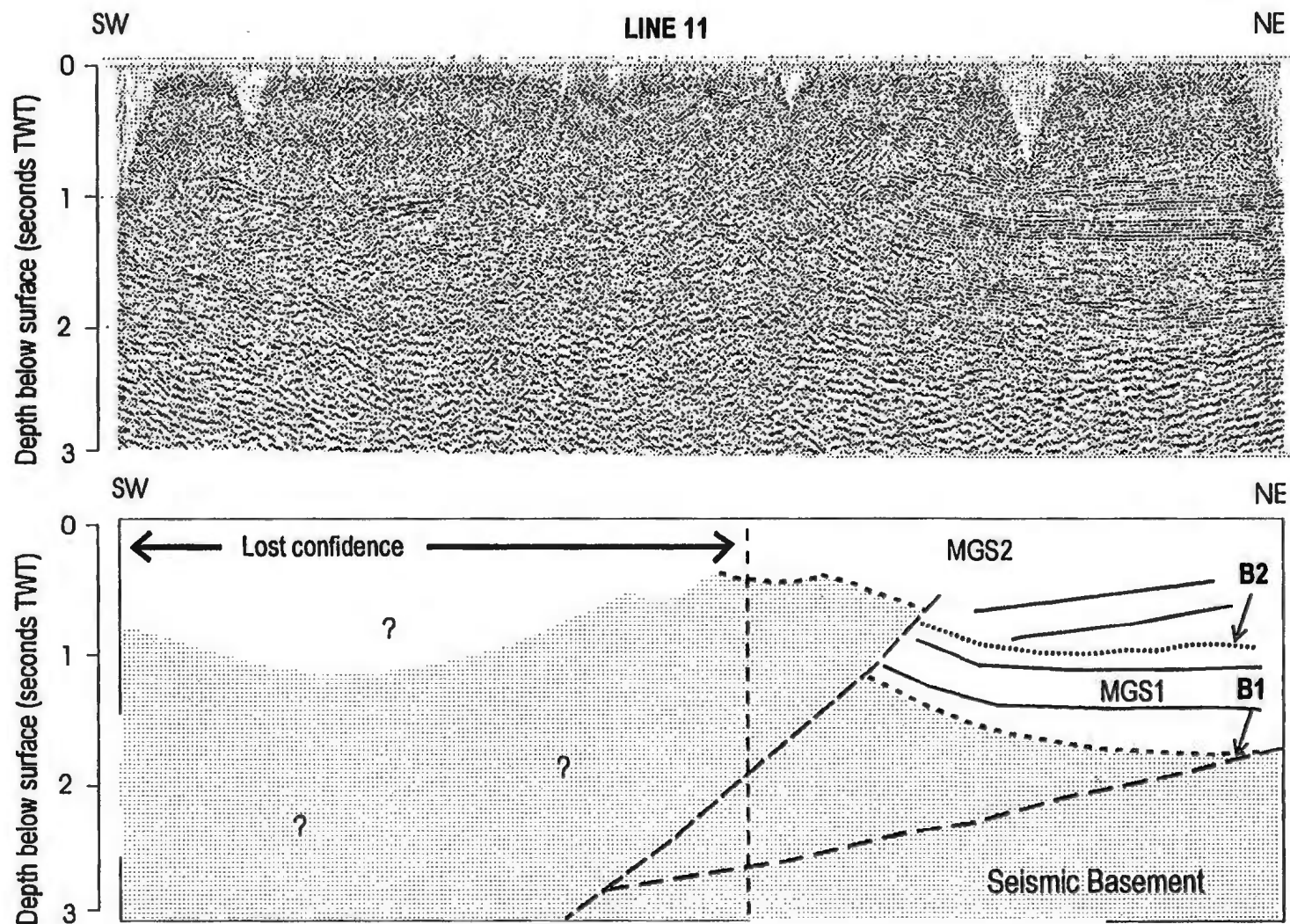


Figure A2: Line 11. Note loss of seismic image in the southwest.

evolution of the basin. The local distribution of the horizon was noted and reported within text Section 2.2.

Isochore maps reflect the vertical thickness distribution in time (seconds TWT), of i) the Miocene to recent basin fill ($t = 0$ to B1) ii) Megasequence 1 (B1 to B2) and iii) the Tortonian to Recent basin fill ($t = 0$ to B2). Data for both the time-structure and isochore maps were collected from seismic profiles using a ten-point divider and scaled reference measures. Equidistant data points (every 20 shot points) and a contour interval of 500 milliseconds were selected to account for standard weighting and smoothing operations that are applied by the SURFER software. Data were tabulated in an EXCEL spreadsheet. A high-resolution isochore map was also generated for seismic Unit 2. The data were collected every 10 shot points and a contour interval of 50 milliseconds was used to construct the high-resolution map.

Structure Mapping Procedures

The base map for the structure map was generated in AUTOCAD 2000, and paper copies of the base map were generated for the mapping exercise. The finalized positions of structural features on the paper base map were digitized into the AUTOCAD drawing (using a digitizing tablet) to maintain spatial relationships. The final map was exported from AUTOCAD to COREL DRAW 8 for annotation. The mapping of prominent structures in the Miocene succession required an iterative cross-line correlation procedure as outlined below:

In the northern portion of the basin, prominent thrust faults have tip lines lying with variable positions within the lower-middle portion of the Miocene succession. Sub-surface mapping at these tip lines was found to be difficult due to the poor expression of the tip points in individual seismic lines. Hence an approach was taken to map the main thrust faults as traces of the hanging wall cutoffs for the B1 unconformity (see Figure A3). This procedure maps the thrust fault positions at a structural level, below and towards the hanging wall side of the tip lines of the faults. The locations of each hanging wall cutoff were projected vertically to surface, and plotted on the base map with the corresponding structural symbol (shark teeth on hanging wall side of the fault trace). The position of ramp anticlines and frontal synclines were also located, vertically projected and plotted to increase confidence in correlations of individual thrust faults and their related fold structures.

In the eastern portion of the study area, the position of a basin-bounding culmination wall was located, projected vertically to surface and plotted on the base map. Seismic signal is greatly reduced in the vicinity of the culmination wall (e.g. Figure A2). Prominent reverse faults imaged on profiles in the east were

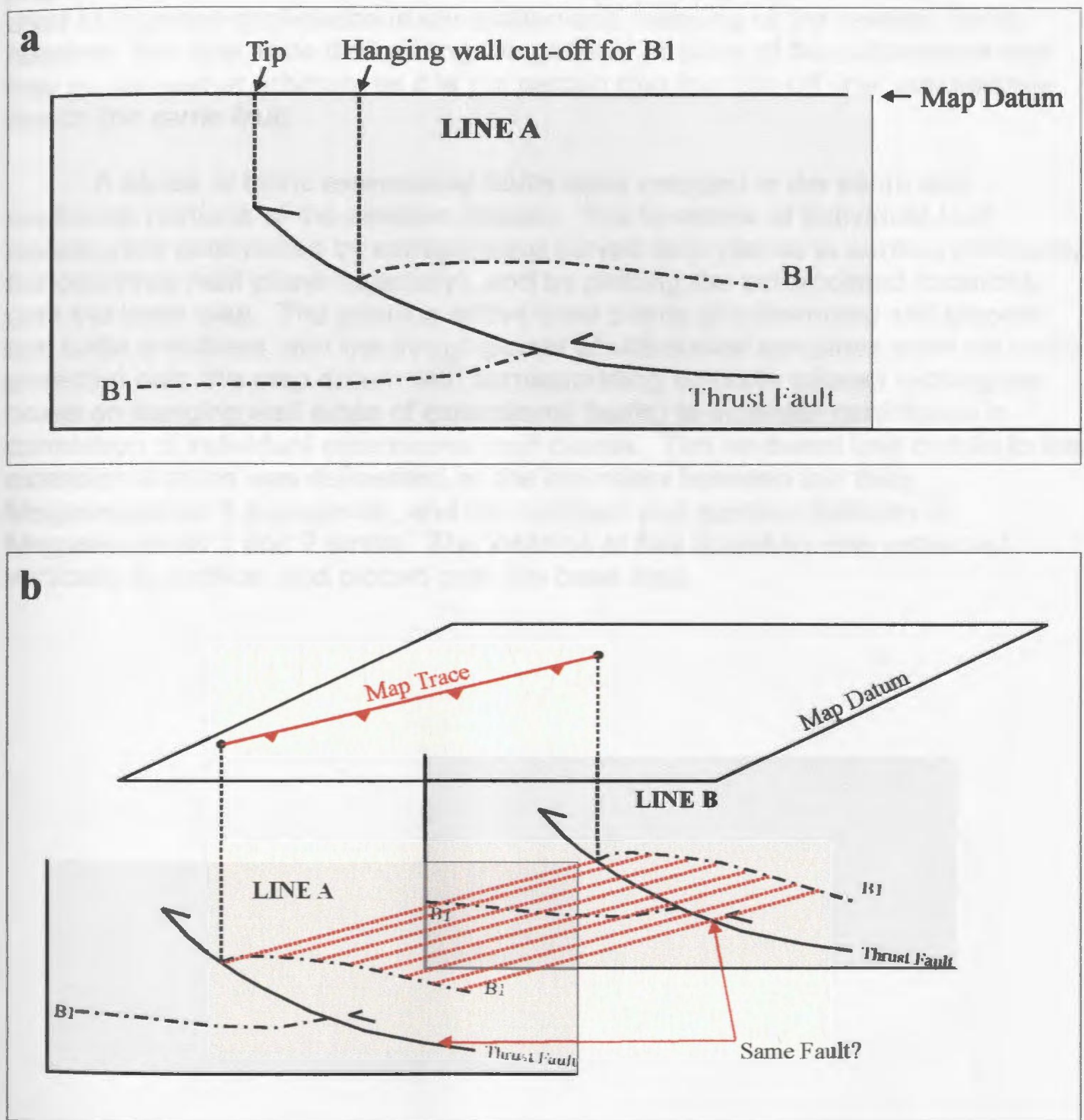


Figure A3: Illustration of mapping techniques used for mapping of thrust fault structures shown in Figure 3.1. Thrust faults and hanging wall cut-offs for the B1 unconformity are identified in seismic reflection profiles (a). Thrust faults are represented on the map pattern by the vertical projection of hanging wall cut-off points of the B1 unconformity (a). Projected points along a common fault plane are correlated and joined to provide representative traces for sub-surface thrust faults features (b). Shark teeth are positioned along the hanging wall side of fault traces.

examined for hanging wall cutoffs for the B1 unconformity, which were vertically projected onto the map. Cross-line correlations through the seismic grid were used to increase confidence in correlation and mapping of the reverse faults; however, the map trace delineating the general position of the culmination wall may be somewhat arbitrary as it is not certain that the “cut-off line” consistently lies on the same fault.

A series of listric extensional faults were mapped in the south and southwest portions of the seismic dataset. The locations of individual fault planes were determined by extrapolating curved fault planes to surface (following the observed fault plane trajectory), and by plotting the extrapolated locations onto the base map. The position of the crest points of intervening salt diapirs and turtle anticlines, and the trough points of withdrawal synclines were vertically projected onto the map datum with corresponding symbols (closed rectangular boxes on hanging wall sides of extensional faults) to increase confidence in correlation of individual extensional fault planes. The landward limit or sole to the extensional faults was delineated as the boundary between the thick Megasequence 3 succession, and the northern and eastern platform of Megasequence 1 and 2 strata. The location of this boundary was projected vertically to surface, and plotted onto the base map.

APPENDIX B – STRATIGRAPHIC CONTROL DATA

APPENDIX B: STRATIGRAPHIC CONTROL DATA

INDEX

TABLE B1: Summary of Available Well Data in the Adana Region.

TABLE B2: Summary of Biostratigraphic Data in the Adana Region.

Table B.1: Summary of available well data in the Adana Basin, with emphasis on regionally correlated lithostratigraphic contacts. Well data compiled from Turkish Petroleum internal reports and Pralle (1994).

Lithologies: Sandstone (SS); Shale (SH), Conglomerate (CONG), Limestone (LS), Limestone Breccia (LSB), Pelagic Limestone (PLS), Clay lenses (CL), Carbonates (CARB), Marl (MARL).

WELL ID (REFER TO FIGURE 1.7 FOR LOCATIONS)		CONTACT NAME		ABOVE CONTACT SURFACE		BELOW CONTACT SURFACE		DISTANCE FROM HORIZONTAL DATUM (T=0, D=0) TO CONTACT	
#	NAME	PRALLE, 1994	THIS STUDY	FORMATION	LITHOLOGY	FORMATION	LITHOLOGY	DEPTH (D) IN METRES	TIME (T) IN SECONDS TWO WAY TRAVEL TIME
1	EMELCIK-1	M3/M2	B2	Absent	Absent	Absent	Absent	Absent	Absent
		M2/M1	B1a	Guvenc	SH	Karaisali	LS, PLS	1182	0.77
		M1/Bsmt.	B1	Karaisali	LS	Basement	Basement (LS)	1241	0.8
2	GILBAS-2	M3/M2	B2	Kuzgun	SS, SH	Guvenc	SH	300	0.22
		M2/M1	B1	Cingoz	CONG, SS, LSB, SH	Gildirli	CONG	2500	1.45
3	SEVINCLI-2	M3/M2	B2	Absent	Absent	Absent	Absent	Absent	Absent
		M2/M1	B1a	Cingoz	SS, LS, MARL, CONG	Karaisali	LS	1800	1.13
4	SEVINCLI-1	M3/M2	B2	Absent	Absent	Absent	Absent	Absent	Absent
		M2/M1	B1a	Cingoz	CONG	Karaisali	LS	1865	1.25
5	YENICE-3	TORT. TOP	L1	Kosan Shale	SH	Kuzgun	LS, SS, SH	1230	0.6
		M3/M2	B2	Not Apparent	Not Apparent	Not Apparent	Not Apparent	Not Apparent	Not Apparent
		M2/M1	B1a	Cingoz	SH	Karaisali	LS	1780	1.5
7	AKKUYU-1	M3/M2	B2	Kuzgun	CONG, SS	Guvenc	SH	1070	0.86
		M2/M1	B1	Cingoz / Kopekli	MARL, CONG, SS, SH	Gildirli	SH	4000	2.6
8	GOZTEPE-1/A	TORT. TOP	L1	Kuransa	CONG	Kuzgun	SH	190	0.18
		M2/M1	B1	Not Penetrated	Not Penetrated	Not Penetrated	Not Penetrated	Not Penetrated	Not Penetrated
9	GOZTEPE-2	M3/M2	B2	Kuzgun	SS, SH, CARB	Guvenc	SS, SH	1080	1.2
		M2/M1	B1	Not Penetrated	Not Penetrated	Not Penetrated	Not Penetrated	Not Penetrated	Not Penetrated
10	K.MIHMANDAR	M3/M2	B2	Kuzgun	CONG, SS, SH	Guvenc	SH	1000	1.1
		THRUST	THRUST	Kuzgun & Guvenc	SH, MARL	Kuzgun & Guvenc	MARL, SH, LSB	1900	1.8
11	GEMISURA	M3/M2	B2	Kuzgun	SS, SH	Guvenc	SH	1180	0.95
		M2/M1	B1	Not Penetrated	Not Penetrated	Not Penetrated	Not Penetrated	Not Penetrated	Not Penetrated
12	YUMURTALIK-1	THRUST	THRUST	Kuzgun	SS	Cingoz	SH, CL, SS, CONG	400	0.2
		THRUST	THRUST	Guvenc	SH, CL	Kuzgun	SH, SS	1050	0.6
13	DERMITAS	MID. KUZGUN	KUZGUN WEDGE	Kuzgun	SS, LSB, SH	Kuzgun	SH	950	Not Available
		M2/M1	B1	Not Penetrated	Not Penetrated	Not Penetrated	Not Penetrated	Not Penetrated	Not Penetrated

Table B.2a: Summary of biostratigraphic data for the Adana Basin.

Lithologic unit	Age	Fossil assemblage	Author/date
Handere Fm	Messinian- early Pliocene	gastropods, ostracods, rare planktonic foraminifera	Gürbüz and Gökçen, 1985; Yetiş 1988a
Kuzgun Fm <i>Memişli</i> <i>Member</i>	Tortonian- Messinian	Ostrea, bivalves, gastropods, ostracods, rare planktonic foraminifera vertebrate teeth (<i>Hippariansp.</i>), gastropods	Tanar, 1985; Gürbüz and Gökçen, 1985; Inal A., cited in Yetiş 1988a
<i>Salbaş Tuffite</i> <i>Member</i>	Tortonian	benthic foraminifera, bivalves, gastropods, <i>Hippariansp</i> teeth	Yetiş, 1988a Yetiş, 1988a
<i>Kuzgun Member</i>	Serravalian- Tortonian		
Güvenç Fm	Burdigalian-lower Tortonian	planktonic foraminifera, discoaster-type nannofossils; <i>Braarudosphaera discula</i> ; <i>Braarudosphaera bigelowi</i> -type nannofossils; {benthic foraminifera also present}	Özelik, 1993
Cingöz Fm	Burdigalian- Serravalian	foraminiferal assemblages	Nazik and Gürbüz, 1992
Karaisalı Fm	Burdigalian- Serravalian	small benthic foraminifera and algae {corals, echinoderms, molluscs, bryzoa, wormtubes also present}	Yetiş, 1988a
Kaplankaya Fm	Burdigalian-early Langhian	benthic foraminiferal assemblage {echinoids, bivalves, gastropods, algae, corals also present}	Yetiş, 1988a
	Burdigalian	foraminiferal assemblage	Benda et al., 1977
Karsanti Fm	Oligocene	<i>Globigerina tripartita</i> Koch; <i>Globigerina cipercensis</i> <i>angulisuturalis</i> Bolli; <i>Globigerina cipercensis</i> <i>angustiumbilocata</i> Bolli; <i>Globigerina ouachitaensis</i> <i>ouachitaensis</i> Howe and Wallace; <i>Hemicyprideis montasa</i> Keen; <i>Echinocythereis</i> sp	Unluğenç et al., 1993

Table B.2b Summary of biostratigraphic data for the Misis Mountains

Isali Fm	Oligocene- Aquitainian	<i>globigerinoidesprimordius</i> Blow and Banner <i>Catapsydraxdissimilis</i> Cushman and Bermudaz	Gökçen et al., 1986 Gökçen et al., 1991
Karataş Fm	Burdigalian - early Tortonian	planktonic foraminiferal assemblages	Kelling et al, 1997; Gökçen et al., 1991
Kızıldere Fm	Tortonian	Ostrea, ostracods, gastropods	Schmidt, 1961; Gökçen et al., 1991
Kadirli Fm	Late Miocene- Pliocene		Schmidt, 1961

APPENDIX C – SURFER DATA

DATA SPREADSHEET

LINE #	FIX	LONG	LAT	B1	B2	MGS1	UNIT1
add8820:	110	37.1683	35.1367	-1.35	-0.1	1.1	0.15
		37.1683	35.14	-1.35	-0.1	1.1	0.15
		37.1683	35.1433	-1.4	-0.15	1.05	0.2
		37.1683	35.1467	-1.4	-0.15	1.05	0.2
		37.1683	35.15	-1.4	-0.18	1.07	0.15
		37.1683	35.153	-1.4	-0.2	1.1	0.1
		37.1683	35.156	-1.4	-0.2	1.1	0.1
		37.1683	35.1583	-1.4	-0.23	1.07	0.1
		37.1683	35.1613	-1.45	-0.25	1.1	0.1
		37.1683	35.1643	-1.45	-0.25	1.15	0.05
		37.1683	35.1667	-1.45	-0.25	1.15	0.05
		37.1683	35.17	-1.45	-0.26	1.14	0.05
		37.1683	35.1733	-1.45	-0.28	1.12	0.05
		37.1683	35.1767	-1.45	-0.3	1.05	0.1
		37.1683	35.18	-1.45	-0.32	1.03	0.1
		37.1683	35.1812	-1.4	-0.35	0.9	0.15
		37.1683	35.1827	-1.35	-0.35	0.8	0.2
		37.1683	35.1833	-1.35	-0.35	0.8	0.2
		37.1683	35.185	-1.35	-0.35	0.8	0.2
		37.1683	35.1867	-1.35	-0.37	0.88	0.1
		37.1683	35.1875	-1.35	-0.37	0.93	0.05
		37.1683	35.1883	-1.45	-0.37	0.98	0.1
		37.1683	35.1917	-1.6	-0.37	1.03	0.2
		37.1683	35.1967	-1.65	-0.4	1.05	0.2
		37.1683	35.2	-1.65	-0.4	1.15	0.1
		37.1683	35.2017	-1.75	-0.43	1.22	0.1
370		37.1683	35.2033	-1.8	-0.45	1.2	0.15
380		37.1683	35.2067	-1.85	-0.45	1.3	0.1
		37.1683	35.21	-1.9	-0.46	1.34	0.1
		37.1683	35.2133	-1.95	-0.46	1.39	0.1
		37.1683	35.2158	-2	-0.46	1.49	0.05
		37.1683	35.2188	-2.05	-0.5	1.5	0.05
		37.1683	35.2217	-2.15	-0.5	1.5	0.15
		37.1683	35.2242	-2.15	-0.53	1.52	0.1

LINE #	FIX	LONG	LAT	B1	B2	MGS1	UNIT1
		36.9783	35.3783	-2.75	-0.9	1.85	0
		36.9733	35.3783	-2.75	-0.9	1.85	0
110		36.97	35.3783	-2.75	-0.9	1.85	0
add8820:	100	37.1183	35.4283	-2.6	-0.8	1.8	0
		37.12	35.4283	-2.6	-0.8	1.8	0
		37.1217	35.4283	-2.6	-0.8	1.8	0
		37.125	35.4283	-2.6	-0.8	1.8	0
		37.1267	35.4283	-2.6	-0.8	1.8	0
		37.1283	35.4283	-2.6	-0.8	1.8	0
		37.1292	35.4283	-2.6	-0.75	1.85	0
		37.13	35.4275	-2.6	-0.75	1.85	0
		37.1333	35.4275	-2.6	-0.7	1.9	0
		37.1367	35.4275	-2.6	-0.7	1.9	0
		37.14	35.4275	-2.55	-0.65	1.9	0
		37.1425	35.4275	-2.5	-0.65	1.85	0
		37.145	35.4275	-2.5	-0.6	1.9	0
230		37.1467	35.4275	-2.45	-0.6	1.85	0
240		37.15	35.4275	-2.4	-0.55	1.85	0
		37.1517	35.4275	-2.35	-0.55	1.8	0
		37.1542	35.4275	-2.3	-0.5	1.8	0
		37.1583	35.4275	-2.25	-0.5	1.75	0
		37.16	35.4275	-2.25	-0.5	1.75	0
		37.1617	35.4275	-2.2	-0.45	1.75	0
		37.1633	35.4275	-2.2	-0.45	1.75	0
		37.165	35.4275	-2.2	-0.45	1.75	0
		37.1667	35.4275	-2.2	-0.4	1.8	0
		37.17	35.4275	-2.2	-0.4	1.8	0
		37.1733	35.4275	-2.2	-0.4	1.8	0
		37.1767	35.4275	-2.2	-0.4	1.8	0
		37.18	35.4275	-2.25	-0.4	1.85	0
		37.1817	35.4275	-2.25	-0.4	1.85	0
		37.1833	35.4275	-2.3	-0.4	1.9	0
		37.185	35.4275	-2.3	-0.35	1.95	0
		37.1867	35.4275	-2.3	-0.35	1.95	0

		37.1683	35.2267	-2.15	-0.55	1.55	0.05			37.1883	35.4275	-2.3	-0.35	1.95	0
		37.1683	35.2283	-2.2	-0.55	1.6	0.05			37.19	35.4275	-2.3	-0.35	1.95	0
		37.1683	35.2317	-2.2	-0.58	1.62	0			37.1917	35.4275	-2.3	-0.3	2	0
		37.1683	35.235	-2.25	-0.6	1.6	0.05			37.1933	35.4275	-2.3	-0.3	2	0
		37.1683	35.2367	-2.3	-0.6	1.65	0.05			37.195	35.4267	-2.3	-0.3	2	0
		37.1683	35.2383	-2.3	-0.6	1.65	0.05			37.1975	35.4267	-2.3	-0.3	2	0
		37.1683	35.2408	-2.35	-0.63	1.62	0.1			37.2	35.4267	-2.3	-0.3	2	0
		37.1683	35.2442	-2.35	-0.63	1.62	0.1			37.2025	35.4267	-2.25	-0.25	2	0
		37.1683	35.2475	-2.35	-0.65	1.6	0.1			37.205	35.4267	-2.25	-0.25	2	0
540		37.1683	35.25	-2.3	-0.65	1.65	0			37.2067	35.4267	-2.2	-0.25	1.95	0
add8300	100	37.1883	35.15	-1.5	0	1.4	0.1		510	37.21	35.4267	-2.2	-0.25	1.95	0
		37.1917	35.1483	-1.5	0	1.5	0		520	37.2125	35.4267	-2.2	-0.2	2	0
		37.195	35.1458	-1.5	0	1.5	0			37.215	35.4267	-2.15	-0.2	1.95	0
		37.1975	35.1433	-1.4	0	1.4	0			37.2175	35.4267	-2.15	-0.2	1.95	0
		37.2033	35.1417	-1.3	0	1.3	0			37.22	35.4267	-2.1	-0.2	1.9	0
		37.2083	35.1392	-1.2	0	1.1	0.1			37.2217	35.4267	-2.1	-0.2	1.9	0
		37.2125	35.137	-1.2	0	1.05	0.15			37.2242	35.4267	-2.1	-0.2	1.9	0
		37.2167	35.135	-1.2	0	1.05	0.15			37.2267	35.4267	-2.05	-0.15	1.9	0
180		37.2183	35.1333	-1.25	0	1.05	0.2			37.2283	35.4267	-2	-0.15	1.85	0
190		37.2233	35.1317	-1.2	0	1.05	0.15			37.23	35.4267	-1.95	-0.1	1.85	0
		37.225	35.1292	-1.15	0	1.05	0.1			37.2317	35.4267	-1.9	-0.1	1.8	0
		37.2292	35.1267	-1.1	0	1.1	0			37.2333	35.4267	-1.85	-0.05	1.8	0
		37.2342	35.1242	-1.1	0	1.1	0			37.2358	35.4267	-1.8	-0.05	1.75	0
		37.2383	35.1217	-1.05	0	1.05	0			37.2383	35.4267	-1.75	0	1.75	0
240		37.2433	35.1192	-1	0	1	0			37.24	35.4267	-1.7	0	1.7	0
		37.2467	35.1167	-1	0	1	0			37.2417	35.4267	-1.65	0	1.65	0
		37.2508	35.115	-1	0	0.95	0.05			37.2433	35.4267	-1.6	0	1.6	0
		37.255	35.1125	-1	0	0.9	0.1			37.2458	35.4267	-1.55	0	1.55	0
		37.2583	35.11	-0.9	0	0.85	0.05			37.2483	35.4267	-1.55	0	1.55	0
		37.265	35.1075	-0.85	0	0.85	0			37.2517	35.4267	-1.55	0	1.55	0
300		37.27	35.105	-0.85	0	0.85	0			37.2533	35.4267	-1.5	0	1.5	0
add87300	100	37.1533	35.0333	-0.6	0	0.6	0			37.2567	35.4258	-1.5	0	1.5	0
		37.1538	35.0375	-0.6	0	0.6	0			37.2583	35.4258	-1.45	0	1.45	0
		37.1543	35.0417	-0.6	0	0.6	0			37.26	35.4258	-1.45	0	1.45	0
		37.1548	35.0458	-0.6	0	0.5	0.1			37.2617	35.4258	-1.45	0	1.45	0

	37.1553	35.0517	-0.6	0	0.4	0.2		37.2633	35.4258	-1.4	0	1.4	0
	37.1562	35.0567	-0.65	0	0.45	0.2		37.265	35.4258	-1.4	0	1.4	0
	37.1572	35.0633	-0.7	0	0.5	0.2		37.2667	35.4258	-1.4	0	1.4	0
	37.1583	35.07	-0.7	0	0.6	0.1		790 37.27	35.4258	-1.4	0	1.4	0
	37.1597	35.075	-0.75	0	0.65	0.1		800 37.2733	35.4258	-1.4	0	1.4	0
	37.1605	35.08	-0.85	0	0.75	0.1		37.275	35.4258	-1.4	0	1.4	0
	37.1617	35.0833	-0.95	0	0.85	0.1		37.2767	35.4258	-1.4	0	1.4	0
	37.1622	35.0867	-1	0	0.9	0.1		37.28	35.4258	-1.4	0	1.4	0
220	37.1628	35.0933	-1.1	0	0.95	0.15		37.2817	35.4258	-1.4	0	1.4	0
230	37.1633	35.0967	-1.15	0	1	0.15		37.2833	35.4258	-1.4	0	1.4	0
240	37.1642	35.1033	-1.25	0	1.1	0.15		37.2867	35.4258	-1.4	0	1.4	0
	37.1645	35.1092	-1.3	-0.05	1.15	0.1		37.2883	35.4258	-1.4	0	1.4	0
	37.165	35.115	-1.35	-0.05	1.3	0		37.2917	35.4258	-1.4	0	1.4	0
	37.1655	35.1183	-1.5	-0.05	1.45	0		37.2933	35.4258	-1.4	0	1.4	0
	37.1658	35.1217	-1.45	-0.1	1.35	0		37.295	35.4258	-1.35	0	1.35	0
290	37.1663	35.1267	-1.4	-0.1	1.2	0.1		37.2967	35.4258	-1.35	0	1.35	0
	37.1667	35.1317	-1.4	-0.1	1.1	0.2		37.2983	35.4258	-1.3	0	1.3	0
	37.1675	35.1367	-1.4	-0.1	1.05	0.25		37.3	35.4258	-1.3	0	1.3	0
	37.1687	35.1433	-1.4	-0.15	1.05	0.2		37.3017	35.4258	-1.25	0	1.25	0
	37.17	35.15	-1.45	-0.15	1.2	0.1		37.305	35.4258	-1.25	0	1.25	0
	37.1713	35.1533	-1.45	-0.18	1.12	0.15		37.3075	35.4258	-1.2	0	1.2	0
	37.1723	35.1558	-1.4	-0.2	1.15	0.05		37.31	35.4258	-1.15	0	1.15	0
	37.1735	35.1617	-1.4	-0.2	1.1	0.1		37.3125	35.4258	-1.1	0	1.1	0
	37.1745	35.1658	-1.35	-0.25	1	0.1		37.315	35.4258	-1.05	0	1.05	0
	37.175	35.17	-1.35	-0.25	0.95	0.15		37.3175	35.4258	-1	0	1	0
	37.1758	35.1767	-1.35	-0.28	0.72	0.35		37.32	35.4258	-0.95	0	0.95	0
	37.1783	35.1867	-1.35	-0.3	0.75	0.3		1020 37.3233	35.4258	-0.95	0	0.95	0
	37.1792	35.2	-1.35	-0.3	0.95	0.1	had8810i	100 37.3567	35.4967	-1	0	1	0
420	37.18	35.2167	-1.35	-0.3	0.95	0.1		37.3517	35.4967	-1	0	1	0
add8630i	370 37.0167	35.0525	-2.35	-1.05	1.2	0.1		37.3467	35.4967	-1.1	0	1.1	0
	37.02	35.055	-2.3	-1.05	1.25	0		37.3417	35.4967	-1.1	0	1.1	0
	37.0217	35.0575	-2.2	-1.05	1.15	0		37.3383	35.4967	-1.1	0	1.1	0
	37.0267	35.0767	-2.15	-1	1.15	0		37.3358	35.4975	-1.1	0	1.1	0
	37.0283	35.0633	-2.1	-1	1.05	0.05		37.3317	35.4975	-1.05	0	1.05	0
320	37.0317	35.0658	-2.05	-0.98	0.97	0.1		37.3267	35.4975	-1.05	0	1.05	0

310	37.0367	35.0683	-2.05	-0.95	0.95	0.15			37.3217	35.4975	-1.05	0	1.05	0
	37.0383	35.0708	-2.1	-0.95	0.95	0.2			37.3167	35.4975	-1.05	0	1.05	0
	37.045	35.075	-2.15	-0.95	1.05	0.15			37.3133	35.4983	-1.05	0	1.05	0
	37.0517	35.0775	-2.2	-0.95	1.1	0.15			37.3083	35.4983	-1.05	0	1.05	0
	37.0617	35.08	-2.25	-0.95	1.05	0.25			37.305	35.4983	-1.05	0	1.05	0
	37.0683	35.0817	-2.25	-0.95	1.05	0.25			37.3	35.4983	-1	0	1	0
	37.0767	35.0833	-2.3	-0.95	1.1	0.25			37.2967	35.4983	-1	0	1	0
	37.078	35.0858	-2.3	-0.95	1.1	0.25			37.2917	35.4988	-1.05	0	1.05	0
	37.0787	35.0883	-2.3	-0.95	1.2	0.15			37.2875	35.4988	-1.1	0	1.1	0
	37.08	35.0917	-2.35	-0.95	1.3	0.1			37.2833	35.4988	-1.15	0	1.15	0
	37.081	35.0942	-2.3	-0.95	1.3	0.05			37.2783	35.4988	-1.25	0	1.25	0
	37.0817	35.0967	-2.25	-0.95	1.3	0			37.2733	35.4988	-1.35	0	1.35	0
	37.0867	35.0983	-2.23	-0.95	1.28	0			37.2683	35.4992	-1.4	0	1.4	0
	37.09	35.1	-2.2	-0.9	1.2	0.1			37.2642	35.4992	-1.45	0	1.45	0
	37.0933	35.1025	-2.15	-0.85	1.1	0.2			37.26	35.4992	-1.45	0	1.45	0
	37.0967	35.1058	-2.1	-0.85	1.05	0.2			37.255	35.4992	-1.5	0	1.5	0
	37.1	35.1083	-1.95	-0.8	1	0.15			340 37.2517	35.4992	-1.5	0	1.5	0
	37.105	35.1108	-1.85	-0.75	1	0.1	add8730!	90	37.2733	35.4492	-1.4	0	1.4	0
	37.1092	35.1133	-1.85	-0.73	0.82	0.3			37.2683	35.4492	-1.4	0	1.4	0
	37.1125	35.1158	-1.8	-0.7	0.75	0.35			37.2633	35.4492	-1.45	0	1.45	0
	37.115	35.1183	-1.65	-0.65	0.85	0.15			37.2583	35.4492	-1.45	0	1.45	0
100	37.1183	35.1217	-1.55	-0.65	0.85	0.05			37.2533	35.4492	-1.5	0	1.5	0
add8821	1040	37.1317	35.2205	-2.45	-0.88	1.57	0		37.2483	35.4492	-1.6	0	1.6	0
		37.1333	35.2207	-2.45	-0.88	1.57	0		37.2433	35.4492	-1.65	0	1.65	0
		37.1358	35.2208	-2.45	-0.85	1.6	0		37.2383	35.4492	-1.75	0	1.75	0
1010	37.1383	35.22	-2.4	-0.8	1.6	0			37.2333	35.4492	-1.85	0	1.85	0
1000	37.14	35.2217	-2.35	-0.78	1.57	0			37.23	35.4492	-1.95	0	1.95	0
	37.1433	35.2217	-2.25	-0.76	1.49	0			37.2267	35.4492	-2.05	0	2.05	0
	37.1467	35.2222	-2.25	-0.75	1.5	0			37.2233	35.4492	-2.1	-0.05	2.05	0
	37.1492	35.2222	-2.2	-0.75	1.45	0			37.2183	35.4492	-2.15	-0.05	2.1	0
	37.1517	35.2222	-2.2	-0.7	1.45	0.05			37.215	35.4492	-2.2	-0.1	2.1	0
	37.1533	35.2225	-2.15	-0.7	1.4	0.05			37.21	35.4492	-2.25	-0.1	2.15	0
	37.1558	35.2225	-2.15	-0.7	1.35	0.1			37.205	35.4492	-2.3	-0.15	2.15	0
	37.1583	35.2225	-2	-0.65	1.3	0.05			37.2	35.4492	-2.35	-0.15	2.2	0
	37.16	35.223	-2.1	-0.65	1.25	0.2			37.1967	35.4492	-2.4	-0.15	2.2	0

	37.1617	35.223	-2.1	-0.6	1.25	0.25		37.1933	35.4492	-2.4	-0.2	2.2	0	
	37.1633	35.223	-2.05	-0.58	1.32	0.15		37.1883	35.4492	-2.4	-0.2	2.2	0	
	37.165	35.2233	-2	-0.55	1.4	0.05		37.1833	35.4492	-2.4	-0.25	2.15	0	
	37.175	35.2233	-2	-0.53	1.47	0		37.1783	35.4492	-2.45	-0.25	2.2	0	
	37.1692	35.2235	-1.95	-0.5	1.45	0		37.175	35.4492	-2.45	-0.3	2.15	0	
860	37.1717	35.2235	-1.9	-0.45	1.4	0.05		37.17	35.4492	-2.45	-0.35	2.1	0	
	37.1733	35.2235	-1.85	-0.43	1.32	0.1		37.165	35.4492	-2.5	-0.4	2.1	0	
	37.1758	35.2237	-1.85	-0.4	1.35	0.1		37.16	35.4492	-2.5	-0.4	2.1	0	
	37.1783	35.2237	-1.85	-0.38	1.32	0.15		37.155	35.4492	-2.55	-0.45	2.1	0	
	37.18	35.2238	-1.85	-0.35	1.35	0.15		360	37.15	35.4492	-2.6	-0.55	2.05	0
	37.1817	35.2238	-1.8	-0.35	1.35	0.1		370	37.1467	35.4492	-2.6	-0.6	2	0
	37.1833	35.2243	-1.8	-0.34	1.41	0.05		37.1433	35.4492	-2.6	-0.65	1.95	0	
	37.185	35.2248	-1.8	-0.32	1.48	0		37.1383	35.4492	-2.6	-0.65	1.95	0	
	37.1867	35.2252	-1.8	-0.3	1.5	0		37.135	35.4492	-2.6	-0.7	1.9	0	
	37.1883	35.2255	-1.8	-0.3	1.4	0.1		37.1317	35.4492	-2.6	-0.75	1.85	0	
	37.1908	35.2258	-1.8	-0.25	1.35	0.2		37.1267	35.4492	-2.55	-0.75	1.8	0	
	37.1933	35.2262	-1.8	-0.2	1.35	0.25		37.1217	35.4492	-2.55	-0.75	1.8	0	
740	37.195	35.2265	-1.8	-0.25	1.3	0.25		37.1167	35.4492	-2.55	-0.8	1.75	0	
730	37.1967	35.2267	-1.8	-0.2	1.35	0.25		37.1117	35.4492	-2.55	-0.85	1.7	0	
	37.1983	35.2267	-1.8	-0.2	1.4	0.2		37.1083	35.4492	-2.55	-0.9	1.65	0	
	37.2008	35.2267	-1.8	-0.15	1.5	0.15		37.1033	35.4492	-2.55	-0.95	1.6	0	
	37.2033	35.2267	-1.8	-0.15	1.55	0.1		37.0983	35.4492	-2.55	-0.95	1.6	0	
	37.2058	35.2267	-1.8	-0.1	1.6	0.1		37.0933	35.4492	-2.6	-0.95	1.65	0	
	37.2083	35.2267	-1.85	-0.1	1.65	0.1		37.0883	35.4492	-2.75	-0.9	1.85	0	
	37.2108	35.2267	-1.85	-0.1	1.7	0.05		37.085	35.4492	-2.7	-0.95	1.75	0	
	37.2133	35.2283	-1.85	0	1.85	0		37.08	35.4492	-2.7	-0.95	1.75	0	
	37.215	35.2283	-1.85	0	1.85	0		37.0767	35.4492	-2.7	-1	1.7	0	
	37.2167	35.2283	-1.85	0	1.85	0		37.0717	35.4492	-2.7	-1	1.7	0	
	37.2192	35.2283	-1.85	0	1.85	0		37.0667	35.4492	-2.7	-1	1.7	0	
	37.2217	35.2283	-1.8	0	1.8	0		37.0633	35.4492	-2.65	-1	1.65	0	
	37.2242	35.2283	-1.8	0	1.8	0		37.0583	35.4492	-2.65	-1	1.65	0	
	37.2267	35.2283	-1.8	0	1.8	0		37.0533	35.4492	-2.6	-1	1.6	0	
	37.2283	35.2283	-1.8	0	1.8	0		37.0483	35.4492	-2.6	-1	1.6	0	
	37.23	35.2292	-1.85	0	1.85	0		37.045	35.4492	-2.55	-1	1.55	0	
	37.2317	35.2292	-1.85	0	1.85	0		37.0417	35.4492	-2.55	-0.95	1.6	0	

37 2333	35 2292	-1.85	0	1.85	0		37 0367	35 4492	-2.5	-0.9	1.6	0
37 235	35 2292	-1.9	0	1.9	0		37 0317	35 4492	-2.5	-0.9	1.6	0
37 2383	35 2292	-1.9	0	1.9	0		37 0267	35 4492	-2.45	-0.9	1.55	0
37 2408	35 2292	-1.9	0	1.9	0		37 0217	35 4492	-2.4	-0.9	1.5	0
37 2433	35 2292	-1.9	0	1.9	0		660 37 0183	35 4492	-2.35	-0.9	1.45	0
37 245	35 2292	-1.85	0	1.85	0	had8810:	110 37 335	35 5467	-1.05	0	1.55	0
37 2467	35 23	-1.8	0	1.8	0		37 325	35 5467	-1.05	0	1.4	0
37 2483	35 23	-1.75	0	1.75	0		37 3167	35 5458	-1.05	0	1.45	0
37 25	35 23	-1.7	0	1.7	0		37 31	35 5458	-1.05	0	1.5	0
37 2533	35 23	-1.65	0	1.65	0		37 3033	35 545	-1.15	0	1.5	0
460 37 2567	35 23	-1.65	0	1.65	0		210 37 2967	35 545	-1.25	0	1.55	0
450 37 2583	35 23	-1.6	0	1.6	0		37 29	35 5442	-1.3	0	1.55	0
37 26	35 23	-1.6	0	1.6	0		37 2808	35 5433	-1.4	0	1.55	0
37 2625	35 23	-1.55	0	1.55	0		37 2717	35 5433	-1.55	-0.1	1.45	0
37 265	35 23	-1.6	0	1.5	0.1		37 2642	35 5425	-1.6	-0.15	1.45	0
37 2683	35 23	-1.55	0	1.4	0.15		37 2567	35 5425	-1.7	-0.15	1.55	0
37 2717	35 23	-1.55	0	1.4	0.15		37 2483	35 5417	-1.8	-0.2	1.6	0
37 2742	35 23	-1.55	0	1.35	0.2		310 37 2383	35 5417	-2	-0.2	1.8	0
37 2767	35 23	-1.55	0	1.35	0.2		37 2283	35 5417	-2.05	-0.2	1.85	0
37 2783	35 23	-1.5	0	1.35	0.15		37 2183	35 5417	-2.05	-0.3	1.85	0
37 28	35 23	-1.45	0	1.35	0.1		37 21	35 5417	-2.05	-0.4	1.85	0
37 2817	35 23	-1.5	0	1.35	0.15		37 2	35 5417	-2.2	-0.4	1.8	0
37 2842	35 23	-1.5	0	1.35	0.15		410 37 1917	35 5417	-2.25	-0.5	1.75	0
37 2867	35 23	-1.5	0	1.35	0.15		37 1817	35 5417	-2.3	-0.6	1.7	0
37 2892	35 23	-1.5	0	1.35	0.15		37 1733	35 5408	-2.4	-0.65	1.75	0
37 2917	35 23	-1.45	0	1.35	0.1		37 165	35 5408	-2.45	-0.75	1.7	0
37 2933	35 23	-1.45	0	1.4	0.05		37 1567	35 5408	-2.45	-0.85	1.6	0
37 295	35 23	-1.45	0	1.4	0.05		510 37 1467	35 5408	-2.5	-0.8	1.7	0
37 2967	35 23	-1.4	0	1.4	0		37 1367	35 5408	-2.5	-0.7	1.8	0
37 2983	35 23	-1.35	0	1.35	0		37 1283	35 5408	-2.45	-0.45	2	0
37 3017	35 23	-1.35	0	1.35	0		37 12	35 5408	-2.4	-0.4	2	0
37 3033	35 23	-1.3	0	1.3	0		37 1117	35 54	-2.3	-0.4	1.9	0
37 305	35 23	-1.3	0	1.3	0		610 37 1033	35 54	-2.2	-0.4	1.8	0
37 3083	35 23	-1.3	0	1.3	0		37 095	35 5392	2.15	-0.3	1.85	0
37 3117	35 23	-1.3	0	1.3	0		37 0867	35 5392	-2.1	-0.25	1.85	0

	37 315	35 23	-1.3	0	1.3	0		37 08	35 5392	-2.05	-0.2	1.85	0	
	37 3167	35 23	-1.3	0	1.3	0		37 0717	35 5383	-2.55	-0.2	2.35	0	
	37 3183	35 23	-1.25	0	1.25	0		710	37.06	35 5383	-2.55	-0.225	2.35	0
180	37.32	35 23	-1.25	0	1.25	0		37.0483	35 5375	-2.55	-0.25	2.3	0	
170	37.3217	35 23	-1.2	0	1.2	0		37.04	35 5375	-2.55	-0.2	2.35	0	
	37 3233	35 23	-1.2	0	1.2	0		37.03	35 5375	-2.55	-0.15	2.4	0	
	37 3267	35 23	-1.15	0	1.15	0		37.02	35 5367	-2.55	-0.1	2.45	0	
	37 3292	35 23	-1.2	0	1.1	0.1		810	37 0117	35 5367	-2.5	-0.05	2.45	0
	37 3317	35 23	-1.2	0	1.1	0.1		37.0017	35 5367	-2.45	0	2.45	0	
	37.3333	35 23	-1.2	0	1.05	0.15		36.995	35 5367	-2.35	0	2.35	0	
110	37 335	35 23	-1.2	0	1.1	0.1		36.9867	35 5367	-2.25	0	2.25	0	
add8820:	100	37.1617	35.3133	-2.3	-0.75	1.45	0.1	36.9783	35 5358	-2.15	0	2.15	0	
	37.1633	35.3133	-2.3	-0.73	1.47	0.1		910	36.9717	35 5358	-2.05	0	2.05	0
	37.165	35.3133	-2.3	-0.7	1.5	0.1		36.965	35 5358	-1.95	0	1.95	0	
	37.1667	35.3133	-2.3	-0.7	1.5	0.1		36.9583	35 5358	-1.3	0	1.3	0	
	37.1683	35.3133	-2.3	-0.67	1.53	0.1		36.9517	35 5358	-1.3	0	1.3	0	
	37.17	35.3142	-2.3	-0.65	1.5	0.15		990	36.945	35 535	-1.3	0	1.3	0
	37.1733	35.3142	-2.3	-0.63	1.52	0.15	had8820:	100	37.0442	35 5933	-2.1		0	
	37.1767	35.3142	-2.3	-0.6	1.5	0.2		37.0442	35 5875					
	37.18	35.3142	-2.3	-0.59	1.46	0.25		37.0442	35 5817					
	37 1833	35.3142	-2.3	-0.57	1.48	0.25		37.0442	35 5767					
	37.185	35.315	-2.3	-0.55	1.5	0.25		37.0442	35 5717					
	37.1883	35.315	-2.3	-0.53	1.52	0.25		37.045	35 5667					
	37.1908	35.315	-2.3	-0.5	1.6	0.2		37.045	35 5617	-2.4			0	
	37 1933	35.315	-2.25	-0.5	1.65	0.1		37.045	35 555	-2.4			0	
	37 195	35.315	-2.25	-0.5	1.65	0.1		37.045	35 5483	-2.45			0	
	37.1967	35.315	-2.25	-0.45	1.7	0.1		37.045	35 5433	-2.5			0	
	37.1992	35.315	-2.25	-0.43	1.72	0.1		37.045	35 5383	-2.6			0	
	37 2083	35.315	-2.2	-0.4	1.75	0.05		37.045	35 5333	-2.6			0	
	37 2033	35.315	-2.2	-0.4	1.75	0.05		37.0458	35 5283	-2.6			0	
290	37 205	35.315	-2.2	-0.4	1.7	0.1		37.0458	35 5233	-2.6			0	
300	37 2067	35.315	-2.2	-0.4	1.7	0.1		37.0458	35 5183	-2.6			0	
	37 2087	35.315	-2.2	-0.36	1.74	0.1		37.0458	35 5133	-2.6			0	
	37 2108	35.315	-2.2	-0.35	1.75	0.1		37.0458	35 5083	-2.6			0	
	37 2122	35.315	-2.15	-0.32	1.78	0.05		37.0458	35 5033	-2.7			0	

37 2133	35 315	-2.1	-0.3	1.8	0			37 0458	35 4983	-2.8			0
37 215	35 315	-2.1	-0.28	1.82	0			37 0458	35 4933	-2.9			0
37 2167	35 315	-2.1	-0.25	1.85	0.05			37 0467	35 4883	-2.6	-0.6	2	0
37 2192	35 315	-2.1	-0.2	1.9	0.05			37 0467	35 4833	-2.6	-0.6	2	0
37 2217	35 315	-2.1	-0.2	1.9	0.05			37 0467	35 4783	-2.6	-0.65	1.95	0
37 225	35 315	-2.05	-0.18	1.87	0			37 0467	35 4733	-2.6	-0.7	1.9	0
37 2267	35 315	-2.05	-0.15	1.9	0			37 0467	35 4683	-2.6	-0.7	1.9	0
37 2283	35 315	-2.05	-0.1	1.9	0.05			37 0475	35 4633	-2.6	-0.8	1.8	0
37 23	35 315	-2.05	-0.08	1.92	0.05			37 0475	35 4583	-2.6	-0.9	1.7	0
37 2317	35 315	-2.05	-0.05	1.9	0.1			37 0475	35 4533	-2.6	-1	1.6	0
37 2342	35 315	-2.05	-0.03	1.87	0.15			37 0475	35 4483	-2.6	-1.05	1.55	0
37 2367	35 315	-2.05	0	1.9	0.15			37 0475	35 4433	-2.6	-1.05	1.55	0
37 2383	35 315	-2.05	0	1.9	0.15			37 0475	35 4383	-2.6	-1.1	1.5	0
37 2417	35 315	-2.05	0	1.9	0.15			37 0483	35 4333	-2.65	-1.15	1.5	0
37 245	35 315	-2	0	1.85	0.15			37 0483	35 4283	-2.65	-1.15	1.5	0
37 2483	35 315	-2	0	1.85	0.15			37 0483	35 4233	-2.65	-1.2	1.45	0
37 25	35 315	-1.95	0	1.8	0.15			37 0483	35 4183	-2.65	-1.2	1.45	0
37 2517	35 315	-1.95	0	1.8	0.15			37 0483	35 4117	-2.65	-1.15	1.5	0
37 2542	35 315	-1.85	0	1.75	0.1			37 0483	35 4042	-2.65	-1.15	1.5	0
37 2567	35 315	-1.85	0	1.75	0.1			37 0483	35 3967	-2.65	-1.15	1.5	0
37 26	35 315	-1.8	0	1.7	0.1			37 0483	35 39	-2.7	-1.15	1.55	0
37 26	35 315	-1.75	0	1.7	0.05			37 0483	35 3833	-2.75	-1.2	1.55	0
37 2633	35 315	-1.7	0	1.7	0			37 0483	35 3783	-2.75	-1.25	1.5	0
570 37 265	35 315	-1.7	0	1.7	0			37 0483	35 3733	-2.8	-1.3	1.5	0
580 37 2667	35 315	-1.7	0	1.7	0			37 0483	35 3683	-2.8	-1.35	1.45	0
37 2692	35 315	-1.65	0	1.65	0			960 37 0483	35 3633	-2.8	-1.4	1.4	0
37 2717	35 315	-1.6	0	1.6	0	had8810:	110	37 1583	35 6583	-0.1	-0.1	0	0
37 2733	35 315	-1.55	0	1.55	0			37 1483	35 6583	-0.2	-0.2	0	0
37 275	35 315	-1.55	0	1.55	0			37 1383	35 6583	-0.3	-0.2	0.1	0
37 2767	35 315	-1.5	0	1.5	0			37 13	35 6583	-0.55	-0.2	0.35	0
37 2783	35 315	-1.45	0	1.45	0			37 1217	35 6575	-0.85	-0.15	0.7	0
37 28	35 315	-1.4	0	1.4	0			37 1133	35 6575	-0.8	-0.15	0.65	0
37 2817	35 315	-1.4	0	1.4	0			37 1042	35 6575	-0.75	-0.1	0.65	0
37 2842	35 315	-1.4	0	1.35	0.05			37 095	35 6575	-0.65	-0.1	0.55	0
37 2867	35 315	-1.4	0	1.3	0.1			37 0858	35 6567	-0.5	-0.1	0.4	0

		37.29	35.315	-1.4	0	1.25	0.15			37.0767	35.6567	-0.3	-0.05	0.25	0
		37.2925	35.315	-1.35	0	1.2	0.15			37.0683	35.6567	-0.35	0	0.35	0
		37.295	35.315	-1.35	0	1.2	0.15			330 37.0592	35.6567	-0.4	0	0.4	0
		37.2975	35.315	-1.3	0	1.15	0.15			37.05	35.6558	-0.45	0	0.45	0
		37.2983	35.315	-1.25	0	1.15	0.1			37.0408	35.6558	-0.45	0	0.45	0
		37.3	35.315	-1.2	0	1.15	0.05			37.0317	35.6558	-0.45	0	0.45	0
	750	37.3025	35.315	-1.2	0	1.1	0.1			37.0233	35.6558	-0.5	0	0.5	0
add8821l	100	37.0825	35.17	-2.65	-1.1	1.55	0			430 37.0183	35.655	-0.55	0	0.55	0
		37.085	35.17	-2.65	-1.1	1.55	0	had8810:	530	37.175	35.6217	0	0	0	0
		37.0867	35.17	-2.55	-1.1	1.45	0			37.1633	35.6217	-0.15	-0.05	0.1	0
		37.09	35.17	-2.6	-1.1	1.45	0.05			37.1542	35.6208	-0.45	-0.1	0.35	0
		37.0933	35.1708	-2.55	-1.1	1.4	0.05			37.145	35.6208	-0.55	-0.2	0.35	0
		37.0967	35.1708	-2.55	-1.1	1.35	0.1			37.1367	35.6208	-0.6	-0.3	0.3	0
	160	37.0983	35.1708	-2.55	-1.05	1.4	0.1			37.1275	35.62	-0.8	-0.4	0.4	0
		37.1	35.1708	-2.55	-1.05	1.35	0.15			37.1183	35.62	-1	-0.4	0.6	0
	180	37.1008	35.1708	-2.5	-1.05	1.35	0.1			37.1083	35.62	-1.2	-0.4	0.8	0
	190	37.1017	35.1717	-2.5	-1	1.35	0.15			37.1	35.6192	-1.3	-0.4	0.9	0
	200	37.105	35.1717	-2.5	-1	1.3	0.2			37.0917	35.6192	-1.35	-0.4	0.95	0
	210	37.1083	35.1717	-2.5	-1	1.25	0.25			37.0833	35.6192	-1.45	-0.4	1.05	0
	220	37.1117	35.1733	-2.5	-1	1.3	0.2			37.075	35.6183	-1.5	-0.35	1.15	0
	230	37.115	35.1733	-2.5	-0.95	1.35	0.2			37.065	35.6183	-1.65	-0.3	1.35	0
	240	37.1183	35.1733	-2.55	-0.93	1.52	0.1			37.055	35.6183	-1.6	-0.3	1.3	0
		37.12	35.175	-2.55	-0.91	1.54	0.1			37.0467	35.6175	-1.5	-0.3	1.2	0
		37.1217	35.175	-2.55	-0.9	1.55	0.1			37.0375	35.6175	-1.45	-0.15	1.3	0
		37.1233	35.175	-2.5	-0.85	1.55	0.1			37.0283	35.6167	-1.4	-0.15	1.25	0
		37.125	35.1783	-2.5	-0.83	1.57	0.1			37.02	35.6167	-1.4	-0.15	1.25	0
		37.1267	35.1783	-2.45	-0.8	1.55	0.1			37.0133	35.6167	-1.4	-0.1	1.3	0
		37.1283	35.1817	-2.4	-0.78	1.57	0.05			37.005	35.6167	-1.3	0	1.3	0
		37.1317	35.1817	-2.4	-0.75	1.55	0.1			36.9967	35.6167	-1.15	0	1.15	0
		37.1333	35.1817	-2.35	-0.75	1.5	0.1			36.9883	35.6167	-0.95	0	0.95	0
		37.1367	35.1817	-2.35	-0.73	1.47	0.15			100 36.985	35.6167	-0.85	0	0.85	0
		37.14	35.1817	-2.3	-0.7	1.5	0.1	had8810l	110	37.1467	35.7467	-1.3	-0.4	0.9	0
		37.1433	35.1817	-2.3	-0.65	1.5	0.15			37.1467	35.7333	-1.1	-0.35	0.75	0
		37.145	35.1817	-2.3	-0.65	1.5	0.15			37.1467	35.7217	-0.9	-0.35	0.55	0
		37.1467	35.1817	-2.25	-0.63	1.52	0.1			37.1467	35.7117	-0.6	-0.3	0.3	0

	37.1483	35.1822	-2.25	-0.63	1.52	0.1		37.1467	35.7017	-0.3	-0.3	0	0
	37.15	35.1822	-2.2	-0.6	1.55	0.05		37.1483	35.6917	-0.3	-0.3	0	0
	37.1508	35.1825	-2.15	-0.58	1.52	0.05		37.1483	35.6808	-0.25	-0.25	0	0
	37.1512	35.183	-2.15	-0.55	1.55	0.05		37.1483	35.67	-0.25	-0.25	0	0
	37.1517	35.1833	-2.05	-0.53	1.47	0.05		37.1483	35.6592	-0.2	-0.2	0	0
	37.1533	35.1833	-2	-0.5	1.45	0.05		37.15	35.6483	-0.15	-0.15	0	0
	37.1567	35.1833	-1.95	-0.48	1.47	0		37.15	35.6383	0	0	0	0
	37.16	35.1833	-1.85	-0.45	1.4	0		37.15	35.6267	-0.2	-0.1	0.1	0
	37.1633	35.1833	-1.8	-0.43	1.37	0		37.1517	35.6167	-0.55	-0.15	0.4	0
470	37.1658	35.1833	-1.75	-0.4	1.3	0.05		37.1517	35.6067	-1.6	-0.3	1.3	0
480	37.1667	35.1833	-1.7	-0.4	1.3	0		37.1517	35.5967	-1.85	-0.35	1.5	0
	37.1692	35.1833	-1.55	-0.35	0.95	0.25		37.1533	35.5883	-2	-0.45	1.55	0
	37.173	35.1842	-1.45	-0.35	0.75	0.35		37.1533	35.5767	-2.1	-0.5	1.6	0
	37.175	35.1842	-1.35	-0.3	0.75	0.3		37.1533	35.565	-2.2	-0.55	1.65	0
	37.1783	35.1842	-1.35	-0.25	1.05	0.05		37.1533	35.5542	-2.3	-0.55	1.75	0
	37.1817	35.1842	-1.35	-0.23	1.02	0.1		37.1533	35.5433	-2.45	-0.6	1.85	0
	37.185	35.185	-1.35	-0.2	1	0.15		37.155	35.5333	-2.6	-0.6	2	0
	37.1867	35.185	-1.3	-0.18	1.02	0.1		37.155	35.5225	-2.7	-0.6	2.1	0
	37.1883	35.185	-1.3	-0.15	1	0.15		37.155	35.5117	-2.7	-0.6	2.1	0
	37.19	35.185	-1.3	-0.13	1.02	0.15		37.155	35.5017	-2.7	-0.65	2.05	0
	37.1908	35.185	-1.35	-0.1	1.1	0.15		37.155	35.4933	-2.7	-0.65	2.05	0
	37.1933	35.185	-1.4	-0.08	1.17	0.15		610 37.1567	35.485	-2.7	-0.65	2.05	0
600	37.195	35.185	-1.45	-0.05	1.25	0.15	had8810	550 37.0683	35.7317	0	0	0	0
610	37.1967	35.185	-1.45	0	1.3	0.15		37.0692	35.7158	0	0	0	0
	37.1983	35.185	-1.45	0	1.25	0.2		37.07	35.7	0	0	0	0
	37.2	35.1867	-1.5	0	1.3	0.2		37.0703	35.6917	0	0	0	0
	37.2025	35.1867	-1.55	0	1.35	0.2		37.0708	35.6817	-0.4	-0.2	0.2	0
	37.205	35.1867	-1.6	0	1.45	0.15		37.0712	35.6717	-0.55	-0.1	0.45	0
	37.2067	35.1867	-1.65	0	1.45	0.2		37.0713	35.66	-0.4	-0.05	0.35	0
	37.2083	35.1883	-1.65	0	1.5	0.15		37.0717	35.6483	-0.25	0	0.25	0
680	37.2117	35.1883	-1.75	0	1.6	0.15		37.072	35.6375	-0.85	-0.3	0.55	0
	37.215	35.1883	-1.75	0	1.6	0.15		37.0723	35.6267	-1.5	-0.35	1.15	0
	37.2167	35.1892	-1.75	0	1.6	0.15		37.0727	35.6167	-1.8	-0.35	1.45	0
	37.2183	35.1892	-1.75	0	1.55	0.2		37.073	35.6067	-1.9	-0.3	1.6	0
	37.22	35.19	-1.75	0	1.55	0.2		37.0733	35.5967	-2.05	-0.3	1.75	0

	37.2217	35.19	-1.75	0	1.55	0.2			37.0737	35.5858	-2.1	-0.3	1.8	0
740	37.2233	35.19	-1.75	0	1.6	0.15			37.074	35.575	-2.15	-0.4	1.75	0
750	37.225	35.1908	-1.75	0	1.6	0.15			37.0743	35.565	-2.15	-0.35	1.8	0
	37.2267	35.1908	-1.75	0	1.65	0.1			37.0747	35.5542	-2.15	-0.3	1.85	0
	37.2292	35.1908	-1.75	0	1.65	0.1			37.075	35.5433	-2.1	-0.3	1.8	0
	37.2317	35.1908	-1.7	0	1.7	0			37.0753	35.5333	-2.1	-0.25	1.85	0
	37.2333	35.1917	-1.6	0	1.6	0			37.0757	35.5225	-2.1	-0.25	1.85	0
800	37.2358	35.1917	-1.5	0	1.5	0			37.076	35.5117	-2.2	-0.35	1.85	0
	37.2383	35.1917	-1.45	0	1.45	0			37.0763	35.5008	-2.3	-0.45	1.85	0
	37.24	35.1917	-1.45	0	1.45	0			110 37.0767	35.49	-2.35	-0.5	1.85	0
	37.2417	35.1925	-1.45	0	1.45	0	had8820:	110	37.09	35.755	-0.4	-0.4	0	0
	37.2442	35.1925	-1.4	0	1.4	0			37.0903	35.75	-0.45			0
	37.2475	35.1925	-1.4	0	1.4	0			37.0907	35.745	-0.45			0
	37.25	35.1933	-1.35	0	1.35	0			37.091	35.74	-0.4			0
	37.2525	35.1933	-1.3	0	1.3	0			37.0913	35.735	-0.4			0
	37.2558	35.1942	-1.3	0	1.3	0			37.0917	35.73	-0.35			0
	37.2583	35.1942	-1.25	0	1.25	0			37.092	35.725	-0.35			0
	37.2617	35.195	-1.25	0	1.25	0			37.0923	35.72	-0.35			0
	37.265	35.195	-1.2	0	1.2	0			37.0927	35.7167	-0.35			0
	37.2675	35.1958	-1.2	0	1.2	0			37.093	35.7117	-0.35			0
930	37.27	35.1967	-1.15	0	1.15	0			37.0933	35.7067	-0.4			0
add8820:	1100 37.0825	35.23	-2.85	-1.4	1.4	0.05			37.0937	35.7	-0.4			0
	37.0842	35.23	-2.85	-1.4	1.4	0.05			37.094	35.695	-0.4			0
	37.0867	35.23	-2.85	-1.35	1.45	0.05			37.0943	35.69	-0.5	-0.4	0.1	0
	37.0892	35.2308	-2.85	-1.35	1.45	0.05			37.0947	35.685	-0.6	-0.35	0.25	0
	37.0917	35.2308	-2.85	-1.3	1.5	0.05			37.095	35.68	-0.65	-0.25	0.4	0
	37.095	35.2308	-2.85	-1.3	1.45	0.1			37.0953	35.675	-0.7	-0.25	0.45	0
	37.0983	35.2317	-2.85	-1.3	1.45	0.1			37.0957	35.67	-0.7	-0.2	0.5	0
	37.1	35.2317	-2.8	-1.25	1.5	0.05			37.096	35.6633	-0.65	-0.2	0.45	0
	37.1025	35.2317	-2.8	-1.25	1.5	0.05			37.0963	35.6583	-0.65	-0.1	0.55	0
	37.105	35.2317	-2.8	-1.25	1.5	0.05			37.0967	35.6533	-0.65	-0.05	0.6	0
	37.1067	35.2325	-2.8	-1.2	1.55	0.05			37.097	35.6483	-0.55	0	0.55	0
	37.1083	35.2325	-2.8	-1.2	1.5	0.1			37.0973	35.6433	-0.6	-0.2	0.4	0
	37.11	35.2325	-2.8	-1.2	1.4	0.2			37.0977	35.6383	-0.85	-0.35	0.5	0
	37.1117	35.2325	-2.8	-1.15	1.5	0.15			37.098	35.6333	-1.05	-0.45	0.6	0

37.1133	35.2325	-2.75	-1.15	1.55	0.05	37.0983	35.6283	-1.25	-0.45	0.8	0
37.115	35.2325	-2.75	-1.1	1.65	0	37.099	35.6233	-1.35	-0.45	0.9	0
37.1167	35.2333	-2.7	-1.1	1.6	0	37.0997	35.6183	-1.65	-0.45	1.2	0
37.12	35.2333	-2.7	-1.1	1.6	0	37.1	35.6133	-1.75	-0.45	1.3	0
37.1233	35.2333	-2.7	-1.05	1.65	0	37.1005	35.6083	-1.85	-0.4	1.45	0
37.1267	35.2342	-2.7	-1.05	1.65	0	37.101	35.6033	-1.9	-0.4	1.5	0
37.13	35.2342	-2.7	-1	1.7	0	37.1013	35.5958	-1.95	-0.4	1.55	0
37.1305	35.2342	-2.7	-1	1.7	0	37.1017	35.59	-2	-0.35	1.65	0
37.1325	35.235	-2.65	-0.95	1.6	0.1	37.1022	35.585	-2.05	-0.35	1.7	0
37.1342	35.235	-2.6	-0.95	1.55	0.1	37.1027	35.58	-2.1	-0.3	1.8	0
37.1367	35.235	-2.6	-0.95	1.45	0.2	37.103	35.575	-2.15	-0.3	1.85	0
37.1392	35.235	-2.55	-0.9	1.45	0.2	37.1033	35.57	-2.2	-0.3	1.9	0
37.1417	35.235	-2.55	-0.9	1.4	0.25	37.1038	35.565	-2.2	-0.25	1.95	0
830 37.1433	35.235	-2.5	-0.85	1.45	0.2	37.1043	35.56	-2.25	-0.3	1.95	0
820 37.145	35.235	-2.5	-0.85	1.45	0.2	37.1047	35.555	-2.3	-0.3	2	0
37.1467	35.235	-2.45	-0.8	1.5	0.15	37.105	35.55	-2.4	-0.35	2.05	0
800 37.1483	35.235	-2.45	-0.8	1.5	0.15	37.1053	35.545	-2.45	-0.4	2.05	0
37.1492	35.2358	-2.45	-0.8	1.55	0.1	37.1057	35.5392	-2.45	-0.4	2.05	0
37.15	35.2358	-2.35	-0.75	1.55	0.05	37.106	35.5333	-2.45	-0.4	2.05	0
37.1525	35.2358	-2.35	-0.75	1.5	0.1	37.1063	35.5283	-2.45	-0.4	2.05	0
37.155	35.2358	-2.35	-0.73	1.47	0.15	37.1067	35.5233	-2.45	-0.4	2.05	0
37.1575	35.2358	-2.35	-0.7	1.45	0.2	37.107	35.5175	-2.45	-0.4	2.05	0
37.16	35.2367	-2.35	-0.68	1.42	0.25	37.1073	35.5117	-2.5	-0.5	2	0
37.1625	35.2367	-2.35	-0.65	1.4	0.3	37.1077	35.5067	-2.55	-0.55	2	0
37.165	35.2367	-2.35	-0.63	1.37	0.35	37.108	35.5017	-2.6	-0.6	2	0
700 37.1667	35.2367	-2.35	-0.6	1.4	0.35	37.1083	35.4967	-2.6	-0.65	1.95	0
37.17	35.2375	-2.35	-0.58	1.42	0.35	37.1087	35.4917	-2.55	-0.65	1.9	0
37.1717	35.2375	-2.35	-0.55	1.45	0.35	37.109	35.4867	-2.55	-0.7	1.85	0
37.175	35.2375	-2.35	-0.53	1.52	0.3	37.1093	35.4817	-2.6	-0.7	1.9	0
37.1767	35.2375	-2.3	-0.5	1.55	0.25	37.1097	35.4767	-2.7	-0.75	1.95	0
37.1792	35.2375	-2.3	-0.48	1.57	0.25	37.11	35.4717	-2.8	-0.75	2.05	0
37.1817	35.2375	-2.25	-0.45	1.65	0.15	37.1103	35.4667	-2.9	-0.75	2.15	0
37.1833	35.2383	-2.2	-0.43	1.67	0.1	37.1107	35.4617	-3	-0.8	2.2	0
37.1867	35.2383	-2.2	-0.4	1.65	0.15	37.111	35.4567	-3	-0.8	2.2	0
37.19	35.2383	-2.15	-0.38	1.72	0.05	37.1113	35.4517	-2.95	-0.8	2.15	0

600	37 1933	35 2383	-2.1	-0.35	1.65	0.1			37 1117	35 4467	-2.9	-0.8	2.1	0
	37 1967	35 2383	-2.1	-0.45	1.5	0.15			37 1122	35 4417	-2.85	-0.8	2.05	0
	37 1983	35 2392	-2.05	-0.43	1.57	0.05			37 1125	35 4367	-2.85	-0.8	2.05	0
	37.2	35 2392	-2.05	-0.4	1.5	0.15	had8820:	110	37 26	35.4017	-1.4	0	1.4	0
	37 2017	35 2392	-2.05	-0.35	1.5	0.2			37 26	35 4067	-1.4	0	1.4	0
550	37 2033	35 2392	-2	-0.33	1.47	0.2			37 26	35.4117	-1.4	0	1.4	0
540	37.205	35 2392	-2	-0.3	1.5	0.2			37 26	35.4167	-1.35	0	1.35	0
530	37.2075	35 2392	-2	-0.28	1.52	0.2			37 26	35.4217	-1.4	0	1.4	0
	37.21	35.24	-2	-0.25	1.55	0.2			37 26	35.4267	-1.45	0	1.45	0
	37 2117	35.24	-2	-0.2	1.65	0.15			37 26	35.4317	-1.5	0	1.5	0
500	37 2142	35.24	-2	-0.18	1.72	0.1			37 26	35.4367	-1.5	0	1.5	0
	37 2167	35.24	-1.95	-0.15	1.8	0			37 2592	35 4417	-1.5	0	1.5	0
	37 2192	35.24	-2	-0.13	1.87	0			37 2592	35 4475	-1.5	0	1.5	0
	37 2217	35.24	-2.05	-0.1	1.95	0			37 2592	35 4533	-1.45	0	1.45	0
	37 2233	35.24	-2.05	-0.08	1.97	0			37 2592	35 4583	-1.45	0	1.45	0
	37 225	35 2408	-2.05	-0.05	2	0			37 2592	35 4633	-1.4	0	1.4	0
	37 227	35 2408	-2	0	2	0			37 2592	35 4683	-1.4	0	1.4	0
	37 2292	35 2408	-2	0	2	0			37 2592	35 4733	-1.4	0	1.4	0
	37 2317	35 2408	-2	0	2	0			37 2592	35 4783	-1.45	0	1.45	0
	37 2333	35 2408	-1.95	0	1.95	0			37 2592	35 4833	-1.5	0	1.5	0
400	37 235	35 2408	-1.85	0	1.85	0			37 2592	35 4892	-1.55	0	1.55	0
	37 2367	35 2408	-1.85	0	1.8	0.05			37 2592	35 495	-1.55	0	1.55	0
	37 2392	35 2408	-1.85	0	1.75	0.1			37 2583	35 5017	-1.55	0	1.55	0
	37 2417	35 2417	-1.8	0	1.7	0.1			37 2583	35 5083	-1.5	0	1.5	0
	37 2442	35 2417	-1.8	0	1.7	0.1			37 2583	35 5133	-1.45	0	1.45	0
	37 2467	35 2417	-1.75	0	1.65	0.1			37 2583	35 5183	-1.4	0	1.4	0
	37 2483	35 2417	-1.75	0	1.65	0.1			37 2583	35 5233	-1.35	-0.05	1.3	0
	37.25	35 2417	-1.7	0	1.6	0.1			37 2583	35 5283	-1.35	-0.1	1.25	0
	37.25	35 2417	-1.7	0	1.6	0.1			37 2583	35 5333	-1.35	-0.1	1.25	0
	37 255	35 2433	-1.65	0	1.55	0.1			37 2575	35 5383	-1.4	-0.1	1.3	0
300	37 26	35 2433	-1.6	0	1.5	0.1			37 2575	35 5433	-1.5	-0.15	1.35	0
	37 2633	35 2433	-1.55	0	1.45	0.1			37 2575	35 5483	-1.55	-0.15	1.4	0
	37 265	35 245	-1.6	0	1.4	0.2			37 2575	35 5533	-1.5	-0.15	1.35	0
	37 2667	35 245	-1.5	0	1.3	0.2			37 2575	35 5567	-1.5	-0.15	1.35	0
260	37 2675	35 245	-1.5	0	1.3	0.2			37 2575	35 5617	-1.45	-0.15	1.3	0

250	37.2683	35.245	-1.5	0	1.3	0.2	37.2575	35.5667	-1.45	-0.2	1.25	0	
	37.2717	35.2458	-1.45	0	1.3	0.15	37.2567	35.5717	-1.45	-0.2	1.25	0	
	37.275	35.2458	-1.45	0	1.3	0.15	37.2567	35.5767	-1.5	-0.25	1.25	0	
	37.2783	35.2458	-1.45	0	1.3	0.15	37.2567	35.5817	-1.55	-0.25	1.3	0	
	37.2817	35.2458	-1.4	0	1.3	0.1	37.2567	35.5867	-1.5	-0.25	1.25	0	
	37.2833	35.2467	-1.35	0	1.35	0	37.2567	35.5933	-1.5	-0.25	1.25	0	
190	37.2858	35.2467	-1.35	0	1.35	0	37.2567	35.5992	-1.55	-0.25	1.3	0	
180	37.2883	35.2467	-1.25	0	1.25	0	37.2567	35.605	-1.55	-0.25	1.3	0	
	37.29	35.2467	-1.2	0	1.2	0	37.2567	35.6117	-1.6	-0.3	1.3	0	
	37.2917	35.2467	-1.15	0	1.15	0	37.2567	35.6167	-1.6	-0.3	1.3	0	
	37.2933	35.2472	-1.15	0	1.15	0	37.2567	35.6217	-1.5	-0.25	1.25	0	
	37.2967	35.2472	-1.1	0	1.1	0	37.2558	35.625	-1.4	-0.25	1.15	0	
130	37.2992	35.2472	-1.1	0	1.1	0	37.2558	35.63	-1.3	-0.25	1.05	0	
	37.3017	35.2472	-1.15	0	1.15	0	37.2558	35.6333	-1.25	-0.15	1.1	0	
	37.305	35.2472	-1.25	0	1.15	0.1	37.2558	35.6383	-1.15	-0.15	1	0	
100	37.3067	35.2475	-1.2	0	1.15	0.05			-0.15				
add8820!	1360	37.1483	35.1217	-1.8	-0.35	1.35	0.1	37.2558	35.6458	-1	-0.15	0.85	0
		37.1467	35.125	-1.8	-0.35	1.35	0.1	37.2558	35.65	-0.95	-0.15	0.8	0
		37.1467	35.1283	-1.85	-0.35	1.4	0.1	37.2558	35.6558	-0.85	-0.2	0.65	0
		37.1467	35.1317	-1.85	-0.37	1.38	0.1	37.2558	35.6625	-0.75	-0.2	0.55	0
		37.1467	35.135	-1.85	-0.38	1.37	0.1	37.2558	35.6667	-0.65	-0.2	0.45	0
		37.1458	35.1375	-1.9	-0.4	1.4	0.1	37.2558	35.6717	-0.2	-0.2	0	0
		37.1458	35.14	-1.9	-0.43	1.37	0.1	37.2558	35.6767	-0.2	-0.2	0	0
		37.1458	35.1433	-2	-0.45	1.45	0.1	37.2558	35.6817	-0.2	-0.2	0	0
		37.1458	35.1467	-2	-0.45	1.45	0.1	37.255	35.6867	-0.25	-0.25	0	0
		37.1458	35.15	-2	-0.45	1.45	0.1	37.255	35.6917	-0.3	-0.3	0	0
1260		37.145	35.1533	-2.05	-0.47	1.48	0.1	37.255	35.6933	-0.35	-0.35	0	0
1250		37.145	35.155	-2.05	-0.5	1.45	0.1	37.255	35.7033	-0.4	-0.4	0	0
		37.145	35.1583	-2.05	-0.5	1.45	0.1	37.255	35.7075	-0.4	-0.4	0	0
		37.1442	35.1617	-2.05	-0.52	1.43	0.1	37.255	35.7117	-0.45	-0.45	0	0
		37.1442	35.1633	-2.05	-0.53	1.42	0.1	37.255	35.7167	-0.45	-0.45	0	0
		37.1442	35.165	-2.05	-0.55	1.4	0.1	37.255	35.7217	-0.4	-0.4	0	0
		37.1442	35.1667	-2.1	-0.55	1.4	0.15	37.255	35.7267	-0.35	-0.35	0	0
		37.1442	35.1683	-2.1	-0.57	1.38	0.15	37.2542	35.7317	-0.35	-0.35	0	0
		37.1433	35.17	-2.15	-0.57	1.38	0.2	37.2542	35.7367	-0.35	-0.35	0	0

	37.1433	35.175	-2.15	-0.6	1.45	0.1			37.2542	35.7417	-0.35	-0.35	0	0
	37.1433	35.1783	-2.2	-0.6	1.55	0.05			37.2542	35.7467	-0.35	-0.35	0	0
	37.1433	35.1817	-2.2	-0.62	1.58	0			37.2542	35.7533	-0.3	-0.3	0	0
	37.1433	35.1842	-2.2	-0.65	1.55	0			37.2542	35.7592	-0.15	-0.15	0	0
	37.1433	35.1867	-2.2	-0.66	1.54	0			37.2542	35.765	-0.25	-0.25	0	0
	37.1425	35.1892	-2.15	-0.68	1.47	0			37.2542	35.77	-0.25	-0.25	0	0
	37.1425	35.1917	-2.15	-0.69	1.46	0			37.2542	35.775	-0.3	-0.3	0	0
	37.1425	35.195	-2.15	-0.7	1.4	0.05			37.2533	35.78	-0.35	-0.35	0	0
	37.1425	35.1967	-2.15	-0.7	1.3	0.15			37.2533	35.785	-0.35	-0.35	0	0
	37.1417	35.1983	-2.15	-0.72	1.28	0.15			37.2533	35.79	-0.35	-0.35	0	0
	37.1417	35.2008	-2.15	-0.73	1.27	0.15			37.2533	35.795	-0.35	-0.35	0	0
	37.1417	35.2033	-2.15	-0.75	1.25	0.15			37.2533	35.8	-0.35	-0.35	0	0
	37.1417	35.205	-2.15	-0.75	1.25	0.15			37.2533	35.805	-0.35	-0.35	0	0
	37.1413	35.2083	-2.2	-0.77	1.28	0.15			37.2517	35.81	-0.35	-0.35	0	0
	37.1413	35.2125	-2.2	-0.77	1.33	0.1			37.2517	35.8167	-0.35	-0.35	0	0
	37.1413	35.215	-2.2	-0.77	1.38	0.05			37.2517	35.8217	-0.3	-0.3	0	0
	37.1408	35.2175	-2.25	-0.77	1.43	0.05			37.2508	35.8267	-0.3	-0.3	0	0
	37.1408	35.2183	-2.25	-0.79	1.41	0.05	had8820	110	37.305	35.77	-0.25	-0.25	0	0
	37.1408	35.2217	-2.3	-0.8	1.4	0.1			37.305	35.7667	-0.2	-0.2	0	0
980	37.1408	35.225	-2.35	-0.82	1.43	0.1			37.305	35.7617	-0.15	-0.15	0	0
970	37.1408	35.2267	-2.4	-0.83	1.42	0.15			37.305	35.7567	-0.1	-0.1	0	0
	37.1408	35.2292	-2.4	-0.84	1.41	0.15			37.3042	35.7517	-0.05	-0.05	0	0
	37.1408	35.2317	-2.45	-0.85	1.45	0.15			37.3042	35.7467	-0.15	-0.15	0	0
	37.1408	35.2333	-2.5	-0.86	1.44	0.2			37.3042	35.7417	-0.2	-0.2	0	0
	37.1408	35.2367	-2.5	-0.87	1.48	0.15			37.3042	35.7367	-0.25	-0.25	0	0
	37.1408	35.24	-2.5	-0.88	1.47	0.15			37.3042	35.7317	-0.25	-0.25	0	0
	37.1408	35.2433	-2.5	-0.9	1.5	0.1			37.3042	35.7267	-0.25	-0.25	0	0
	37.1405	35.2467	-2.5	-0.9	1.5	0.1			37.3033	35.7217	-0.25	-0.25	0	0
	37.1405	35.2492	-2.45	-0.91	1.44	0.1			37.3033	35.7167	-0.25	-0.25	0	0
	37.1405	35.2508	-2.45	-0.92	1.43	0.1			37.3033	35.7117	-0.3	-0.25	0.05	0
	37.1405	35.2533	-2.45	-0.93	1.42	0.1			37.3033	35.7067	-0.4	-0.25	0.15	0
	37.1405	35.2542	-2.45	-0.94	1.41	0.1			37.3033	35.7017	-0.45	-0.25	0.2	0
	37.1405	35.255	-2.45	-0.95	1.45	0.05			37.3025	35.6967	-0.55	-0.25	0.3	0
	37.1405	35.2583	-2.5	-0.95	1.5	0.05			37.3025	35.6917	-0.6	-0.25	0.35	0
	37.1405	35.2625	-2.5	-0.95	1.5	0.05			37.3025	35.6867	-0.65	-0.25	0.4	0

	37.1405	35.265	-2.55	-0.95	1.55	0.05		37.3025	35.68	-0.7	-0.25	0.45	0
	37.1405	35.2667	-2.55	-0.95	1.55	0.05		37.3025	35.6733	-0.85	-0.25	0.6	0
	37.1405	35.27	-2.55	-0.95	1.5	0.1		37.3017	35.6667	-0.95	-0.3	0.65	0
	37.14	35.2717	-2.55	-0.95	1.5	0.1		37.3017	35.66	-1	-0.3	0.7	0
	37.14	35.275	-2.55	-1	1.45	0.1		37.3017	35.655	-1.05	-0.3	0.75	0
	37.14	35.2783	-2.55	-1	1.4	0.15		37.3017	35.65	-1.05	-0.3	0.75	0
	37.14	35.2817	-2.55	-1	1.4	0.15		37.3017	35.645	-1	-0.3	0.7	0
	37.1383	35.285	-2.55	-1	1.45	0.1		37.3008	35.64	-0.95	-0.25	0.7	0
	37.1383	35.287	-2.55	-1	1.45	0.1		37.3008	35.635	-1	-0.25	0.75	0
	37.1383	35.2892	-2.6	-1	1.5	0.1		37.3008	35.63	-1.05	-0.2	0.85	0
	37.1383	35.2917	-2.6	-1.05	1.5	0.05		37.3008	35.625	-1.05	-0.15	0.9	0
	37.1367	35.2933	-2.6	-1.05	1.5	0.05		37.3008	35.62	-1.05	-0.1	0.95	0
700	37.1367	35.295	-2.6	-1.03	1.52	0.05		37.3	35.615	-1.05	-0.05	1	0
690	37.1367	35.2983	-2.6	-1.03	1.52	0.05		37.3	35.61	-1.05	0	1.05	0
	37.135	35.3017	-2.55	-1.03	1.47	0.05		37.3	35.605	-0.95	0	0.95	0
	37.135	35.3033	-2.55	-1.03	1.42	0.1		37.3	35.6	-0.95	0	0.95	0
	37.1348	35.305	-2.5	-1	1.4	0.1		37.3	35.595	-0.9	-0.05	0.85	0
	37.1348	35.3075	-2.5	-1	1.4	0.1		37.2992	35.59	-1	-0.1	0.9	0
	37.1348	35.31	-2.5	-0.98	1.37	0.15		37.2992	35.585	-1.2	-0.1	1.1	0
	37.1345	35.3133	-2.5	-0.95	1.4	0.15		37.2992	35.58	-1.25	-0.05	1.2	0
	37.1345	35.3158	-2.5	-0.95	1.4	0.15		37.2992	35.575	-1.3	-0.05	1.25	0
	37.1345	35.3183	-2.5	-0.93	1.42	0.15		37.2983	35.57	-1.3	0	1.3	0
	37.1342	35.3217	-2.5	-0.92	1.43	0.15		37.2983	35.565	-1.25	0	1.25	0
	37.1342	35.325	-2.45	-0.9	1.4	0.15		37.2983	35.56	-1.25	0	1.25	0
	37.1342	35.3283	-2.45	-0.9	1.35	0.2		37.2975	35.555	-1.35	0	1.35	0
	37.1342	35.3317	-2.45	-0.9	1.35	0.2		37.2975	35.5483	-1.35	0	1.35	0
	37.1338	35.3333	-2.4	-0.9	1.35	0.15		37.2975	35.5433	-1.25	0	1.25	0
	37.1338	35.335	-2.35	-0.88	1.32	0.15		37.2967	35.5383	-1.15	0	1.15	0
	37.1338	35.338	-2.35	-0.88	1.32	0.15		37.2967	35.5333	-1.15	0	1.15	0
	37.1338	35.34	-2.35	-0.88	1.37	0.1		37.2958	35.5283	-1.1	0	1.1	0
	37.1338	35.3425	-2.35	-0.87	1.38	0.1		37.2958	35.5233	-1.05	0	1.05	0
	37.1338	35.345	-2.35	-0.85	1.35	0.15		37.2958	35.5183	-1.05	0	1.05	0
	37.1338	35.3467	-2.35	-0.85	1.35	0.15		37.295	35.5133	-1.05	0	1.05	0
	37.1333	35.3492	-2.35	-0.85	1.35	0.15		37.295	35.5067	-1.05	0	1.05	0
	37.1333	35.3508	-2.35	-0.85	1.35	0.15		37.295	35.5	-1.05	0	1.05	0

	37.1333	35.3517	-2.35	-0.85	1.4	0.1			37.295	35.4283	-1.1	0	1.1	0
	37.1333	35.355	-2.35	-0.85	1.4	0.1			37.295	35.49	-1.1	0	1.1	0
	37.1328	35.3567	-2.4	-0.85	1.45	0.1			37.2942	35.485	-1.15	0	1.15	0
	37.1328	35.3587	-2.4	-0.88	1.42	0.1			37.2942	35.4967	-1.2	0	1.2	0
	37.1328	35.3617	-2.45	-0.9	1.45	0.1			37.2942	35.475	-1.25	0	1.25	0
420	37.1325	35.3642	-2.45	-0.88	1.47	0.1			37.2942	35.47	-1.25	0	1.25	0
410	37.1325	35.3667	-2.45	-0.87	1.48	0.1			37.2942	35.465	-1.3	0	1.3	0
	37.1317	35.3717	-2.45	-0.85	1.5	0.1			37.2933	35.46	-1.35	0	1.35	0
	37.1317	35.375	-2.45	-0.85	1.5	0.1			37.2933	35.455	-1.35	0	1.35	0
	37.1308	35.3783	-2.45	-0.85	1.5	0.1			37.2933	35.45	-1.35	0	1.35	0
	37.1308	35.3817	-2.45	-0.85	1.5	0.1			37.2925	35.445	-1.3	0	1.3	0
	37.13	35.385	-2.45	-0.8	1.5	0.15			37.2925	35.44	-1.3	0	1.3	0
	37.13	35.3883	-2.45	-0.78	1.47	0.2			37.2917	35.435	-1.3	0	1.3	0
	37.13	35.3917	-2.45	-0.75	1.5	0.2			37.2917	35.43	-1.3	0	1.3	0
	37.13	35.3933	-2.45	-0.78	1.52	0.15			37.2917	35.425	-1.3	0	1.3	0
	37.13	35.395	-2.5	-0.78	1.57	0.15			37.2908	35.42	-1.3	0	1.3	0
	37.13	35.3967	-2.5	-0.78	1.62	0.1			37.2908	35.415	-1.3	0	1.3	0
	37.13	35.4	-2.5	-0.75	1.65	0.1			37.29	35.41	-1.3	0	1.3	0
	37.13	35.4033	-2.5	-0.75	1.65	0.1	had8810'	110	37.21	35.4017	-2.05	-0.3	1.75	0
	37.13	35.405	-2.5	-0.75	1.65	0.1			37.21	35.4117	-2.05	-0.3	1.75	0
	37.13	35.4067	-2.55	-0.75	1.7	0.1			37.21	35.4217	-2.15	-0.3	1.85	0
	37.13	35.41	-2.55	-0.75	1.75	0.05			37.21	35.4317	-2.25	-0.3	1.95	0
	37.13	35.4117	-2.55	-0.75	1.8	0			37.21	35.4417	-2.15	-0.3	1.85	0
	37.13	35.4133	-2.55	-0.75	1.8	0			37.2092	35.4533	-2.15	-0.25	1.9	0
230	37.13	35.415	-2.6	-0.75	1.85	0			37.2092	35.4642	-2.1	-0.25	1.85	0
add8201t	750	37.2283	35.0833	-1	0	0.85	0.15		37.2092	35.4733	-2.1	-0.25	1.85	0
	37.2308	35.0883	-1.05	0	0.9	0.15			37.2092	35.4833	-2.05	-0.25	1.8	0
	37.2333	35.0933	-1.1	0	0.95	0.15			37.2092	35.4942	-2.05	-0.3	1.75	0
	37.235	35.0983	-1.1	0	0.95	0.15			37.2083	35.505	-2.05	-0.4	1.65	0
	37.2367	35.1	-1.1	0	1	0.1			37.2083	35.515	-2.05	-0.45	1.6	0
	37.2383	35.1033	-1.1	0	1	0.1			37.2083	35.5258	-2.05	-0.45	1.6	0
	37.2408	35.11	-1.1	0	1.05	0.05			37.2083	35.5375	-2.05	-0.45	1.6	0
	37.2433	35.115	-1.05	0	1.05	0			37.2083	35.5492	-2.05	-0.4	1.65	0
	37.245	35.12	-1.05	0	1.05	0			37.2075	35.56	-2.05	-0.4	1.65	0
	37.2467	35.125	-1	0	1	0			37.2075	35.57	-2	-0.4	1.6	0

	37 2483	35 1317	-0.9	0	0.9	0			37 2075	35 5808	-1.75	-0.35	1.4	0
	37 2508	35 1367	-0.9	0	0.85	0.05			37 2075	35 5917	-1.65	-0.25	1.4	0
	37 2533	35 1433	-0.9	0	0.75	0.15			37 2075	35 6025	-1.45	-0.25	1.2	0
	37 255	35 1483	-0.95	0	0.75	0.2			37 2067	35 6133	-1.25	-0.35	0.9	0
	37 2567	35 155	-1	0	0.8	0.2			37 2067	35 6233	-0.7	-0.25	0.45	0
	37 2583	35 1633	-1.05	0	0.85	0.2			37 2067	35 6333	-0.35	-0.3	0.05	0
	37 26	35 1667	-1.1	0	0.9	0.2			37 2067	35 6433	-0.35	-0.35	0	0
	37 2617	35 1708	-1.1	0	0.95	0.15			37 2058	35 6533	-0.3	-0.35	0.05	0
	37 2633	35 175	-1.15	0	1	0.15			37 2058	35 6733	-0.3	-0.3	0	0
	37 265	35 1792	-1.15	0	1	0.15			37 2058	35 6833	-0.3	-0.3	0	0
	37 2667	35 1833	-1.15	0	1	0.15			37 2058	35 695	-0.3	-0.3	0	0
	37 27	35 1875	-1.2	0	1.05	0.15			37 2058	35 7067	-0.55	-0.35	0.2	0
	37 2717	35 1917	-1.2	0	1.1	0.1			37 205	35 7183	-0.5	-0.35	0.15	0
	37 275	35 1967	-1.2	0	1.2	0			37 205	35 73	-0.55	-0.4	0.15	0
510	37 2767	35 2008	-1.25	0	1.25	0			37 205	35 7417	-0.55	-0.45	0.1	0
	37 2783	35 205	-1.25	0	1.25	0			37 205	35 7533	-0.65	-0.45	0.2	0
	37 28	35 21	-1.35	0	1.2	0.1			37 2033	35 765	-0.55	-0.45	0.1	0
480	37 2817	35 215	-1.35	0	1.2	0.15	had8810-	950	37 3517	35 5883	-1.15	0	1.15	0
470	37 2833	35 22	-1.4	0	1.25	0.2			37 3467	35 5883	-1.15	0	1.15	0
	37 2842	35 2283	-1.4	0	1.3	0.2			37 3383	35 5883	-1.1	0	1.1	0
	37 285	35 2333	-1.4	0	1.35	0.2			37 3275	35 5883	-1.05	0	1.05	0
	37 2867	35 2383	-1.4	0	1.35	0.2			37 3192	35 5875	-1.05	0	1.05	0
	37 2883	35 2433	-1.4	0	1.35	0.2			37 31	35 5875	-1	0	1	0
	37 29	35 2467	-1.4	0	1.35	0.2			37 3017	35 5875	-1.05	0	1.05	0
	37 2908	35 25	-1.35	0	1.35	0.15			37 2933	35 5867	-1.15	-0.1	1.05	0
	37 2917	35 2533	-1.35	0	1.35	0.15			37 2833	35 5867	-1.2	-0.15	1.05	0
	37 2925	35 2583	-1.35	0	1.35	0.15			37 275	35 5858	-1.3	-0.2	1.1	0
	37 2933	35 2633	-1.35	0	1.35	0.15			37 2667	35 5858	-1.4	-0.25	1.15	0
	37 295	35 2683	-1.35	0	1.35	0.1			37 2583	35 2525	-1.45	-0.25	1.2	0
	37 2958	35 275	-1.3	0	1.3	0.05			37 2483	35 2517	-1.5	-0.3	1.2	0
	37 2967	35 28	-1.3	0	1.3	0			37 2417	35 2517	-1.6	-0.3	1.3	0
	37 2975	35 2833	-1.25	0	1.25	0			37 2333	35 5842	-1.7	-0.4	1.3	0
	37 2992	35 2883	-1.2	0	1.25	0			37 225	35 5842	-1.75	-0.4	1.35	0
	37 3	35 2933	-1.15	0	1.25	0			37 215	35 5842	-1.8	-0.5	1.3	0
	37 3008	35 2983	-1.15	0	1.2	0			37 205	35 5833	-1.85	-0.4	1.45	0

	37.3017	35.3017	-1.15	0	1.15	0		37.195	35.5833	-1.95	-0.4	1.55	0		
	37.302	35.305	-1.15	0	1.15	0		37.185	35.5833	-2	-0.4	1.6	0		
	37.3023	35.31	-1.2	0	1.15	0.1		37.1767	35.5833	-2	-0.45	1.55	0		
	37.3027	35.315	-1.2	0	1.15	0.15		37.1683	35.5833	-2	-0.5	1.5	0		
	37.303	35.32	-1.2	0	1.15	0.15		37.16	35.5825	-1.95	-0.5	1.45	0		
	37.3033	35.3267	-1.2	0	1.15	0.15		37.15	35.5825	-1.95	-0.5	1.45	0		
	37.3038	35.3308	-1.15	0	1.1	0.1		37.1417	35.5825	-1.95	-0.5	1.45	0		
	37.304	35.3367	-1.15	0	1.1	0.1		37.1333	35.5825	-1.85	-0.4	1.45	0		
	37.3042	35.3433	-1.15	0	1	0.1		37.125	35.5825	-1.85	-0.35	1.5	0		
	37.3045	35.3475	-1.15	0	1	0.1		37.115	35.5817	-1.85	-0.35	1.5	0		
200	37.305	35.35	-1.15	0	1	0.1		37.1033	35.5817	-1.85	-0.35	1.5	0		
190	37.3067	35.355	-1.1	0	1.05	0		37.095	35.5817	-1.8	-0.4	1.4	0		
	37.3083	35.36	-1.1	0	1.05	0		37.0867	35.5817	-1.8	-0.4	1.4	0		
	37.31	35.365	-1.1	0	1.05	0		37.0783	35.5808	-2.1	-0.4	1.7	0		
	37.3117	35.3717	-1.1	0	1.05	0		37.07	35.5808	-2.05	-0.25	1.8	0		
	37.3133	35.38	-1.1	0	1.05	0		37.0617	35.5808	-2.05	-0.2	1.85	0		
	37.3138	35.3833	-1.1	0	1.05	0		37.0533	35.5808	-2	-0.1	1.9	0		
	37.3143	35.3867	-1.1	0	1.05	0		37.045	35.5808	-1.95	-0.05	1.9	0		
	37.315	35.3917	-1.05	0	1.05	0		37.0367	35.5808	-1.9	0	1.9	0		
	37.3158	35.3967	-1.05	0	1.05	0		37.0283	35.5803	-1.85	0	1.85	0		
100	37.3167	35.4	-1	0	1	0		37.02	35.5803	-1.8	0	1.8	0		
add87311	100	37.1667	35.2817	-2.35	-0.7	1.55	0.1	37.0133	35.5803	-1.7	0	1.7	0		
		37.1667	35.2867	-2.35	-0.7	1.55	0.1	37.0067	35.58	-1.6	0	1.6	0		
		37.1667	35.2917	-2.4	-0.7	1.6	0.1	36.9967	35.58	-1.55	0	1.55	0		
		37.1667	35.2967	-2.4	-0.75	1.55	0.1	36.985	35.58	-1.5	0	1.5	0		
		37.1667	35.3017	-2.4	-0.75	1.55	0.1	add8710	110	36.9617	35.5383	-1.6	0	1.6	0
		37.1667	35.3067	-2.4	-0.7	1.6	0.1			36.9533	35.5317	-1.6	0	1.6	0
		37.1667	35.3117	-2.35	-0.7	1.55	0.1			36.9467	35.525	-1.55	0	1.55	0
		37.1667	35.3167	-2.3	-0.65	1.55	0.1			36.94	35.5183	-1.55	0	1.55	0
		37.1667	35.3225	-2.3	-0.6	1.6	0.1			36.9333	35.5117	-1.5	0	1.5	0
		37.1667	35.3283	-2.25	-0.55	1.6	0.1			36.9267	35.505	-1.4	0	1.4	0
		37.1667	35.3333	-2.2	-0.55	1.55	0.1			36.9183	35.4983	-1.3	0	1.3	0
		37.1667	35.3383	-2.1	-0.5	1.5	0.1			36.91	35.4917	0	0	0	0
		37.1667	35.3442	-2.1	-0.5	1.5	0.1			36.9033	35.485	0	0	0	0
		37.1667	35.35	-2.05	-0.5	1.4	0.15			36.8967	35.4783	0	0	0	0

	37.1667	35.3558	-2	-0.5	1.35	0.15		36.89	35.4717	0	0	0	0
	37.1667	35.3617	-2	-0.5	1.35	0.15		36.8817	35.465	0	0	0	0
	37.1667	35.3667	-2.1	-0.55	1.45	0.1		36.875	35.46	0	0	0	0
	37.1667	35.3717	-2.2	-0.55	1.5	0.15		36.8683	35.455	0	0	0	0
	37.1667	35.3767	-2.1	-0.55	1.55	0		36.8617	35.45	0	0	0	0
	37.1667	35.3817	-2.1	-0.6	1.5	0		36.855	35.4433	0	0	0	0
	37.1667	35.385	-2.1	-0.6	1.5	0		36.8483	35.435	0	0	0	0
	37.1665	35.39	-2.15	-0.6	1.55	0		36.8417	35.4267	0	0	0	0
	37.1665	35.395	-2.15	-0.55	1.6	0		36.835	35.42	0	0	0	0
	37.1665	35.4	-2.2	-0.55	1.65	0		36.8283	35.4133	0	0	0	0
	37.1663	35.4067	-2.25	-0.55	1.7	0		36.8217	35.4067	0	0	0	0
	37.1663	35.4133	-2.25	-0.5	1.75	0		530 36.8133	35.4	0	0	0	0
	37.1663	35.4183	-2.25	-0.5	1.75	0	ad42	110 36.9667	35.495	-1.85	-0.6	1.25	0
370	37.1663	35.4233	-2.25	-0.45	1.8	0		36.96	35.505	-2	-0.8	1.2	0
380	37.1662	35.4283	-2.25	-0.45	1.8	0		36.9533	35.5167	-2.05	-1	1.05	0
	37.1662	35.4333	-2.3	-0.4	1.9	0		36.9467	35.5283	-1.7	-0.55	1.15	0
	37.1662	35.4383	-2.35	-0.4	1.95	0		36.94	35.54	-1.6	-0.55	1.05	0
	37.166	35.4433	-2.4	-0.4	2	0		36.935	35.55	-1.65	-0.06	1.59	0
	37.166	35.4492	-2.45	-0.4	2.05	0		36.93	35.56	-1.9	-0.75	1.15	0
	37.166	35.4542	-2.5	-0.4	2.1	0		250 36.925	35.57	-2.1	-1	1.1	0
	37.1658	35.46	-2.55	-0.4	2.15	0	add8833f	110 36.6867	35.14	-4.1	-2.4	1.7	0
	37.1658	35.465	-2.6	-0.4	2.2	0		36.6933	35.1467	-4.1	-2.4	1.7	0
	37.1657	35.47	-2.65	-0.45	2.2	0		36.7	35.1533	-4.1			0
	37.1657	35.475	-2.7	-0.5	2.2	0		36.7067	35.16	-4.1			0
	37.1657	35.48	-2.7	-0.55	2.15	0		36.7133	35.17	-4.1			0
	37.1655	35.4842	-2.7	-0.55	2.15	0		36.72	35.175	-4.1			0
	37.1655	35.4883	-2.7	-0.6	2.1	0		36.7267	35.1817	-4.1			0
	37.1655	35.4933	-2.7	-0.65	2.05	0		36.7333	35.1883	-4	-2.35	1.65	0
	37.1653	35.4983	-2.7	-0.7	2	0		36.74	35.195	-4	-2.35	1.65	0
	37.1653	35.5042	-2.65	-0.75	1.9	0		36.7467	35.2017	-3.9	-2.3	1.6	0
	37.1653	35.51	-2.65	-0.75	1.9	0		36.7533	35.2083	-3.8	-2.1	1.7	0
	37.1652	35.515	-2.6	-0.75	1.85	0		36.76	35.215	-3.75	-1.95	1.8	0
	37.1652	35.5208	-2.6	-0.75	1.85	0		36.7667	35.2217	-3.7	-1.8	1.9	0
570	37.165	35.5267	-2.6	-0.7	1.9	0		36.7733	35.2283	-3.65	-1.75	1.9	0
add8731f	100 37.2817	35.3867	-1.5	0	1.4	0.1		36.78	35.235	-3.6	-1.75	1.85	0

	37.2667	35.3867	-1.5	0	1.4	0.1		36.7867	35.2417	-3.5	-1.7	1.8	0
	37.2617	35.3865	-1.5	0	1.4	0.1		36.7933	35.2483	-3.45	-1.55	1.9	0
	37.2567	35.3863	-1.55	0	1.4	0.15		36.8	35.255	-3.35	-1.45	1.9	0
	37.2517	35.3862	-1.6	0	1.4	0.2		36.8067	35.2617	-3.25	-1.45	1.8	0
	37.2467	35.386	-1.55	0	1.4	0.15	490	36.8133	35.2683	-3.2	-1.5	1.7	0
	37.2417	35.3858	-1.6	0	1.45	0.15		36.8217	35.2733	-3.15	-1.5	1.65	0
	37.2383	35.3857	-1.6	0	1.5	0.1		36.8283	35.28	-3.1	-1.55	1.55	
	37.2333	35.3855	-1.65	0	1.55	0.1		36.835	35.2867	-3.1	-1.55	1.55	
	37.2283	35.3853	-1.7	-0.05	1.6	0.05		36.8417	35.2933	-3	-1.55	1.45	
	37.2225	35.3852	-1.75	-0.1	1.65	0		36.8483	35.3017	-2.9	-1.5	1.4	
	37.2183	35.385	-1.85	-0.1	1.75	0		36.8567	35.31	-2.9	-1.5	1.4	
	37.2133	35.3848	-1.9	-0.15	1.75	0		36.865	35.3183	-2.9	-1.45	1.45	
	37.2092	35.3847	-1.95	-0.25	1.7	0							
	37.205	35.3845	-2	-0.3	1.7	0		36.8783	35.3283	-3	-1.4	1.6	
	37.2017	35.3843	-2	-0.35	1.65	0		36.885	35.335	-2.9	-1.2	1.7	
	37.1967	35.3842	-2.05	-0.35	1.7	0		36.8917	35.3417	-2.85	-1.2	1.65	
	37.1917	35.384	-2.1	-0.4	1.7	0		36.8983	35.3483	-2.8	-1.25	1.55	
	37.1867	35.3838	-2.15	-0.4	1.65	0.1		36.905	35.355	-2.8	-1.2	1.6	
	37.1825	35.3837	-2.2	-0.4	1.7	0.1		36.9117	35.3617	-2.8	-1.2	1.6	
	37.1783	35.3835	-2.2	-0.45	1.6	0.15		36.92	35.37	-2.8	-1.1	1.7	
	37.1733	35.3833	-2.25	-0.5	1.6	0.15		36.9267	35.3783	-2.8	-0.95	1.85	
	37.1683	35.3832	-2.3	-0.55	1.6	0.15		36.9333	35.385	-2.9	-0.85	2.05	
	37.1633	35.383	-2.3	-0.6	1.6	0.1		36.94	35.39	-2.95	-0.85	2.1	
	37.1583	35.3828	-2.3	-0.6	1.65	0.05		36.9467	35.3967	-2.95	-0.95	2	
	37.1533	35.3827	-2.35	-0.65	1.7	0		36.9533	35.4017	-3	-0.95	2.05	
	37.15	35.3825	-2.45	-0.65	1.8	0		36.9617	35.4083	-2.5	-0.95	1.55	
	37.1467	35.3823	-2.5	-0.7	1.8	0		36.9683	35.415	-2.35	-0.85	1.5	
	37.1417	35.3822	-2.55	-0.75	1.8	0		36.975	35.4217	-2.35	-0.8	1.55	
	37.1367	35.382	-2.5	-0.75	1.75	0		36.9817	35.4267	-2.35	-0.75	1.6	
	37.1333	35.3818	-2.45	-0.8	1.65	0		36.99	35.4317	-2.5	-0.8	1.7	
410	37.13	35.3817	-2.35	-0.8	1.55	0		36.9967	35.4367	-2.55	-0.85	1.7	
add8730	90	37.285	35.405	-1.4	0	1.4	0	1030	37.005	35.4433	-2.55	-0.85	1.7
		37.2833	35.405	-1.4	0	1.4	0	add86321	390	36.7667	35.32	0	0
		37.2792	35.405	-1.4	0	1.4	0			36.7617	35.3267	0	0
		37.275	35.405	-1.4	0	1.4	0			36.7567	35.3333	0	0

	37.2708	35.405	-1.4	0	1.4	0			36.7517	35.34	0	0	0
	37.2667	35.405	-1.4	0	1.4	0			36.7467	35.3467	0	0	0
	37.2633	35.405	-1.4	0	1.4	0			36.7417	35.3533	0	0	0
	37.2583	35.405	-1.4	0	1.4	0			36.7367	35.36	0	0	0
	37.2533	35.405	-1.4	0	1.4	0			36.7325	35.3667	0	0	0
	37.2483	35.405	-1.45	0	1.45	0			36.7283	35.375	0	0	0
	37.2433	35.405	-1.55	0	1.55	0			36.7233	35.3817	0	0	0
	37.2383	35.405	-1.65	0	1.65	0			36.7183	35.39	0	0	0
	37.235	35.405	-1.7	-0.05	1.65	0			36.7133	35.3983	0	0	0
	37.23	35.405	-1.8	-0.1	1.7	0			36.7083	35.4067	0	0	0
	37.225	35.405	-1.9	-0.15	1.75	0			36.7033	35.415	0	0	0
	37.22	35.405	-2	-0.2	1.8	0			36.6983	35.4233	0	0	0
	37.2167	35.405	-2.15	-0.2	1.85	0.1			36.6933	35.4317	0	0	0
	37.2117	35.405	-2.15	-0.25	1.8	0.1			36.6867	35.4417	0	0	0
	37.2067	35.405	-2.15	-0.3	1.75	0.1			36.68	35.45	0	0	0
	37.2017	35.405	-2.2	-0.35	1.75	0.1			36.6733	35.4583	0	0	0
	37.1983	35.405	-2.25	-0.35	1.8	0.1			36.6683	35.4667	0	0	0
	37.195	35.405	-2.3	-0.4	1.8	0.1			36.6617	35.4733	0	0	0
	37.1917	35.405	-2.3	-0.45	1.8	0.05			36.6567	35.4817	0	0	0
	37.1867	35.405	-2.35	-0.45	1.8	0.1			36.6517	35.4883	0	0	0
	37.1817	35.405	-2.35	-0.5	1.75	0.1			830 36.6467	35.4967	0	0	0
	37.1783	35.405	-2.35	-0.5	1.75	0.1	ad31	550	36.7367	35.2208	-4	-2	2
	37.175	35.405	-2.35	-0.5	1.8	0.05			36.7467	35.2275	-4	-2	2
360	37.17	35.405	-2.4	-0.55	1.75	0.1			36.76	35.2383	-3.9	-2	1.9
370	37.165	35.405	-2.4	-0.55	1.75	0.1			36.7667	35.245	-3.8	-2	1.8
	37.16	35.405	-2.4	-0.55	1.75	0.1			36.7733	35.2517	-3.7	-1.95	1.75
	37.155	35.405	-2.35	-0.6	1.65	0.1			36.78	35.2583	-3.65	-1.9	1.75
	37.15	35.405	-2.35	-0.6	1.65	0.1			36.7867	35.265	-3.6	-1.85	1.75
	37.1458	35.405	-2.35	-0.65	1.6	0.1			36.795	35.27	-3.5	-1.9	1.6
	37.1417	35.405	-2.35	-0.65	1.65	0.05			36.8017	35.275	-3.35	-1.9	1.45
	37.1367	35.405	-2.4	-0.7	1.7	0			36.8083	35.2817	-3.3	-1.95	1.35
	37.1317	35.405	-2.45	-0.75	1.7	0			36.815	35.2883	-3.3	-1.7	1.6
	37.1267	35.405	-2.5	-0.8	1.7	0			36.8217	35.2967	-3.4	-1.55	1.85
	37.1217	35.405	-2.55	-0.85	1.7	0			36.8283	35.305	-3.4	-1.6	1.8
	37.1167	35.405	-2.55	-0.85	1.7	0			36.8383	35.3133	-3.5	-1.75	1.75

		37.115	35.405	-2.55	-0.85	1.7	0			36.845	35.32	-3.5	-1.8	1.7
		37.11	35.405	-2.55	-0.9	1.65	0			36.8517	35.3267	-3.5	-1.85	1.65
		37.105	35.405	-2.6	-0.95	1.65	0			36.8567	35.3333	-3.5	-1.85	1.65
		37.1	35.405	-2.6	-0.95	1.65	0			36.8617	35.3383	-3.5	-1.9	1.6
		37.0958	35.405	-2.6	-1	1.6	0			36.8667	35.345	-3.5	-1.95	1.55
		37.0917	35.405	-2.6	-1	1.6	0			36.8733	35.3517	-3.4	-1.95	1.45
		37.0875	35.405	-2.6	-1.05	1.55	0			36.88	35.3583	-3.3	-1.3	2
		37.0833	35.405	-2.6	-1.05	1.55	0			36.8867	35.365	-3.3	-1.15	2.15
		37.08	35.405	-2.6	-1.05	1.55	0			36.8933	35.3733	-3.35	-1.2	2.15
		37.075	35.405	-2.6	-1.1	1.5	0	Add8830	210	36.9967	34.9117	-0.95	-0.35	0.6
		37.07	35.405	-2.6	-1.1	1.5	0			36.99	34.92	-1.1	-0.35	0.75
		37.065	35.405	-2.6	-1.1	1.5	0			36.9833	34.9283	-1.25	-0.65	0.6
		37.06	35.405	-2.6	-1.1	1.5	0			36.9783	34.9367	-1.5	-0.75	0.75
		37.0567	35.405	-2.6	-1.1	1.5	0			36.9717	34.945	-1.65	-0.85	0.8
		37.0533	35.405	-2.6	-1.1	1.5	0			36.9667	34.9533	-1.75	-1	0.75
		37.05	35.405	-2.55	-1.15	1.4	0			36.9617	34.9617	-1.95	-1.1	0.85
640		37.0467	35.405	-2.5	-1.2	1.3	0			36.955	34.97	-2.15	-1.2	0.95
add8830i	100	37.2583	35.5	-1.5	0	1.5	0			36.9483	34.98	-2.35	-1.35	1
		37.2533	35.5	-1.55	0	1.55	0			36.9433	34.995	-2.45	-1.45	1
		37.2483	35.5	-1.55	0	1.55	0			36.9383	34.99	-2.55	-1.55	1
		37.2433	35.4998	-1.6	0	1.6	0			36.9333	34.985	-2.6	-1.6	1
		37.2383	35.4998	-1.65	0	1.65	0			36.9283	35.0117	-2.6	-1.7	0.9
		37.2333	35.4997	-1.7	0	1.7	0			36.9233	35.02	-2.65	-1.8	0.85
		37.23	35.4997	-1.75	-0.1	1.65	0			36.9183	35.0283	-2.7	-1.9	0.8
		37.225	35.4995	-1.85	-0.15	1.7	0			36.9117	35.0367	-2.75	-1.95	0.8
		37.2217	35.4993	-1.9	-0.2	1.7	0			36.905	35.045	-2.8	-2.05	0.75
		37.2183	35.4992	-1.9	-0.25	1.65	0			36.8983	35.0533	-2.85	-2.1	0.75
		37.2133	35.499	-1.95	-0.3	1.65	0			36.8917	35.0617	-2.9	-2.2	0.7
		37.2083	35.4988	-2	-0.35	1.65	0			36.885	35.07	-3	-2.3	0.7
		37.2033	35.4985	-2.15	-0.4	1.75	0			36.88	35.0783	-3.1	-2.4	0.7
		37.1983	35.4983	-2.2	-0.4	1.8	0			36.8733	35.0867	-3.2	-2.5	0.7
		37.1942	35.4983	-2.3	-0.4	1.9	0			36.8633	35.095	-3.25	-2.55	0.7
		37.19	35.4983	-2.4	-0.45	1.95	0			36.8583	35.1017	-3.3	-2.55	0.75
		37.185	35.4983	-2.5	-0.45	2.05	0			36.8533	35.1083	-3.4	-2.55	0.85
		37.1817	35.4983	-2.55	-0.5	2.05	0			36.8483	35.115	-3.5	-2.6	0.9

37.1783	35.4975	-2.6	-0.5	2.1	0		36.845	35.1233	-3.55	-2.6	0.95
37.175	35.4975	-2.6	-0.55	2.05	0		36.8417	35.1317	-3.6	-2.6	1
37.17	35.4975	-2.55	-0.55	2	0	add8830:	710 37.0333	34.925	0	0	0
37.165	35.4975	-2.6	-0.6	2	0		37.0267	34.9333	-0.15	0	0.15
37.16	35.4967	-2.65	-0.6	2.05	0		37.02	34.9417	-0.35	-0.25	0.1
37.1542	35.4967	-2.7	-0.65	2.05	0		37.015	34.9483	-0.75	-0.4	0.35
37.1483	35.4967	-2.8	-0.65	2.15	0		37.01	34.955	-1	-0.45	0.55
37.1433	35.4967	-2.8	-0.7	2.1	0		37.005	34.9617	-1.25	-0.55	0.7
37.14	35.4967	-2.8	-0.7	2.1	0		37	34.9667	-1.45	-0.7	0.75
370 37.1367	35.4958	-2.75	-0.65	2.1	0		36.9933	34.9717	-1.55	-0.75	0.8
380 37.1333	35.4958	-2.75	-0.65	2.1	0		36.9883	34.9783	-1.8	-0.85	0.95
37.1283	35.4958	-2.7	-0.65	2.05	0		36.9833	34.9883	-2	-1.05	0.95
37.1233	35.4958	-2.65	-0.65	2	0		36.9767	34.9967	-2.15	-1.2	0.95
37.1183	35.4958	-2.6	-0.65	1.95	0		36.9683	35.005	-2.3	-1.3	1
37.1133	35.4958	-2.55	-0.65	1.9	0		36.9617	35.0133	-2.45	-1.4	1.05
37.1083	35.495	-2.5	-0.65	1.85	0		36.955	35.0217	-2.6	-1.45	1.15
37.1033	35.495	-2.5	-0.65	1.85	0		36.95	35.03	-2.65	-1.55	1.1
37.0983	35.495	-2.45	-0.6	1.85	0		36.945	35.0383	-2.75	-1.65	1.1
37.095	35.495	-2.45	-0.6	1.85	0		36.94	35.0467	-2.8	-1.75	1.05
37.0917	35.495	-2.45	-0.6	1.85	0		36.935	35.055	-2.9	-1.85	1.05
37.0875	35.495	-2.4	-0.6	1.8	0		36.93	35.0633	-2.95	-1.95	1
37.0833	35.495	-2.4	-0.55	1.85	0		36.925	35.0667	-3	-2	1
37.0783	35.495	-2.4	-0.5	1.9	0		36.92	35.0717	-2.8	-2.05	0.75
37.075	35.4943	-2.35	-0.45	1.9	0		36.9117	35.08	-2.8	-2.05	0.75
37.07	35.4943	-2.35	-0.45	1.9	0		36.9033	35.0883	-3	-2.05	0.95
37.065	35.4938	-2.3	-0.4	1.9	0		36.8967	35.0967	-3.2	-2.3	0.9
37.06	35.4938	-2.35	-0.45	1.9	0		36.89	35.105	-3.25	-2.4	0.85
37.055	35.4933	-2.45	-0.45	2	0		36.8833	35.1133	-3.3	-2.45	0.85
37.0508	35.4933	-2.55	-0.5	2.05	0		36.8767	35.1217	-3.3	-2.45	0.85
37.0467	35.4925	-2.6	-0.5	2.1	0		36.87	35.13	-3.4	-2.5	0.9
37.0417	35.4925	-2.6	-0.55	2.05	0		36.8667	35.1383	-3.4	-2.6	0.8
37.0417	35.4922	-2.6	-0.6	2	0		36.8617	35.1467	-3.4	-2.6	0.8
37.0333	35.4922	-2.6	-0.6	2	0		36.8567	35.1533	-3.4	-2.6	0.8
37.03	35.4922	-2.6	-0.65	1.95	0	ad14	410 36.9067	35.38	-3.4	-1.25	2.15
620 37.0267	35.492	-2.6	-0.8	1.8	0		36.9133	35.3867	-3.4	-1.35	2.05

add8830	490	37.1367	35.3783	-2.3	-0.85	1.45	0			36.92	35.3933	-3.4	-1.35	2.05	
		37.1317	35.3783	-2.35	-0.85	1.5	0			36.925	35.4	-3.4	-1.25	2.15	
		37.1267	35.3783	-2.4	-0.9	1.5	0			36.93	35.4067	-3.4	-1.25	2.15	
		37.1217	35.3783	-2.5	-0.9	1.6	0			36.935	35.4133	-3.4	-1.35	2.05	
		37.1167	35.3783	-2.5	-0.9	1.6	0			36.9417	35.42	-3.4	-1.45	1.95	
		37.1133	35.3783	-2.55	-0.95	1.6	0			36.9483	35.4267	-3.4	-1.4	2	
		37.11	35.3783	-2.6	-1	1.6	0			36.955	35.4333	-3.05	-1.4	1.65	
		37.1067	35.3783	-2.65	-1.05	1.6	0			36.9617	35.44	-3	-1.4	1.6	
		37.1017	35.3783	-2.7	-1.05	1.65	0			36.97	35.4467	-2.9	-1.4	1.5	
		37.0967	35.3783	-2.75	-1.1	1.65	0			36.9767	35.4533	-2.85	-1.35	1.5	
		37.0917	35.3783	-2.8	-1.1	1.7	0			36.9817	35.46	-2.85	-1.3	1.55	
		37.0875	35.3783	-2.8	-1.15	1.65	0			36.9883	35.4667	-2.8	-1.3	1.5	
		37.0833	35.3783	-2.9	-1.2	1.7	0			36.995	35.4733	-2.8	-1.4	1.4	
		37.0792	35.3783	-2.9	-1.25	1.65	0			37.0033	35.48	-2.8	-1.45	1.35	
		37.075	35.3783	-2.85	-1.3	1.55	0			37.01	35.4867	-2.8	-1.55	1.25	
		37.07	35.3783	-2.85	-1.3	1.55	0			37.0167	35.4933	-2.8	-1.55	1.25	
		37.065	35.3783	-2.8	-1.3	1.5	0			37.0217	35.5	-2.8	-1.3	1.5	
		37.0617	35.3783	-2.8	-1.3	1.5	0			37.0283	35.5067	-2.8	-1.15	1.65	
		37.0575	35.3783	-2.8	-1.3	1.5	0			37.0333	35.5133	-2.9	-1.1	1.8	
		37.0533	35.3783	-2.8	-1.3	1.5	0			37.0383	35.52	-2.9	-1.15	1.75	
		37.0483	35.3783	-2.8	-1.3	1.5	0			37.045	35.5267	-2.8	-1.05	1.75	
		37.0433	35.3783	-2.8	-1.3	1.5	0			37.0517	35.5383	-2.75	-0.9	1.85	
		37.0383	35.3783	-2.75	-1.3	1.45	0			37.06	35.54	-2.25	-0.75	1.5	
		37.0333	35.3783	-2.75	-1.3	1.45	0			37.0683	35.5467	-2.2	-0.65	1.55	
		37.03	35.3783	-2.8	-1.3	1.5	0			37.075	35.5533	-2.2	-0.7	1.5	
		37.0267	35.3783	-2.9	-1.3	1.6	0			37.0817	35.56	-2.2	-0.8	1.4	
	230	37.0233	35.3783	-2.9	-1.3	1.6	0			37.0883	35.5667	-2.2	-0.9	1.3	
	220	37.02	35.3783	-2.9	-1.3	1.6	0			37.0933	35.5733	-2.2	-0.9	1.3	
		37.015	35.3783	-2.9	-1.3	1.6	0			37.0983	35.58	-2.2	-0.9	1.3	
		37.0117	35.3783	-2.9	-1.3	1.6	0		had8730	500	36.9167	35.5967	0	0	0
		37.005	35.3783	-2.9	-1.3	1.6	0				36.9017	35.65	0	0	0
		37	35.3783	-2.9	-1.3	1.6	0				36.8833	35.69	0	0	0
		36.9975	35.3783	-2.85	-1.1	1.75	0				36.8683	35.7383	0	0	0
		36.9925	35.3783	-2.8	-1.05	1.75	0		add8730	200	36.9067	35.4833	0	0	0
		36.9883	35.3783	-2.75	-1	1.75	0			150	36.9017	35.5067	0	0	0

36 9833	35 3783	-2 75	-0 9	1 85	0	100 36 8967	35 5333	0	0	0
---------	---------	-------	------	------	---	-------------	---------	---	---	---

